Aalto University
School of Chemical
Technology

School of Chemical Technology
Degree Programme of Materials Science and Engineering

Simon Yliaho

DISTRIBUTION OF GALLIUM, GERMANIUM, INDIUM AND TIN BETWEEN LEAD BULLION AND SLAG

Master's thesis for the degree of Master of Science in Technology submitted for inspection, Espoo, January 12th, 2016.

Supervisor **Professor Pekka Taskinen**

Instructor **M.Sc. (Tech.) Katri Avarmaa**

Aalto University
School of Chemical
Technology

Aalto University, P.O. BOX 11000, 00076 AALTO
www.aalto.fi

Abstract of master's thesis

Author Simon Yliaho

Title of thesis Distribution of gallium, germanium, indium and tin between lead bullion and slag

Department Materials Science and Engineering

Professorship Metallurgy/Thermodynamics and modelling **Code of professorship** MT-37

Thesis supervisor Prof. Pekka Taskinen

Thesis advisor(s) / Thesis examiner(s) M.Sc.(Tech) Katri Avarmaa

Date 12.01.2016 **Number of pages** 95+55 **Language** English

Abstract

This work examines the distribution of the trace elements gallium, germanium, indium and tin at lead smelting conditions. First part of the work is a literature overview and the latter part is an experimental part where a laboratory work on the distribution of the trace elements between lead and slag is presented. The work is concentrating on modern direct smelting technologies, because these are the promising technologies for the future.

The experimental work was performed at 1150 °C (1423 K). The aim of the work is to research how the elements distribute when the oxygen partial pressure is changed. Oxygen partial pressures used in the experiments (10^{-7}-10^{-12} atm) are around the same values that are used in industrial processes. The experimental method employed consists of three main stages: equilibration at high temperature, fast quenching and EPMA-analyses. The EPMA-analyses were implemented by the Geological survey of Finland (GTK). A pseudo-wollastonite crucible was used to hold the lead and slag.

The conclusions were that gallium dissolves in the slag, germanium has the oxidation state Ge^{2+} during reducing conditions and Ge^{+} during oxidating conditions, indium has the oxidation state In^{2+} and tin has the oxidation state close to Sn^{2+}. The distribution coefficients were 0.01-0.8 for gallium, 0.1-8 for germanium, 0.003-11 for indium and 0.002-4 for tin. The concentrations were close to the detection limits but it was possible to make conclusions from the results.

Keywords Lead smelting, gallium, germanium, indium, tin, distribution

Aalto-universitetet
Högskolan för
kemiteknik

Aalto-universitetet, PB 11000, 00076 AALTO
www.aalto.fi

Sammandrag av diplomarbetet

Författare	Simon Yliaho
Titel	Fördelning av gallium, germanium, indium och tenn mellan bly och slagg
Examensprogram	Materialteknik
Huvudämne	Metallurgi/Termodynamik och modellering
Huvudämnets kod	MT-37
Ansvarig lärare	Prof. Pekka Taskinen
Handledare	DI Katri Avarmaa
Datum	12.01.2016
Sidantal	95+55
Språk	Engelska

Sammandrag

I det här diplomarbetet undersöks fördelningen av spårämnena gallium, germanium, indium och tenn under blysmältningsförhållanden. Första delen av det här arbetet består av en litteraturöversikt och den andra delen av en experimentell del, där det gjordes ett laboratoriearbete på fördelningen av spårämnen mellan bly och slagg. Det här arbetet tar i beaktande moderna blysmältningsmetoder eftersom de är de mest lovande metoderna för framtiden.

Det experimentella arbetet blev gjort i en temperatur på 1150 °C (1423 K). Målet med det här arbetet är att undersöka hur spårämnena fördelar sig mellan det smälta blyet och den smälta slaggen. De partialtryck som syret har i dessa experiment är liknande de som används i industriella processer. Den använda experimentella metoden består av tre skeden: jämvikt vid hög temperatur, släckning och EPMA-analys. EPMA-analyserna blev gjorda vid Geologiska forskningscentralen (GTK). Det användes en smältdegel av pseudo-wollastonit för att hålla blyet och slaggen under experimenten.

Slutledningen i arbetet var att gallium löser sig i slaggen, germanium har oxidationstalet +2 under reducerande förhållanden och +1 under oxiderande förhållanden, indium har oxidationstalet +2 och tenn har ett oxidationstal nära +2. Fördelningskoefficienterna mellan bly och slagg blev 0.01-0.8 för gallium, 0.1-8 för germanium, 0.003-11 för indium och 0.002-4 för tenn. Koncentrationerna var nära gränsen för observation, men det var möjligt att göra slutsatser utgående från resultatena.

Nyckelord Blysmältning, gallium, germanium, indium, tenn, fördelning

Aalto-yliopisto
Kemian tekniikan
korkeakoulu

Aalto-yliopisto, PL 11000, 00076 AALTO
www.aalto.fi
Diplomityön tiivistelmä

Tekijä Simon Yliaho		
Työn nimi Galliumin, germaniumin, indiumin ja tinan jakautuminen lyijyn ja kuonan välillä		
Laitos Materiaalitekniikka		
Professuuri Metallurgia/Termodynamiikka ja mallinnus		**Professuurikoodi** MT-37
Työn valvoja Prof. Pekka Taskinen		
Työn ohjaaja(t)/Työn tarkastaja(t) DI Katri Avarmaa		
Päivämäärä 12.01.2016	**Sivumäärä** 95+55	**Kieli** Englanti

Tiivistelmä

Tämä diplomityö tarkastelee hivenaineiden gallium, germanium, indium ja tina jakautumista lyijysulatuksen olosuhteissa. Työn ensimmäinen osuus koostuu kirjallisuuskatsauksesta ja toinen osuus kokeellisesta osuudesta, jossa esitetään tehty laboratoriotyö hivenaineiden jakautumisesta lyijyn ja kuonan välillä. Tämä työ keskittyy moderneihin lyijyn suoravalmistusprosesseihin, koska ne ovat tulevaisuuden lupaavat teknologiat.

Kokeet suoritettiin lämpötilassa 1150 °C (1423 K). Työn tavoite on tutkia kuinka alkuaineet jakautuvat hapen osapainetta muuttaessa. Tässä työssä käytössä olevat hapen osapaineet (10^{-7}-10^{-12} atm) ovat samankaltaisia kuin teollisuudessa käytössä olevat. Kokeellinen menetelmä kostuu kolmesta vaiheesta: tasapainotus, nopea sammutus ja EPMA-analyysi. Näytteiden EPMA-analyysit toteutti Geologinen tutkimuskeskus (GTK). Lyijy ja kuona olivat pseudo-wollastoniittiupokkaassa kokeiden aikana.

Tuloksissa päädyttiin siihen, että gallium liukenee kuonaan, germaniumilla on hapetusaste Ge^{2+} pelkistävissä olosuhteissa ja Ge^{+} hapettavissa olosuhteissa, indiumilla on hapetusaste In^{2+} ja tinalla on hapetusaste lähellä Sn^{2+}. Jakautumiskertoimet olivat 0.01-0.8 galliumille, 0.1-8 germaniumille, 0.003-11 indiumille ja 0.002-4 tinalle. Vaikka pitoisuudet olivat lähellä havainnointirajoja, tuloksista oli mahdollista tehdä edellä mainitut johtopäätökset.

Avainsanat Lyijyn sulatus, gallium, germanium, indium, tina, jakautuminen

Foreword

This work is done as a research work for the company CLEEN Oy (Click Innovations Oy) and as a part of the ARVI program. It is done in cooperation between Aalto University, Kuusakoski Oy and Outotec Oyj. The work has been executed in the research group for thermodynamics and modelling at Aalto University.

I want to thank Professor Pekka Taskinen who gave me the opportunity to do my thesis in the laboratory at the university. It was a great experience and I also met many interesting persons. Without my instructor M.Sc. Katri Avarmaa I would have been completely lost and I give great thanks to her as well. I wish the best to everyone in the thermodynamics and modelling research group. And finally I thank Maria for encouraging me to accomplish my thesis.

In Espoo, January 12th 2016 _____

Simon Yliaho

Table of contents

Symbols

a	activity
γ	activity coefficient
γ°	limiting activity cefficient
$\Delta_f G^0$	Gibbs standard-state free energy of transformation
G	Gibbs energy
K	reaction constant
$L_X^{Pb/s}$	distribution ratio of X between lead phase and slag phase
$\Delta\ L_X$	error for distribution ratio
$\%X$	weight-% of metal
n_T	number of mole per 100 g
N	atom percentage
p	partial pressure
R	gas constant
T	temperature
XO_v	metal oxide
X	metal
[X] or []	concentration of metal in metal phase
(XO_v) or ()	concentration of metal in slag phase
(g)	gas phase
(l)	liquid phase
(s)	solid phase

Introduction

The demand for different rare metals is growing due to the expanding fabrication of new electronic devices. Many of these metals are already attached in the electronic devices that we use today. Thus we can and we should reuse the metals that are in these old devices called waste electric and electronic equipment (WEEE)/e-scrap. This is done by smelting e-scrap and extracting the metals. However, to fully understand how to recover different metals that are often mixed and in small portions in e-scrap, the thermodynamics of the smelting needs to be investigated.

Distribution coefficients for a vast amount of trace elements and other metals between lead and slag can be found from literature. These elements include copper, antimony, arsenic, tin, indium, germanium, silver, cadmium, zinc, cobalt, thallium and bismuth (Matyas & Mackey, 1976) (Fischer II & Bennington, 1991; Rytkönen et al., 1985; Toubartz, 1991; Yan & Swinbourne, 2003; Rytkönen & Klarin, 1987; Rytkönen & Taskinen, 1986; Henao et al., 2010; Hoang & Swinbourne, 2007; Johnson et al., 1983; Moon et al., 1998). Gold and silver distribution between lead, speiss and matte has also been investigated (Ermisch, 1953). However, the distribution results are not inconsistent and include high uncertainties. This work includes one element, gallium, which have not been investigated ever before in direct lead smelting processes.

This work provides an understanding on gallium, germanium, indium and tin distributions between lead bullion and slag in the lead smelting conditions. The work consists of a theoretical part where the up-to-date knowledge on the lead smelting processes and the behaviour of the trace elements of interest in lead smelting is presented. The experimental part consists of the method description employed, the execution of the experiments and in the end the results are discussed and compared with the previous research.

The used experimental method consists of three stages. These are equilibrium at high temperature, quick quenching in ice water and EPMA-analyses. Pure lead was

employed in the experiments and the slag were made from synthetic materials. Three different slags were tested. The trace elements were added to lead-slag system as oxides or metals. The crucibles that were used in the experiments were pseudo-wollastonite substrates produced from calcium oxide (CaO) and silica (SiO_2). The experiments were conducted at a temperature of 1150 °C and at oxygen partial pressures of 10^{-7}, 10^{-8}, 10^{-9}, 10^{-10}, 10^{-11} and 10^{-12} atm. The oxygen partial pressures were reached by controlling carbon monoxide (CO) and carbon dioxide (CO_2) volumetric flows. The phase analyses were carried out with SEM-EDS and EPMA.

Theory part

1 Lead smelting processes

This chapter represents different processes of smelting lead concentrates and further processes of reduced lead. There are different types of smelting methods depending on the way the lead is produced. The most common mineral that is processed is the natural sulphide galena, PbS. The mostly used pyrometallurgical process is the lead blast furnace, but nowadays there are multiple direct smelting processes in use. This work concentrates on the direct smelting technologies. After lead is smelted, it also has to be refined. The refining processes are just mentioned briefly in this work.

The pyrometallurgical processes for lead are smelting and producing of lead bullion, and refining of the lead bullion. After smelting stage, the lead concentration in the bullion is between 90-99.9 % depending on the process type and its control. The refined lead has even higher percentage. (Davidson et al., 2000) Nowadays most lead produced in the world comes from recycled car batteries (Blanpain et al., 2014; Davidson et al., 2000). When lead is produced, also other metals are extracted and will appear in the metal making circuit of lead.

1.1 Direct smelting

Nowadays, the direct smelting method is one of the most promising processes for smelting of lead concentrates, as it consumes less energy than the older methods where the concentrates are first sintered before they are fed to a blast furnace. Because of the less energy used, the direct smelting is also a more environmental friendly process. (Matyas & Mackey, 1976) In direct smelting of lead from the galena ore the net reaction equation is:

$$PbS(s) + O_2(g) \rightarrow Pb(l) + SO_2(g) \quad (1)$$

Direct smelting consists of two stages: a so called flash reaction stage were the oxidation reactions take part and a reduction stage were for example carbon or hydrocarbon gas is injected. The lead concentrate is direct reduced with oxygen to molten lead according to reaction (1). Plenty of sulphur dioxide is produced, which is more strong than the gas produced in a blast furnace. Carbon is employed to reduce the lead oxides. Then as a consequence a great amount of carbon monoxide and carbon dioxide is released. Following reaction chemistry is suggested (King et al., 2014; Davidson et al., 2000):

$$PbS(s) + 2C^0(s) + \frac{5}{2}O_2(g) \rightarrow Pb^0(l) + SO_2(g) + CO(g) + CO_2(g) \quad (2)$$

$$2PbS(s) + 3O_2(g) \rightarrow 2PbO(l) + 2SO_2(g) \quad (3)$$

$$2PbO(l) + C(s) \rightarrow 2Pb(l) + CO_2(g) \quad (4)$$

$$PbS(s) + 2PbO(l) \rightarrow 3Pb(l) + SO_2(g). \quad (5)$$

In reactions (2-5), it can be seen that the galena ore reacts with oxygen and carbon in different stages to form pure lead and also lead oxide. Other metals in the system will also react during the smelting stage, for example iron forms iron oxide and zinc forms zinc oxide, as presented in reactions (6-7) (Helin et al., 2012). At high oxygen partial pressures also hematite and magnetite can be formed from iron. These oxides form the slag with CaO and SiO_2 as the fluxes.

$$FeS(s) + \frac{3}{2}O_2(g) \rightarrow FeO(l) + SO_2(g) \quad (6)$$

$$2ZnS(s) + 3O_2(g) \rightarrow 2ZnO(l) + 2SO_2(g) \quad (7)$$

Direct smelting is possible using the right conditions, as seen in Figure 1 (Matyas & Mackey, 1976). One disadvantage of direct lead smelting is that a significant amount of lead dissolves to slag phase as lead oxides. The lead content in slag can increase up to 50 wt-%. Figure 1 presents the equilibrium diagram of the Pb-S-O system at 1200 °C (Matyas & Mackey, 1976). From this diagram it is possible to see where the different processes and process stages can take place and what products are

recovered, depending on the process conditions. For example, the direct smelting operates in a somewhat higher oxygen partial pressure range than the conventional lead blast furnace.

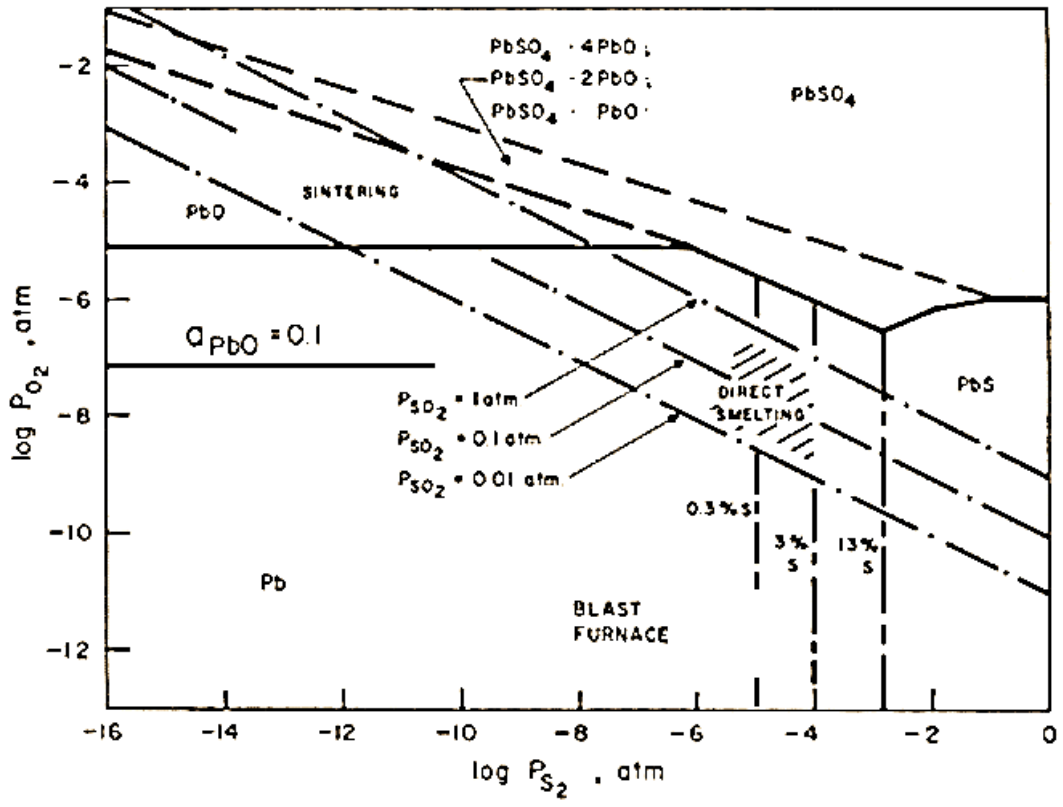

Figure 1 Equilibrium diagram of the Pb-S-O system at 1200 °C (Matyas & Mackey, 1976)

Figure 2 represents the constrained Pb-S-O system and it can be seen from the system that at above temperature of 1100 °C and oxygen partial pressures of 10^{-8} atm, lead is in the form of pure lead and lead oxide, depending on the prevailing oxygen partial pressure.

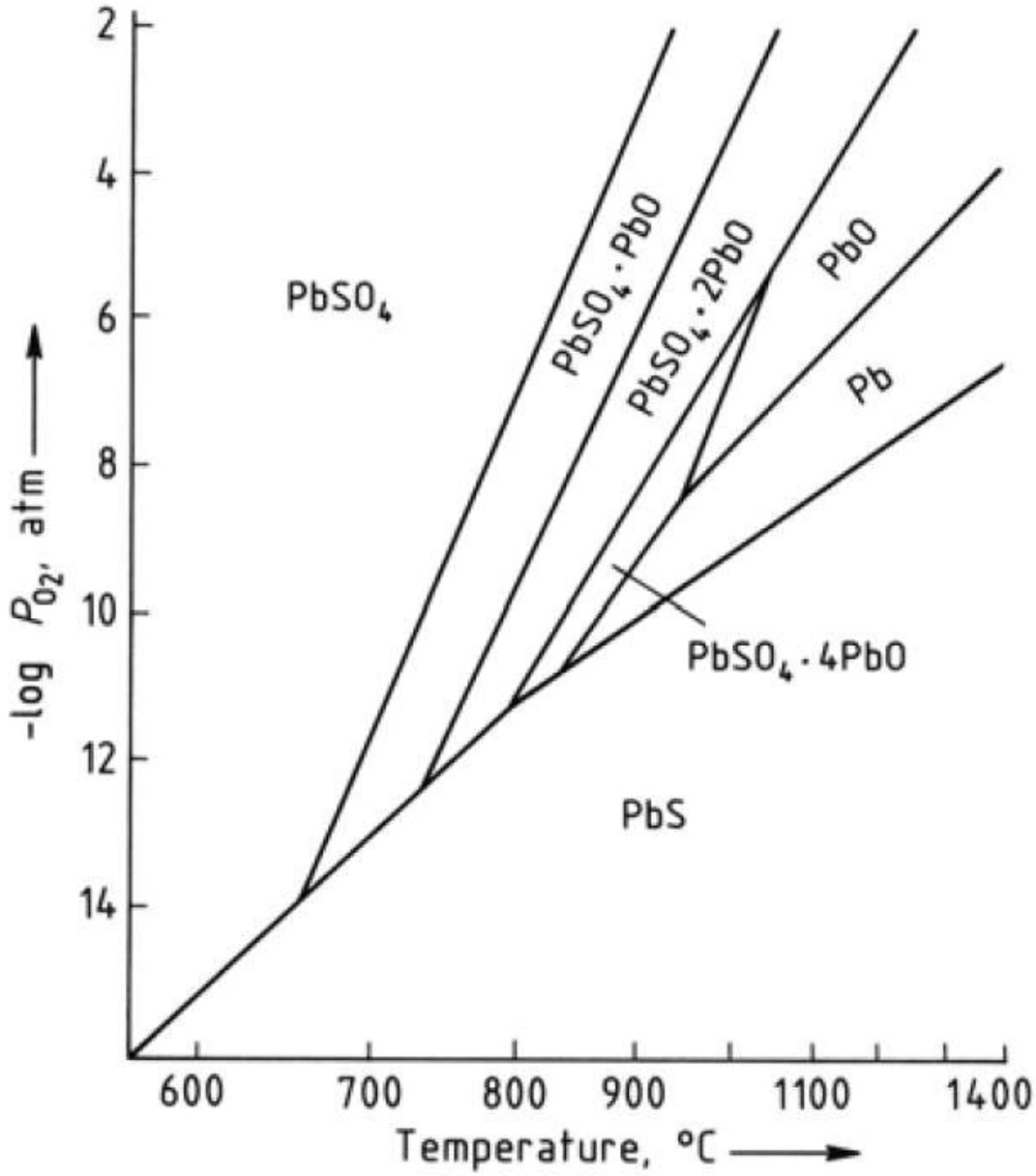

Figure 2 Pb-S-O system, SO_2 pressure 0.2 atm (Davidson et al., 2000).

According to Taskinen et al. (1984) and Matyas & Mackey (1976) there are two types of direct smelting processes for lead ores and concentrates. One is producing a lead bullion with high sulphur content and then discarding the slag. The other one is to produce low-sulphur-content bullion, where after the slag formed has to be cleaned due to its high lead content.

E-scrap is also recycled with direct smelting processes. When e-scrap is recycled there is no sulphur present. This changes the way of observing and operating the e-scrap smelting operation. (van Schaik & Reuter, 2014)

1.2 Smelters

There are different smelters depending on the type of the used concentrate; ores or e-scrap. The concentrates include different concentrations of lead. Some of the smelters can operate both with mineral ores and recyclables to produce lead bullion. (Davidson et al., 2000)

During the 19th century and the beginning of the 20th century, most lead was produced with blast furnaces where the lead concentrate had to be sintered and desulphurised before feeding to the furnace. Because of environmental directives and stricter pollution control, the lead industry has been forced to develop various new direct smelting technologies. (Davidson et al., 2000)

Nowadays the QSL, KIVCET, Kaldo, Ausmelt/Isasmelt and SKS are the smelter types that are the most adopted because they meet the pollution regulations better than the old processes that combines sintering and Blast Furnace or Imperial Smelting. The Varta process is a smelting process were recycled batteries are smelted in a shaft furnace. (Blanpain et al., 2014) The working conditions for QSL, KIVCET, Isasmelt and Kaldo furnaces are presented in Table 1 (Toubartz, 1991; European Commission, 2001; Siegmund, 2003; Matousek, 2011). There are both conditions shown in the table; the oxidation stage and the reduction stage, for each smelting process.

Table 1 Working conditions for direct smelting methods, modified from (Toubartz, 1991), (European Commission, 2001), (Siegmund, 2003), (Matousek, 2011)

	QSL	Ausmelt/Isasmelt	KIVCET		Kaldo
Oxidation					
Temperature (°C)					
Slag/Lead	1100 - 1200	1150 - 1200	1270 - 1300		
Off gas	1100	1050	1300		
Oxidation gas	O_2 (techn.)	Air (27 - 30 % O_2)	O_2 (techn.)		O_2 (techn.)
			Ox	Red	
log pO_2 (atm)	-8.8 - -7.8	-5.6	-5.0	< -9.0	
a_PbO	0.05 - 0.1	> 0.1	> 0.1	< 0.1	
% Pb (Slag)	25 - 40	> 50	> 50	< 10	50
% S (Lead)	0.5 - 1	< 0.5	< 0.05		
% SO_2 (Off gas)	10 - 20	7 - 10	21		4 - 5
Reduction					
Temperature (°C)					
Slag/Lead	1200 - 1250	1150 - 1200	1300 / 750 (bullion discharge 850-950)		
Off gas	1200	1350	1100		
log pO_2 (atm)	-10 - -9	-9	-12		
% Pb (Slag)	< 2	2 - 5	< 2		2 - 4
% S (Slag)	0.4		1.4		

According to European Commission (2014), in 2013 the last smelter in EU-28, working with sintering and shaft furnace, changed its processing technology to direct smelting. Even though countries in EU have changed to direct smelting processes, there are still multiple blast furnaces in use around the world.

1.2.1 KIVCET

The KIVCET smelting process is an old Russian technique for handling copper concentrates. The KIVCET smelter that processes copper concentrates has a cyclone where the reactions happen. (Melcher et al., 1976; Müller, 1976) Later on, this process was adopted to produce lead from complex concentrates. The smelter for lead concentrates includes a shaft where the oxidation reactions happen, instead of the cyclone. (Chaudhuri et al., 1980; Müller, 1976) During the oxidation reactions an oxide melt is generated. The smelter also consists of an electric furnace section where

the graphite electrodes heat up the slag and coal or coke is added to execute the reduction processes. (King et al., 2014)

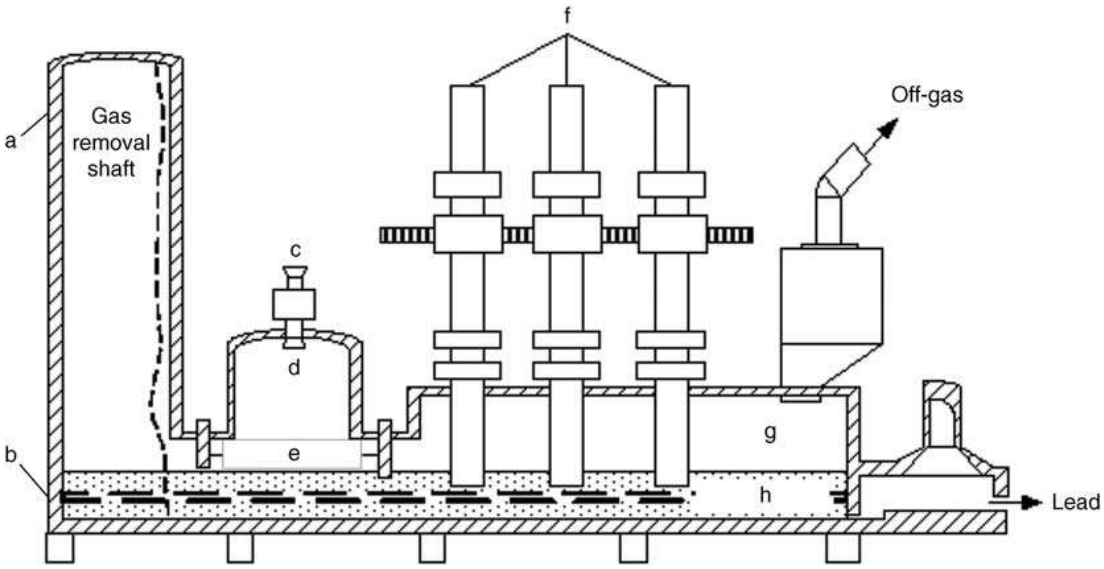

Figure 3 The KIVCET furnace (Davidson et al., 2000).

The KIVCET smelting furnace is presented in Figure 3. One of the first KIVCET smelters for lead smelting was presented by Müller (1976) and Chaudhuri, Koch & Patino (1980). This was a smelter that were able to handle complex ores. According to Siegmund (2003) there are two smelters in Canada and Italy working with the KIVCET technology today. In addition to lead produced, the KIVCET smelter can recover zinc from the smelting fumes and flue dust (King et al., 2014).

1.2.2 Ausmelt/Isasmelt

The Ausmelt/Isasmelt technology is ranked as the best available technology (BAT) of EU for lead smelting (European Commission, 2014; European Commission, 2001). It can be adopted for primary or secondary lead smelting. The Ausmelt/Isasmelt furnace adopts both oxidation and reduction processes. (Errington et al., 2005; Blanpain et al., 2014). First, the Ausmelt/Isasmelt furnace produces lead bullion and a slag with a high lead content. Then the slag is fed to the blast furnace or to a second Ausmelt/Isasmelt furnace or the same furnace again, by changing the parameters, to

reduce the slag and its lead oxide. In China there exist also some lead production sites that combines Ausmelt/Isasmelt technology and blast furnace. (Zhao et al., 2008)

The Outotec Ausmelt process consists of two stages: the smelting of concentrates and cleaning of the slag. The Ausmelt/Isasmelt technology is a modern smelting method that uses a lance to blow gases and fuel into the smelt bath. The top submerged lance is used to control the oxygen partial pressure in the smelting. It is of great importance that the oxygen partial pressure is regulated properly to make sure the right reactions happen. The Ausmelt furnace is presented schematically in Figure 4. (Wood et al., 2009)

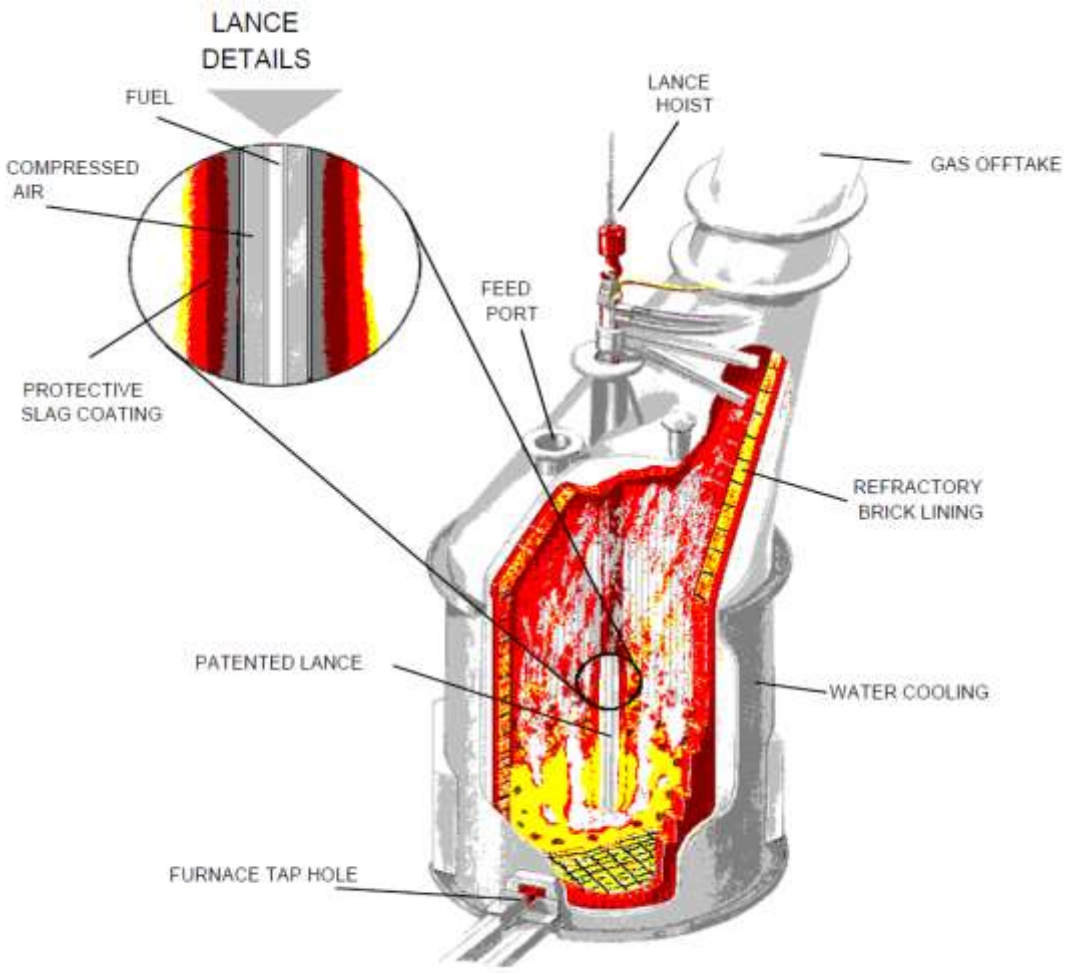

Figure 4 Ausmelt/Isasmelt furnace (Siegmund, 2003).

There are also drawbacks with the Ausmelt/Isasmelt technology, for example a lot of waste gases are formed and a lot of coal is needed for the reduction processes. A flow sheet over these processes is presented in Figure 5 (Wood et al., 2009).

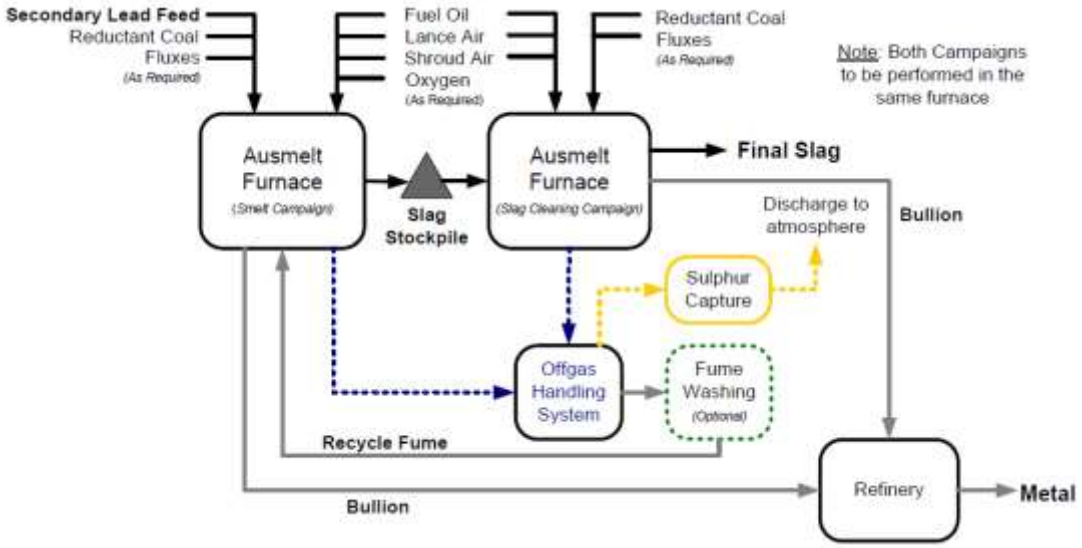

Figure 5 Ausmelt process flow sheet (Wood et al., 2009).

1.2.3 Kaldo, QSL, SKS

In Sweden, a top blown rotary furnace called Kaldo process is used to produce lead from secondary resources, mainly from batteries (Davidson et al., 2000). This furnace can also be used for copper concentrates. The furnace works similar to the Ausmelt/Isasmelt furnace as it includes both the oxidation stage and subsequently the reduction stage in the same furnace. (Siegmund, 2003)

Queneau, Schumann, Lurgi (QSL) is a furnace used in Germany. It is a smelter where the oxidation reactions happen in the feed-end of the reactor and the reduction reactions in the end part of the reactor. So, one end of the reactor the lead concentrate is fed to the furnace and in the opposite side the lead is tapped out. (Siegmund, 2003; Blanpain et al., 2014)

SKS (Shuikoushan) is a lead smelting technology developed and adopted in China. It is a reactor where the oxygen is blown from the bottom of the reactor instead of top-

blowing as for example in the Kaldo furnace and in the Ausmelt/Isasmelt furnace. (Chai et al., 2015; Blanpain et al., 2014)

1.3 Lead refining

After refining the lead bullion, the lead receives a purity of 99.99 to 99.9999 %, depending on the factory and technology used (Crowson, 2006). There are different types of refining processes and stages for the lead bullion. In these refining stages the impurities and trace elements in lead are removed and recovered for further extraction and utilization. There are pyrometallurgical, electrolytic and hydrometallurgical processes to refine the lead bullion, and they are often combined in different stages at the same place. (Blanpain et al., 2014) Here are few examples presented how the lead bullion can be refined and some trace elements recovered.

Some of the metals in the lead bullion can be extracted by cooling down the bullion after which the metals form a dross on the bullion bath. This is usually the first refining stage and its purpose is to remove mainly copper from the lead bullion. (Davidson et al., 2000; Blanpain et al., 2014) The Port Pirie process is another type of decoppering technology where sulphur is added to the bullion in order to remove the copper as copper sulphide from the lead. (Davidson et al., 2000)

Tin is removed with selective oxidation or the Harris process depending on the complexity of the lead bullion (Blanpain et al., 2014). These are called softening processes because they make the lead softer. (Davidson et al., 2000; Crowson, 2006) Air or oxygen injection is employed in the selective oxidation processes to remove tin from the lead bullion (Blanpain et al., 2014). UMICORE adopts the Harris process also to gain indium from the lead to dross. The Harris process consists of pyrometallurgical steps where caustic soda and sodium nitrate are mixed with the lead bullion in order to recover indium and some other metals. Indium will dissolve to the salt mixture, which will be re-treated to separate and recover indium. (Davidson et al., 2000; Alfantazi & Moskalyk, 2003; Han & Park, 2015; Hoang & Swinbourne, 2007)

The Parkes process is used to extract metals especially silver and copper. By adding zinc to the lead bullion and cooling it down, silver and zinc forms a crust on top of the lead bullion. Then this crust can be separated from the lead. (Davidson et al., 2000)

1.4 Secondary lead processes

Recycled lead can be processed with the same technologies as primary lead. The Ausmelt technology can be adopted to produce lead from recycled products, e.g. in Germany an Ausmelt furnace is employed to produce lead from recycled lead batteries. The Varta process is a technology where emptied and crushed batteries are fed to a shaft furnace. (Blanpain et al., 2014)

Today, more lead smelters are operating as recycling facilities and in the recycled products many different materials are mixed and will end up in the smelting processes (Matsura et al., 2011). A new lead smelter, which smelts cathode ray tubes (CRT) of old televisions, is operating in England. In this smelting process, pure lead is extracted from glass in a scale glass furnace. Sweep Kuusakoski uses the furnace developed by Nulife Glass. (Recycling Today, 2012)

A process for utilizing lead and zinc from slags are presented in a paper by Hecker et al. (2004). This process employs an electric arc furnace to recover metals from the slag.

1.5 Slags in lead smelting

The slags in lead smelting are mostly formed by the CaO-SiO_2-FeO slag system. The slags generally contain some lead and zinc, too. (Reuter et al., 2004) The purpose of the slags is to maintain a layer on the molten lead and to make sure that the impurities are dissolved in the slag in order to make a pure lead bullion. Matousek (2011) presented different oxidation potentials in various lead smelter slags. The

components in the slag affect the melting and the viscosity of the slag (Fischer II & Bennington, 1991). CaO-bearing slags are environmentally stable (Han & Park, 2015).

Nowadays, some of the trace elements are also wanted to deport in the lead bullion because then it is possible, depending on other treatment after the smelting, to recover these elements and utilize them. There were some examples of lead refining treatments in chapter 1.3.

Developments in lead smelting slags were discussed by Jak & Hayes (2010). From the slag phase diagram in Figure 6 can it be seen what type of slags are used in different industrial smelters.

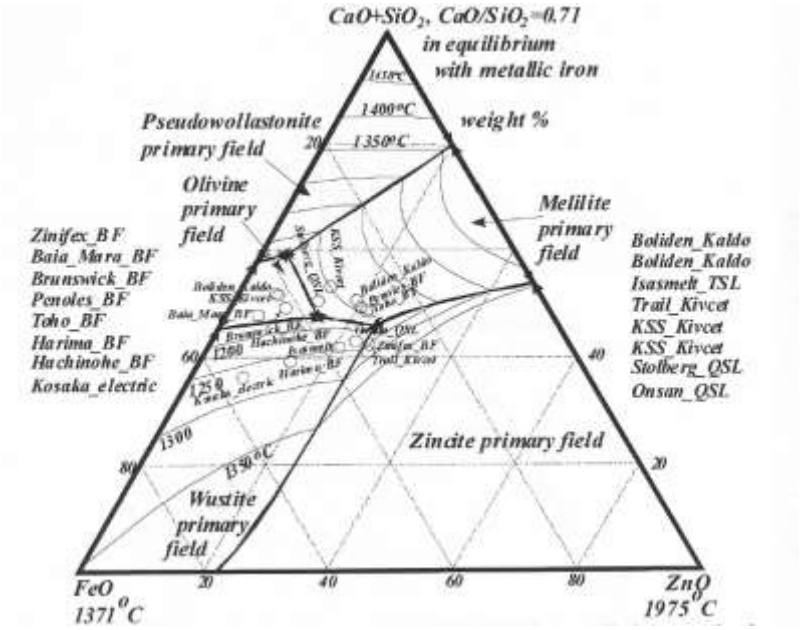

Figure 6 Slags for different lead smelters (Jak & Hayes, 2010).

The slags that occur in the direct smelting of lead in the Ausmelt/Isasmelt technology can have high percent of lead in them. But the slags are then reduced in either an Ausmelt/Isasmelt furnace or in a separate blast furnace, as discussed before (Zhao et al., 2008). Figure 7 shows the target slag composition in the Ausmelt reduction step at 1200 °C and the oxygen partial pressure 10^{-8} (atm) pointed out (Hughes et al., 2008).

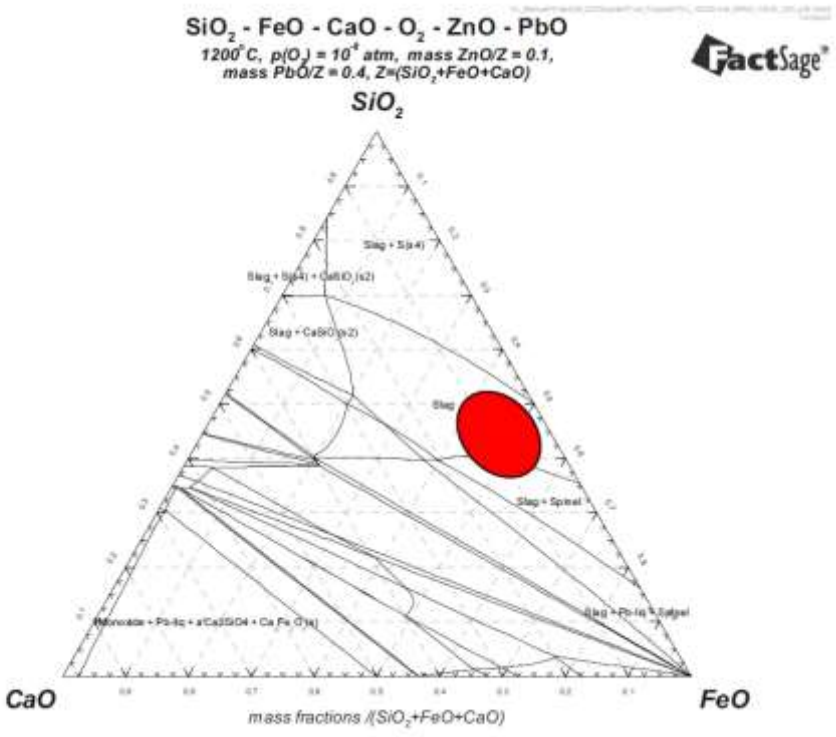

Figure 7 Target for slag chemistry for the Ausmelt slag reduction process (Hughes et al., 2008).

Taskinen et al. (1984) analysed different slag compositions in lead smelting and gained information on the thermodynamics and equilibrium of the lead-slag systems. The slag used in that research was a composition of PbO-SiO_2-CaO-FeO_x with different CaO/SiO_2-ratios and Fe/SiO_2-ratios. In order to make a low PbO slag, silica content needs to be lowered and more lime and more iron will be needed.

During the 1980's, there were discussions on which types of slags would be most suitable for the direct smelting of lead. There were studies about calcium ferrite slags and lead-iron silicate slags. The conclusions made at that time were that lead dissolution is lower in ferrite slags than in silica slags, and that some specific minor elements such as Cu, Sb, As, Sn and Zn dissolve in the calcium ferrite slag whereas Bi and Ag do not. (Rytkönen & Klarin, 1987)

1.6 Gallium, germanium, indium and tin in lead production

The elements that are of interest in this work are four metals that can occur in the different concentrates of lead, and also as trace elements in different types of recyclables. These elements, such as gallium and indium, can be attached in some electronic devices and therefore they are often produced from recycled end-of-life equipment (van Schaik & Reuter, 2014). The aim in the production of these elements is to get them collected already in an early stage of the pyrometallurgical process so that it would not be necessary to develop many different post-treatment processes for extracting the elements. Gallium, indium and tin have volatile species that can be recovered if the right metallurgical process for smelting is chosen (van Schaik & Reuter, 2014).

Indium and germanium distributions have gained interest during the latest years, and there has been done some research about how they divide between lead and slag. It is possible to modify slags in the lead smelting processes, depending on how the trace elements should be distributed. Either the elements are wanted in the molten metal or in the slag, and in some cases to gas or flue dust phase depending on the element properties and the downstream treatment processes.

Gallium, germanium, indium and tin are mostly produced as by-products when another metal is produced (Alfantazi & Moskalyk, 2003). Indium can be present in zinc concentrates. Gallium can be present in aluminium ores and in some zinc ores. Gallium, germanium and indium are expected to be recovered from old lead smelting slag dumps. (Moskalyk, 2003) The parameters for the reduction stage in the lead smelters affect greatly how the indium distributes between lead and slag. (Hoang & Swinbourne, 2007) One research paper suggests that germanium ends up in the slag in the lead smelting and goes further to the zinc refining stages. (Yan & Swinbourne, 2003)

2 Thermodynamics, equilibrium and distribution

There exist only a few investigations on the distributions of gallium, germanium, indium and tin in lead smelting. The interest for researching the behaviour of these elements, in lead smelting processes, has recently gained attention. The behaviour of other minor elements in lead smelting has been investigated during the years with different experimental methods (Fischer II & Bennington, 1991; Henao et al., 2010; Hoang & Swinbourne, 2007; Rytkönen & Taskinen, 1986; Moon et al., 1998; Johnson et al., 1983; Toubartz, 1991; Ermisch, 1953). Some of these methods have concentrated on certain smelting technologies, such as the blast furnace, KIVCET or QSL. However, the results are applicable to several other processes. In this chapter, thermodynamics of lead smelting are presented.

2.1 Equilibrium in lead smelting

The equilibrium is dependent on the components (Pb, Fe, Si, Ca, O, S) in the system, the phases (gas, slag, bullion), the temperature and the pressures of gases in the system. Moon et al. (1997) studied the phase equilibrium between lead and slag for the QSL smelting process. Activity coefficients and activity were obtained for lead and lead oxide. Also Toubartz (1991) calculated activity coefficients for lead oxide and oxides of trace elements in the slag with reference to the QSL lead smelting process. From the equilibrium diagram in Figure 1 by Matyas & Mackey (1976), it is possible to see the equilibrium conditions in lead smelting and also the thermodynamics and ratios of the phases.

In the direct smelting, a flash smelting happens when the concentration is fed to the furnace and the final slag and bullion formation reactions occur in the bath. (Matyas & Mackey, 1976) Equilibrium reaction for lead between bullion and slag can be expressed as:

$$Pb(l) + \frac{1}{2}O_2(g) = PbO(l), \quad (8)$$

where the oxidation product, liquid PbO is dissolved in slag and thus its activity is less than that of pure liquid PbO. Iron also reacts and form oxides in the slag. The equilibrium between lead and lead oxide was investigated by Taskinen et al. (1984) in Fe_xO-SiO_2-CaO slags with different compositions, by changing the FeO/SiO_2-ratio and CaO/SiO_2-ratio.

In previous studies, suggestions were presented for the reactions of different trace elements. The oxidation reactions depend on the circumstances in the furnace. The oxidation reactions between bullion and slag (9) are as follows:

$$X + v/2\ O_2\ \rightarrow XO_v, \tag{9}$$

where X is the reacting metal and v the stoichiometric number of reacting oxygen. The trace elements can react and form different oxides. Here are possible forms and reactions presented for lead and the trace elements during lead smelting (equations 10-18). The temperature of interest for the lead smelting in this work is 1150 °C and therefore the values of thermodynamic properties presented here are for the same boundary condition. Both gallium and indium have volatile compounds and therefore they are taken in the consideration here. The Gibbs energy of formation for oxidation of lead is presented, when molten lead reacts to molten lead oxide, as:

$$\Delta G^0_{Pb/PbO} = -189713 + 74.31\ T\ (kJ/kmol) \qquad \text{(Toubartz, 1991)} \tag{10}$$

Yan & Swinbourne (2003) suggested that at 1200 °C germanium dissolves into slag according to the the following formula:

$$Ge(l) + \frac{1}{2}O_2(g) = GeO(l) \tag{11}$$

However, Henao et al. (2010) proposed that germanium dissolves in the slag at 1200 °C in another form:

$$Ge(l) + O_2(g) = GeO_2(l) \quad (12)$$

Depending on the conditions, indium can dissolve in the slag in many ways. Here are three suggestions from previous studies. Hoang & Swinbourne (2007) proposed this reaction at 1200 °C to occur as:

$$In(l) + \frac{1}{2}O_2(g) = InO(g) \quad (13)$$

Henao et al. (2010) concluded that the following oxide form of indium was dissolved in the slag at 1200 °C:

$$2In(l) + \frac{3}{2}O_2(g) = In_2O_3(l) \quad (14)$$

Han & Park (2015) suggested that indium dissolves as In_2O in the slag at 1300 °C. They also calculated the enthalpy of formation. In that study, pure indium was used and no lead-indium alloys. This is the oxidation equation by Han & Park (2015):

$$2In(s) + \frac{1}{2}O_2(g) = In_2O(g), \qquad \Delta H_f^0 = -33.2\ (kJ/mol). \quad (15)$$

Tin can form many oxides and Toubartz (1991) found that at 1150 – 1300 °C tin forms the divalent oxide SnO:

$$Sn(l) + \frac{1}{2}O_2(g) = SnO(l) \quad (16)$$

From the values in Table 2, conclusions can be made to decide the probability of which the reactions will happen.

Table 2 Standard Gibbs free energy (energy of formation) for reactions at 1150 °C (HSC).

Reaction	$\Delta_f G^0$ / (kJ/mol) (1150°C)	Reference
$Ga(l) + \frac{1}{2}O_2(g) = GaO(g)$	50.380	[HSC]
$2Ga(l) + \frac{3}{2}O_2(g) = Ga_2O_3(l)$	−599.017	[HSC]
$Ge(l) + \frac{1}{2}O_2(g) = GeO(l)$	−161.291	[HSC]
$Ge(l) + O_2(g) = GeO_2(l)$	−103.857	[HSC]
$In(l) + \frac{1}{2}O_2(g) = InO(g)$	73.850	[HSC]
$2In(l) + \frac{3}{2}O_2(g) = In_2O_3(l)$	−431.852	[HSC]
$2In(s) + \frac{1}{2}O_2(g) = In_2O(g)$	−120.156	[HSC]
$Sn(l) + \frac{1}{2}O_2(g) = SnO(l)$	−141.959	[HSC]
$Sn(l) + O_2(g) = SnO_2(l)$	−282.719	[HSC]

Because the Gibbs free energy of formation for gaseous gallium(II)oxide and indium(II)oxide have positive values, they will most probably not form these oxides at 1150 °C. However, liquid gallium(III)oxide will probably be formed and dissolve in slag because of the low ΔG^0 value. The other elements also have the probability to form oxides rather than stay as pure metal, due to the low values of the Gibbs energy. It is worth mentioning that some of the values are for gaseous species and not for liquids.

The possible reactions between the slag and gas in the reduction smelting step were presented by Zhao et al. (2008):

$$PbO + CO \rightarrow Pb(l) + CO_2 \quad (17)$$

$$Fe_2O_3 + CO \rightarrow 2FeO + CO_2(g) \quad (18)$$

$$FeO + CO \rightarrow Fe + CO_2(g) \quad (19)$$

$$Pb(l) \rightarrow Pb(g) \quad (20)$$

Lead oxide can be reduced by carbon monoxide and it forms pure lead. Lead can also evaporate. Iron oxidizes according to equation (21):

$$Fe(s) + \frac{1}{2}O_2(g) = 'FeO'(l) \text{ (Matsura et al., 2011)} \quad (21)$$

$$\Delta G^0_{Fe/FeO} = -214800 + 34.98\,T \text{ (Matsura et al., 2011)} \quad (22)$$

In the smelting stage, the forming slag contains some Fe^{3+} (or $FeO_{1.5}$) but its fraction is negligible in the reduction slag.

2.2 Solubility of lead in slag

Lead concentration in slag should be low in order to make an environmental friendly slag and utilise the full potential of the resource efficiency. Lead forms oxides that become part of the slag. Lead forms mainly lead oxide in the slag according to equation (8). The solubility of lead can be expressed as weight-% Pb in slag. When the basicity of the slag is raised, less lead dissolves in slag. (Moon et al., 1997; Matsuzaki et al., 2000; Yazawa et al., 1981; Kudo et al., 2000; Fischer II & Bennington, 1991)

The lead distribution between lead bullion and ferrite or silicate slag at 1200 °C is presented in Figure 8 (Yazawa et al., 1981). As can be seen, lead dissolves in a ferrite slag less than in a silicate slag. Also, soda and chromium reduce the solubility of lead in the slag (Matsura et al., 2011).

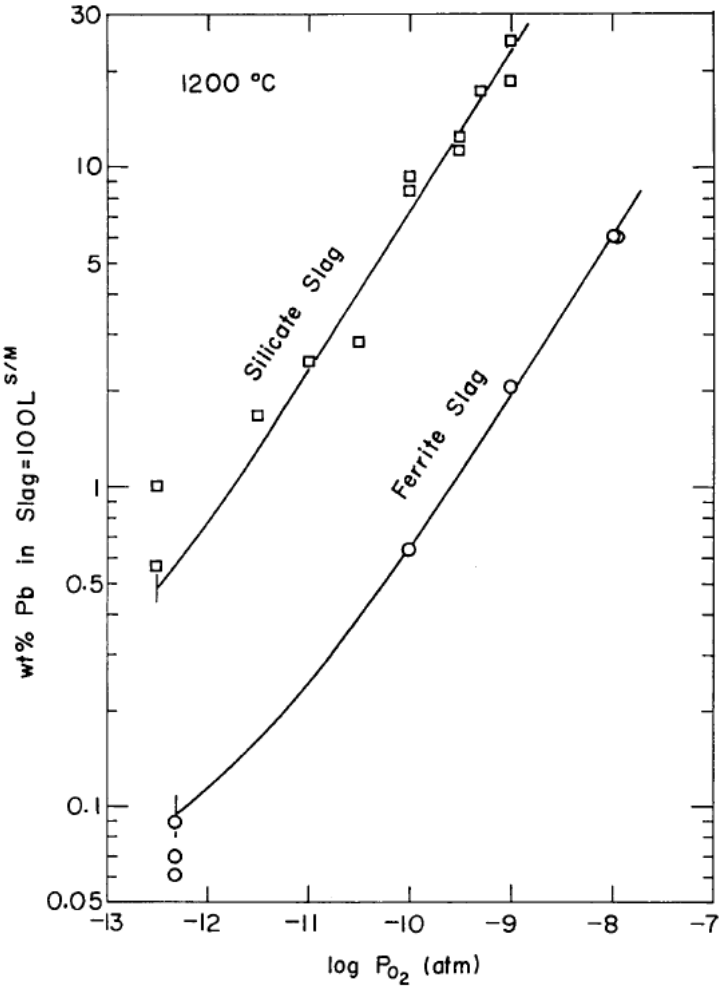

Figure 8 Solubility of lead in two different slags (Yazawa et al., 1981).

Taskinen et al. (1984) executed experiments at 1300 °C with different slag compositions and concluded that with all the slag compositions employed more lead oxide was formed in slag as the oxygen partial pressure increased. The slags consisted of PbO, SiO_2, CaO and FeO. Also according to Henao et al. (2010), lead will form more lead oxide in slag when the oxygen partial pressure is raised (Figure 9). This is due to higher chemical potential of oxygen that allows oxygen to react with the lead.

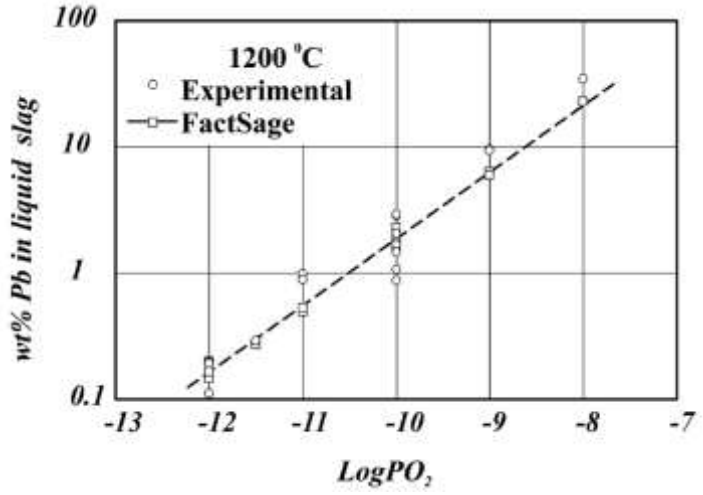

Figure 9 Wt-% of lead in slag dependent on oxygen partial pressure. CaO/SiO_2=0.48-0.59, Fe/SiO_2=0.63-1.0. (Henao et al., 2010)

According to Henao et al. (2010), the lower the temperature is, the higher the lead concentration is in the slag at constant oxygen pressures. This is presented in Figure 10.

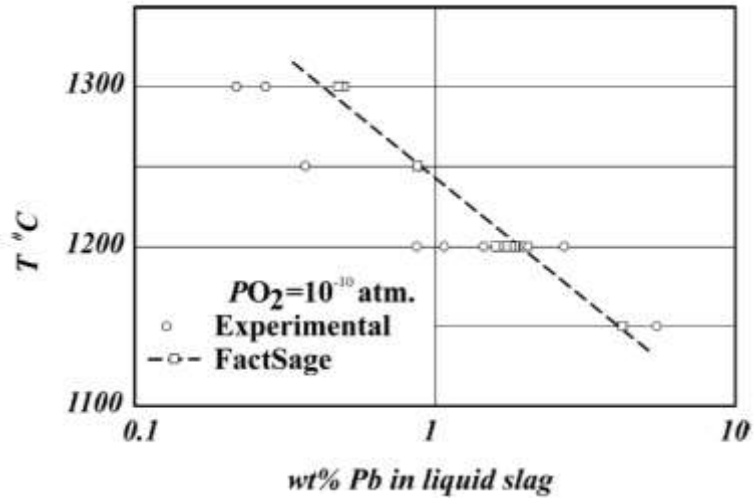

Figure 10 Wt-% of lead in slag dependent on temperature in constant oxygen pressure. CaO/SiO_2=0.53-0.67, Fe/SiO_2=0.83-1.0. (Henao et al., 2010)

2.2.1 Activity of lead and lead oxide

Activity of lead in experiments is close to 1 because it is added as a pure metal (and standard state is set to pure lead). In an industrial process, the activity can be less because there are other materials involved in the metal phase. The activity coefficients are of great importance to understand the behaviour of specific elements in lead-slag-gas systems. (Matsura et al., 2011) Activity of lead oxide in the slag decreases as the concentration of lead oxide decreases. When more materials are mixed the activity decreases. The activity coefficient is a function of temperature and slag composition. (Kudo et al., 2000; Matsura et al., 2011) K_1 is the equilibrium constant of reaction (8).

$$K_1 = \frac{a_{PbO}}{a_{Pb} \cdot {p_{O_2}}^{\frac{1}{2}}} = exp(-\frac{\Delta G^0}{RT}) \quad (23)$$

$$\Delta G^0(J) = -190.900 + 75.52\,T \quad (24)$$

Gibbs energy of formation of lead oxide is taken from Matsura et al. (2011). The previously presented Gibbs energy of formation for lead oxide by Toubartz (1991) differs only slightly from this value. The activity coefficient of lead in a slag is derived from the equation for the equilibrium coefficient.

$$(\gamma_{PbO}) = K \cdot M_{Pb} \cdot (n_T) \cdot p_{O_2}^{\frac{1}{2}} / (wt - \%\, Pb) \quad (25)$$

Matsura et al. (2011) calculated activity coefficients for lead oxide in slags with sodium and chrome and compared them. (Matsura et al., 2011) Activity coefficients of lead oxide were 0.15 to 3 in one study (Kudo et al., 2000). These variations were dependent on the slag compositions. In Figure 11, the activity of lead oxide is presented as function of concentration of lead oxide in slag. As the lead oxide content is increased the activity increases. These are the results from Taskinen et al. (1984) on how lead oxide activity behaves in the direct lead smelting.

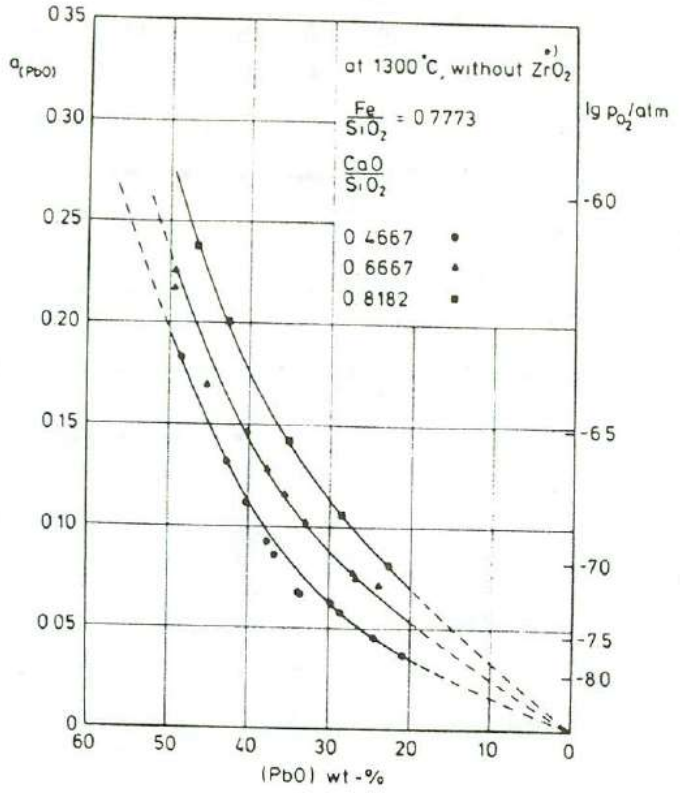

Figure 11 Activity of lead oxide in slag with Fe/SiO_2-ratio=0.7773, standard state $a_{PbO(l)}$=1 in pure Pb-PbO system. (Rytkönen et al., 1985; Taskinen et al., 1984)

When the iron concentration is raised, the activity of lead oxide decreases somewhat. This can be seen in Figure 12 and comparing with the results given in Figure 11. The oxygen partial pressure is also presented in these graphs and the relation between the pressure, the activity and the lead oxide content is depicted. (Rytkönen et al., 1985; Rytkönen & Taskinen, 1986)

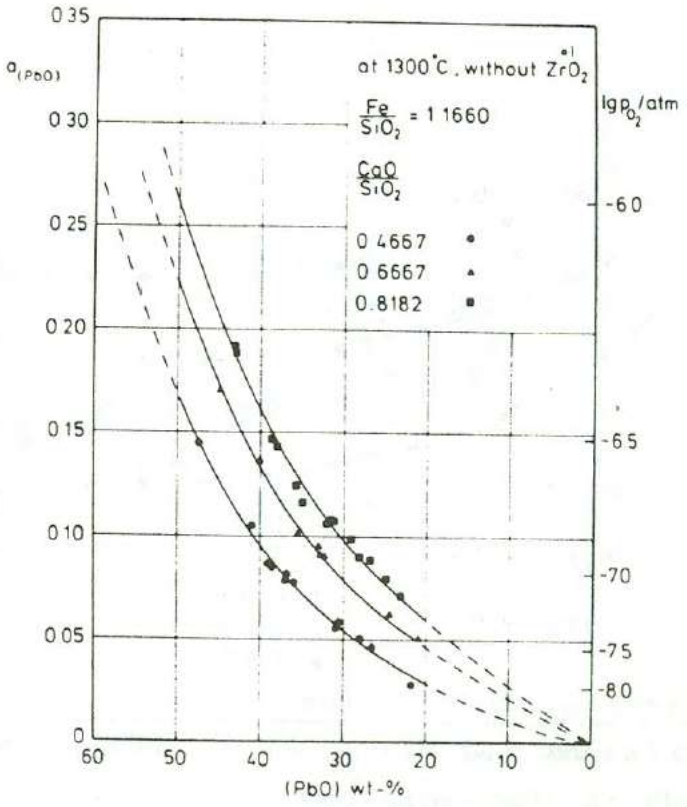

Figure 12 Activity of lead oxide in slag and Fe/SiO_2-ratio=1.1660, standard state $a_{PbO(l)}$=1 in pure Pb-PbO system. (Rytkönen et al., 1985)

Lead has an activity value close to 1 if it is present as pure lead. Activity coefficient of lead in bullion have positive deviation from the value 1 when gallium is mixed with lead (Katayama et al., 2002). When comparing the trace elements with lead, the trace elements are present in really small quantities and therefore the activity of lead is assumed as 1, and the activities for the trace elements are low.

2.3 Solubilities of trace elements in lead smelting

Trace elements will preferentially form either metals or oxides in the lead smelting and sulphides if sulphur is present. The solubility is dependent on the smelting conditions such as temperature, oxygen pressure and slag composition. The solubilities of different elements depend on the elements' ability to form oxides, metals, sulphides or evaporate. The thermodynamic properties of the elements affect the way the elements behave in the lead smelting processes. The trace

elements exist often in the form of oxides in slag and as alloys in the metal phase. Studies (Han & Park, 2015; Han et al., 2015; Henao et al., 2010; Moon et al., 1998; Rytkönen & Klarin, 1987; Rytkönen & Taskinen, 1986; Toubartz, 1991; Yan & Swinbourne, 2003; Hoang & Swinbourne, 2007) on the behaviour of trace elements and impurities have been executed to clarify what oxides the elements form in various lead smelting slags.

2.4 Distribution of trace elements in lead smelting

The distributions of different elements are dependent on temperature, slag composition and the oxygen potential used in industrial processes or laboratory experiments. The elements under investigation can deport either to the smelted slag or the smelted lead. The impurity (metal) or a trace element (X) in the lead bullion-slag system is oxidized to the slag according to the following generic reaction:

$$X(l, metal) + v/4O_2(g) = XO_{v/2}(l, slag) \tag{26}$$

Of this reaction (26), it is possible to write the equilibrium constant (27), obtained from pure substance data of the substances involved, as

$$K = a_{XO_{\frac{v}{2}}}/(a_X \times pO_2^{\frac{v}{4}}) \tag{27}$$

The equilibrium constant can also be described based on the activity coefficients (28):

$$K = \frac{[n_T](\gamma_{XO_{\frac{v}{2}}})(\%X)}{(n_T)[\gamma_X][\%X]p_{O_2}^{\frac{v}{4}}} \qquad \text{(Anindya et al., 2013)} \tag{28}$$

Distribution coefficient between metal (m) and slag (s) in common form is defined by equation (29). In this equation, only the weight percentages of the element X in slag and bullion are required to define the distribution coefficient.

$$L_X^{m/s} = \frac{[wt\%\ X\ in\ alloy]}{\{wt\%X\ in\ liquid\ slag\}} = \frac{[wt\%X]}{\{wt\%X\}} \quad (29)$$

(Henao et al., 2010; Hoang & Swinbourne, 2007)

The following equation (30) is derived from equations (28) and (29) for the equilibrium coefficient (28) when the logarithm is taken of it:

$$logL_X^{m/s} = -v/4logp_{O_2} + A \quad (30)$$

The distribution coefficients can be plotted graphically by setting the logarithm of the oxygen partial pressure on the x-axle and the logarithm of the distribution coefficient on the y-axle. From the slope, the oxidation state of the dissolved metal in the slag under observation can be determined. An example in lead smelting is that if the slope of the plot is ½ the v becomes 2. This means that the oxidation product is XO and so the oxidation state in the slag is X^{2+}.

2.4.1 Activity of trace elements in lead

The activities of trace elements are less in lead bullion than if they were present as pure elements. Activity coefficients for the trace elements are needed to be able to do thermodynamic calculations in computer programs.

The activity of gallium in lead-gallium alloys was measured by Katayama et al. (2002). The gallium-lead binary system was investigated by Manasijevic et al. (2003) and gained activity values for gallium in a lead-gallium alloy. The experiments were executed at temperatures lower than in lead smelting and the interesting feature is that gallium and lead form two liquid phases, and do not mix. Activity of gallium has a positive deviation from ideal behaviour. The temperature dependence on the activity is not large. The miscibility gap in lead-gallium alloys has also been investigated by Plevachuk et al. (2003).

When the activities for the trace elements deviate positively from Raoult's law it means that the activity coefficients are greater than 1. Morachevskii (2014) presented the limiting activty coefficients for the elements of interest in this work. They are shown in Table 3 together with the activity coefficients used by Hoang and Swinbourne (2006) and Jia et al. (2012). Activity of tin in lead was studied by Jia et al. (2013). They also predicted the activity coefficients for tin in lead.

Table 3 Limiting activity coefficients in dilute lead alloys (Pb-X) (Hoang & Swinbourne, 2007; Jia et al., 2013; Morachevskii, 2014).

Trace element	Temperature (°C)	Limiting activity coefficients in lead γ°	Reference
Ga	727	8.33	Morachevskii (2014)
Ge	1000	11.0-13.5	Morachevskii (2014)
In	400	1.342	Morachevskii (2014)
In	1200	1.35	Hoang and Swinbourne (2007)
Sn	1200	3.65	Jia et al. (2012)
Sn	777	6.816	Morachevskii (2014)

Activity coefficients for trace elements in lead can either be found from the literature or calculated from binary phase diagrams. There are no data for the system Pb-Ga-Ge-In-Sn so the applicable phase diagrams for this study are the binary ones with lead and one of the trace elements.

2.4.2 Activity of trace elements in slags

The activity coefficients for the trace element oxides in the slag can be derived when temperature, Gibbs energies, distribution coefficients and activity coefficients for trace elements in lead are known.

$$\gamma_{XO_v} = \frac{K(n_T)[\gamma_X]p_{O_2}^{v/2}}{[n_T]L_X^{s/m}} \qquad \text{(Anindya et al., 2013)} \qquad (31)$$

Studies on indium in slags in the lead smelting were presented by Han & Park (2015). The solubility of indium in a slag was studied. Though, they did not present any activity coefficients.

Activity coefficients for SnO in slags were calculated by Toubartz (1991). Activity and activity coefficients for germanium oxide were calculated in the work of Yan & Swinbourne (2003).

Hoang and Swinbourne (2007) calculated activity coefficients for InO at 1200 °C. The activity coefficients by these authors are presented in Table 4.

Table 4 Activity coefficients in lead smelting slags (Toubartz, 1991; Yan & Swinbourne, 2003; Hoang & Swinbourne, 2007).

Trace element	Temperature (°C)	Activity coefficients in lead smelting slags γ	Reference
GeO	1250	1.44-2.55	Yan and Swinbourne (2003)
InO	1200	$4x10^{-8}$ - $3x10^{-7}$	Hoang and Swinbourne (2007)
SnO	1150-1300	0.33-6.43	Toubartz (1991)
SnO	1150	0.36-3.55	Toubartz (1991)

3 Distributions of minor elements between lead bullion and slag

There exist only little research on the distributions of gallium, germanium, indium and tin in lead smelting. In this chapter, previous findings on the distribution ratios for these elements are presented. Some differences can be observed in the conclusions in the research papers, but it is due to the different experimental methods and analysing equipment used. Older research often employed EMF (electromotive force) measurements and the lead and slag were analysed chemically. Newer research methods involve three steps: reaching equilibria in a hot furnace, quenching and analysing with mass spectrometry or X-ray microanalysis.

In some experiments, only inductively coupled plasma atomic emission spectrometry (ICP-AES) was adopted to define the metal distributions using sampling (Yan & Swinbourne, 2003), (Hoang & Swinbourne, 2007), (Henao et al., 2010). In other hand some studies adopted inductively coupled plasma mass spectrometry (ICP-MS) to analyse metal phase and the electron probe X-ray microanalysis (EPMA) in quenched samples for the slag phase (Henao et al., 2010). EPMA was expected to provide more accurate results. (Henao et al., 2010)

3.1 Distribution of gallium

There are no data in the literature on the distribution of gallium between lead bullion and slag. Gallium oxide can according to thermodynamics be reduced by carbon monoxide. Depending on the circumstances and the correct process, gallium can be recovered from different phases in pyrometallurgical reactors and to some extent from the gas phase and its flue dust. (van Schaik & Reuter, 2014)

There exist one research paper on the distribution of gallium in iron blast furnace processing (Chernousov et al., 2010). They concluded that most gallium dissolves into the pig iron and only a small amount in the slag. The temperature of that experiment was 1400 °C and the gas atmosphere was 90 vol-% nitrogen and 10 vol-% hydrogen.

The gallium content was analysed by mass spectrometry. The results are shown in Table 5. (Chernousov et al., 2010)

Table 5 Distribution of gallium in iron smelting, modified from Chernousov et al. (2010).

Method of gallium introduction into system	Slag type	Gallium content at end of test, g/ton		$L_{Ga}^{iron/slag}$
		in pig iron	in slag	
In pig iron composition	Basic	0.74–5.59	0.014–0.022	52.86-254.09
	Acid	0.88–5.15	0.013–0.020	67.69-257.5
In slag composition	Basic	0.58–1.43	0.017–0.022	34.12-65
	Acid	1.94	0.018	107.78

3.2 Distribution of germanium

Few studies how germanium is distributed between lead bullion, $CaO\text{-}SiO_2\text{-}FeO\text{-}Al_2O_3$ slag and gas can be found in the literature. Yan and Swinbourne (2003) executed experiments on germanium distribution in lead blast furnace. They did not find any prior research for the germanium distribution under lead smelting conditions. Most germanium dissolved in the slag in their experiments (Figure 13).

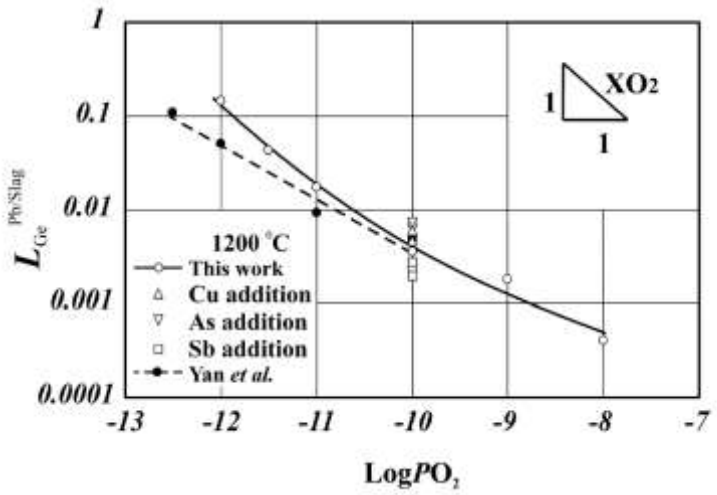

Figure 13 Germanium distribution dependence with oxygen partial pressure. CaO/SiO_2=0.53-0.67. (Yan & Swinbourne, 2003; Henao et al., 2010).

Also Henao et al. (2010) have done measurements on the germanium distribution between lead and slag. In their experiments, germanium evaporated at temperatures of 1250 and 1300 °C and thus was out of the detection limits at these temperatures (Henao et al., 2010). Their results at 1200 °C are presented in Figure 13. They considered that the experimental methods employed by Yan and Swinbourne (2003) included uncertainties such as an unreliable analysing method.

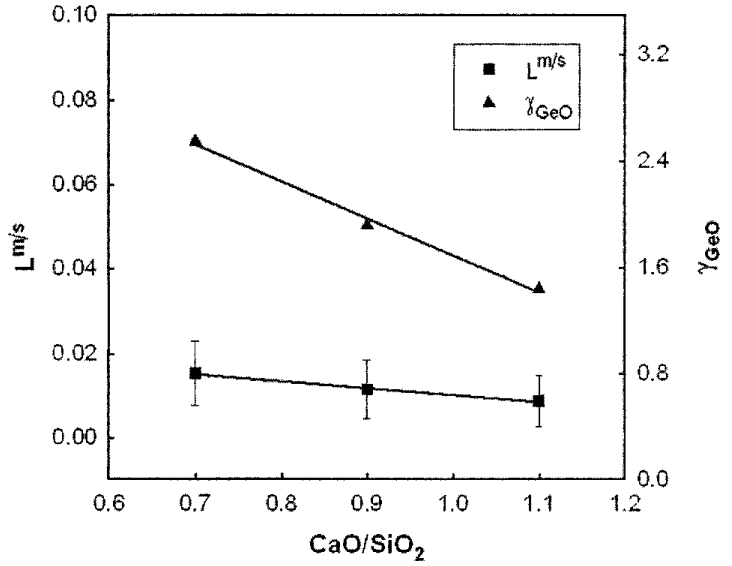

Figure 14 Effect of slag composition on the metal-to-slag distribution of germanium at 1250 °C and 10^{-11} atm (Yan & Swinbourne, 2003).

The distribution coefficient for germanium was not much affected by the change in slag basicity, but the activity coefficient of germanium oxide increases as the slag basicity is raised. Figure 14 shows the effect of slag composition on the activity coefficient of GeO and on the metal-to-slag distribution of germanium.

3.3 Distribution of indium

In the 1980's, experimental series were performed to study the distribution of indium between lead bullion and slag (Johnson et al., 1983). These results were later compared with the experiments executed by Hoang & Swinbourne (2007). The results in these two studies were hard to compare because Johnson et al. (1983) made the experiments at single oxygen partial pressure only. However, some contradictions in

the dependence on the basicity of the slag were found between these studies. Also Henao et al. (2010) have done experiments on the indium distribution in lead smelting. That work differs from the other two with its experimental technique and their tests were executed in several oxygen partial pressures. Indium formed different oxides in slag in the mentioned studies.

The analysing equipment EPMA was employed in the work by Henao et al. (2010) but the indium concentrations were close to the detection limit of EPMA. EPMA was used for analysing the slag. The distribution results of these three studies have been represented in Figure 15.

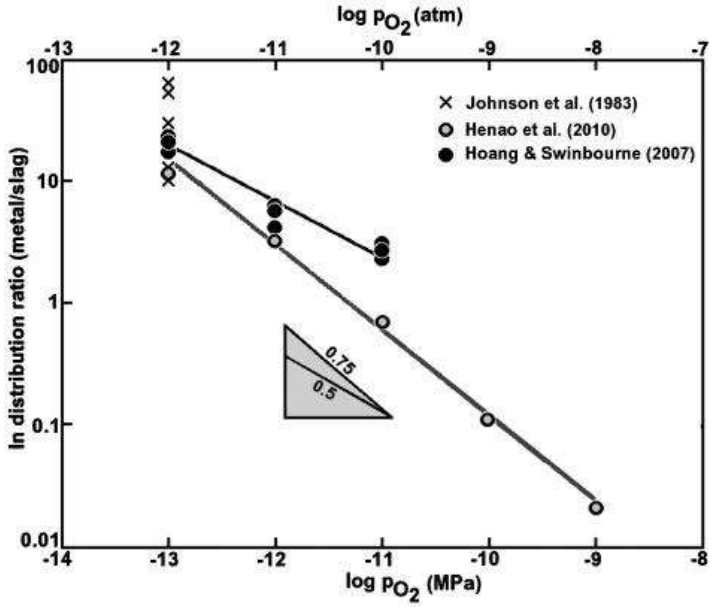

Figure 15 Comparison of indium distribution between lead and slag at 1200 °C. (Anindya et al., 2014)

Han & Park (2015) investigated indium solubility in a FeO-SiO_2-Al_2O_3-5CaO-MgO_{sat} slag. They concluded that low-silica calcium oxide slags and low oxygen partial pressures are needed to get a good indium recovery. Han & Park (2015) stated that oxygen potentials need to be very low, otherwise indium dissolves to the slag. Indium distribution in copper smelting was investigated by Anindya et al. (2014) and the results were compared with the earlier studies in lead smelting. It is shown that more indium distributes to the slag the higher the oxygen partial pressure is (Hoang &

Swinbourne, 2007). They also noticed that the iron content of the slag affects the distribution coefficient of indium (Figure 16), but not very much the CaO/SiO_2 basicity.

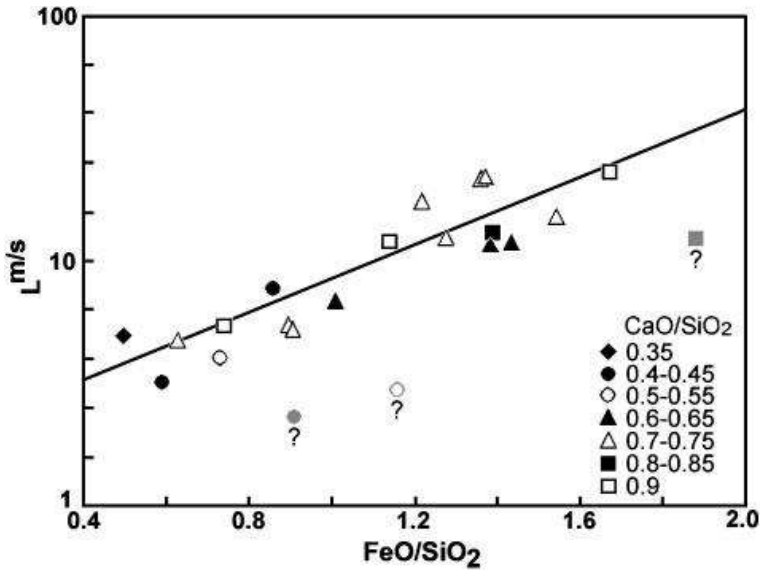

Figure 16 Indium distribution coefficient dependent on iron content in slag. (Hoang & Swinbourne, 2007)

3.4 Distribution of tin

The distribution of tin in lead smelting has been the topic of research for many years, because it is often present in the ores used in lead smelting. Tin in slag forms SnO_2 or SnO depending on the slag, temperature and the oxygen partial pressure (Anindya et al., 2013; Toubartz, 1991). Anindya et al. (2013) investigated distribution of tin in copper smelting at 1300 °C. Rytkönen & Taskinen (1986) and Rytkönen & Klarin (1987) studied the tin distribution in lead smelting at 1200 °C, but they adopted another type of research method (EMF measurements) than Anindya et al. (2013). Rytkönen & Klarin (1987) came to the conclusion that tin dissolves easier in calcium ferrite slags than in silicate slags.

Toubartz (1991) investigated tin distribution between lead and slag in the QSL reactor. This data are comparable with the data provided by Rytkönen & Klarin (1987). Toubartz (1991) experimented the distribution with EMF measurement methods similarly as Rytkönen & Taskinen (1986) and Rytkönen & Klarin (1987).

Anindya et al. (2013) found from the literature that in the slag, tin is as tin monoxide (SnO) when the oxygen partial pressure is under 10^{-9} MPa and as tin dioxide (SnO_2) when the pressure is higher in calcium ferrite slags and calcium magnesium silicate slags. The study done by Anindya et al. (2013) concluded that tin is present as SnO for oxygen partial pressures over 10^{-9} atm in copper-saturated $CaO\text{-}SiO_2\text{-}FeO_x$ slags.

In calcium ferrite slag, tin is as tetravalent SnO_2 and in silicate slags as divalent SnO (Rytkönen & Klarin, 1987). In silicate slags, tin stays as oxide (SnO) in the slag in every investigated environment (Rytkönen & Taskinen, 1986). Toubartz (1991) compared the results with studies from Rytkönen & Taskinen (1986) and Solf (1987). Solf's results in silicate slags was that tin had the oxidation state Sn^{2+} (SnO) when oxygen partial pressure was less than 10^{-8} atm and Sn^{4+} (SnO_2) when partial pressure was greater than 10^{-8} atm.

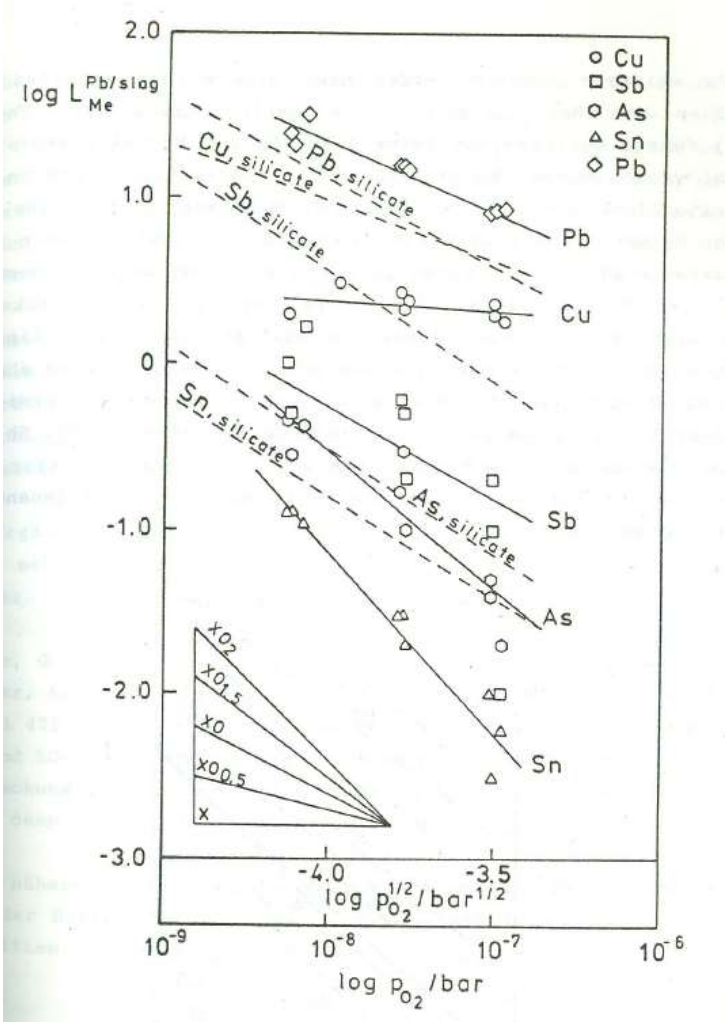

Figure 17 Distributions of elements as function of oxygen partial pressure. Calcium ferrite slags (solid line) and silicate slags (dotted line) in comparison. (Rytkönen & Klarin, 1987)

In Figure 17 by Rytkönen & Klarin (1987), the differences in the distributions between lead silicate and calcium ferrite slags can be clearly seen. Tin can appear in many oxide forms and be present in both SnO and SnO_2 forms at the same time. It can be concluded that the dissolved form is very dependent on the process conditions including temperature, slag compositions and oxygen partial pressure. The results of Toubartz (1991) are presented in Figure 18.

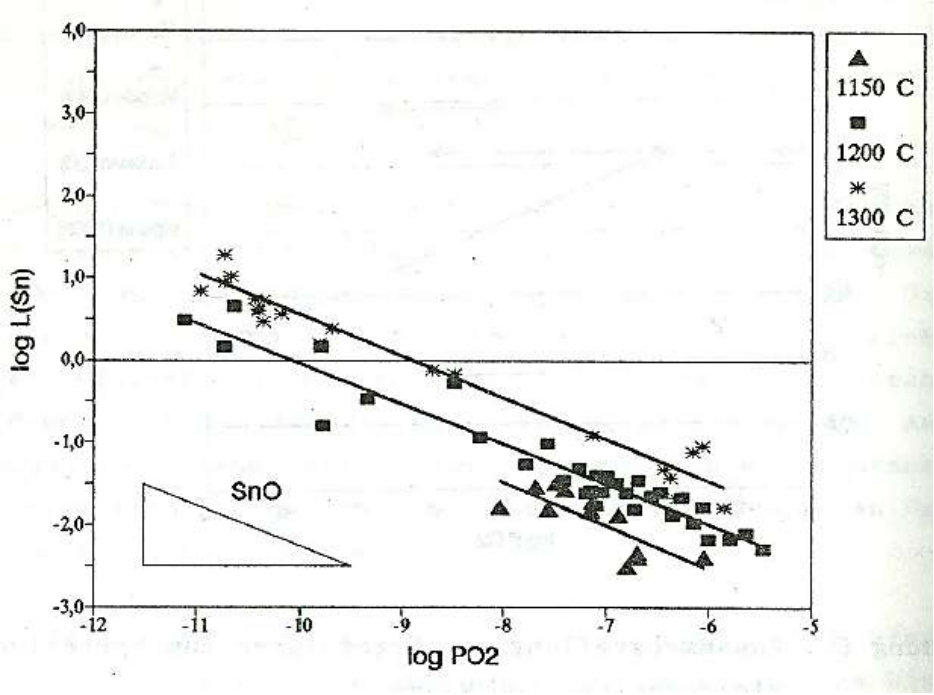

Figure 18 Tin distribution between lead and slag (Toubartz, 1991).

3.5 Temperature dependence of distribution

Yan & Swinbourne (2003) studied germanium distribution in a temperature range 1150–1250 °C (Figure 19). No dependency between the distribution coefficient and temperature was noticed.

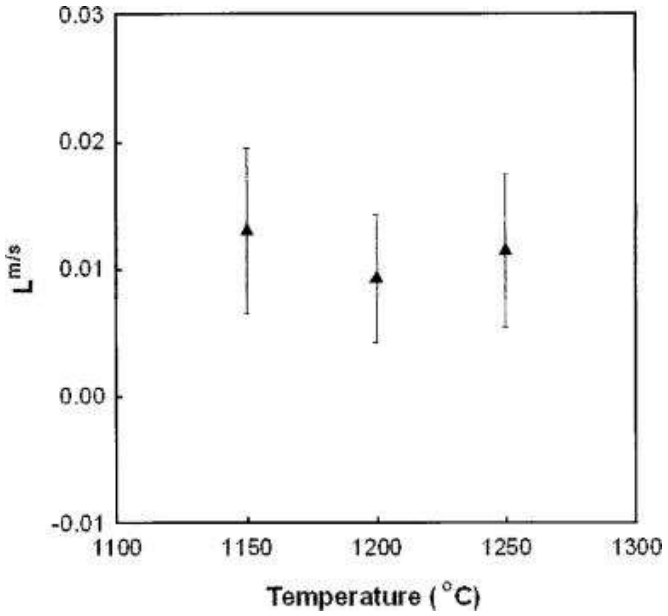

Figure 19 Distribution coefficient of germanium and its dependence on temperature (Yan & Swinbourne, 2003).

According to Henao et al. (2010), no major variations were detected in the distribution for germanium between 1150 °C and 1200 °C. However, for indium the distribution coefficient increased as temperature was increased from 1150 °C to 1300 °C (Figure 20). Problems occurred as germanium evaporized at temperatures from 1250 °C to 1300 °C.

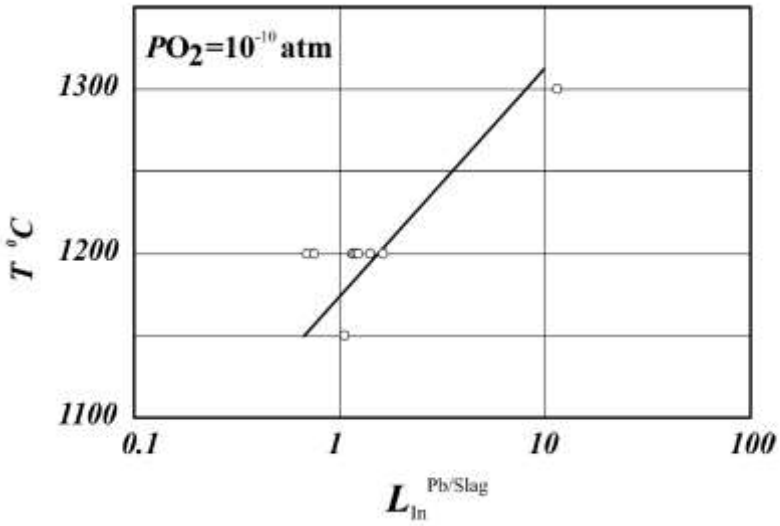

Figure 20 Temperature dependence of the metal-slag distribution coefficient (Henao et al., 2010).

For tin it can be clearly seen in Figure 18 (Toubartz, 1991) that the higher the temperature is, the greater the metal–slag distribution coefficient is. A similar behaviour of tin was also detected in the research series by Rytkönen et al. (1985) and Rytkönen & Klarin (1987).

Experimental part

4 Procedure

This section describes the methods and arrangements involved in the experimental work. The distributions of gallium, germanium, indium and tin between lead and a slag were investigated by high temperature quenching experiments. The experiments consisted of preparing the mixtures of reagents for the samples, putting the samples into the furnace, and after reaching equilibrium the samples were quenched very fast in a bath of ice water. Furthermore, the samples were cast in epoxy and analysed with SEM, to ensure that every phase needed was present in the samples. After the desired phases were found to be present, the samples were analysed with EPMA in order to achieve more accurate analyses of the phases and distribution results.

In earlier studies by Yan & Swinbourne (2003), Johnson et al. (1983), Hoang & Swinbourne (2007) and Matsura et al. (2011), much larger quantities of lead and slag were used in the experiments. As in this work, small (~0.1 g) samples were employed, the quenching can is much faster than in previous studies. Moreover, the phase analysis are more accurate with proper quenching. The lead and slag were not separated in this work, which give the opportunity to analyse directly from the phases and give more accurate results from the analysis with EPMA. This is the first work using this type of analysing method for investigating distribution coefficients in lead smelting. Also new in this work is the use of pseudo-wollastonite crucibles in order to provide pseudo-wollastonite saturation into the system. Pseudo-wollastonite substrates have been used previously in one other experimental phase equilibrium study (Nikolic et al., 2008). However, this work was the first to adopt these crucibles in the lead smelting conditions.

In industrial processes using lead sulphide minerals, sulphur is present in smelting. In these laboratory experiments, no sulphur was present and therefore this has to be

noticed when analysing results and comparing the data with the industrial processes. The experiments in this study were actually executed in simulated secondary lead smelting conditions.

4.1 Experimental procedure

In this work, the distribution of four elements (Ga, Ge, In, Sn) between lead and slag are investigated. The experiments were executed at a temperature of 1150 °C and in six oxygen partial pressures (10^{-7}, 10^{-8}, 10^{-9}, 10^{-10}, 10^{-11} and 10^{-12} atm). Carbon monoxide and carbon dioxide mixtures were used to gain the right oxygen partial pressures. Two series of experiments were completed and in both series two experiments were executed in six oxygen partial pressures, except the second series where just one experiment was done at 10^{-12} atm. The trace elements were present in oxide forms in the first series and in pure metallic form in the second series, except gallium that was added as oxide in both series. The experimental procedure consisted of three main steps: equilibrium, quenching and analysis with EPMA. The lead and the slag were thus smelted and equilibrated with a controlled gas atmosphere.

Pseudo-wollastonite crucibles produced from calcium oxide and silica were employed in the experiments. Primary substrate method was adopted in order to avoid extra elements contamination in the system (Nikolic et al., 2008). The crucible had almost the same CaO/SiO_2-ratio as the mixed slag involved.

The sample was quenched in ice water in order to preserve the phases and their compositions that formed at the equilibration temperature. Afterwards, metallographic examination were executed using polished sections of the samples. The pictures of the microstructures were taken and the pre-analyses were performed with SEM-EDS. The distribution coefficients were calculated from the final results conducted by EPMA.

4.2 Experimental apparatus

The experiments were performed in high temperature conditions at 1150 °C. A schematic picture of the furnace with the gas handling equipment is presented in Figure 21 and a picture of the furnace is in Figure 22.

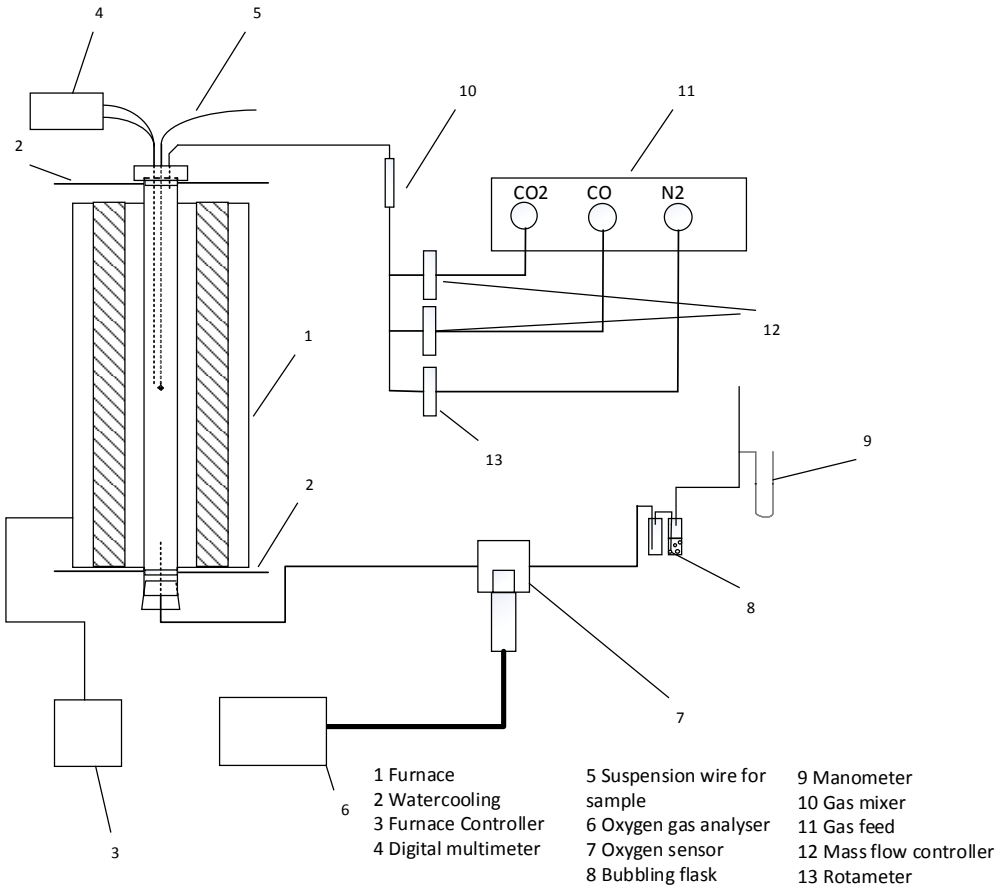

Figure 21 The equipment used in the experiments.

The furnace used in the experiments was a vertical tube furnace of the type Lenton silicon carbide resistance model LTF 16/45/450. The furnace controller was a Eurotherm 3216 PID. The temperature measurement was executed with an S-Type Pt/90%Pt-10%Rh-thermopair connected to a Keithley 2000 and a Keithley 2010 digital multimeters. The program for the temperature measurement data collection was a NI LabVIEW temperature logging program. The wire for hanging the samples and as the sample holder during the experiments was a Kanthal-D wire.

The carbon monoxide and carbon dioxide gases were controlled by mass flow controllers from Aalborg. The controller for CO_2 operated in the range of 0-500 ml/min and the controllers for CO in 0-20 ml/min (10^{-7}-10^{-9} atm) or 0-200 ml/min (10^{-10}-10^{-12} atm). The model of the controllers was a DFC26 with an accuracy of +/- 1 % of full scale. For low carbon monoxide flows the controller was changed to a controller with a smaller range to have higher accuracy at lower flow rates. The program DFC control terminal 2.05 was employed to control the digital flow controllers. The nitrogen gas was controlled by a rotameter also from Aalborg, model 052-01-SA. The nitrogen was applied to flush the furnace after the experiments.

Figure 22 Picture of the furnace and other equipment used in the experiments.

The oxygen sensor was adopted to measure and check the oxygen concentration of the off-gas. From this data, the precise oxygen partial pressure was defined for each experiment. The oxygen sensor is presented in Figure 23.

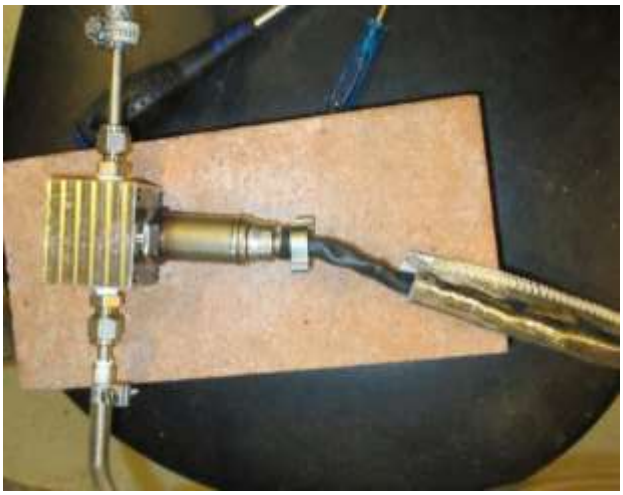

Figure 23 Oxygen sensor.

The operating temperature for the oxygen sensor was 650 °C. The model of the oxygen analyser was Cambridge Sensotec Rapidox 2100 and can be seen from Figure 24. The oxygen sensor was calibrated before the experiments started in this work. The program used to collect the data is called Rapidox Data Logger 7.0.71 and provided by Cambridge Sensotec.

Figure 24 Oxygen sensor analyser, Cambridge Sensotec rapidox 2100.

The samples were prepared using traditional dry metallographic methods. Samples were moulded in epoxy and then dry grinded with sandpaper abrasives until the needed phases were shown. The grinding was done in stages from 240 µm to 2000 µm using the machine in Figure 25.

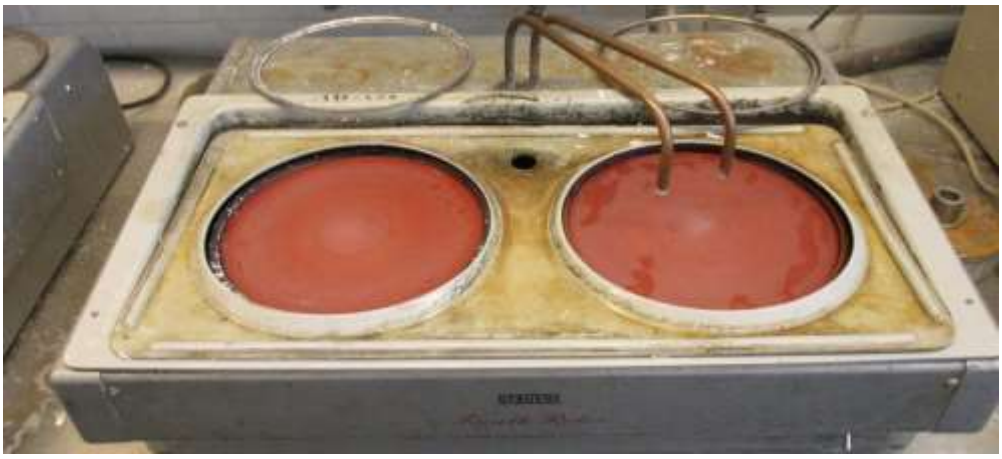

Figure 25 Struers grinding machine.

After grinding, the samples were polished with the machine shown in Figure 26 with 1 and 3 µm diamond polishing sprays (DP Spray P, Struers) on a soft felt polishing wheel. DP Brown lubricant from Struers was sprayed on to make the polishing smoother.

Figure 26 Struers polishing machine.

After polishing, the samples were cleaned in an ultrasonic purifier and coated with carbon to make sure they conduct properly in the SEM-EDS and in EPMA analysers. The carbon coating apparatus was a Leica EM SCD050. A picture of this equipment is shown in Figure 27.

Figure 27 Leica carbon coating equipment.

Samples were analysed with SEM-EDS and the proper full analysis employing EPMA. Experiments done earlier with this type of samples have showed that the EPMA analysing equipment is not sensitive enough to determine small concentrations in lead phase (Henao et al., 2010). The SEM-EDS used was operated at Aalto University. The EPMA equipment was a Cameca SX100. The analysing was performed at Geological Survey of Finland (GTK, Geologian tutkimuskeskus).

4.3 Gas atmosphere in experiments

The gases used were provided by AGA and they were carbon monoxide (CO), carbon dioxide (CO_2) and nitrogen (N_2). The purity of CO was 4.7 and the purity of CO_2 was 5.3. Table 6 presents the gas flow ratios employed to achieve the right oxygen partial pressure in the furnace. The total gas flow was 300 ml/min (STP) and consisted of carbon monoxide and carbon dioxide. 300 ml/min nitrogen gas was employed to

flush the furnace for 10-15 min after every experiment. The gas ratio is calculated from the equilibrium reaction between CO, O_2 and CO_2:

$$CO(g) + \frac{1}{2}O_2(g) = CO_2(g) \quad (32)$$

Table 6 Calculated gas ratios for the experiments and the prevailing oxygen pressures.

Temperature °C	Log pO_2 atm	CO ml/min	CO_2 ml/min	Sample (SYxx)
1150	-7	1.4	298.6	48, 49, 50, 51
1150	-8	4.3	295.7	31, 33, 34, 37
1150	-9	13.2	286.8	11, 23, 25, 47
1150	-10	38.0	262.0	13, 27, 29, 30
1150	-11	94.3	205.7	14, 15, 41, 42
1150	-12	177.5	122.5	16, 45, 46

From equation (33), it is possible to see that the product of equilibrium coefficient and the square root of the desired oxygen partial pressures equals the ratio for CO_2 and CO:

$$K_2 \cdot p_{O_2}^{\frac{1}{2}} = \frac{CO_2}{CO} \quad (33)$$

The equilibrium coefficient of reaction (32) from HSC6 is

$$K(1150\ ℃) = 6.897 \cdot 10^5. \quad (34)$$

From this conclusion, the needed CO_2 or CO flows can be calculated using 300 ml/min as total flow. The oxygen partial pressure was checked with the oxygen sensor to ensure the right pressure had been obtained. Because the oxygen sensor operated at a temperature of 650 °C, the data from that measurement had to be changed to be recalculated to the conditions in the furnace and at 1150 °C. In appendix 6 the calculated mole-% is presented, where the Log(mole-%) = -5 equals to 10^{-7} atm. From the graphs it is possible to see that the higher the temperature is the higher is the

mole-% and so the partial pressure is higher at higher temperatures if the same amounts or flow rates are used in the mixture. Equilibrium coefficient (35) for reaction (32) at 650 °C is:

$$K(650\ ℃) = 2.790 \cdot 10^{11} \tag{35}$$

The calculated oxygen partial pressure measured in the oxygen sensor (36) is:

$$p_{O_2}^{\frac{1}{2}} = \frac{VCO_2}{K \cdot VCO} \rightarrow p_{O_2} = \left(\frac{VCO_2}{K \cdot VCO}\right)^2 \tag{36}$$

When these values are known it is possible to calculate the (logarithmic) oxygen partial pressure in the equilibration furnace from the off-gas data:

$$log\ p_{O_2}(furnace) = \frac{log\ p_{O_2}(wanted) \cdot log\ p_{O_2}(sensor)}{log\ p_{O_2}(calculated\ sensor)} \tag{37}$$

An example (SY23, 10^{-9} atm) of results for oxygen concentration in the oxygen sensor is presented in Figure 28. It can be clearly seen that during the last hour of the experiment the oxygen concentration stabilizes. The average partial pressure from the sensor is taken from the last hour of the experiment. The total deviation of log pO_2 during the whole equilibration period is only ±0.1. The oxygen partial pressures used in the graphs for presenting the results are calculated from the measured oxygen partial pressures.

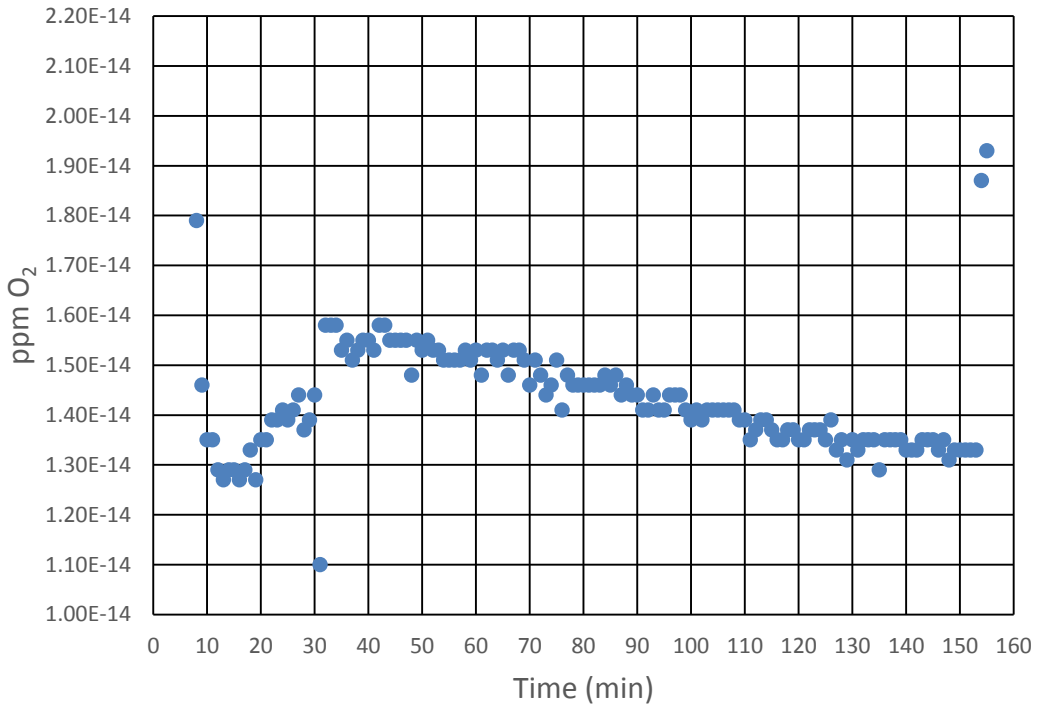

Figure 28 Sample SY23 in 10^{-9} atm at 1150 °C. The data from the sensor that operated at 650 °C in the gas outlet.

5 Experimental arrangements

In this chapter, the different materials used for the experiments are presented. The making of the crucibles required a lot of work, therefore the procedure for making them are also described. After the crucibles were prepared, the experiments in the furnace were ready to be made. The samples were then analysed with SEM-EDS to make sure that the trace elements were found in the lead and slag phases.

5.1 Reagent materials

Every material used in the experiments was a commercially available product and every mixture was made in the laboratory to the desired composition. The reagent materials for the substrate (crucible) are presented in Table 7. They were mixed in the proportion SiO_2/CaO=0.6 in weight-% ratio (w/w).

Table 7 Reagents used for crucibles.

Crucible			
Reagent	Manufacturer	Purity	Form
SiO_2	Sigma-Aldrich	Fumed	Powder, 0.2-0.3 µm
CaO	Sigma-Aldrich	99.9 %	Powder

Lead was of purity 99.95 % and delivered from Alfa Aesar (Table 8). The aimed weight of lead for each sample was 0.125 g.

Table 8 Lead used in experiments.

Lead			
Reagent	Manufacturer	Purity	Form
Pb	Alfa Aesar	99.95 %	Atomized powder, -100 mesh

The slag reagents and the manufacturers are presented in Table 9. The preparation of the slag mixtures are explained in detail in chapter 6.1.2. The trace elements used in the experiments are presented in Table 10.

Table 9 Slag reagents used in experiments.

Slag			
Reagent	Manufacturer	Purity	Form
PbO	Alfa Aesar	99.99 %	Powder
Fe	Alfa Aesar	99.5 %	Powder <10 µm
Fe_2O_3	Alfa Aesar	99.99 %	Powder
SiO_2	Sigma-Aldrich	99.995 %	Powder
CaO	Sigma-Aldrich	99.9 %	Powder

Table 10 Trace elements used in experiments.

Trace elements			
Reagent	Manufacturer	Purity	Form
Ge	Alfa Aesar	99.999 %	Powder, -100 mesh
GeO_2	Alfa Aesar	99.999 %	Powder
Ga_2O_3	Alfa Aesar	99.99 %	Powder, -50 mesh
In	Alfa Aesar	99.99 %	Powder, -325 mesh
In_2O_3	Alfa Aesar	99.9 %	Powder, -325 mesh
Sn	Alfa Aesar	99.85 %	Powder, -100 mesh
SnO	Alfa Aesar	99.9 %	Powder, -100 mesh

The trace elements were mixed together in such a way that in the first series the oxides were mixed and in the second series the metals were mixed. Gallium was present in oxide form in both mixtures. The mixtures consisted of 1 wt-% of each element in relation to the lead content. In the first series, gallium and indium concentrations were 2 wt-% of the lead mass. The oxide mix consisted of 0.1675 g Ga_2O_3, 0.0906 g GeO_2, 0.1506 g In_2O_3 and 0.0744 g SnO. It was added 0.0096 g per sample. The metal trace element mix consisted of 0.0423 g Ga_2O_3, 0.0309 g Ge, 0.0323 g In and 0.0325 g Sn. It was added 0.00543 g per sample.

5.2 Substrate preparation

The sample materials need a substrate to keep them together during the experiments. There are different kinds of commercial substrates available, but in this study the crucibles were prepared in the laboratory. These crucibles were produced to a composition close to the slag in the experiments. In this case, the crucible does not bring any new elements to the system, but rather is a part of the equilibrium system. The crucible was made of silica and calcium oxide. The crucibles were heated up to form pseudo-wollastonite ($CaSiO_3$). This type of crucible has not been used before to investigate trace elements in lead smelting conditions. Aluminium oxide and magnesium oxide crucibles have been used in the other studies (Henao et al., 2010; Hoang & Swinbourne, 2007; Yan & Swinbourne, 2003).

The CaO/SiO_2-weight ratio was 0.92 for the crucibles. The preparing of the mixtures were done in small batches. The used silica was a powder with very small particle size. This made the crucibles very compressible. After the two materials were mixed the powder was put into a uni-axial pressing tool (Figure 29) and pressed with Compac HP20 AA/AR (Figure 30) with a force of 20-30 kN to a crucible.

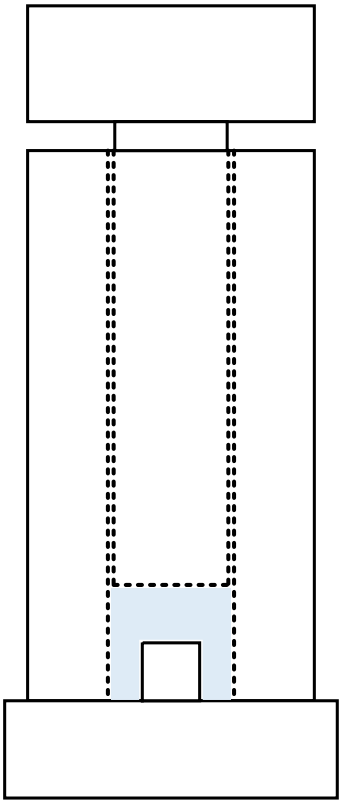

Figure 29 The used pressing tool to make the direct pressed crucibles.

Figure 30 Compac pressing equipment.

Two methods of making the crucibles were applied; either by pressing a pellet with a size of 15 mm, sintering and drilling it or by pressing it to the right form directly and then sinter it. The pressing tool is presented in Figure 29. The pressed pellets had a diameter of 15 mm and the diameter of the hole was approximately 8 mm. The crucibles were heated to 1450 °C in air and kept there for 12 hours. When they were heated they somewhat shrunk. After calcination and heating of the crucibles, they were drilled to form a hole where the lead and the slag can be put. The drilling was done using a dentist drill. Figure 31 represents three drilled crucibles.

Figure 31 Drilled pseudo-wollastonite crucibles.

The furnace used to sinter the crucibles was a Nabertherm P330 model HTC 08/16 presented in Figure 32. The crucibles were put on platina wire that was on an alumina plate during heating, see Figure 33. The composition of the crucibles were identified and studied with SEM-EDS.

Figure 32 Nabertherm chamber furnace used for the heating of the crucibles.

Figure 33 Platina wire on a flat piece of alumina.

5.3 Degrees of freedom in the system under inspection

The Gibbs phase rule can be employed to determine the degrees of freedom. With this formula (38), the needed factors can be calculated for investigating of the system:

$$F = C - P + 2, \tag{38}$$

Where C refers to components (Pb, Fe, Ca, Si and O) and P to phases (lead, slag, gas and pseudo-wollastonite). There are five components and four phases present. The carbon in the gases are presumed to be inert and the trace elements are also excluded from this inspection. This means that there exist three degrees of freedom, but as temperature and the total pressure (1 atm) is also constant, two degrees of freedom stays in the system. Thus, it is possible to determine the equilibrium of the system when the oxygen partial pressure and the CaO/SiO_2 ratio in slag (as that of the crucible) are specified.

6 Implementation

This chapter describes how the experiments were executed and the samples obtained analysed. Moreover, it represents the preparations performed before the distribution experiments.

6.1 Preparations

Before the actual experiments, preparations were executed to make sure the experiments had the right conditions. The slags were prepared and the trace elements were pre-mixed in a batch to be easier to handle when preparing samples. To assure that equilibrium was reached in the experiments, tests were done without trace elements and for different annealing time periods.

6.1.1 Temperature profile for furnace

The temperature profile was measured before the experiments in this work were started. The small Al_2O_3 tube, through which the suspension wire went, was adjusted so that the sample was placed in the middle of the hot zone.

6.1.2 Slag preparation

The slags in this work were made to be similar to industrial slags. First, a mixture of the slag materials was prepared to meet the required composition. Different slags were prepared with different lead oxide concentrations assuring the equilibrium would be reached faster. The lead oxide concentration in the slag mixtures varied between 10-20 %, depending on the target oxygen partial pressure in the experiment. The oxygen partial pressure was adjusted with the gas flows and the pressure should produce the right conditions to form the target slags i.e. the lead-bearing slags were prepared only to quicken the equilibrium formation.

The first slag made had a 20 % PbO concentration. The second slag had a PbO concentration of 10 %. Lead was evaporated greatly from the samples during the

experiments. To prevent this a third pre-melted slag was made in a silica crucible. The pre-melting was executed at 1150 °C for 14 hours in 10^{-9} atm O_2 atmosphere. This slag was used in the second series and also in the higher oxygen partial pressures of the first series. The assays of prepared slags and the CaO/SiO_2-ratios are presented in Table 11.

Table 11 Measured masses (g) for slag components and CaO/SiO_2-ratio for the prepared slags in this work.

Sample (SYXX)	log pO_2 (atm)	Slag	SiO_2	CaO	Fe_2O_3	Fe	PbO	CaO/SiO_2
14, 15, 16, 46	-11, -12	10 wt-% PbO	0.85	0.5069	0.0546	0.6641	0.2484	0.5964
23, 11, 27, 13	-9, -10	20 wt-% PbO	0.9171	0.5503	0.0608	0.4083	0.4994	0.6000
		Pre-melted slag						
50, 51, 31, 37 and series 2	-7, -8 in series 1 and all in series 2	17 wt-% PbO	2.5025	1.5187	1.0048		1	0.6069

Weight of the slag in each sample was 0.10 g. In the results chapter (Chapter 7.4) it can be seen how the slag composition changed, during equilibration, from the ratios presented in Table 11.

6.1.3 Equilibration time

Equilibrium is reached in a system when no changes are happening anymore in the phase assays. To find the equilibrium between metal and slag, there has to be made preliminary experiments. With the experiments, the suitable time can be found when the equilibrium is reached.

The time how long the lead-slag-crucible system takes to equilibrate was investigated with a time-series of experiments. The experiments were done in 1, 2, 3 and 4 hours durations. An oxygen partial pressure of 10^{-9} atm was adopted. Because of evaporation of lead, three more tests with more lead and slag were conducted to see if the lead would stay longer in the crucible. In the search for the equilibration time, only the main slag components and pure lead were used.

Table 12 Concentrations of slag components in the first time-test series by SEM-EDS.

t/h	O/wt-%	Si/wt-%	Ca/wt-%	Fe/wt-%	Pb/wt-%
1	32.23	16.90	9.71	25.12	15.44
2	32.19	15.94	9.43	26.92	15.52
3	34.24	20.55	11.07	21.35	12.78
4	31.15	18.50	11.10	24.75	14.50

The first tests showed that no relevant changes happened in the slag even for longer equilibration times beyond 2h. This can be noticed from the results in Table 12 and Figure 34.

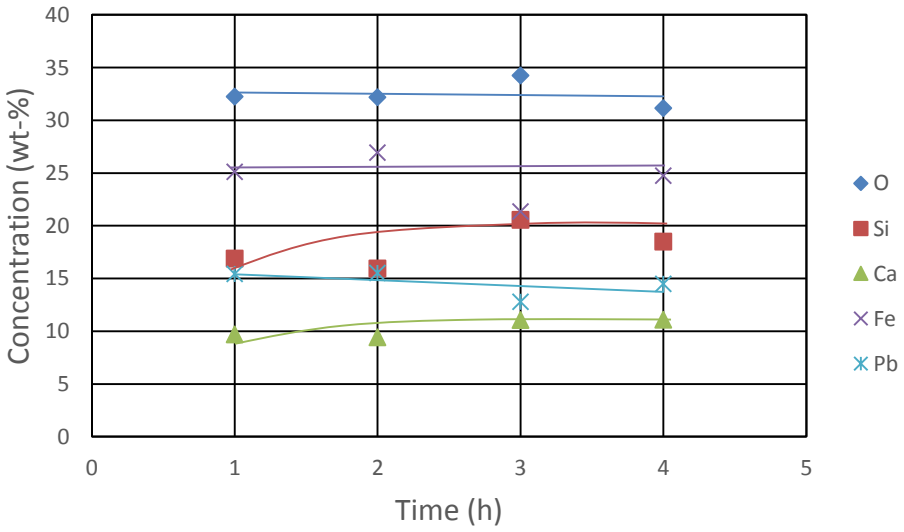

Figure 34 Concentrations of slag components over time in the first test series.

The second attempt with more lead and slag in the crucible made sure that lead did not evaporate completely. Even if the values seem to not change more than in the previous test series there are still not so much difference in the slag assay between two and three hours duration.

Table 13 Concentrations of slag components in the second time-test series.

t/h	O/wt-%	Si/wt-%	Ca/wt-%	Fe/wt-%	Pb/wt-%
1	31.48	14.72	10.73	21.98	21.09
2	33.15	18.72	10.76	14.90	22.48
3	32.62	20.05	7.33	17.62	22.38

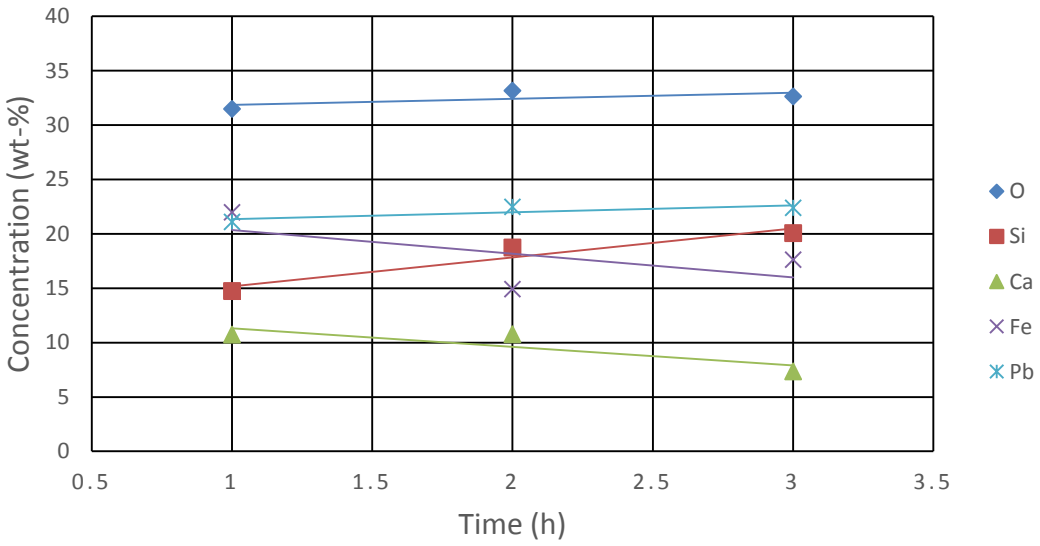

Figure 35 Concentrations of slag components over time in the second pre-test series.

The conclusion was that 2 hours is a enough long time to reach equilibrium in the system. This can be seen in the graphs in Figure 34 and Figure 35, and the compositions in Table 12 and Table 13 indicate that no major changes happen in the slag after two hours.

6.2 Realization of equilibration experiments

The equilibration experiment was started by putting the crucible in the sample holder and then the materials were added in the crucible. Lead, trace elements and slag were pre-weighted in specific portions and put in the pseudo-wollastonite crucible. The total weight of the samples was around 0.24 g (lead+trace elements+slag) and the lead/slag-ratio was 1.25-1.6. Lead was located at the bottom of the crucible, in the middle was the trace element mixture and on top was the slag mixture. When

the crucible was in the holder and the material mixtures in it, the whole holder was attached to the suspension wire in the furnace, by bending the wire end to make a hook to which the holder was intended to hang. Then the wire was pulled up to the cold zone of the furnace and the lower end of the working tube was sealed. A steel pipe was put through the sealing and a rubber hose was connected to the pipe to let the gases flow out of the furnace, see Figure 21 and Figure 22. When the furnace was sealed, the gases were fed to the furnace. A gas sensor device (BW Gasalertmicro 5, Honeywell) was used to make sure there were no leaks during the experiments.

Figure 36 Sample holder made of 0.5 mm Kanthal-D wire.

The sample holders were made out of Kanthal-D steel wire. An example is presented in Figure 36. After stabilising the proper gas atmosphere for half an hour, the wire was pulled up until the sample holder reached the small tube inside the furnace. Now the crucible was in the hot zone and it was kept there for two hours. After two hours, the sample was quenched in ice water. The water was in a small cup that was put beneath the working tube just so that it covered the end of the tube. The sealing was opened and it was possible to drop the sample to the ice water. After the quenching, the furnace was flushed with nitrogen gas for 10-15 minutes.

6.3 Making and analysing of the samples

After the sample was dried post quenching, it was broken down into pieces to make sure both lead and slag was present in the sample. The sample was moulded in an epoxy resin as to prepare it for the SEM-EDS- and EPMA-analyses. After the epoxy had hardened, the sample was grinded and polished. The grinding was done in several stages in order to get a smooth surface. The sample was checked with optical microscope to see if both lead and slag phases were present. When grinding was done, the sample was polished to make sure the surface quality would be good enough for analysing the sample with EPMA.

From both phases (metal and molten slag) at least 10 points were analysed, but for some samples more points were analysed to achieve a better and more reliable average. Only 7 points in the lead phase were analysed for sample SY46, due to the small area of the metal phase. The analysed points were chosen by taking the average of all points except for one slag phase in sample SY11 were only the slag closest to the lead phase were used to take the average value of the elements. In some analysed points there were data that showed zero concentration of an element. These were not used in the calculation of the average value.

The conditions in the EPMA measurements are presented in Table 14. The beam diameter used in measuring the lead phase was narrow because the lead micro structure was porous and in some samples the lead alloy regions were small.

Table 14 EPMA measurement conditions.

Phase	Accelerating voltage	Beam current	Beam diameter
Lead	20 kV	40 nA	1 µm
Slag	20 kV	40 nA	10 µm, 20 µm

Table 15 presents the estimated detection limits in ppm of the EPMA analyses for different elements in the phases in the present samples. Every value in the current results that is over the detection limit is considered as reliable.

Table 15 Average elemental detection limits (ppm) determined by GTK.

O	Si	Ca	Fe	Ga	Ge	In	Sn	Pb
4568	366	232	549	452	613	356	360	2206

7 Results

In this chapter, the results obtained from the EPMA-analyses are presented and discussed. The distribution coefficients are calculated from the normalised compositions of the lead and the slag phases. In appendices 2-5, the results are presented in tables in numerical format. Some of the results are not reliable, as the minor element concentrations in lead were under the detection limits. According to the analyses, the lead phase contains some oxygen, even though there should not be any (Matousek, 2011). In the calculations, the oxygen was not taken into account. The results for lead phase are normalised without oxygen, because oxygen solubility in the experimental conditions was small (Ganesan et al., 2006).

7.1 Microstructure

Figure 37 presents a picture of the microstructure of sample SY47. The white phase is lead and the grey phase is the slag. The darker grey phase is the crucible material.

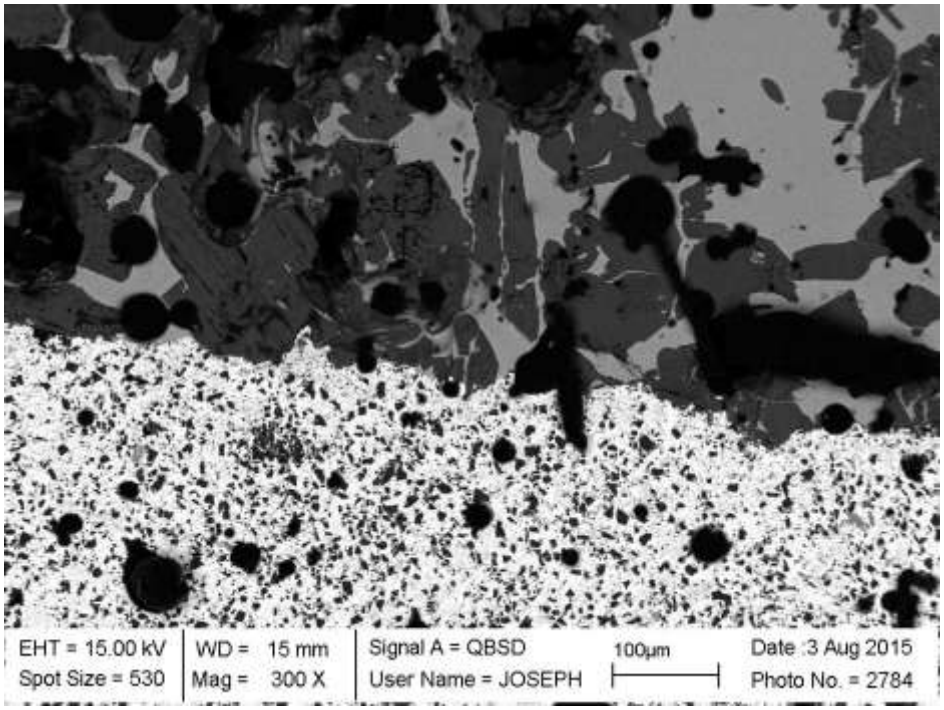

Figure 37 SEM Picture of microstructure of sample SY47. The white phase is lead, the light gray phase is slag and the darker gray phase is the crucible.

In order to determine the phases and the compositions, BSD(back scattered)-pictures were taken. Because the materials have different hardnesses, it was difficult to make smooth surfaces on the samples. The lead phase seems to have many small pores and this also can affect the EPMA results. In some samples (SY46), the lead phase existed only as very small regions, maybe because of evaporation of lead and a high porosity of the crucible.

7.2 Trace elements in lead bullion-slag-system

The EPMA results are presented in Appendix 2 and the calculated distribution coefficients in Appendix 5. The average values for different elements in lead and slag were collected in Appendices 3 and 4. The trace element distribution coefficients were calculated from the average weight percentages of the EPMA results; the concentration of a trace element in lead phase was divided by the concentration of a trace element in the slag phase. The distribution coefficients were thus calculated using the following formula:

$$L_X^{Pb/s} = \frac{[wt\%X]}{(wt\%X)} \tag{39}$$

where X stands for the trace element (Ga, Ge, In, Sn) and lead (Pb), depending on what metal is under investigation. The errors were also calculated for the obtained distribution coefficients and they were derived from the formula:

$$\frac{\Delta L_X}{L_X} = \left|\frac{\Delta x}{x}\right| + \left|\frac{\Delta y}{y}\right| \tag{40}$$

In equation (40), the ΔL is the error for the distribution coefficient, Δx is the standard deviation for the element in lead phase and Δy for the element in slag phase. x is the average value for an element in lead phase and y is the average value for an element in slag phase. The errors for the distribution coefficients are presented graphically in

the next figures and they are also available in numerical format in Appendix 5. The equation for the distribution coefficient error can be derived from expression (40) as:

$$\Delta L_X = \left(\left|\frac{\Delta x}{x}\right| + \left|\frac{\Delta y}{y}\right|\right)\frac{x}{y} \tag{41}$$

The concentrations of the trace elements have a large standard deviation in this work.

7.3 Detection limits of the distribution coefficients for trace elements

The distribution coefficient detection limits are calculated from the detection limits by EPMA. This makes it possible to see how reliable the results are. The detection limits were calculated from equation (39) used in the previous chapter to calculate the distribution coefficients. The EPMA detection limits in Table 15 are used for the minor elements in lead. The minor element concentrations in slag are from the experimental results as they were above the detection limits in every sample. The detection limits of the distribution coefficient for series 1 are presented in Figure 38. The corresponding limits for series 2 are presented in Figure 39.

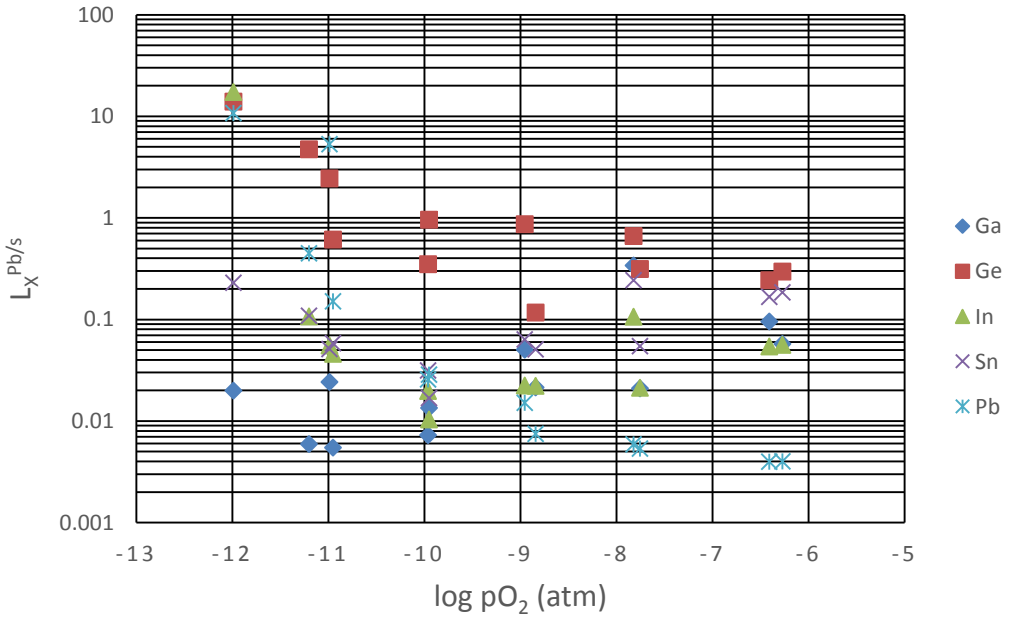

Figure 38 Detection limits for the distribution coefficients in series 1.

The distribution coefficients can be considered reliable when they are larger than those calculated from detection limit. This detection limits are presented along with the experimental results of the distribution coefficients in the coming chapters.

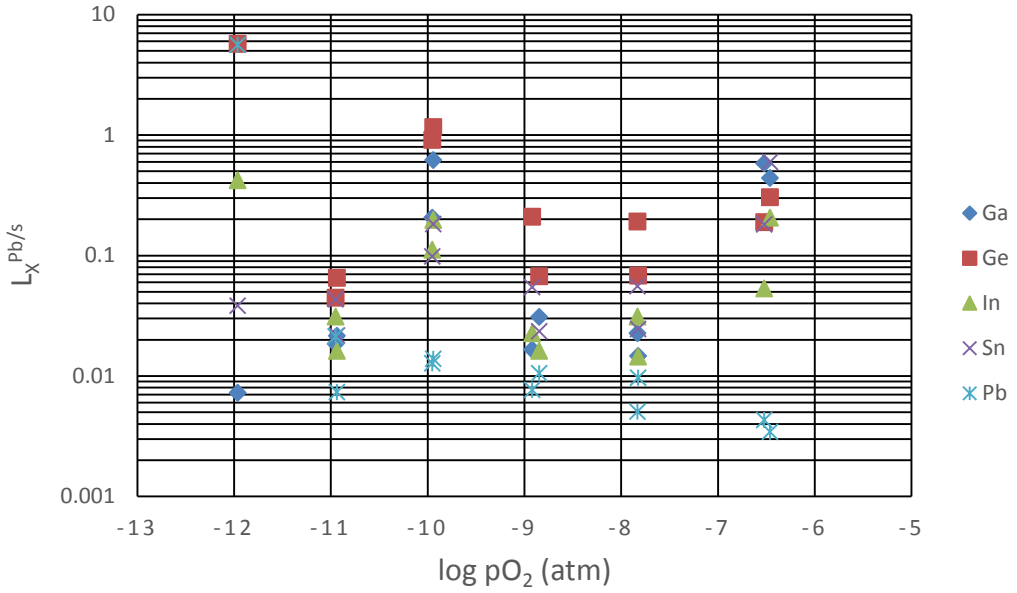

Figure 39 Detection limits for the distribution coefficients in series 2.

7.4 Slag composition after equilibration

This chapter presents the experimental results for the slag composition. The results from the EPMA analyses shows that lead concentration increases while the concentrations of the other components decrease, as the oxygen partial pressure increases. This can be seen in Figure 40 and Figure 41. Figure 40 shows the results for the slag compositions in series 1.

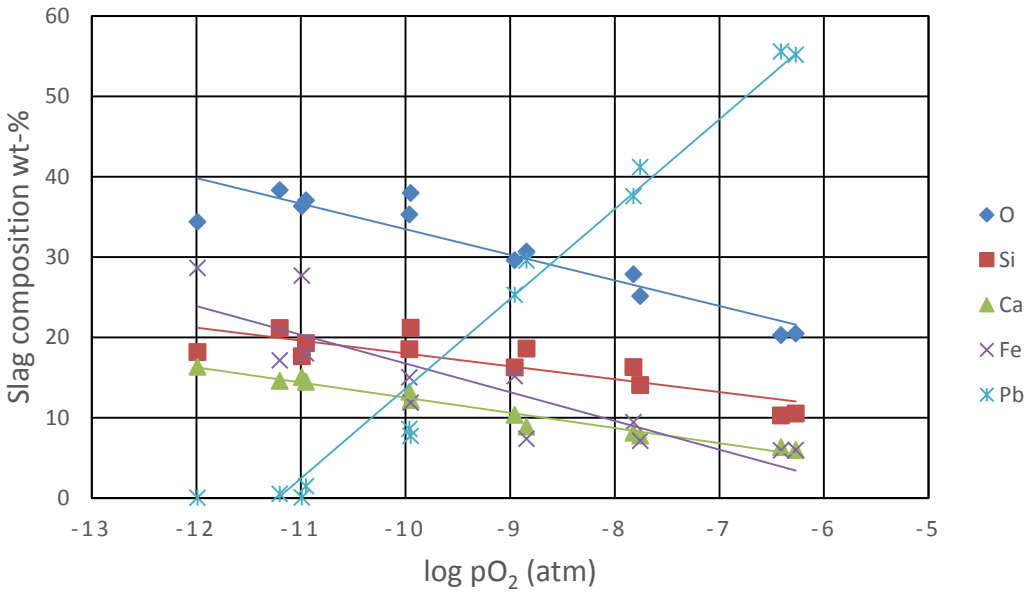

Figure 40 Series 1 slag composition as a function of oxygen pressure.

Figure 41 shows the element concentrations in the slag for experimental series 2. The concentrations show similar trends as series 1. When the lead concentration of the slag increases, the other components in the slag phase decrease.

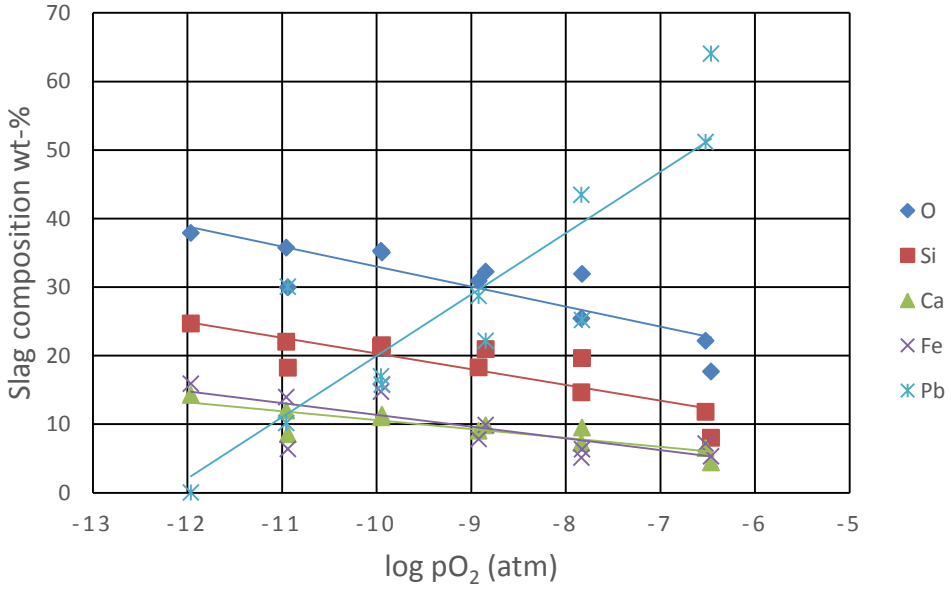

Figure 41 Series 2 slag composition as function of oxygen pressure.

The CaO/SiO_2-ratio of the molten slag is presented in weight-%-ratio for the two series in the following graph (Figure 42). The ratio changes as a function of oxygen pressure around 0.55-0.35 in series 1.

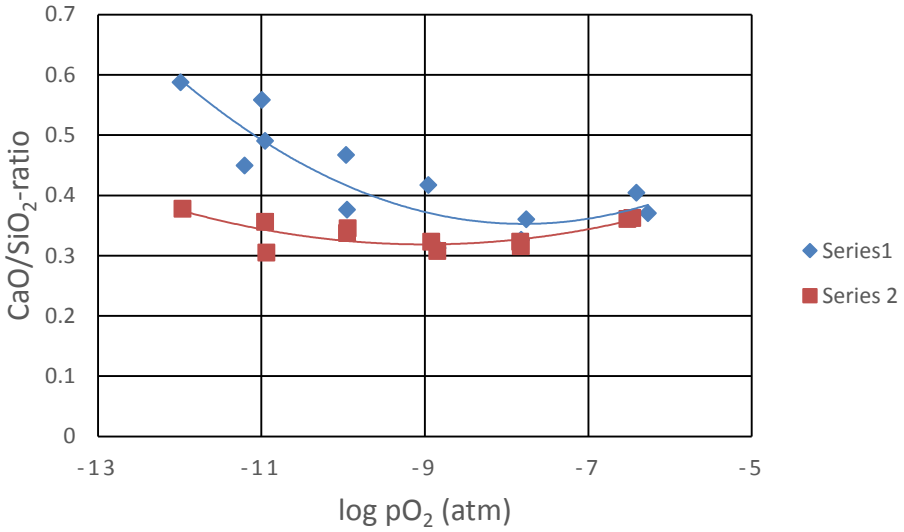

Figure 42 CaO/SiO_2-ratio for series 1 and 2.

In series 2, there is not much change in the CaO/SiO_2-ratio over the experimental oxygen pressure range and the value of the ratio is around 0.34. The pre-smelted slag probably has a more stable CaO/SiO_2-ratio. The CaO/SiO_2-ratio was around 0.6 when measuring the initial sample weight but it seemed to decrease as the samples were heated and molten slag was formed in the equilibration.

Another ratio considering the slag is the Fe/SiO_2-ratio and it is also expressed in weight-%. This ratio does not show any particular trend, but in series 1 it decreases as the oxygen partial pressure increases, as can be seen in Figure 43. The Fe/SiO_2-ratio in the series 2 was around 0.2 and 0.3.

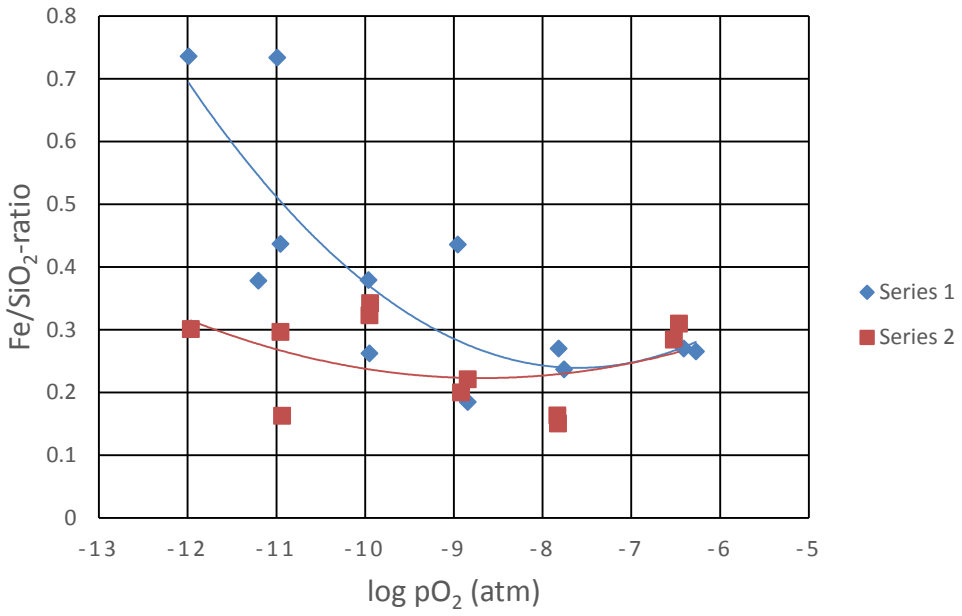

Figure 43 Fe/SiO_2-ratio (w/w) for series 1 and 2.

A slag concentration depth profile of sample SY11 was meaured to investigate the slag composition near the lead phase and further away towards the gas interface. The profile begins at the marked point in Figure 44 and has a length of 1263 µm. 20 points were taken and the beam diameter in EPMA was 5 µm.

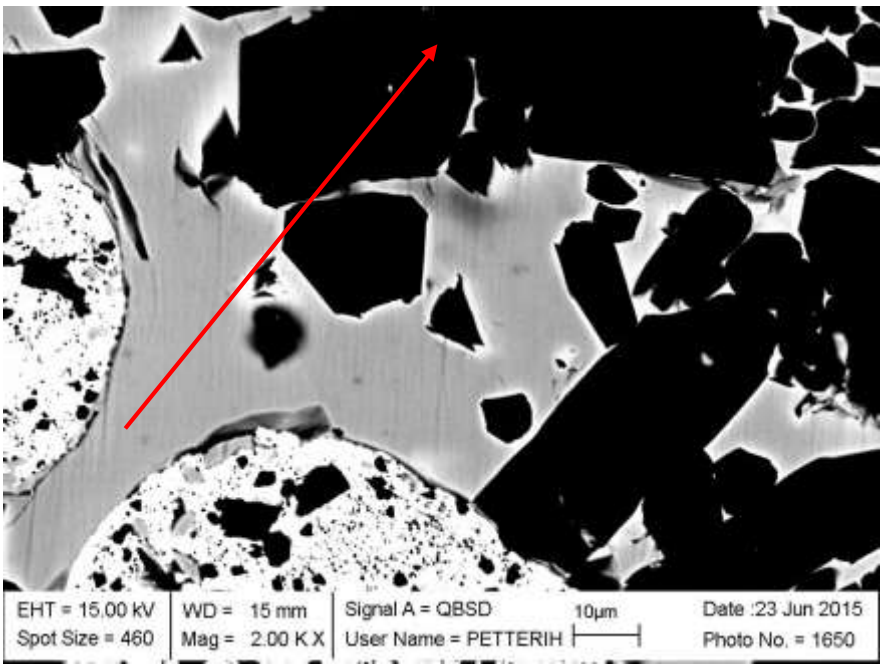

Figure 44 SY11 and arrow showing the slag profile analysis line.

The obtained slag profile is presented in Figure 45. It can be noticed from the profile that the lead content of the slag changes from 25 wt-% near the lead phase to 10 wt-% further away from the lead-slag interface. This indicates a strong trend for vaporisation for PbO from the slag and its transfer to the surrounding gas atmosphere.

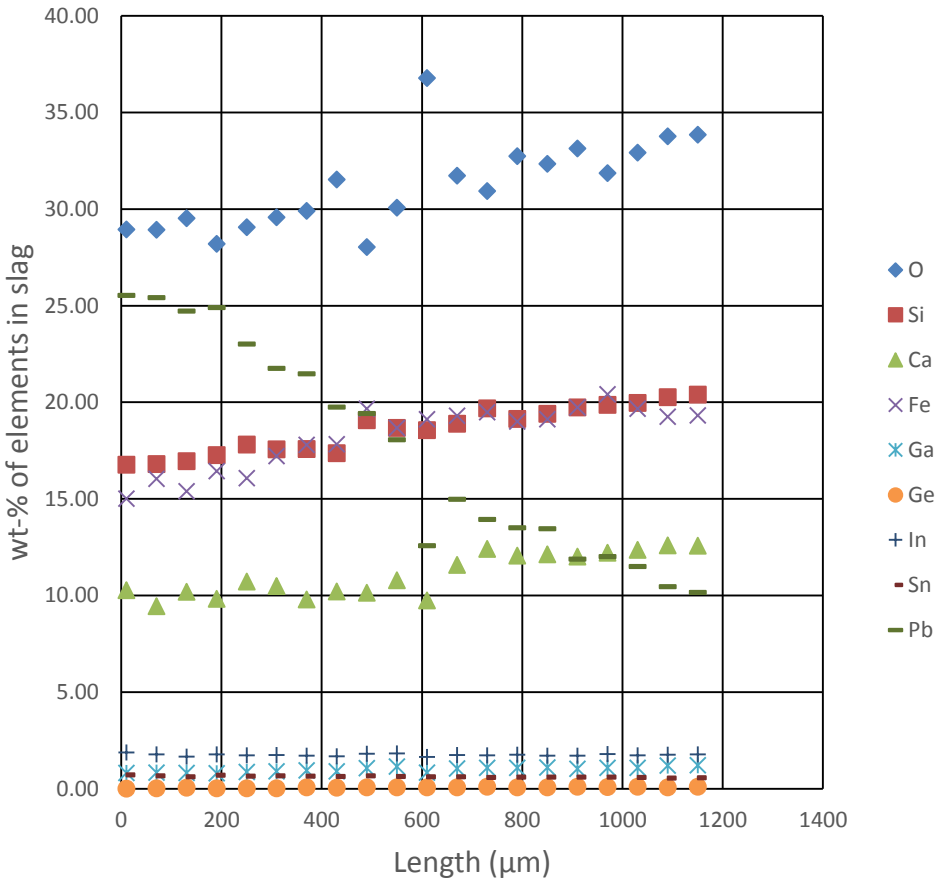

Figure 45 Slag concentration profile of sample SY11. The length is the distance from the lead phase.

A concentration profile of the trace elements in the slag is presented in Figure 46. Gallium and germanium concentrations increase the further away from the lead phase the EPMA points are analysed. Because of this feature, there is a large scatter in the experimental results. Indium and tin concentrations seem to be less dependent on the location and distance from the metal phase.

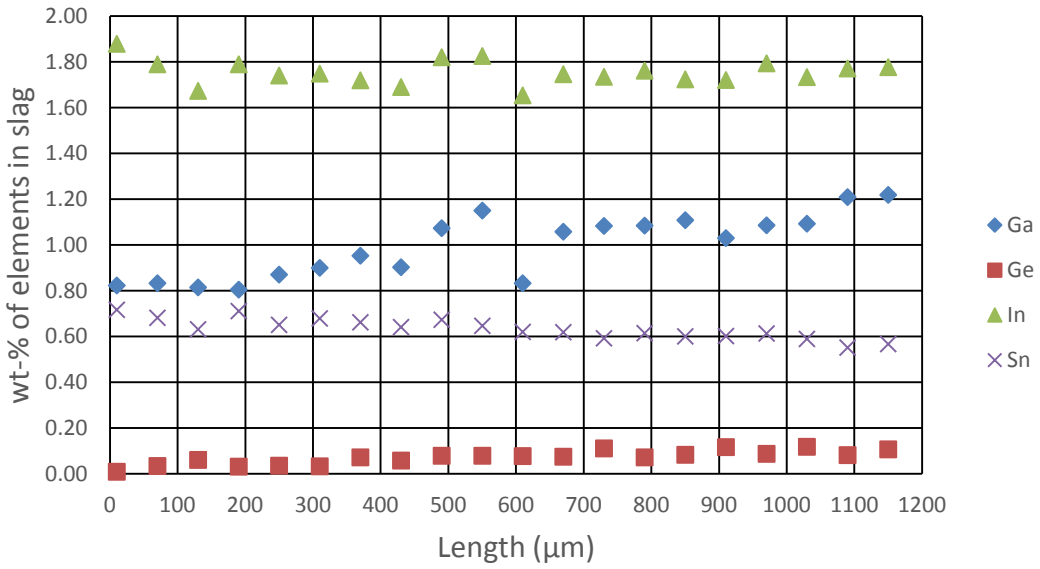

Figure 46 Same concentration profile as in Figure 45, zoomed in on the trace elements.

7.5 Lead distribution between lead bullion and slag

Three different slags were used in the experiments. The lead concentrations in the slags differ, targeted according to variable oxygen pressure of the experimental point.

The concentration of lead in lead phase for series 1 is shown in Figure 47. The lead concentration is lower in the reducing conditions because more trace elements are dissolving to the metal phase. A similar behaviour is also noticed in series 2.

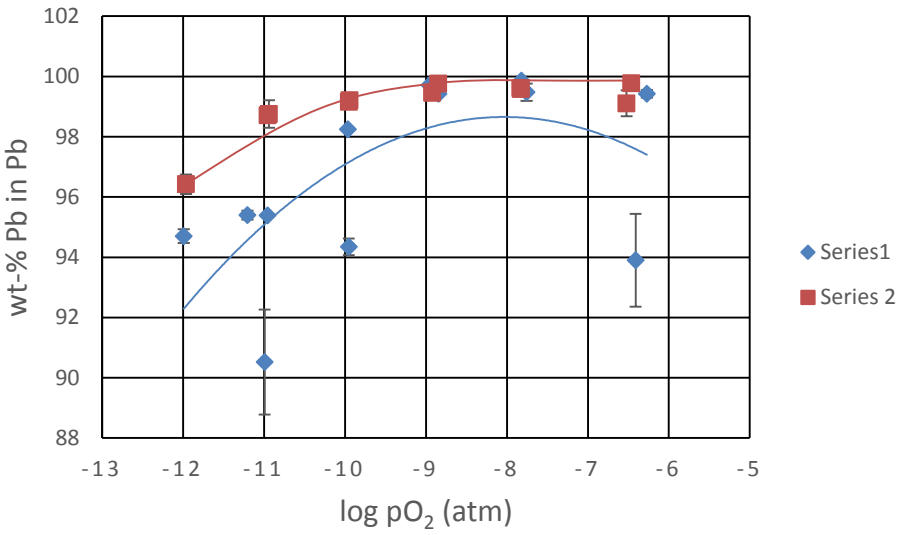

Figure 47 Lead concentration of the metal phase in series 1 and 2.

The following graph shows the slag phases' lead concentration (wt-%) as a function of pO_2 (atm). The more reducing the smelting conditions are, less lead is dissolving in the slag, as can be seen in Figure 48. The samples in the oxygen partial pressures 10^{-7} and 10^{-8} atm in series 1 and every sample in series 2 were using the pre-melted slag. Note the good agreement between the results.

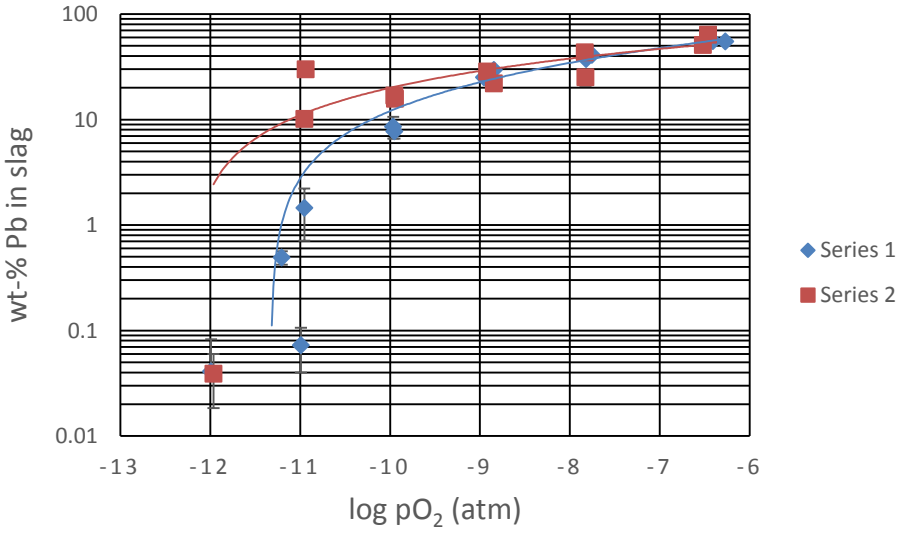

Figure 48 Concentration of lead in slag phase in series 1 and 2.

The lead concentration in the slag in series 2 is not changing that much as in series 1. The Pb concentration is slightly decreasing as the oxygen partial pressure is decreased, but it stays over 10 wt-% in series 2. In series 1, during reducing conditions the lead concentration decreases below 10 wt-%. Both in series 1 and 2 at $pO_2=10^{-12}$ atm the lead concentration is really low (0.04 wt-%).

Distribution coefficients for lead between lead and slag are different in series 1 and 2. As presented in Figure 49, the distribution coefficient increases with decreasing oxygen partial pressure.

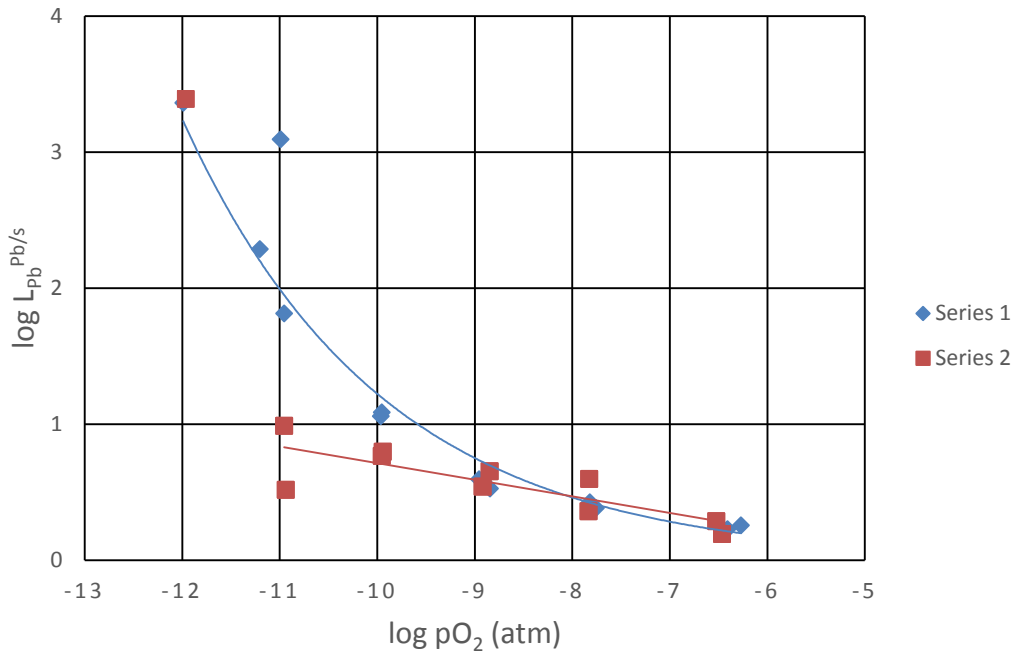

Figure 49 Distribution coefficient for lead between metal and slag in series 1 and 2.

The metal-slag distribution coefficients in series 2 have values between 1 and 10. When comparing the series, it can be concluded that the oxidation state of lead in the two series seem to be different. In series 1, the oxidation state is Pb^{4+} in reducing conditions and close to Pb^{2+} or Pb^{1+} in oxidising conditions. In series 2 the oxidation state is Pb^{1+} and/or Pb^{2+} over the whole experimental region. Lead is in the oxide form of PbO_2, PbO and Pb_2O in the slags.

7.6 Distribution and behaviour of gallium

The results for gallium in lead smelting are presented next and the results do not show any specific relation to the oxygen partial pressure. As mentioned before, there is no previous research on the distribution of gallium in lead smelting, so there is no studies to compare with. In series 1, there is no change on the gallium solubility in lead phase between 10^{-10} and 10^{-7} atm. In pO_2=10^{-11} and 10^{-12} atm the concentration of gallium is a little bit higher. This can be seen from Figure 50.

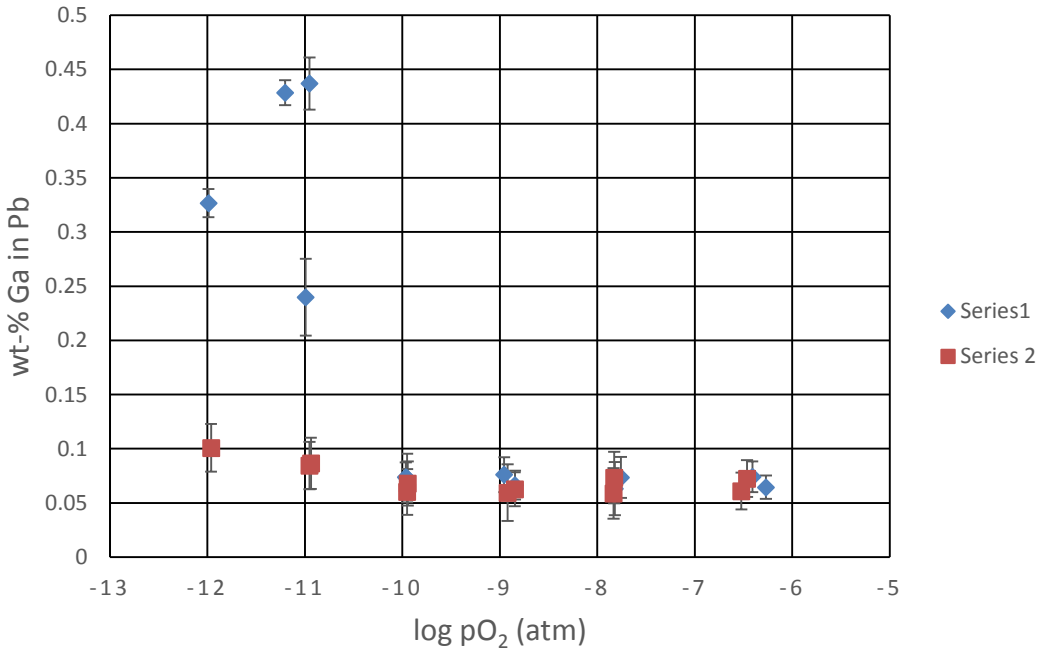

Figure 50 Gallium concentration in the lead phase in series 1 and 2.

In series 2, no greater change is happening to the gallium in the lead phase. From Figure 50 it can be seen that at lower oxygen partial pressures the gallium concentration is around 0.1 wt-%. There is a huge difference in the concentrations of gallium between series 1 and 2 at oxygen partial pressures 10^{-11} and 10^{-12} atm.

Gallium concentration varies more in the slag phase than in the lead phase. The values in the slag phase are in the same concentration region for both series (Figure 51). The dependence on oxygen partial pressure seems to be similar for both series.

The concentration of gallium in the slag increases when the oxygen partial pressure decreases. The concentration of gallium is much higher in the slag than in the lead phase.

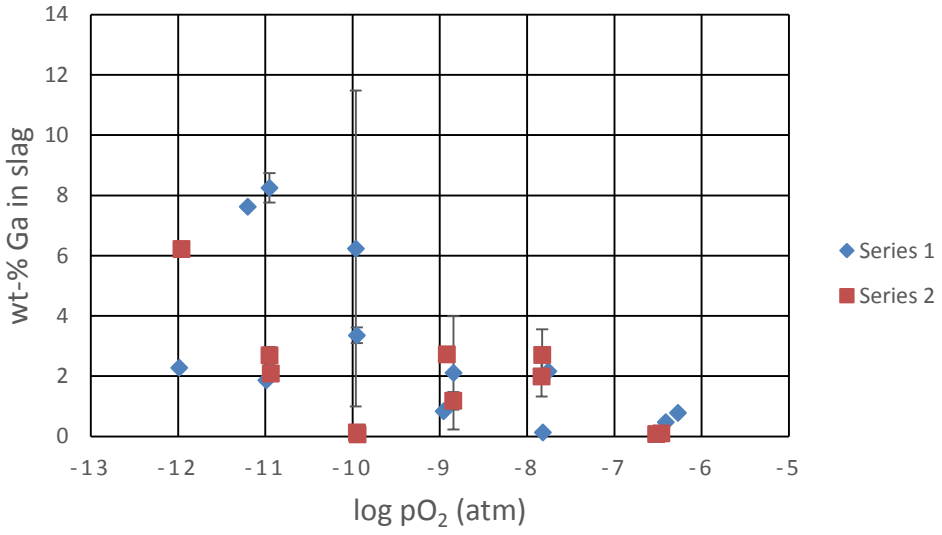

Figure 51 Gallium concentration in the slag phase in series 1 and 2.

The obtained distribution coefficients for gallium are plotted in Figure 52. The dotted lines show the detection limits for the distribution coefficients. The points above the dotted line are the reliable results.

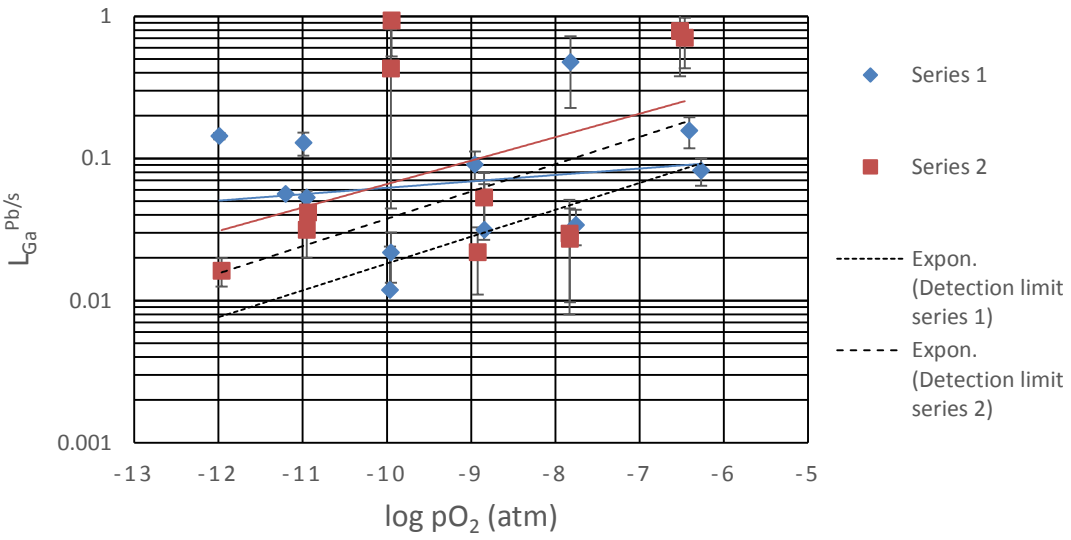

Figure 52 Distribution coefficient of gallium between lead and slag in series 1 and 2.

In series 2, the distribution coefficients are increasing as the oxygen partial pressure is increased. This would mean that more gallium dissolves to the lead phase in oxidising conditions.

7.7 Distribution and behaviour of germanium

The obtained data for germanium in the lead phase are unreliable because many data points in lead are under the detection limit. Still the results give a hint on the distribution for germanium. It is possible to see in Figure 53 that at the lowest (10^{-11} , 10^{-12} atm) oxygen partial pressures the concentration of germanium is higher than at the other partial pressures. This means that more germanium dissolves in the lead phase at low oxygen pressures or in reducing conditions.

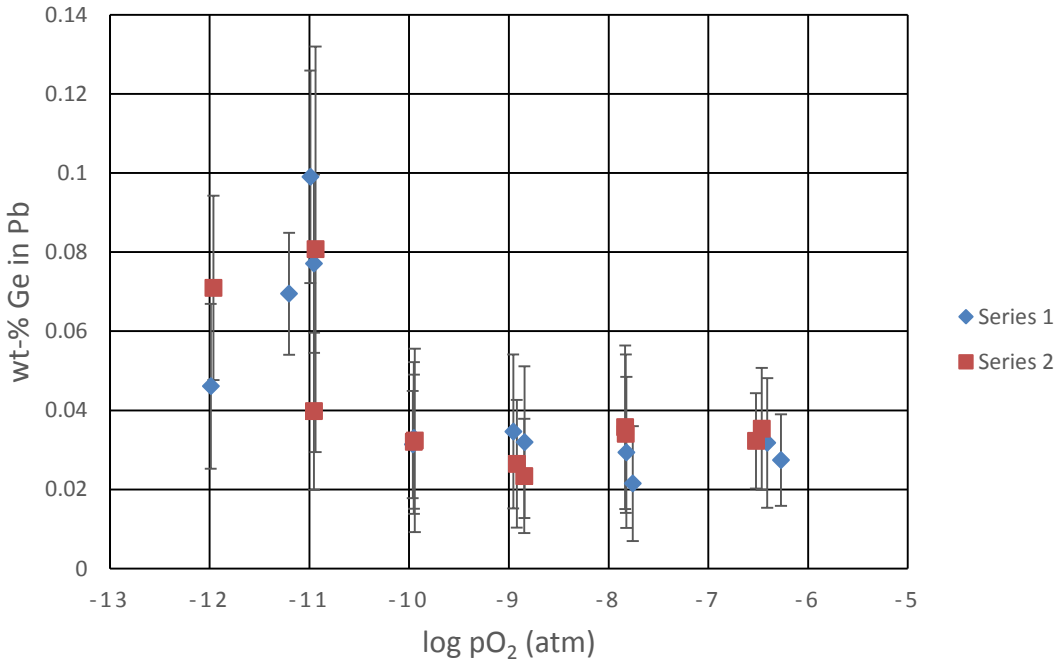

Figure 53 Concentration of germanium in the lead phase in series 1 and 2.

The data for germanium in the lead phase show similar results for series 1 and 2, but the differences are significant. Also the differences for the data in the slag phase for

series 2 are large. The trend for germanium is that the higher the oxygen partial pressure is the more germanium dissolve in the slag, as seen in Figure 54.

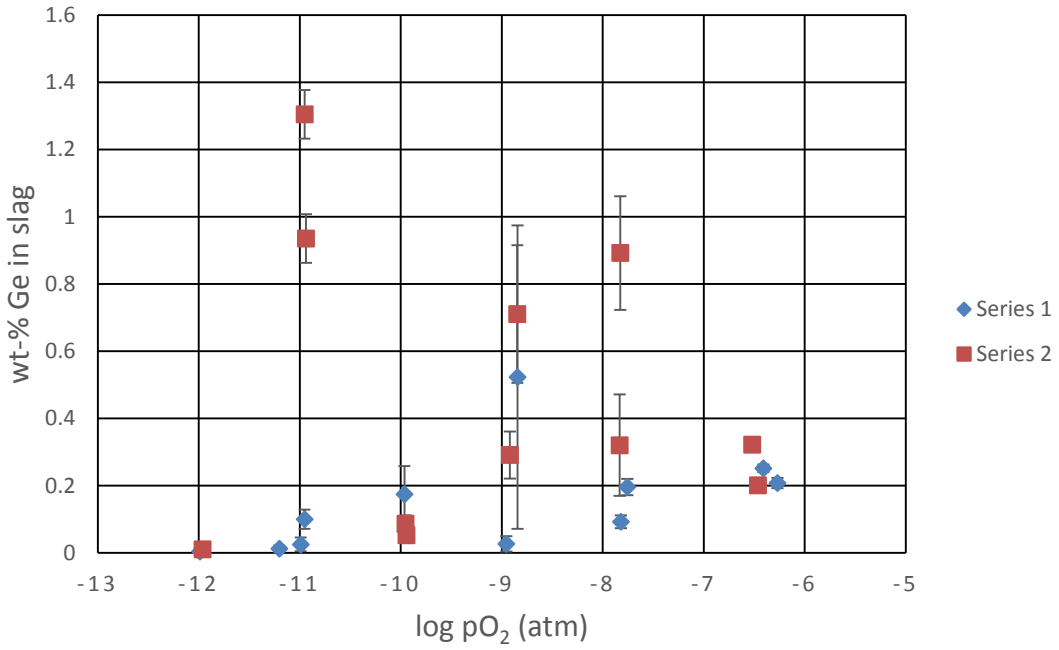

Figure 54 Concentration of germanium in slag phase in series 1 and 2.

The distribution coefficients for series 1 and 2 (Figure 55) show clear trends that during reduction smelting germanium distributes to lead and during oxidation smelting germanium distributes to slag. Of course, many points are under the detection limit meaning that these results only give an estimate on the distribution behaviour of germanium.

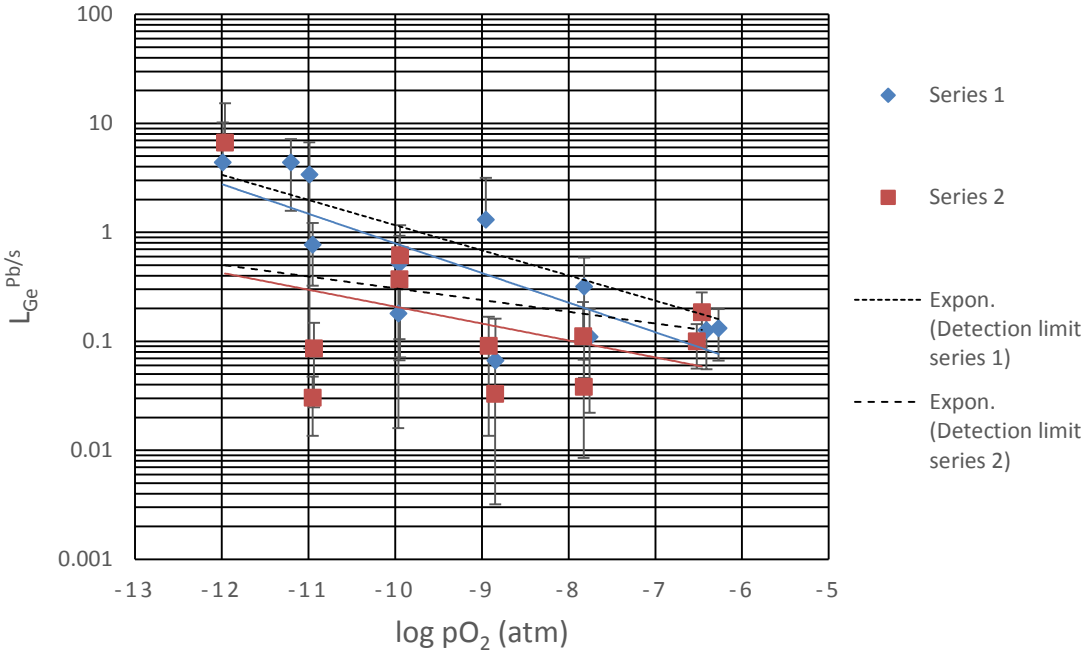

Figure 55 Distribution of germanium between lead and slag in series 1 and 2.

The oxidation state of germanium is Ge^{2+} in reducing conditions and Ge^{+} in oxidising conditions in series 1 in the slag. The oxidation state in series 2 seems to be closer to Ge^{+} but the values for oxygen partial pressure 10^{-11} atm could distort the analysis and therefore the oxidation state could be similar to series 1.

7.8 Distribution and behaviour of indium

A clear trend is shown in the lead phase in both series 1 and 2 indicating that the lower the oxygen partial pressure is the more indium dissolves in lead. This can be clearly seen in Figure 56.

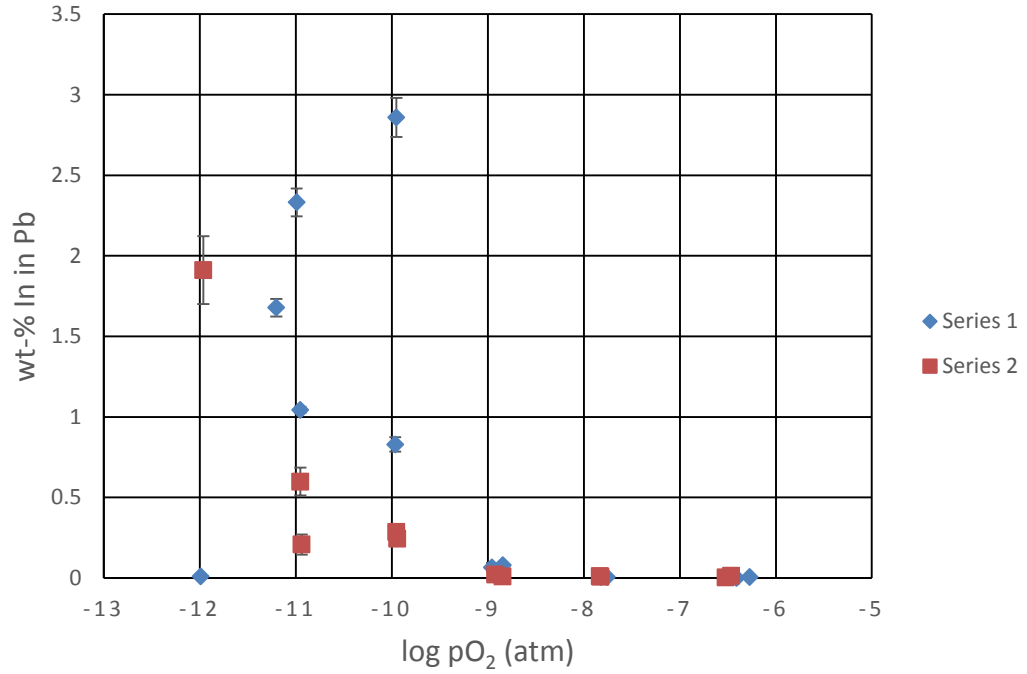

Figure 56 Concentration of indium in the lead phase in series 1 and 2.

Indium concentration in the slag phase shows no direct trend as depicted in Figure 57. Though, it seems that in oxidising conditions indium dissolves in the slag.

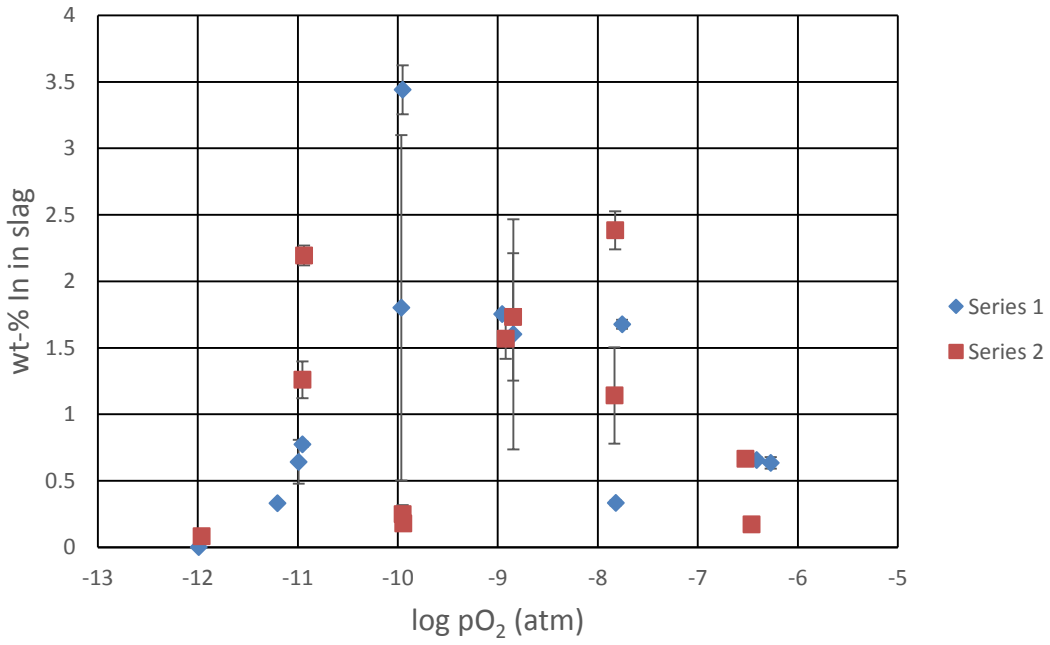

Figure 57 Concentration of indium in the slag phase in series 1 and 2.

The distribution coefficients for indium are presented in Figure 58. Indium behaves in the same way in both series. The data points in the oxidation conditions are unreliable because they are beneath the detection limit in lead. Indium has the oxidation state of In^{2+} in the slag in both series.

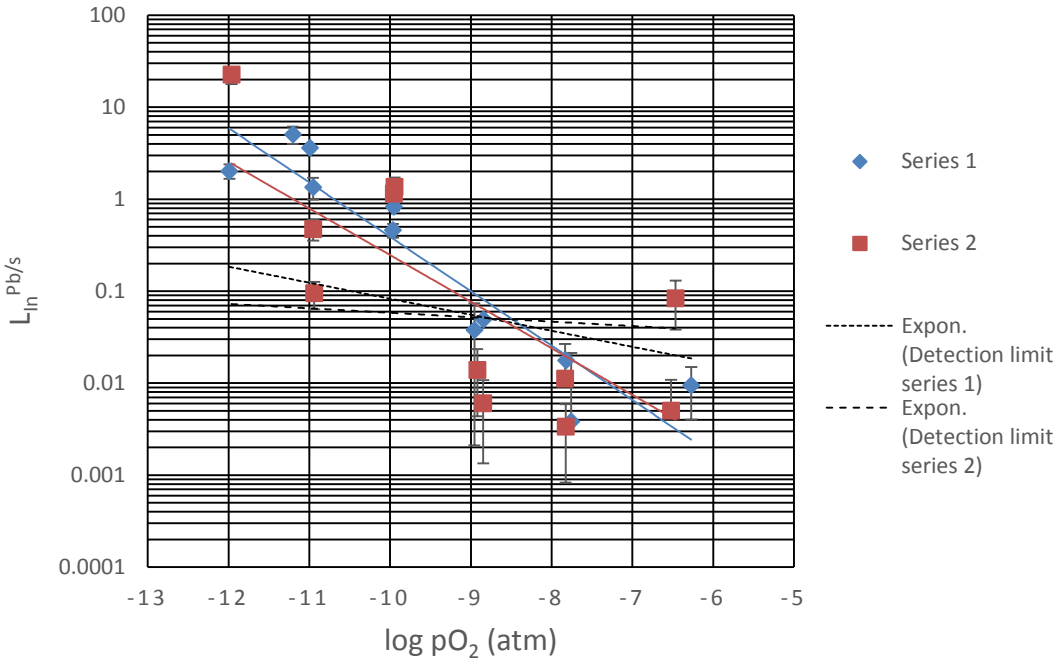

Figure 58 Distribution coefficient of indium between lead and slag in series 1 and 2.

7.9 Distribution and behaviour of tin

In the lead phase tin is dissolving at the reducing conditions. That happens in the first and second series. For both series, tin starts to dissolve in the lead phase at $pO_2 = 10^{-9}$ atm, as seen in Figure 59. The values of lead in oxidising conditions are below the detection limits and so the values for tin in lead are unreliable. There is no trend for the concentration of tin in the slag phase (Figure 60). Clearly more tin is dissolved in the slag at higher oxygen partial pressures than in the lead phase.

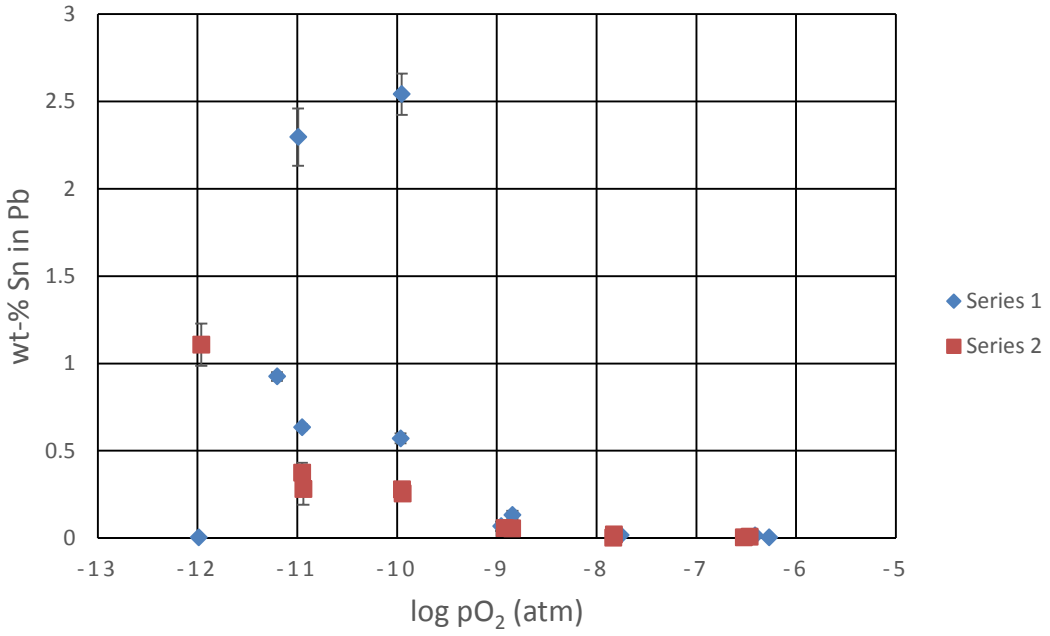

Figure 59 Concentration of tin in the lead phase in series 1 and 2.

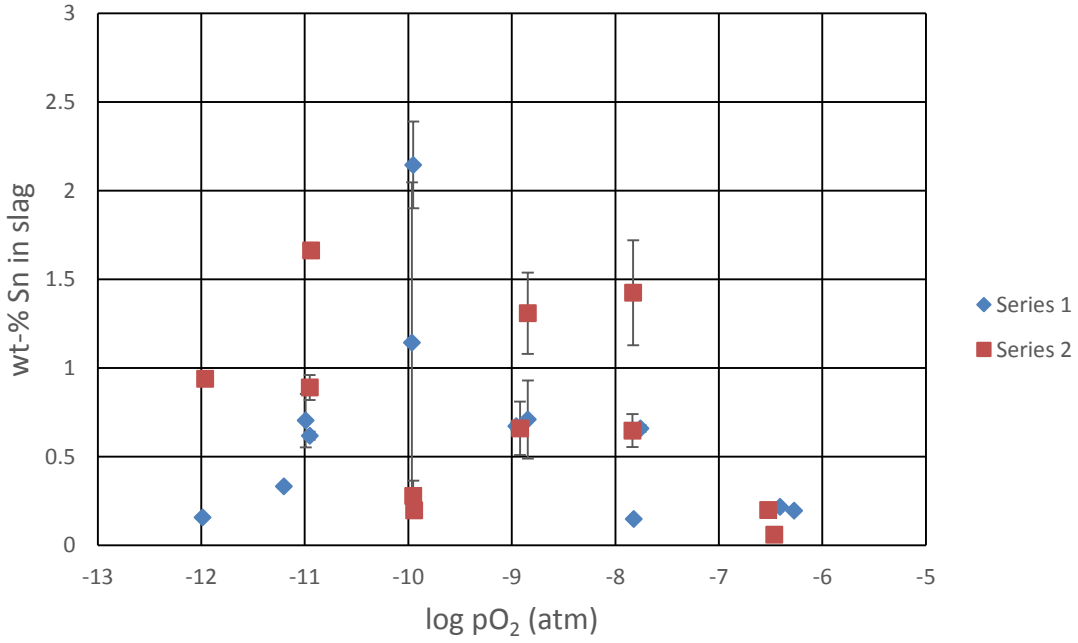

Figure 60 Concentration of tin in the slag phase in series 1 and 2.

The distribution coefficients for tin are presented in Figure 61. The distribution coefficients in the oxidising region are beneath the detection limits, so these results

are not reliable though they give a hint on the distribution for tin. The oxidation state of tin in the slag is close to Sn^{2+} or SnO. There are points that are scattering from the other points for example at oxygen partial pressure 10^{-12} atm in series 1. In series 2 there is scattering in oxidising conditions.

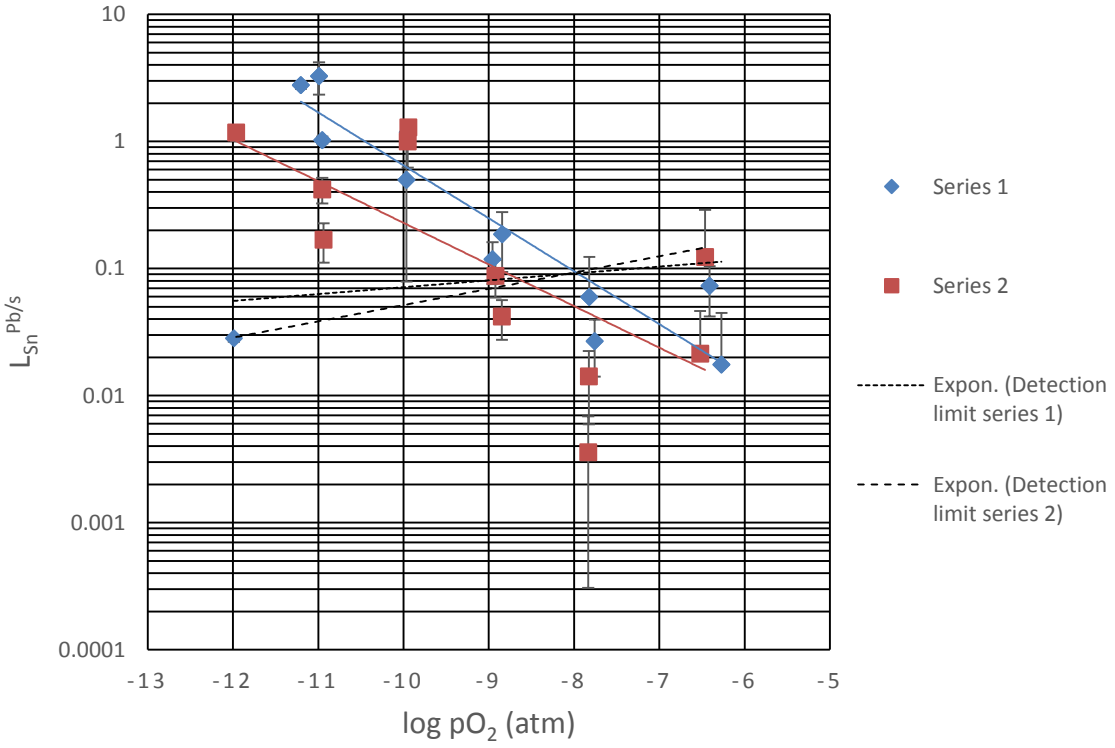

Figure 61 Distribution of tin between lead and slag in series 1 and 2.

8 Discussion

Most of the trace elements showed some kind of trend in solubility in lead or slag, depending on the oxygen partial pressure. In this chapter, the results are compared with the previous research. Lead concentration is decreasing in the lead phase when the oxygen partial pressure is lowered. The decrease is due to the dissolution of trace elements in the lead phase.

A previous study concluded that gallium deports to pig iron in a blast furnace (Chernousov et al., 2010). This is in contradiction with the result in this work were most gallium dissolves in the slag. However, Chernousov et al. (2010) studied the gallium distribution in iron smelting at carbon saturation and this work deals with lead smelting.

The distribution coefficients for gallium in this work have a large scatter. Because of this it is difficult to conclude what oxidation state gallium has in the slag. As mentioned before, there is no previous studies to compare the results with. The conclusions made in this study are that gallium dissolves as pure metal in the slag and more gallium dissolves in slag than in lead phase. The metal-slag distribution coefficients for gallium obtained are between 0.01-0.8.

Germanium seems to be dependent on temperature when comparing the results of this work with the previous studies by Henao et al. (2010) and Yan & Swinbourne (2003) (Figure 62). The slag composition and the type of crucible may also change the distribution coefficients. The temperature in this work was 1150 °C and in the previous works 1200 °C. Also the oxidation state seem to be another (Ge^{+}) in this work compared to the previous ones. The scatter of the data points is great in this work so the results are questionable. Moreover, many points in the alloy were under the detection limit. Henao et al. (2010) mentioned that the temperature does not have any effect on the distribution coefficient but in this work the distribution coefficient varies clearly from the previous studies. The distribution coefficients

between metal and slag in this work are around 0.1-8 and they are about two orders of magnitude higher than obtained earlier.

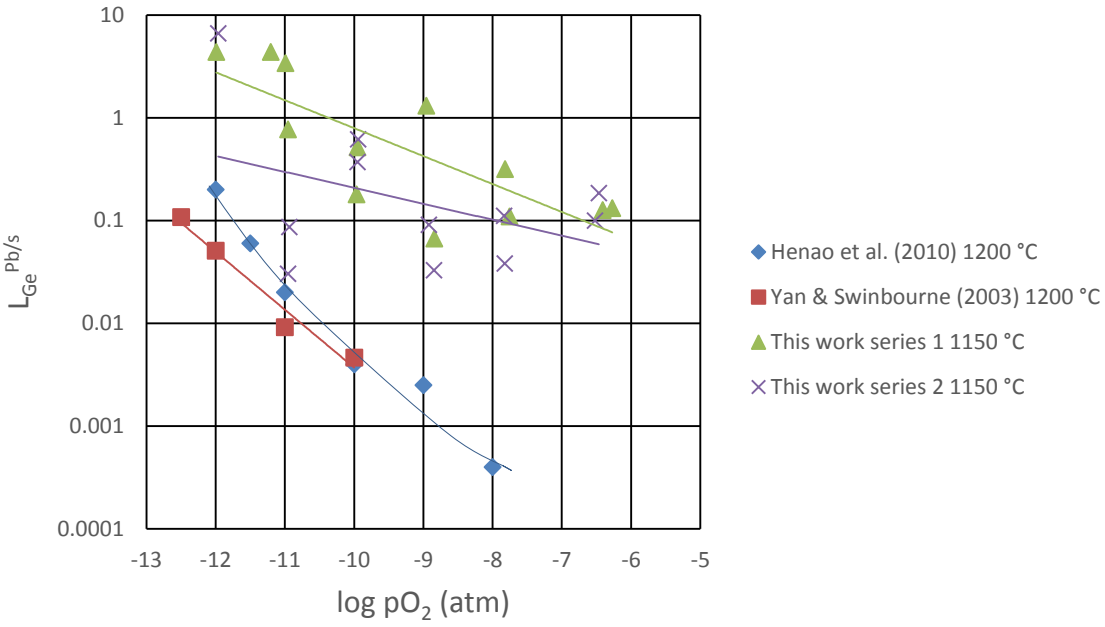

Figure 62 Comparison of germanium distribution coefficients in this work and other works at different temperatures.

The obtained indium distribution between lead and slag is compared with three other studies (Figure 63). Johnson et al. (1983) concluded that indium concentration in slag is 0.02-0.2 % and in bullion 0.5-2.0 %. Henao et al. (2010) showed that if the temperature is raised to 1300 °C indium dissolves even more to lead phase and if it is lowered to 1150 °C indium distribution coefficient decreases only a little. This is also the case in this work. The oxidation state is closer to the results of Yan and Swinbourne (2003). The distribution coefficients between metal and slag are around 0.003-11 for indium in this work.

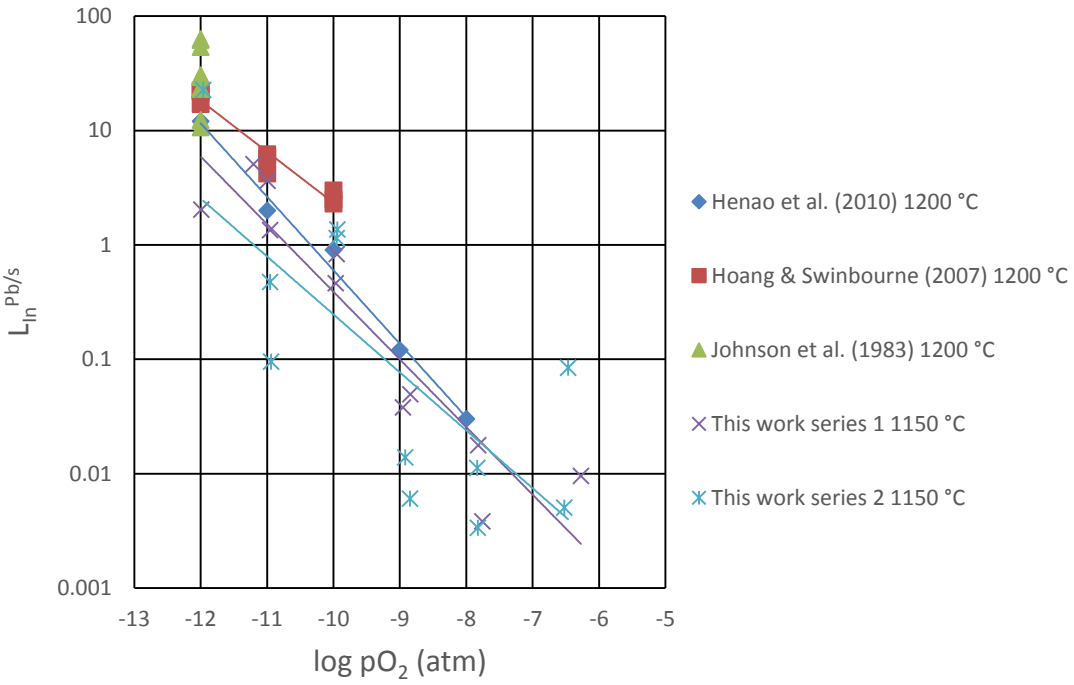

Figure 63 Comparison of indium distribution coefficients in this work and other works at different temperatures.

The results for tin distribution in this work are compared with the previous studies of Toubartz (1991) and Rytkönen et al. (1985, 1987) (Figure 64). It can be noticed in previous studies that in oxidising conditions the slope starts to have a greater angle. This means that the oxidation state of tin is changing to a higher oxidation state when the oxygen partial pressure is raised.

Toubartz (1991) has the only study to include results at 1150 °C and in their study the distribution coefficient seems to decrease as temperature decreases. Overall, the results of this work are similar to the results by Toubartz. The slags that are used in previous works and in this work are different from each other. Rytkönen et al. (1985, 1986, 1987) tested the difference between lead silicate and calcium ferrite slags, and they concluded that tin exist as SnO in silicate slags and as SnO_2 in calcium ferrite slags. In this work, tin is closer to SnO in the slag which is due to the use of silicate slag. The metal-slag distribution coefficients for tin obtained in this work are around 0.002-4.

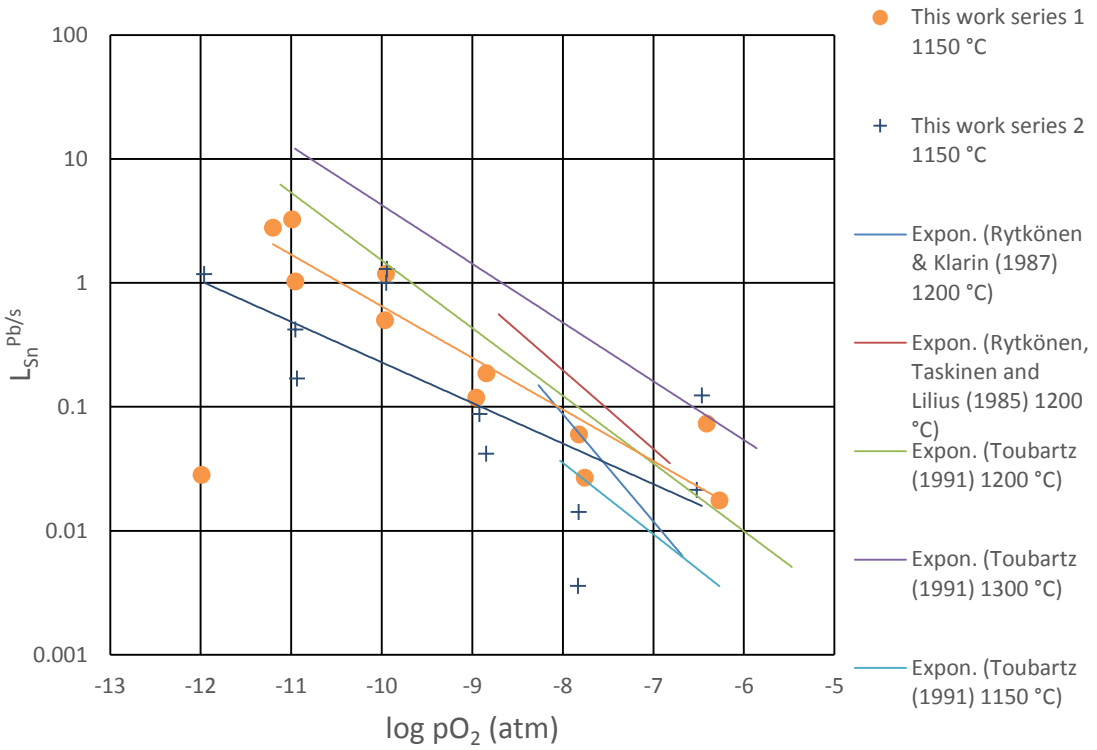

Figure 64 Comparison of tin distribution coefficients in this work and other works at different temperatures.

The experiments in this work were carried out in a sulphur free atmosphere. Previous studies have been executed with both sulphur containing gas and without. Still, the experiments in this work show similar behaviour as previous studies. Many of the results in this work were close (or below) to the detection limits and therefore there is an uncertainty factor present in the results obtained.

9 Summary

The distributions of gallium, germanium, indium and tin between lead and PbO-SiO_2-CaO-FeO-slag at 1150 °C have been investigated in this work. The method for investigation consisted of equilibrium, quick quenching and EPMA analysis. This research method is quite new and have been implemented in the last years. Two series were made with 12 experiments in the first and 11 in the second batch. Trace elements were added as oxides in the first series and as metals in the second series. The flowing gas atmosphere in the experiments consisted of CO and CO_2 and was adjusted to get low oxygen partial pressures (10^{-7}-10^{-12} atm) . The partial pressures and the slag compositions were determined by the programs HSC and MTDATA.

The metal-slag distribution coefficients for the trace elements ($L^{Pb/s}$) were calculated from the EPMA-analyses and were plotted against oxygen partial pressures. From these graphs, it was possible to see if the trace elements dissolve in the slag or if any of them distributes more preferentially to the lead phase. Most of the elements formed pretty clear trends between the distribution coefficient and oxygen partial pressure. The results were also compared with the previous studies in the literature. Overall, the experimental standard deviations were large for several elements. The conclusions are that the more reducing the conditions are the more the elements distribute to the lead phase, except in the case of gallium. The slag compositions affect the oxidation states of different trace elements.

The element concentrations were close or below to the detection limits of EPMA in the lead phase causing uncertainties to the results. Moreover, in many samples the lead phase regions were small and because of this in sample SY46 only 7 points were analysed in the lead phase.

In this work a pseudo-wollastonite crucible was used, which has not been used in similar lead smelting research projects before. The previous studies have been employing magnesia and alumina crucibles. The selection used was to make sure that

the experiments would be executed in true pseudo-wollastonite saturated conditions and without contamination in the slag.

Gallium was investigated for the first time in lead smelting and gave interesting results as the distribution coefficient seem to be nearly constant along the oxygen partial pressure. The temperature seem to affect the distribution of germanium when comparing with previous studies. The crucible and the slag composition could have affected the distribution. Indium showed similar results compared to the previous studies. The temperature or slag composition do not seem to have the similar effect on the distribution of indium as in the case of germanium. Tin showed also similarities with previous works but this work give new understanding of the tin distribution at 1150 °C as it was investigated in more reducing conditions than before. The distribution coefficient for tin seems to be dependent on the temperature. The metal-slag distribution coefficients for the studied trace elements are very low. The trace elements have a tendency to dissolve in the slag and especially at higher oxygen partial pressures in oxidising conditions.

Challenging in the work was that lead had difficulties to stay in the crucibles during the experiments and severe volatilization was observed, in particular in the first experimental series. The distribution coefficients for gallium, germanium, indium and tin were determined in this work. There are not many studies regarding these elements in lead smelting and therefore it would be useful to investigate the behaviour of these elements to get more information and knowledge about them.

10 Proposals for further research

There are a few proposals that could be investigated further regarding the trace element (Ga, Ge, In and Sn) distributions in the lead smelting. This work was performed in one temperature and the knowledge about the element distributions would be expanded if experiments were made in 1200 °C and 1300 °C. Also different slag compositions, CaO/SiO_2-ratios, could be tested to see if they have any effect on the distributions. Investigation is needed on how the slag should be prepared in order to avoid lead losses and volatilization of PbO from the slag.

In this work, EPMA was employed for analysing but to get more accurate results it would be good to analyse some of the samples with laser ablation inductively coupled mass spectrometry (LA-ICP-MS). The results for gallium are still a bit unclear and there are no previous research on the behaviour of gallium in lead smelting and therefore this should be something to investigate even more. The activity coefficients could be defined if more accurate results would be obtained for the trace elements distribution.

11 References

Alfantazi, A. M. & Moskalyk, R. R., 2003. Processing of indium: a review. Minerals Engineering, August, 16(8), pp. 687-694.

Anindya, A., Swinbourne, D. R., Reuter, M. A. & Matusewicz, R. W., 2013. Distribution of elements between copper and FeO_x–CaO–SiO_2 slags during pyrometallurgical processing of WEEE Part 1 – Tin. Mineral Processing and Extractive Metallurgy (Trans. Inst. Min. Metall. C), 122(3), pp. 165-173.

Anindya, A., Swinbourne, D. R., Reuter, M. A. & Matusewicz, R. W., 2014. Distribution of elements between copper and FeO_x–CaO–SiO_2 slags during pyroprocessing of WEEE: Part 2 – indium. Mineral Processing and Extractive Metallurgy (Trans. Inst. Min Metall. C), 123(1), pp. 43-52.

Blanpain, B., Arnout, S., Chintinne, M. & Swinbourne, D. R., 2014. Lead Recycling. In: Handbook of recycling. s.l.:Elsevier, pp. 95-111.

Chai, L.-y.et al., 2015. Behavior, distribution and environmental influence of arsenic in a typical lead smelter. Journal of Central South University, 22(4), pp. 1276-1286.

Chaudhuri, K. B., Koch, M. & Patino, J. L., 1980. The technical-scale realization of the Kivcet Process for lead. CIM Bulletin, May, pp. 146-150.

Chernousov, P. I., Golubev, O. V. & Petelin, A. L., 2010. Study of gallium behavior in blast furnace smelting. Metallurgist, 54(5-6), pp. 285-290.

Crowson, P., 2006. 4 - Lead. In: M. Thompson, ed. Base Metals Handbook (Third edition). Cambridge: Woodhead Publishing, pp. 4-1-4-75.

Davidson, A. et al., 2000. Lead. In: Ullmann's Encyclopedia of Industrial Chemistry. Wiley-VCH Verlag GmbH & Co. KGaA.

Ermisch, D.-I. H., 1953. Über die Verteilung von Silber und Gold auf Blei, Speise und Stein. Berlin-Charlottenburg: Technischen Universität Berlin-Charlottenburg.

Errington, B., Arthur, P., Wang, J. & Dong, Y., 2005. The ISA-YMG Lead Smelting Process. Kyoto, PbZn 2005 Conference, pp. 1-14.

European Commission, 2001. Reference Document on Best Available Techniques in the Non Ferrous Metals Industries,

European Commission, 2014. Best Available Techniques (BAT) Reference Document for the Non-Ferrous Metals Industries, European IPPC Bureau.

Fischer II, G. T. & Bennington, K. O., 1991. Solubility of Lead and Distribution of Minor Elements Beetween Bullion and Calcium Ferrite Slag at 1250 °C, Albany: United States Department of The Interior, Bureau Of Mines.

Ganesan, R., Gnanasekaran, T. & Srinivasa, R. S., 2006. Diffusivity, acticty and solubility of oxygen in liquid lead and lead-bismuth eutectic alloy by electrochemical methods. Journal of Nuclear Materials, 349(1-2), pp. 133-149.

Han, Y. S. & Park, J. H., 2015. Thermodynamics of Indium Dissolution Behavior in FeO-Bearing Metallurgical Slags. Metallurgical and Materials Transaction B, February, Volume 46B, pp. 235-242.

Han, Y. S., Swinbourne, D. R. & Park, J. H., 2015. Thermodynamics of Gold Dissolution Behavior in $CaO-SiO_2-Al_2O_3-MgO_{sat}$ Slag System. Metallurgical and Materials Transactions B, 14 July.pp. 1-9.

Hecker, E., Friedrich, B. & Göhlke, J., 2004. Treatment of lead and zinc slags in hollow electrode DC-EAF in consideration of calculated phase equilibria and thermodynamics. VII International Conference on Molten Slags Fluxes and Salts, The South African Institute of Mining and Metallurgy, pp. 377-383.

Helin, G. et al., 2012. Design and commissioning of the Ausmelt TSL lead smelter at Yunnan Tin Company Limited. In: J. P. Downey, T. P. Battle & J. F. White, eds. International Smelting Technology Symposium (Incorporating the 6th Advances in Sulfide Smelting Symposium). TMS, 2012, pp. 11-21.

Henao, H., Hayes, P., Jak, E. & Richards, G., 2010. Research on Indium and Germanium Distributions between Lead Bullion and Slag at Selected Process Conditions. John Wiley & Sons, Inc., Hoboken, New Jersey, pp. 1145-1160.

Hoang, G. B. & Swinbourne, D. R., 2007. Indium distribution between $FeO-CaO-SiO_2$ slags and lead bullion at 1200°C. Mineral Processing and Extractive Metallurgy (Trans. Inst. Min Metall. C), 116(2), pp. 133-138.

Hughes, S., Reuter, M. A., Baxter, R. & Kaye, A., 2008. Ausmelt technology for lead and zinc processing. Lead and Zinc 2008, The Southern African Institute of Mining and Metallurgy, pp. 147-162.

Jak, E. & Hayes, P. C., 2010. Phase Chemistry of Lead Smelting Slags. Vancouver, Lead-Zinc 2010, John Wiley & Sons, pp. 1161-1176.

Jia, G.-b., Yang, B. & Liu, D.-c., 2013. Deeply removing lead from Pb-Sn alloy with vacuum distillation. Transactions of Nonferrous Metals Society of China, Volume 23, pp. 1822-1831.

Johnson, E. A., Oden, L. L. & Koch, J. N., 1983. Laboratory investigations on the behavior of accessory elements in lead blast furnace smelting, Albany, Oreg: U.S. Dept. of the Interior, Bureau of Mines.

Katayama, I. et al., 2002. Activity Measurment of Ga in Liquid Ga-Pb Alloys by EMF Method with Zirconia Solid Electrolyte. Journal of Mining and Metallurgy, 38B(3-4), pp. 229-236.

Kinaev, N. N., Jak, E. & Hayes, P. C., 2005. Kinetics of reduction of lead smelting slags with solid carbon. Scandinavian Journal of Metallurgy, Issue 34, pp. 150-157.

King, M. et al., 2014. Lead and Lead Alloys. In: Kirk-Othmer Encyclopedia of Chemical Technology. John Wiley & Sons, Inc, pp. 1-55.

Kudo, M. et al., 2000. Lead Solubility in $FeO_x-CaO-SiO_2$ Slags at Iron Saturation. Metallurgical and Materials Transactions B, February, Volume 31B, pp. 15-24.

Lee, S. H., Moon, S. M., Park, J. H. & Min, D. J., 2002. Thermodynamic Behavior of Nickel in CaO-SiO_2-Fe_tO Slag. Metallurgical and Materials Transactions B, February, Volume 33B, pp. 55-59.

Manasijevic, D., Zivkovic, D. & Zivkovic, Z., 2003. Thermodynamic Analysis of The Ga-Pb Binary System. Journal of Mining and Metallurgy, 39B(3-4), pp. 465-474.

Matousek, J. W., 2011. Oxidation Potentials in Lead and Zinc Smelting. JOM, December, 63(12), pp. 63-67.

Matsura, D., Ueda, S. & Yamaguchi, K., 2011. Lead solubility in FeO_x-CaO-SiO_2-$NaO_{0.5}$ and FeO_x-CaO-SiO_2-$CrO_{1.5}$ Slags under Iron Saturation at 1573 K. High Temperature Materials and Processes, 30(4-5), pp. 441-446.

Matsuzaki, K., Ishikawa, T., Tsukada, T. & Ito, K., 2000. Distribution Equilibria of Pb and Cu between CaO-SiO_2-Al_2O_3 Melts and Liquid Copper. Metallurgical and Materials Transactions B, December, Volume 31B, pp. 1261-1266.

Matyas, A. G. & Mackey, P. J., 1976. Metallurgy of the direct smelting of lead. JOM, November, pp. 10-15.

Melcher, G., Müller , E. & Weigel, H., 1976. The KIVCET cyclone smelting process for impure copper concentrates. JOM, July, pp. 4-8.

Moon, N., Hino, M., Lee, Y. & Itagaki, K., 1997. Phase Equilibrium between Metallic Lead and PbO-FeO_x-CaO-SiO_2 or PbO-FeO_x-CaO-SiO_2-ZnO Slag at 1423 K. Shigen-to-Sozai, 113(8), pp. 635-640.

Moon, N., Hino, M., Lee, Y. & Itagaki, K., 1998. Phase Equilibrium and Minor Elements Distribution Between Metallic Lead and PbO-FeO_x-CaO-SiO_2-ZnO Slag at 1423 K. Metallurgical Review of MMIJ, 15(1), pp. 38-62.

Morachevskii, A. G., 2014. Thermodynamic Properties of Dilute Solutions of Various Elements in Liquid Lead. Russian Journal of Applied Chemistry, 87(12), pp. 1783-1803.

Moskalyk, R. R., 2003. Gallium: the backbone of the electronics industry. Minerals Engineering, 16(2003), pp. 921-929.

Müller, E., 1976. Die Verhüttung von Bleikonzentraten nach dem KIVCET-Verfahren. Erzmetall, 29(7/8), pp. 322-327.

Nikolic, S., Hayes, P. C. & Jak, E., 2008. Phase Equilibria in Ferrous Calcium Silicate Slags: Part III. Copper-Saturated Slag at 1250 °C and 1300 °C at an Oxygen Partial Pressure of 10^{-6} atm. Metallurgical and Materials Transactions B, April, 39(2), pp. 200-209.

Plevachuk, Y. et al., 2003. Investigation of the miscibility gap region in liquid Ga-Pb alloys. Zeitschrift für Metallkunde, 94(9), pp. 1034-1039.

Recycling Today, 2012. SWEEEP Kuusakoski Opens Lead Recovery Furnace. [Online]
Available at: http://www.recyclingtoday.com/article/sweeep-kuusakoski-crt-lead-recovery-furnace
[Accessed 13 August 2015].

Reuter, M., Xiao, Y. & Boin, U., 2004. Recycling and environmental issues of metallurgical slags and salt fluxes. VII International Conference on Molten Slags and Salts, The South African Institute of Mining and Metallurgy, pp. 349-356.

Rytkönen, T. K. & Klarin, A. I., 1987. Distribution equilibria of impurities between lead and calcium ferrite slags. Scandinavian Journal of Metallurgy, Volume 16, pp. 210-213.

Rytkönen, T. & Taskinen, A., 1986. Distribution of Impurities between Lead and Lead Silicate Slags. Scandinavian Journal of Metallurgy, Volume 15, pp. 25-29.

Rytkönen, T., Taskinen, A. & Lilius, K., 1985. Epäpuhtauksien käyttäytyminen suorassa lyijyn valmistuksessa, Espoo: TKK Offset.

Siegmund, A., 2003. Modern applied technologies for primary lead smelting at the beginning of the 21st century. San Diego, California, Wiley.

Solf, H., 1987. Untersuchungen zu heterogenen Gleichgewichten im System Pb-S-O-Me (Me für Cu, Sb, Sn und Tl). Aachen: Dissertation RWTH Aachen.

Taskinen, A. I., Toivonen, L. M. & Talonen, T. T., 1984. Thermodynamics of slags in direct lead smelting. Second International Symposium on Metallurgical Slags and Fluxes, Lake Tahoe, Nevada, The Metallurgical Society of AIME, pp. 741-756.

Toubartz, F. E., 1991. Blei-Schlacken-Verteilungsgleichgewichte unter oxidierenden und reduzierenden Bedingungen. Aachen: Fakultät für Bergbau, Hüttenwesen und Geowissenschaften der Rheinisch-Westfälischen Technischen Hochschule Aachen. p. 189.

van Schaik, A. & Reuter, M. A., 2014. Material-Centric (Aluminum and Copper) and Product-Centric (Cars, WEEE, TV, Lamps, Batteries, Catalysts) Recycling and DfR Rules. In: E. Worrell & M. A. Reuter, eds. Handbook of Recycling. Boston: Elsevier, pp. 307-378.

Wood, J., Coveney, J., Hoang, J. & Reuter, M. A., 2009. Small-Scale Secondary Lead Processing using Ausmelt TSL Technology. Macau.

Yan, S. & Swinbourne, D. R., 2003. Distribution of germanium under lead smelting conditions. Mineral Processing and Extractive Metallurgy (Trans.Inst.Min. Metall.C), 112(August), pp. 75-80.

Yazawa, A., Takeda, Y. & Waseda, Y., 1981. Thermodynamic properties and structure of ferrite slags and their process implications. Canadian Metallurgical Quarterly, 20(2), pp. 129-134.

Zhao, B., Errington, B., Jak, E. & Hayes, P., 2008. Gaseous Reduction Of Isasmelt Lead Slag And Lead Blast Furnace Sinters. Durban Harbour, The Southern African Institute of Mining and Metallurgy, pp. 133-146.

Appendix 1 Pictures of microstructures of the samples

First series

SY50

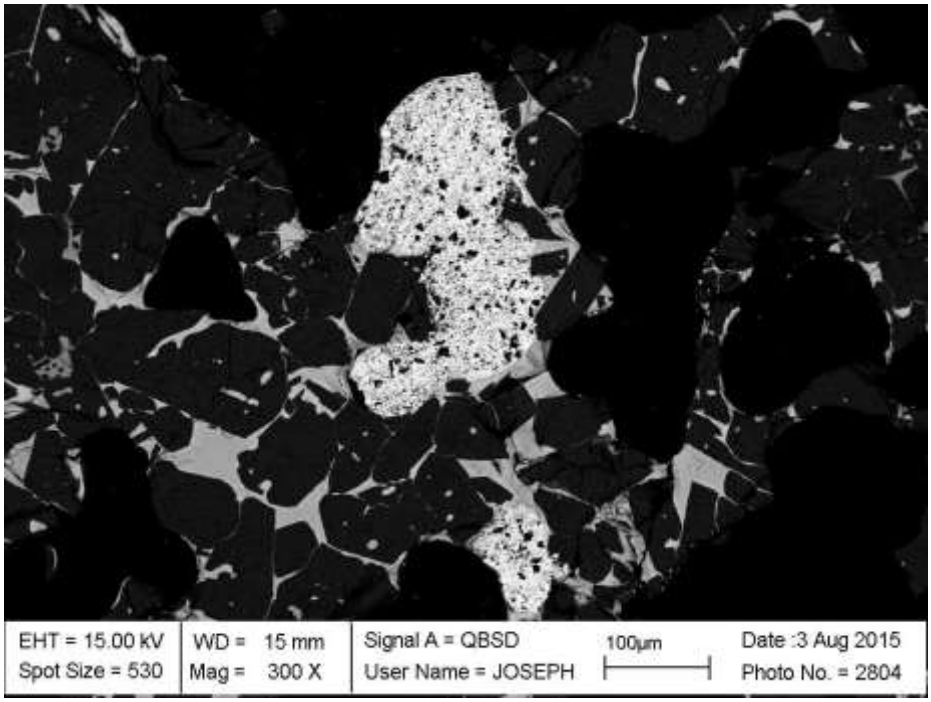

SY51

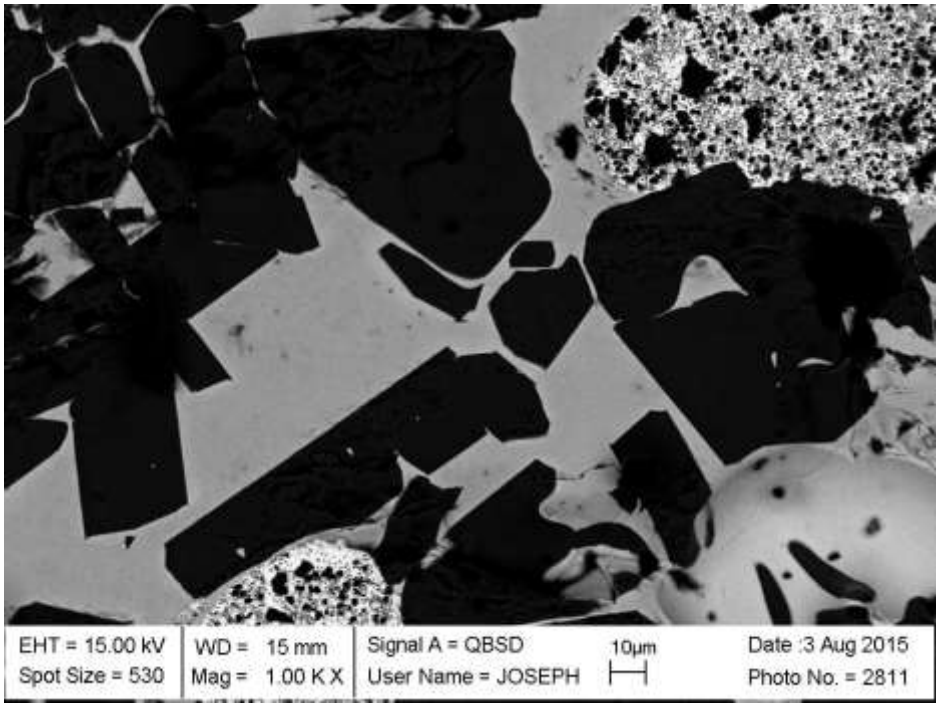

SY31

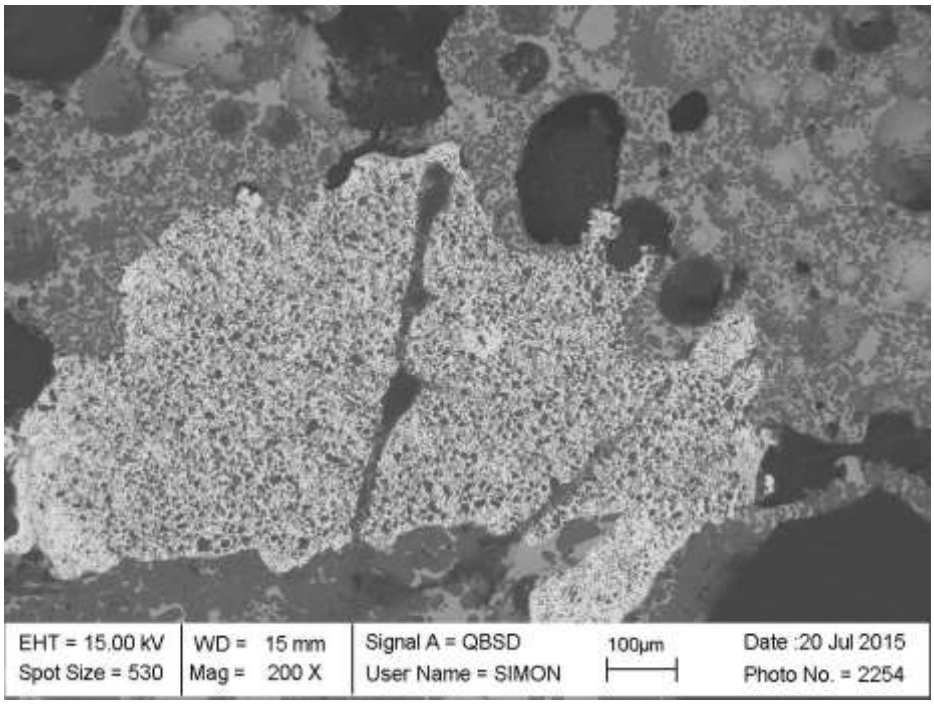
EHT = 15.00 kV
Spot Size = 530
WD = 15 mm
Mag = 200 X
Signal A = QBSD
User Name = SIMON
100µm
Date :20 Jul 2015
Photo No. = 2254

SY37

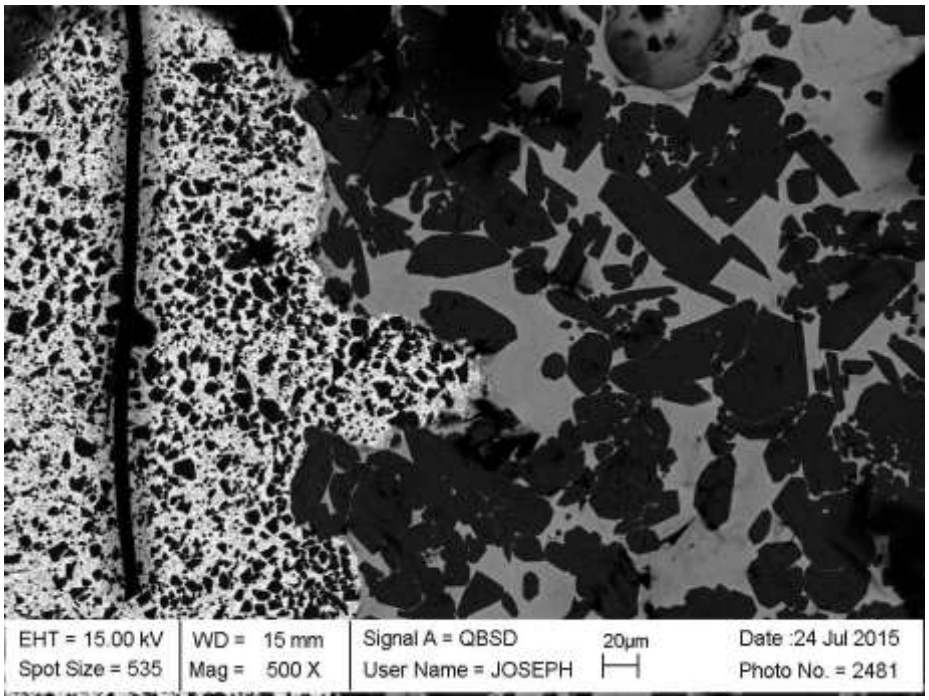
EHT = 15.00 kV
Spot Size = 535
WD = 15 mm
Mag = 500 X
Signal A = QBSD
User Name = JOSEPH
20µm
Date :24 Jul 2015
Photo No. = 2481

SY23

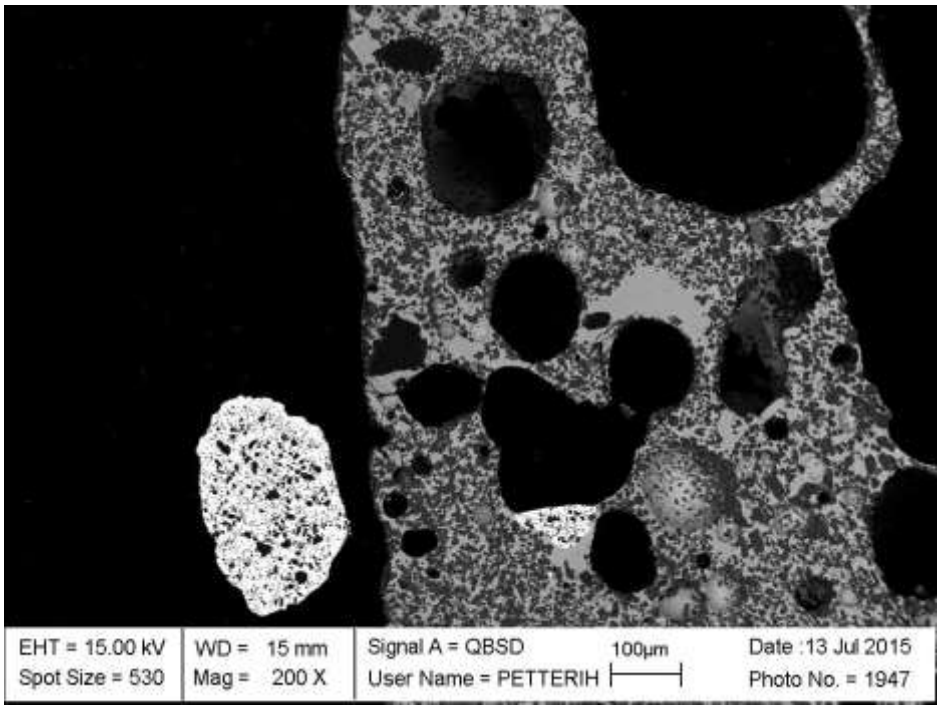
EHT = 15.00 kV
Spot Size = 530
WD = 15 mm
Mag = 200 X
Signal A = QBSD
User Name = PETTERIH
100µm
Date :13 Jul 2015
Photo No. = 1947

SY11

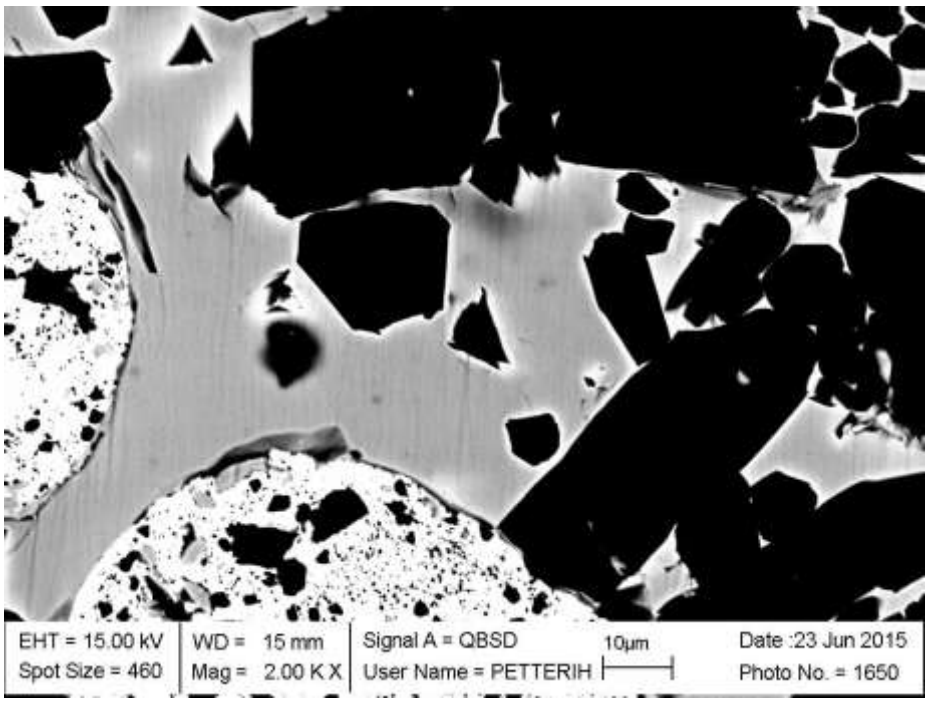
EHT = 15.00 kV
Spot Size = 460
WD = 15 mm
Mag = 2.00 K X
Signal A = QBSD
User Name = PETTERIH
10µm
Date :23 Jun 2015
Photo No. = 1650

SY27

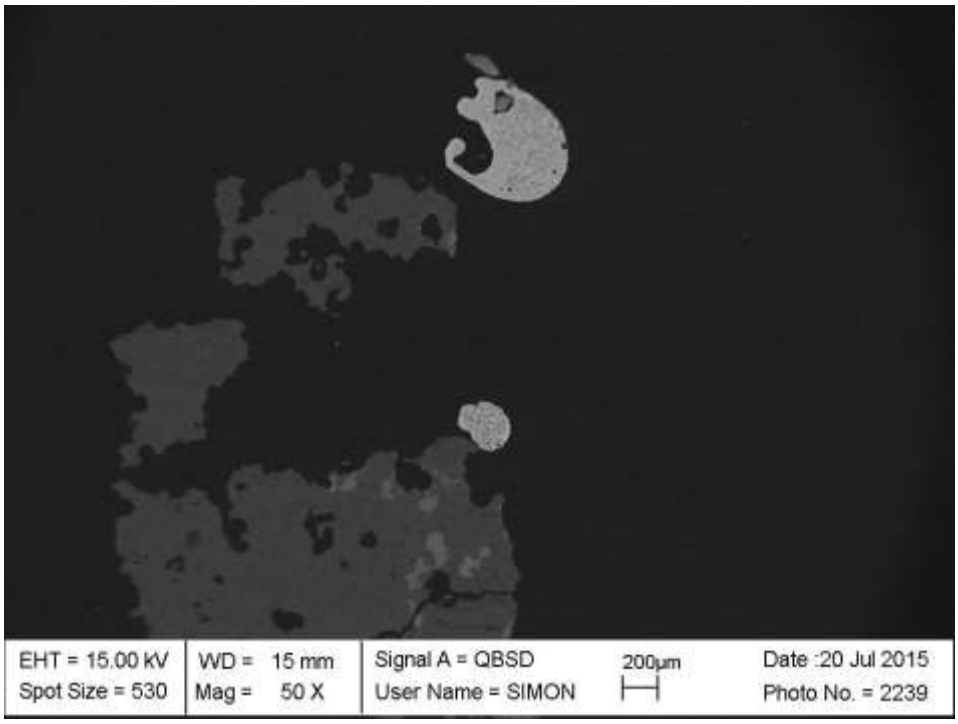
EHT = 15.00 kV
Spot Size = 530
WD = 15 mm
Mag = 50 X
Signal A = QBSD
User Name = SIMON
200µm
Date :20 Jul 2015
Photo No. = 2239

SY13

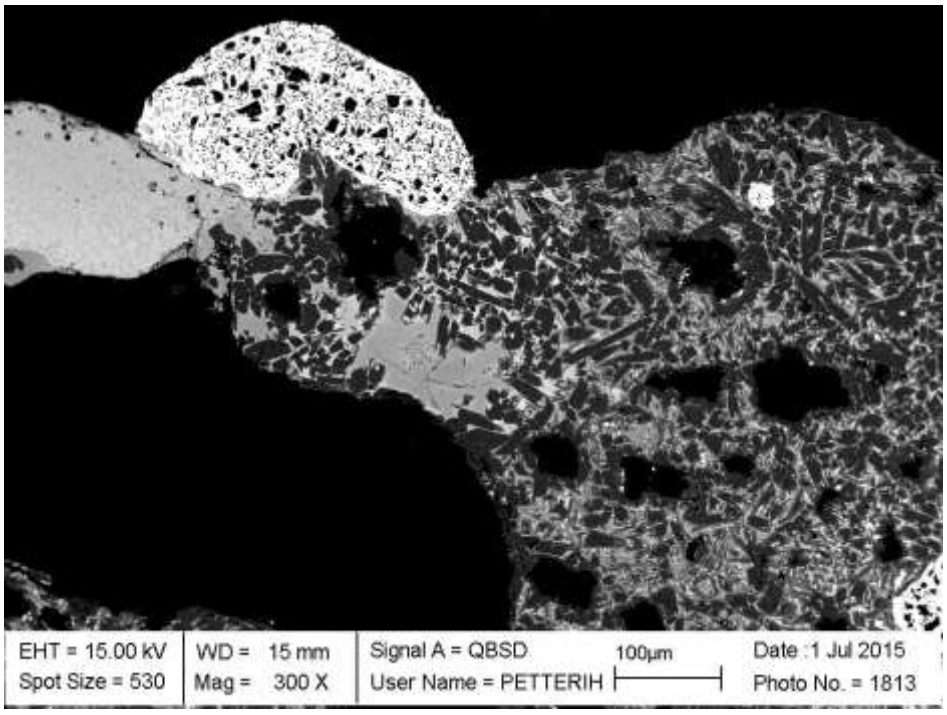
EHT = 15.00 kV
Spot Size = 530
WD = 15 mm
Mag = 300 X
Signal A = QBSD
User Name = PETTERIH
100µm
Date :1 Jul 2015
Photo No. = 1813

SY14

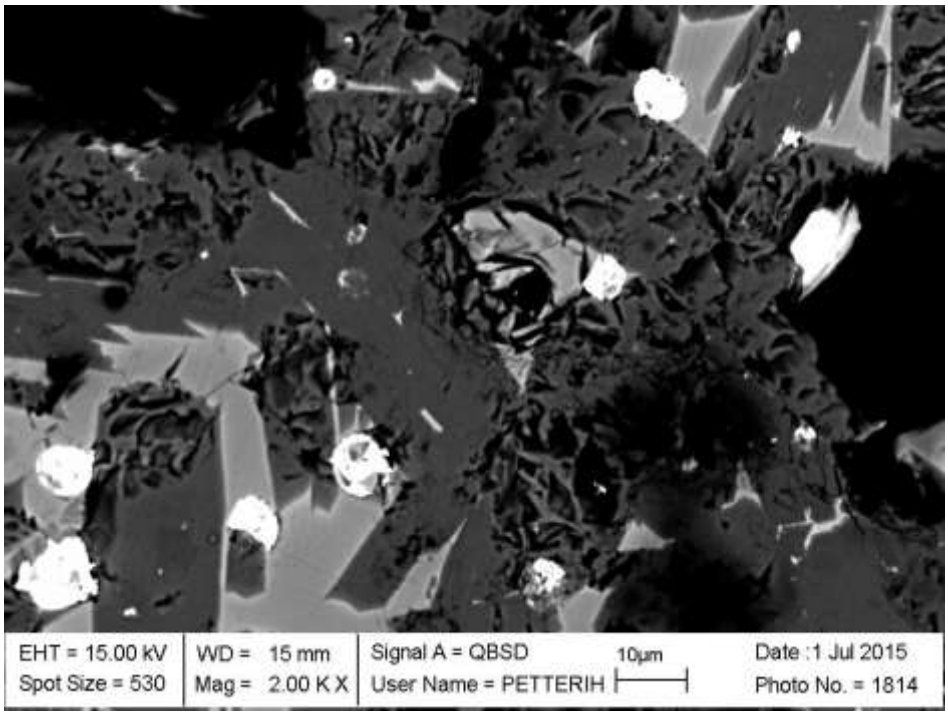
EHT = 15.00 kV
Spot Size = 530
WD = 15 mm
Mag = 2.00 K X
Signal A = QBSD
User Name = PETTERIH
10µm
Date :1 Jul 2015
Photo No. = 1814

SY15

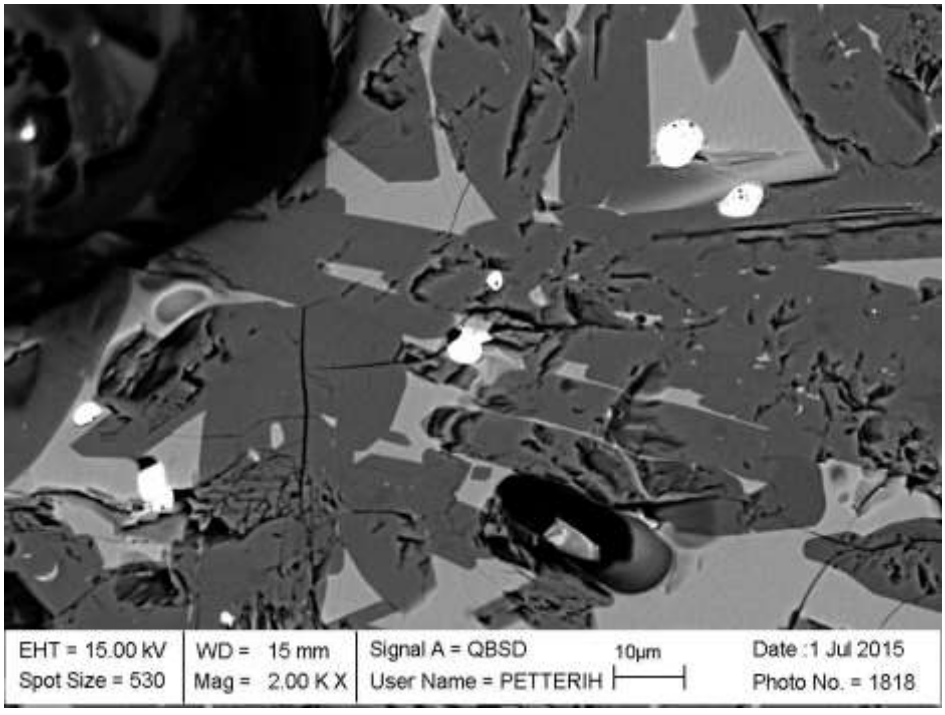
EHT = 15.00 kV
Spot Size = 530
WD = 15 mm
Mag = 2.00 K X
Signal A = QBSD
User Name = PETTERIH
10µm
Date :1 Jul 2015
Photo No. = 1818

SY16

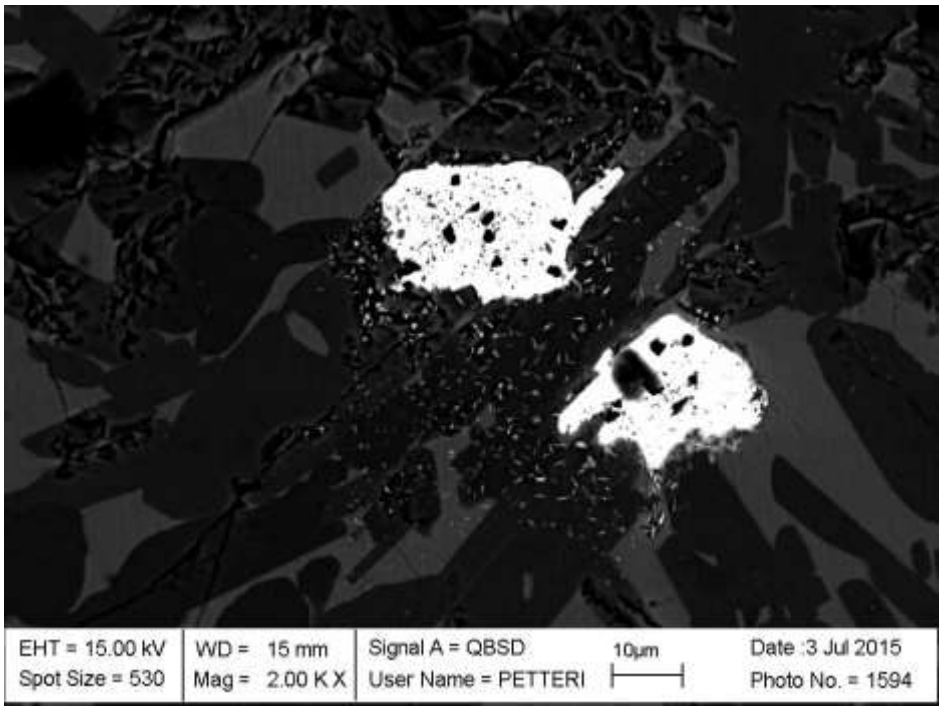
EHT = 15.00 kV
Spot Size = 530
WD = 15 mm
Mag = 2.00 K X
Signal A = QBSD
User Name = PETTERI
10µm
Date :3 Jul 2015
Photo No. = 1594

SY46

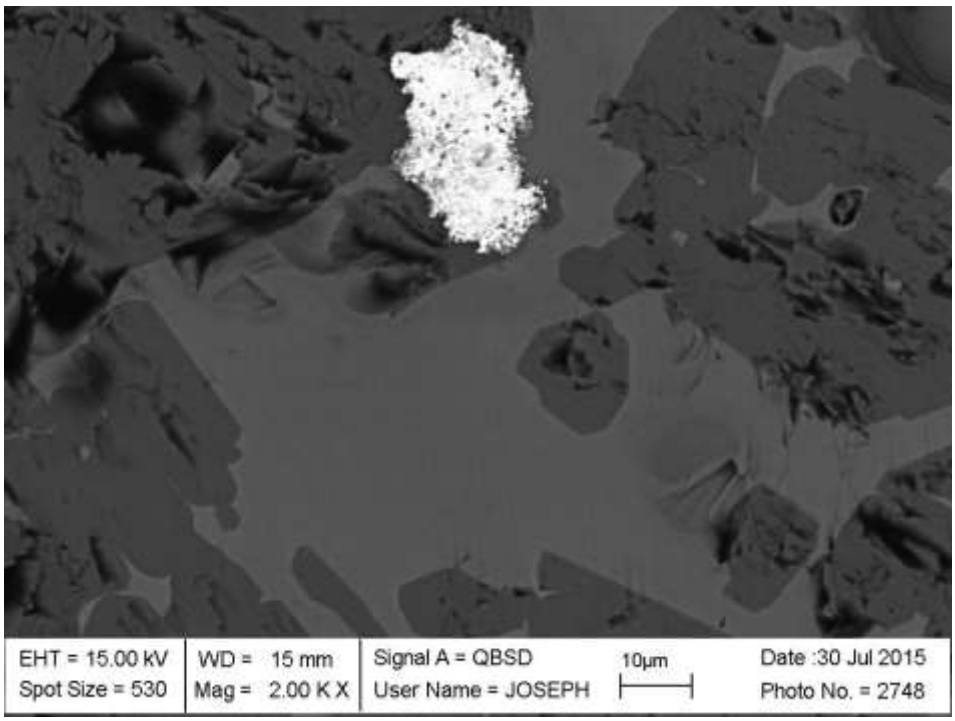
EHT = 15.00 kV
Spot Size = 530
WD = 15 mm
Mag = 2.00 K X
Signal A = QBSD
User Name = JOSEPH
10µm
Date :30 Jul 2015
Photo No. = 2748

Second series

SY48

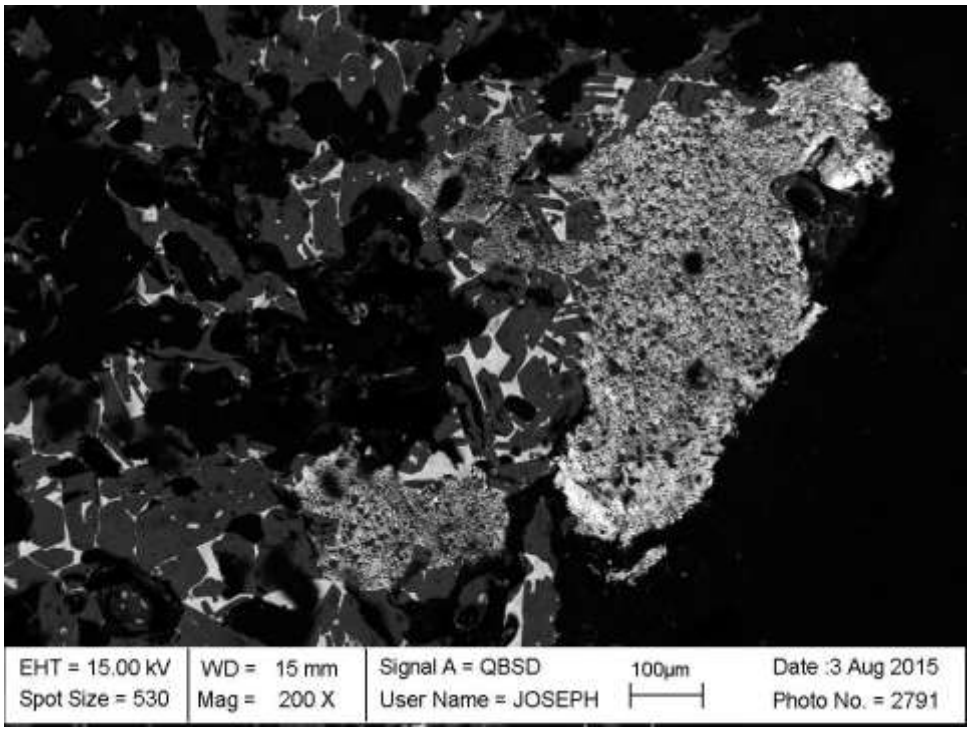

SY49

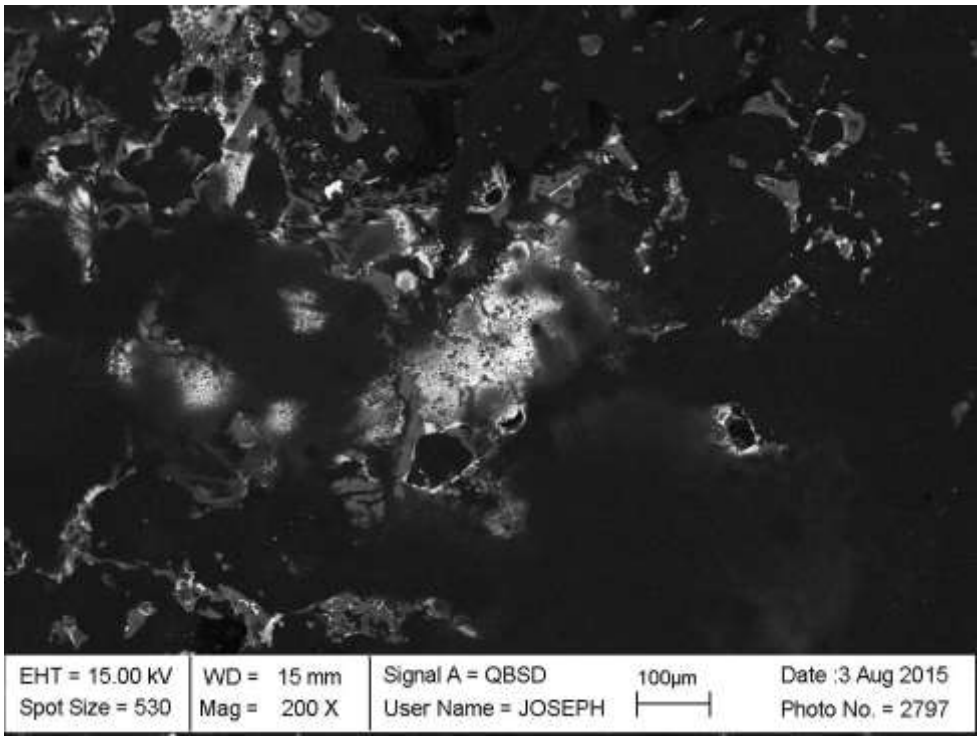

SY33

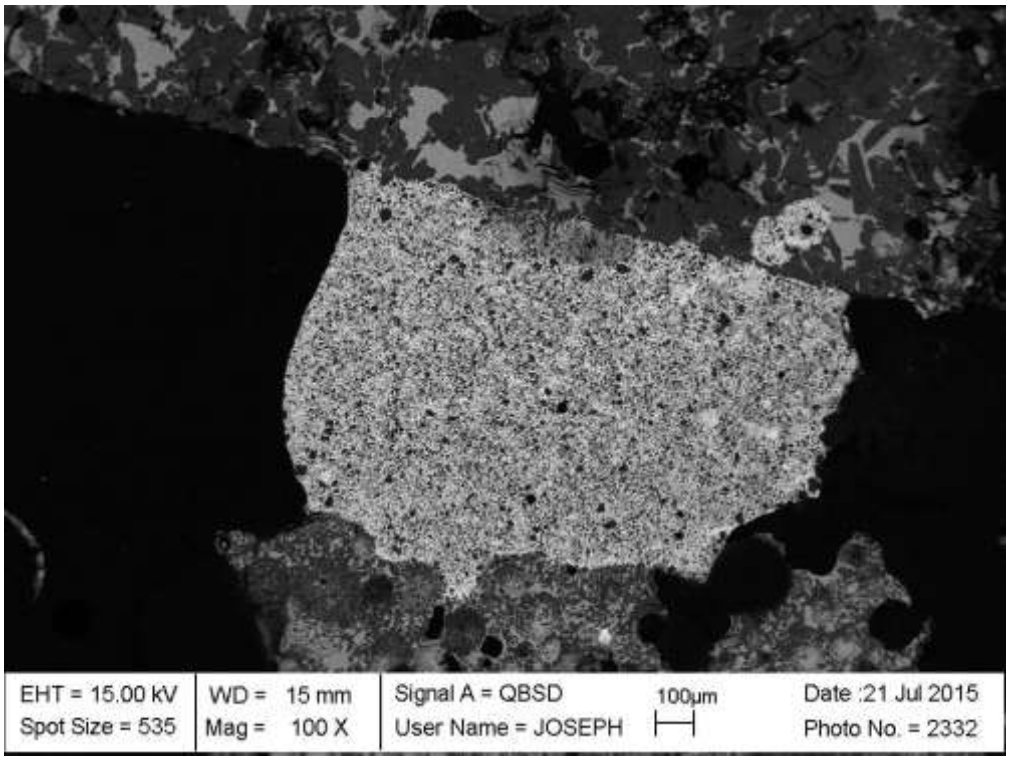
EHT = 15.00 kV
Spot Size = 535
WD = 15 mm
Mag = 100 X
Signal A = QBSD
User Name = JOSEPH
100µm
Date :21 Jul 2015
Photo No. = 2332

SY34

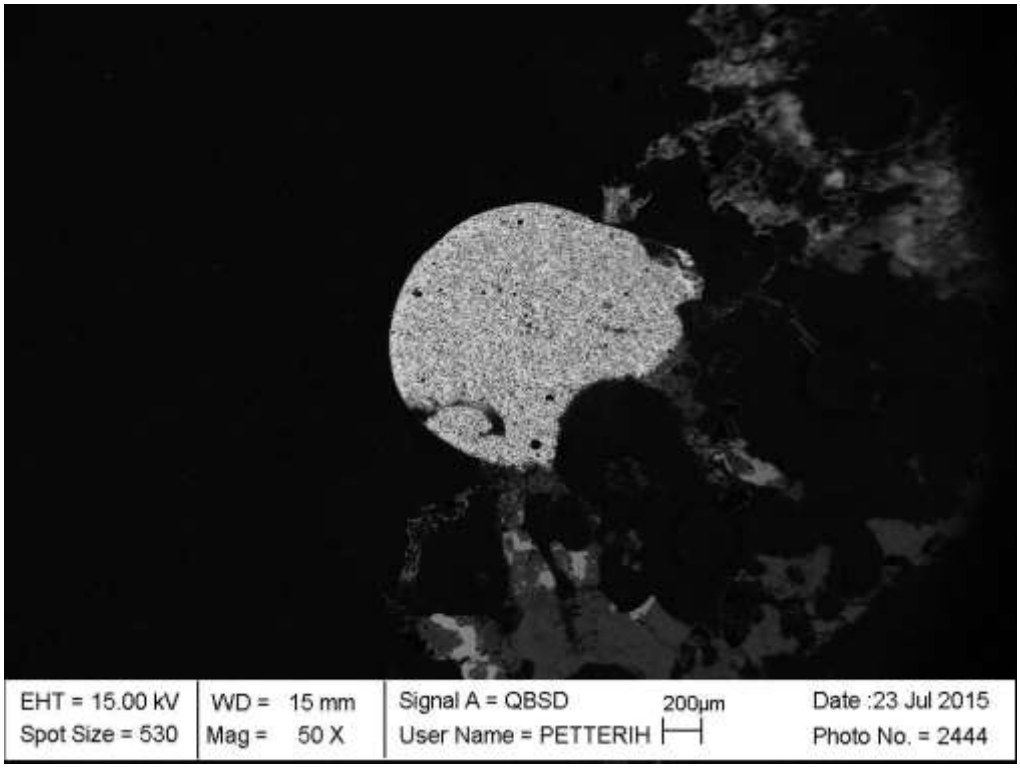
EHT = 15.00 kV
Spot Size = 530
WD = 15 mm
Mag = 50 X
Signal A = QBSD
User Name = PETTERIH
200µm
Date :23 Jul 2015
Photo No. = 2444

SY47

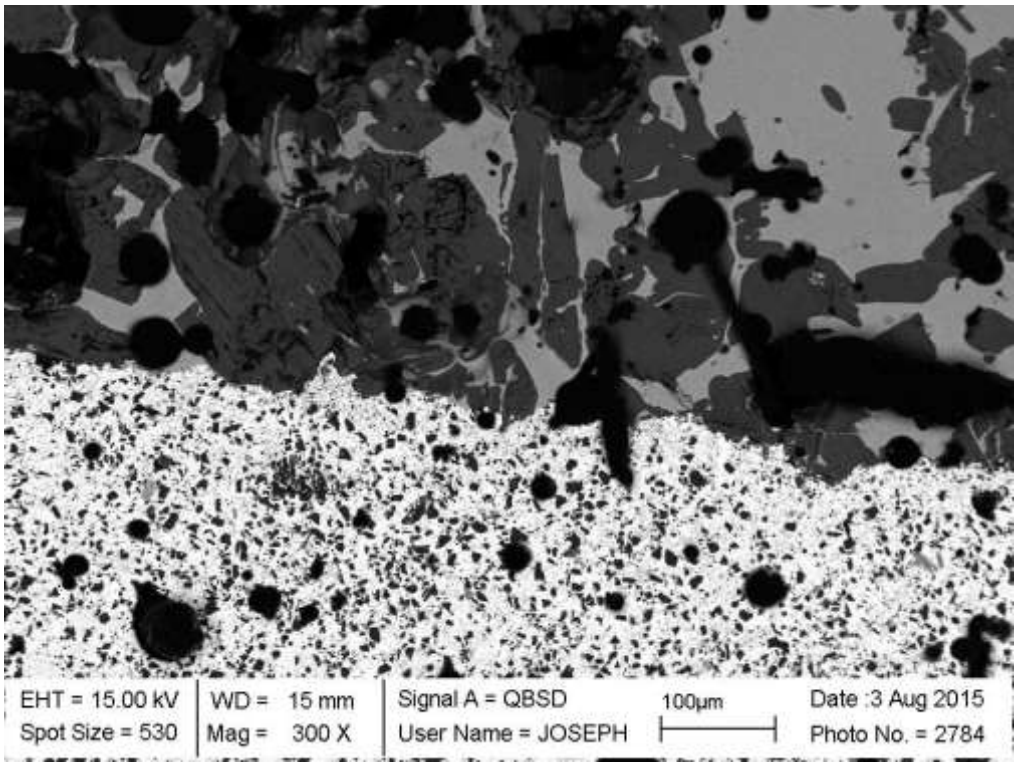
EHT = 15.00 kV
Spot Size = 530
WD = 15 mm
Mag = 300 X
Signal A = QBSD
User Name = JOSEPH
100µm
Date :3 Aug 2015
Photo No. = 2784

SY25

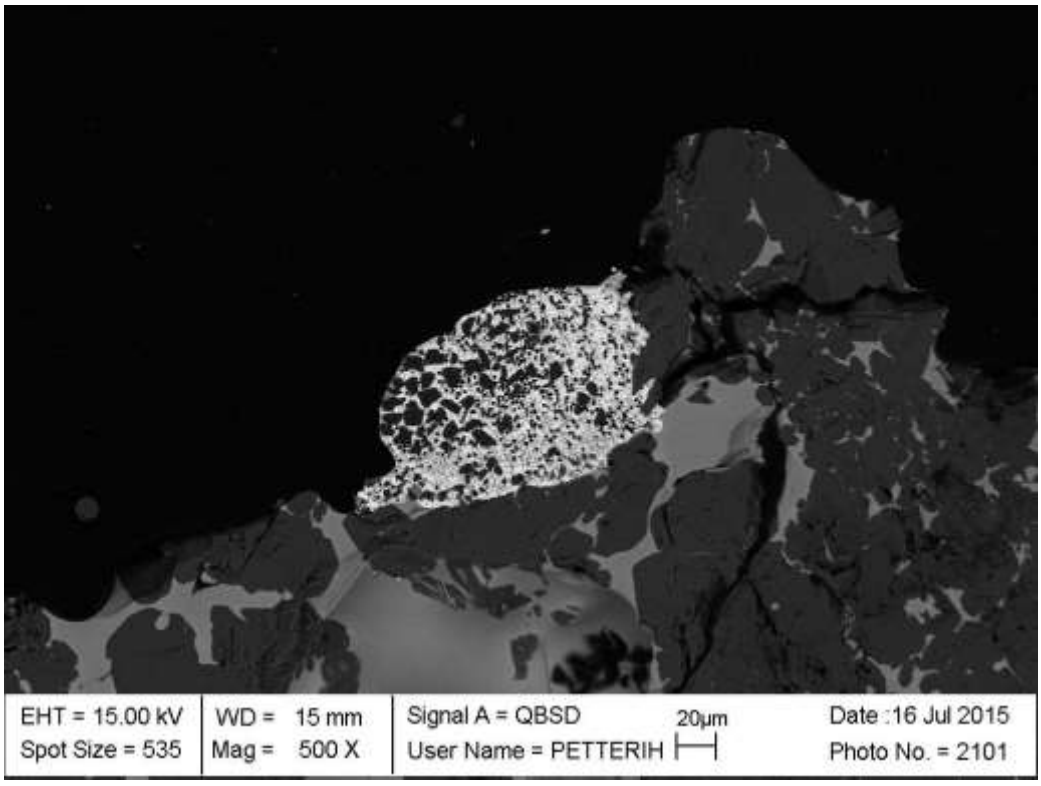
EHT = 15.00 kV
Spot Size = 535
WD = 15 mm
Mag = 500 X
Signal A = QBSD
User Name = PETTERIH
20µm
Date :16 Jul 2015
Photo No. = 2101

SY29

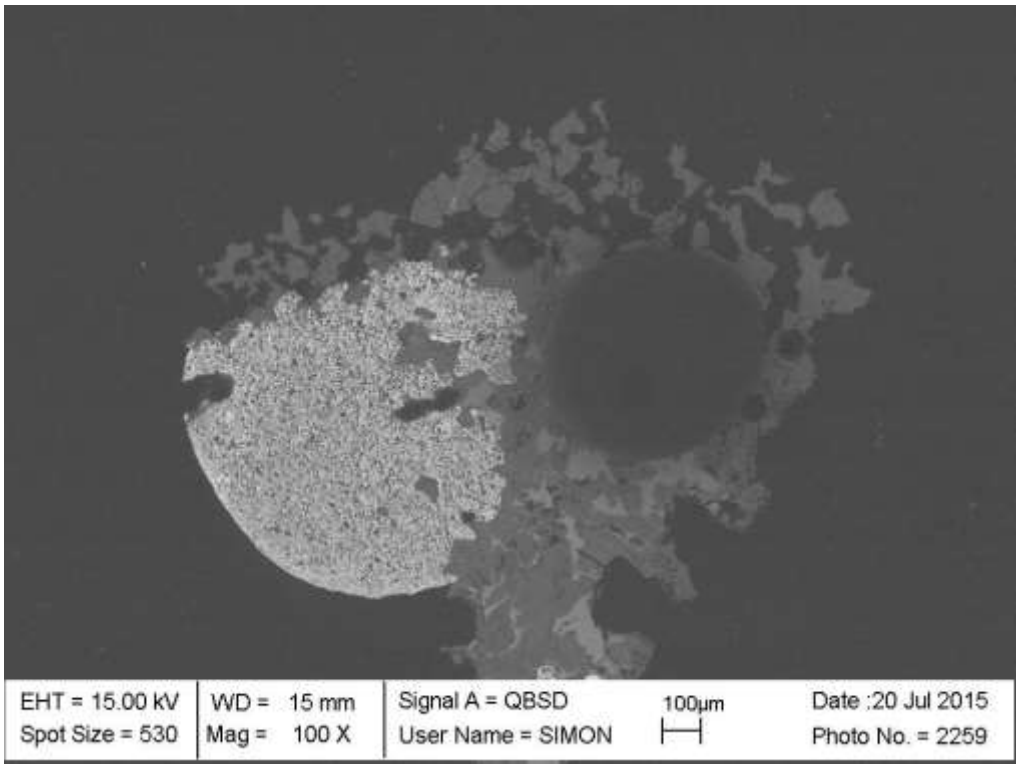
EHT = 15.00 kV
Spot Size = 530
WD = 15 mm
Mag = 100 X
Signal A = QBSD
User Name = SIMON
100µm
Date :20 Jul 2015
Photo No. = 2259

SY30

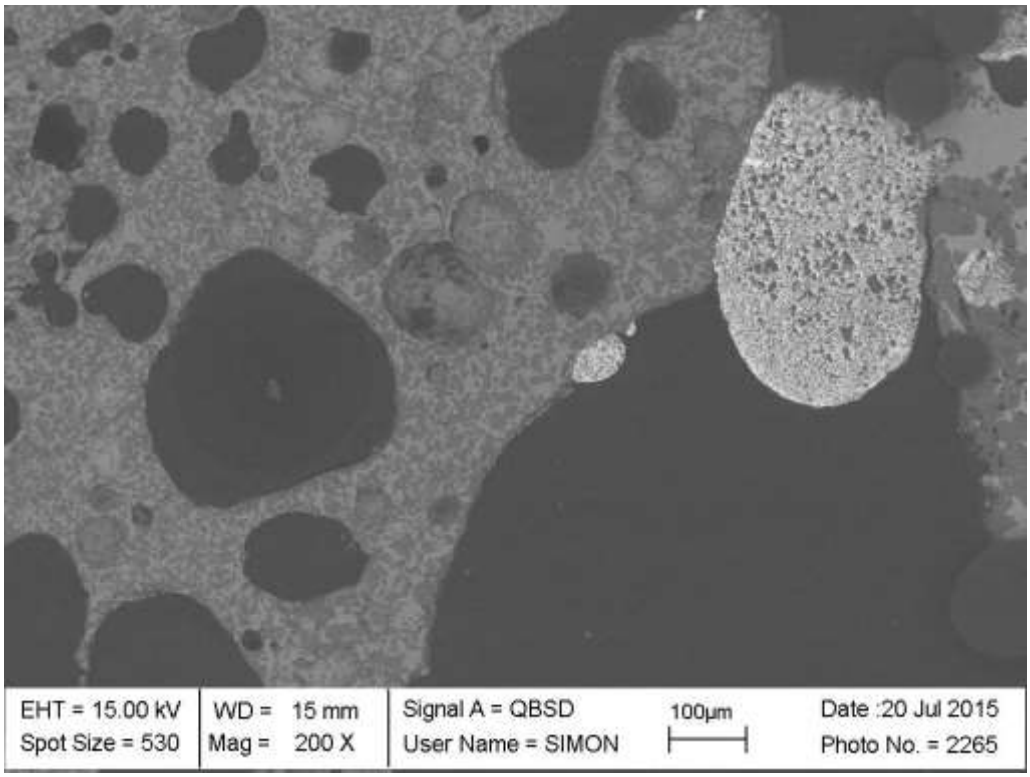
EHT = 15.00 kV
Spot Size = 530
WD = 15 mm
Mag = 200 X
Signal A = QBSD
User Name = SIMON
100µm
Date :20 Jul 2015
Photo No. = 2265

SY41

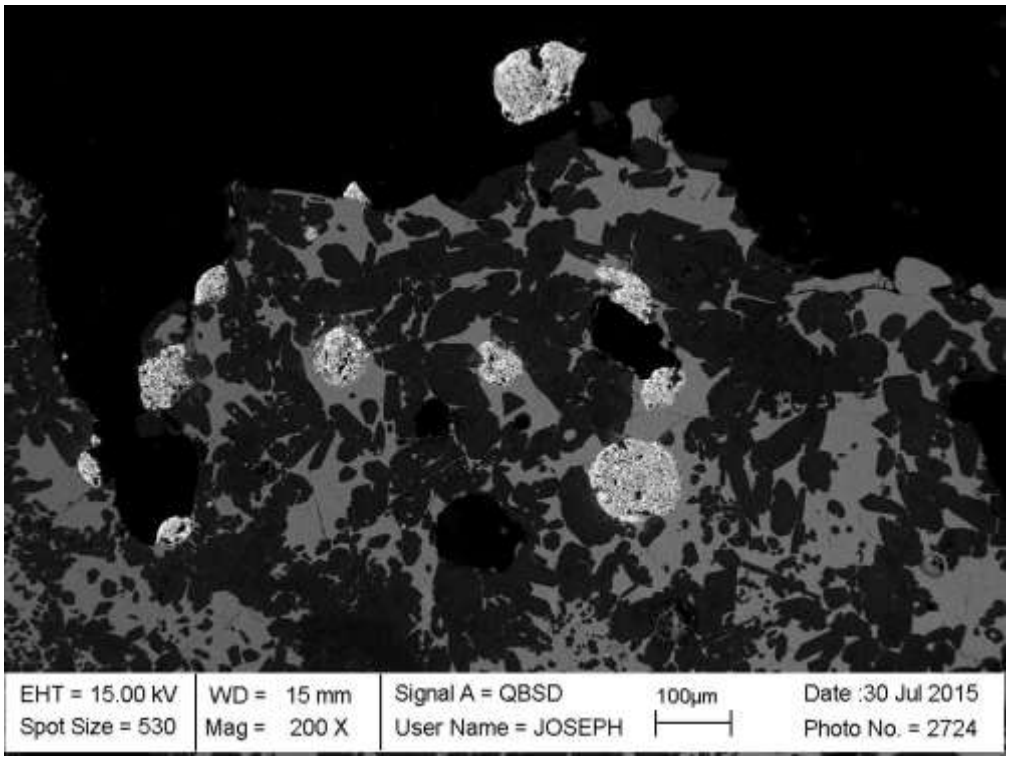
EHT = 15.00 kV
Spot Size = 530
WD = 15 mm
Mag = 200 X
Signal A = QBSD
User Name = JOSEPH
100µm
Date :30 Jul 2015
Photo No. = 2724

SY42

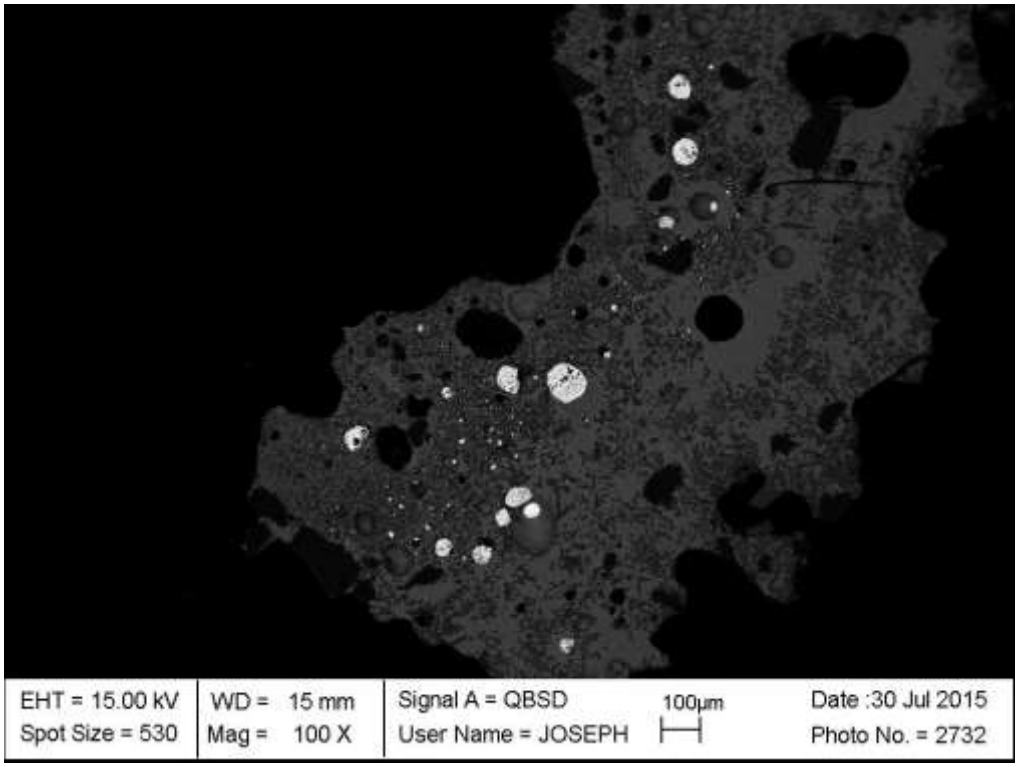
EHT = 15.00 kV
Spot Size = 530
WD = 15 mm
Mag = 100 X
Signal A = QBSD
User Name = JOSEPH
100µm
Date :30 Jul 2015
Photo No. = 2732

SY45

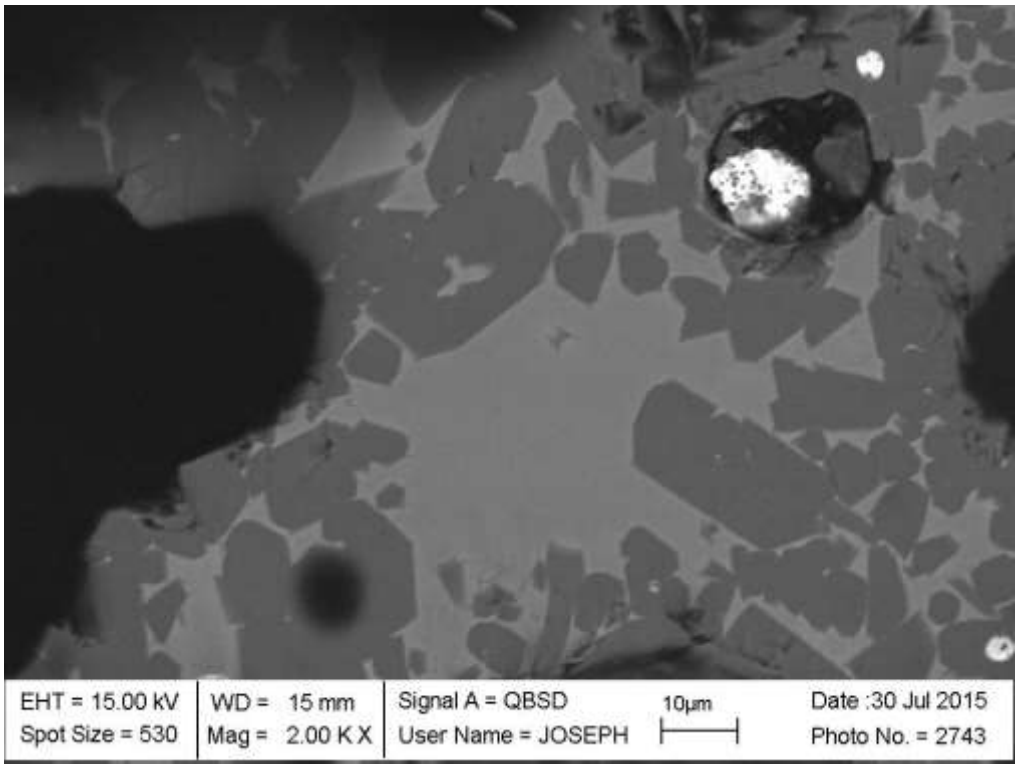
EHT = 15.00 kV
Spot Size = 530
WD = 15 mm
Mag = 2.00 K X
Signal A = QBSD
User Name = JOSEPH
10µm
Date :30 Jul 2015
Photo No. = 2743

Appendix 2 Results from EPMA-analyses

Lead phase wt-%

Weight%										
Sample	O	Si	Ca	Fe	Ga	Ge	In	Sn	Pb	Total
SY_50_kirkas_area1	4.01	0.48	0.31	0.00	0.05	0.02	0.01	0.00	95.86	100.75
SY_50_kirkas_area1	3.73	0.43	0.20	0.00	0.05	0.03	0.00	0.00	96.02	100.46
SY_50_kirkas_area1	3.83	0.37	0.17	0.01	0.08	0.02	0.00	0.00	96.01	100.48
SY_50_kirkas_area1	3.40	0.33	0.14	0.01	0.07	0.02	0.00	0.00	96.00	99.98
SY_50_kirkas_area1	3.34	0.32	0.14	0.01	0.07	0.04	0.01	0.00	95.93	99.85
SY_50_kirkas_area1	3.05	0.32	0.10	0.00	0.08	0.05	0.01	0.00	96.00	99.60
SY_50_kirkas_area1	3.00	0.29	0.11	0.00	0.07	0.03	0.00	0.00	95.73	99.22
SY_50_kirkas_area1	2.96	0.30	0.10	0.01	0.06	0.03	0.00	0.00	95.75	99.20
SY_50_kirkas_area1	2.68	0.30	0.10	0.00	0.06	0.03	0.00	0.01	95.70	98.88
SY_50_kirkas_area1	2.97	0.27	0.09	0.01	0.06	0.01	0.00	0.00	95.72	99.14
SY_50_kirkas_area1	2.77	0.29	0.10	0.00	0.07	0.03	0.00	0.00	95.57	98.83
SY_50_kirkas_area1	3.05	0.29	0.08	0.00	0.05	0.01	0.00	0.00	95.44	98.92
SY_50_kirkas_area1	2.96	0.28	0.08	0.00	0.05	0.03	0.00	0.00	95.43	98.82
SY_51_kirkas_area1	1.97	2.25	0.10	0.00	0.06	0.06	0.00	0.01	94.34	98.79
SY_51_kirkas_area1	1.79	5.89	0.10	0.01	0.10	0.02	0.00	0.00	92.15	100.07
SY_51_kirkas_area1	1.77	7.20	0.12	0.01	0.07	0.04	0.00	0.00	90.26	99.48
SY_51_kirkas_area1	1.75	7.38	0.11	0.00	0.09	0.03	0.00	0.00	90.58	99.93
SY_51_kirkas_area1	1.91	7.38	0.12	0.01	0.06	0.03	0.00	0.02	90.43	99.96
SY_51_kirkas_area1	2.02	6.93	0.11	0.02	0.08	0.02	0.00	0.00	90.97	100.14
SY_51_kirkas_area1	1.75	6.66	0.10	0.01	0.07	0.06	0.00	0.00	90.80	99.45
SY_51_kirkas_area1	2.14	6.55	0.11	0.00	0.08	0.04	0.00	0.00	91.37	100.29
SY_51_kirkas_area1	1.85	5.69	0.11	0.02	0.07	0.04	0.00	0.00	91.84	99.62
SY_51_kirkas_area1	1.90	5.08	0.09	0.02	0.08	0.02	0.00	0.00	92.37	99.56
SY_51_kirkas_area1	1.81	4.92	0.10	0.02	0.06	0.01	0.00	0.00	92.99	99.91
SY_51_kirkas_area1	2.05	4.54	0.10	0.03	0.07	0.01	0.00	0.00	93.55	100.35
SY_51_kirkas_area1	1.94	4.30	0.09	0.00	0.05	0.04	0.00	0.00	93.47	99.90
SY31_kirkas_alue1	2.11	0.00	0.03	0.00	0.05	0.06	0.00	0.00	96.97	99.24
SY31_kirkas_alue1	2.13	0.01	0.03	0.00	0.06	0.05	0.00	0.02	96.90	99.20
SY31_kirkas_alue1	2.38	0.00	0.03	0.00	0.05	0.05	0.00	0.00	96.86	99.37
SY31_kirkas_alue1	2.21	0.00	0.03	0.00	0.05	0.00	0.01	0.00	96.77	99.07
SY31_kirkas_alue1	1.73	0.00	0.04	0.00	0.06	0.03	0.00	0.03	96.63	98.52
SY31_kirkas_alue1	2.44	0.00	0.03	0.00	0.10	0.00	0.00	0.00	96.80	99.38
SY31_kirkas_alue1	2.11	0.03	0.03	0.01	0.03	0.00	0.00	0.00	96.48	98.69
SY31_kirkas_alue1	2.45	0.00	0.03	0.00	0.07	0.04	0.00	0.00	96.37	98.97
SY31_kirkas_alue1	2.04	0.02	0.02	0.01	0.09	0.01	0.00	0.00	96.60	98.80
SY31_kirkas_alue1	1.95	0.02	0.02	0.03	0.06	0.02	0.00	0.01	96.32	98.43
SY31_kirkas_alue1	2.29	0.02	0.01	0.00	0.08	0.04	0.00	0.00	96.29	98.72

SY31_kirkas_alue1	2.31	0.01	0.03	0.01	0.09	0.00	0.00	0.01	95.99	98.45
SY31_kirkas_alue1	2.45	0.02	0.03	0.01	0.02	0.01	0.00	0.00	96.22	98.76
SY31_kirkas_alue1	2.61	0.00	0.02	0.00	0.03	0.02	0.01	0.00	96.34	99.03
SY31_kirkas_alue1	2.45	0.02	0.02	0.04	0.07	0.01	0.00	0.00	95.74	98.35
SY37_kirkas_alue1	2.59	0.60	0.00	0.01	0.08	0.03	0.00	0.02	95.83	99.16
SY37_kirkas_alue1	2.20	0.60	0.01	0.03	0.07	0.02	0.00	0.00	95.55	98.47
SY37_kirkas_alue1	2.61	0.54	0.01	0.00	0.09	0.00	0.00	0.01	96.42	99.68
SY37_kirkas_alue1	3.23	0.75	0.01	0.00	0.10	0.00	0.00	0.00	96.68	100.78
SY37_kirkas_alue1	3.34	0.77	0.01	0.00	0.07	0.03	0.00	0.02	96.34	100.57
SY37_kirkas_alue1	3.11	0.73	0.00	0.00	0.07	0.03	0.00	0.01	96.59	100.55
SY37_kirkas_alue2	2.75	0.19	0.00	0.00	0.06	0.02	0.00	0.00	95.22	98.25
SY37_kirkas_alue2	2.08	0.12	0.01	0.00	0.03	0.00	0.00	0.00	96.11	98.35
SY37_kirkas_alue2	2.28	0.07	0.01	0.01	0.08	0.01	0.00	0.03	95.54	98.03
SY37_kirkas_alue2	2.15	0.15	0.02	0.00	0.06	0.05	0.00	0.00	96.30	98.73
SY37_kirkas_alue2	2.31	0.24	0.01	0.00	0.08	0.00	0.00	0.00	96.60	99.24
SY37_kirkas_alue2	2.18	0.25	0.00	0.01	0.08	0.02	0.00	0.00	96.69	99.22
SY37_kirkas_alue2	2.07	0.15	0.01	0.00	0.06	0.02	0.01	0.02	96.94	99.27
SY23_kirkas_alue1	2.72	0.26	0.00	0.02	0.06	0.01	0.08	0.13	96.38	99.67
SY23_kirkas_alue1	2.93	0.26	0.02	0.00	0.06	0.00	0.06	0.14	96.39	99.86
SY23_kirkas_alue1	2.81	0.27	0.02	0.00	0.07	0.04	0.05	0.15	95.74	99.14
SY23_kirkas_alue1	2.76	0.26	0.00	0.00	0.06	0.05	0.08	0.14	95.93	99.28
SY23_kirkas_alue1	2.84	0.24	0.01	0.00	0.08	0.03	0.06	0.15	96.14	99.54
SY23_kirkas_alue1	2.63	0.24	0.01	0.00	0.04	0.00	0.07	0.12	95.58	98.70
SY23_kirkas_alue1	2.72	0.24	0.01	0.00	0.05	0.05	0.09	0.10	95.65	98.92
SY23_kirkas_alue1	3.25	0.22	0.01	0.00	0.08	0.06	0.07	0.15	95.41	99.24
SY23_kirkas_alue1	2.56	0.22	0.00	0.01	0.07	0.03	0.08	0.15	95.58	98.71
SY23_kirkas_alue1	2.83	0.24	0.02	0.02	0.06	0.04	0.09	0.11	95.40	98.81
SY23_kirkas_alue1	2.66	0.24	0.01	0.03	0.08	0.05	0.08	0.08	95.07	98.28
SY23_kirkas_alue1	2.75	0.23	0.02	0.01	0.05	0.02	0.09	0.10	95.30	98.58
SY11_kirkas_alue1	2.83	0.02	0.00	0.03	0.08	0.01	0.11	0.10	95.65	98.83
SY11_kirkas_alue1	2.96	0.03	0.00	0.00	0.04	0.02	0.04	0.04	95.74	98.86
SY11_kirkas_alue1	2.93	0.02	0.00	0.02	0.07	0.05	0.04	0.04	95.85	99.02
SY11_kirkas_alue1	2.97	0.00	0.01	0.00	0.08	0.01	0.11	0.09	95.75	99.03
SY11_kirkas_alue1	2.98	0.02	0.00	0.01	0.08	0.06	0.05	0.05	95.60	98.84
SY11_kirkas_alue1	3.45	0.01	0.00	0.03	0.07	0.03	0.05	0.09	95.45	99.19
SY11_kirkas_alue1	3.02	0.04	0.00	0.02	0.08	0.04	0.06	0.02	95.72	99.00
SY11_kirkas_alue1	3.30	0.03	0.00	0.05	0.09	0.03	0.05	0.05	95.33	98.92
SY11_kirkas_alue2	2.31	0.05	0.00	0.03	0.07	0.07	0.05	0.08	96.24	98.89
SY11_kirkas_alue2	2.53	0.05	0.00	0.01	0.06	0.00	0.08	0.09	96.35	99.17
SY11_kirkas_alue2	2.27	0.03	0.01	0.01	0.09	0.02	0.06	0.06	96.35	98.90
SY27_kirkas_alue1	2.23	0.10	0.00	0.00	0.07	0.03	2.61	2.44	92.38	99.86
SY27_kirkas_alue1	2.31	0.10	0.02	0.00	0.08	0.02	2.63	2.32	92.73	100.20
SY27_kirkas_alue1	1.95	0.10	0.01	0.02	0.05	0.04	2.72	2.44	92.14	99.48

SY27_kirkas_alue1	1.85	0.08	0.03	0.00	0.07	0.01	2.67	2.35	92.18	99.23
SY27_kirkas_alue1	2.27	0.08	0.01	0.00	0.05	0.08	2.72	2.44	91.79	99.43
SY27_kirkas_alue1	2.38	0.12	0.02	0.00	0.06	0.02	2.72	2.34	91.81	99.47
SY27_kirkas_alue1	2.20	0.09	0.01	0.00	0.06	0.03	2.76	2.39	92.17	99.71
SY27_kirkas_alue2	2.66	0.15	0.03	0.01	0.12	0.01	2.83	2.49	91.22	99.52
SY27_kirkas_alue2	2.83	0.12	0.04	0.01	0.04	0.03	2.86	2.57	91.20	99.70
SY27_kirkas_alue2	2.49	0.13	0.05	0.01	0.08	0.03	2.85	2.49	91.34	99.49
SY27_kirkas_alue2	2.65	0.14	0.03	0.02	0.07	0.03	2.93	2.61	90.95	99.44
SY27_kirkas_alue2	2.63	0.11	0.02	0.02	0.08	0.03	2.89	2.57	90.77	99.11
SY27_kirkas_alue2	2.59	0.14	0.03	0.00	0.11	0.05	2.90	2.65	90.95	99.42
SY13_kirkas_alue1	5.26	0.25	0.02	0.01	0.07	0.03	0.76	0.50	92.63	99.52
SY13_kirkas_alue1	5.27	0.26	0.03	0.00	0.04	0.00	0.75	0.51	92.79	99.66
SY13_kirkas_alue1	5.19	0.24	0.02	0.03	0.06	0.02	0.72	0.52	92.28	99.10
SY13_kirkas_alue1	5.16	0.25	0.01	0.01	0.06	0.01	0.73	0.53	92.61	99.37
SY13_kirkas_alue1	4.99	0.25	0.02	0.00	0.07	0.05	0.73	0.50	92.41	99.02
SY13_kirkas_alue1	4.84	0.24	0.01	0.02	0.08	0.02	0.78	0.53	92.84	99.37
SY13_kirkas_alue1	4.88	0.26	0.03	0.03	0.06	0.00	0.75	0.52	92.34	98.87
SY13_kirkas_alue1	5.87	0.18	0.03	0.02	0.07	0.02	0.81	0.58	92.43	100.01
SY13_kirkas_alue1	5.74	0.17	0.03	0.00	0.10	0.03	0.80	0.55	92.31	99.73
SY13_kirkas_alue1	5.52	0.17	0.02	0.02	0.06	0.02	0.80	0.56	92.07	99.23
SY13_kirkas_alue1	5.59	0.18	0.02	0.03	0.06	0.00	0.81	0.56	92.27	99.52
SY13_kirkas_alue1	5.71	0.17	0.03	0.01	0.07	0.04	0.83	0.56	92.26	99.67
SY13_kirkas_alue1	5.50	0.18	0.02	0.02	0.07	0.05	0.81	0.54	92.15	99.33
SY13_kirkas_alue1	5.56	0.18	0.03	0.01	0.08	0.00	0.85	0.57	92.17	99.44
SY14_kirkas_alue1	6.79	0.51	0.65	1.02	0.40	0.07	0.95	0.61	86.93	97.93
SY14_kirkas_alue1	6.83	0.54	0.67	0.98	0.40	0.05	0.98	0.60	87.77	98.81
SY14_kirkas_alue1	6.89	0.55	0.67	1.01	0.42	0.09	0.99	0.57	87.78	98.97
SY14_kirkas_alue1	6.95	0.51	0.67	1.01	0.40	0.07	0.97	0.58	87.55	98.71
SY14_kirkas_alue1	6.83	0.52	0.65	1.02	0.38	0.09	0.91	0.58	87.40	98.39
SY14_kirkas_alue1	7.53	0.52	0.68	1.07	0.38	0.09	0.96	0.58	87.24	99.07
SY14_kirkas_alue1	6.98	0.53	0.65	1.03	0.40	0.04	0.94	0.59	87.32	98.47
SY14_kirkas_alue1	6.69	0.51	0.67	0.98	0.41	0.07	0.96	0.58	87.43	98.29
SY14_kirkas_alue1	7.13	0.54	0.68	1.01	0.45	0.09	0.97	0.56	87.49	98.91
SY14_kirkas_alue1	7.01	0.53	0.68	1.07	0.37	0.09	0.95	0.58	87.43	98.71
SY14_kirkas_alue1	6.97	0.56	0.66	1.02	0.42	0.07	0.96	0.57	87.07	98.29
SY14_kirkas_alue1	6.93	0.52	0.67	1.04	0.38	0.04	0.94	0.58	87.21	98.32
SY15_kirkas_area1	3.25	0.36	0.63	1.26	0.18	0.09	2.10	1.80	90.32	99.99
SY15_kirkas_area1	3.82	0.42	0.75	1.24	0.20	0.14	2.09	2.05	87.64	98.34
SY15_kirkas_area1	3.95	0.54	0.82	1.29	0.20	0.09	2.07	2.02	86.34	97.32
SY15_kirkas_area1	4.15	0.64	0.92	1.33	0.17	0.10	2.20	2.19	86.77	98.48
SY15_kirkas_area1	4.28	0.72	1.00	1.47	0.22	0.11	2.15	2.15	85.33	97.43
SY15_kirkas_area1	5.21	1.00	1.34	1.65	0.23	0.10	2.25	2.30	84.92	99.00
SY15_kirkas_area1	5.33	1.13	1.43	1.69	0.22	0.09	2.28	2.26	83.68	98.12

SY15_kirkas_area1	5.82	1.29	1.66	1.78	0.22	0.05	2.24	2.33	84.06	99.44
SY15_kirkas_area1	5.88	1.41	1.77	1.95	0.26	0.07	2.18	2.21	82.66	98.40
SY15_kirkas_area1	6.59	1.54	1.84	2.01	0.23	0.08	2.21	2.17	82.86	99.52
SY15_kirkas_area1	6.48	1.57	1.98	2.08	0.25	0.13	2.22	2.11	82.39	99.22
SY15_kirkas_area1	6.19	1.63	2.07	2.01	0.23	0.07	2.19	2.13	82.86	99.38
SY15_kirkas_area1	7.29	1.88	2.32	2.27	0.29	0.07	2.20	2.20	81.43	99.94
SY16_kirkas_area1	4.58	0.26	0.38	0.70	0.43	0.05	1.53	0.89	91.64	100.46
SY16_kirkas_area1	4.33	0.26	0.38	0.68	0.39	0.06	1.56	0.87	91.58	100.11
SY16_kirkas_area1	4.15	0.25	0.42	0.71	0.40	0.05	1.56	0.84	91.88	100.27
SY16_kirkas_area1	4.48	0.28	0.40	0.73	0.41	0.05	1.52	0.86	91.49	100.21
SY16_kirkas_area1	4.43	0.27	0.45	0.73	0.41	0.05	1.66	0.88	91.77	100.66
SY16_kirkas_area1	4.04	0.29	0.42	0.76	0.41	0.07	1.58	0.86	91.28	99.71
SY16_kirkas_area1	4.42	0.27	0.43	0.80	0.40	0.09	1.61	0.89	91.47	100.39
SY16_kirkas_area1	4.44	0.27	0.42	0.76	0.41	0.06	1.63	0.88	91.14	100.00
SY16_kirkas_area1	4.46	0.29	0.45	0.73	0.40	0.09	1.67	0.91	91.21	100.20
SY16_kirkas_area1	4.60	0.31	0.44	0.77	0.41	0.09	1.62	0.91	91.48	100.64
SY16_kirkas_area1	4.50	0.30	0.44	0.78	0.43	0.06	1.65	0.91	91.34	100.40
SY16_kirkas_area1	4.17	0.29	0.44	0.73	0.42	0.07	1.65	0.91	91.34	100.02
SY16_kirkas_area1	4.20	0.31	0.45	0.74	0.42	0.07	1.67	0.91	91.19	99.95
SY46_kirkas_area1	9.02	1.20	2.17	1.43	0.28	0.03	0.00	0.00	84.30	98.43
SY46_kirkas_area1	6.12	1.21	2.01	1.44	0.30	0.02	0.00	0.00	86.96	98.08
SY46_kirkas_area1	5.77	1.07	2.11	1.42	0.32	0.06	0.02	0.00	87.16	97.92
SY46_kirkas_area1	4.83	1.03	1.95	1.44	0.29	0.04	0.00	0.00	87.98	97.56
SY46_kirkas_area1	4.96	0.98	1.96	1.38	0.30	0.08	0.00	0.00	87.72	97.38
SY46_kirkas_area1	5.04	1.00	2.01	1.43	0.30	0.05	0.01	0.00	87.81	97.63
SY46_kirkas_area1	4.96	0.99	1.99	1.44	0.32	0.03	0.01	0.00	87.83	97.56
SY_48_kirkas_area1	2.08	0.04	0.10	0.02	0.08	0.01	0.01	0.00	96.16	98.50
SY_48_kirkas_area1	2.19	0.02	0.10	0.00	0.05	0.05	0.00	0.00	96.33	98.74
SY_48_kirkas_area1	2.17	0.04	0.10	0.01	0.05	0.04	0.00	0.00	96.22	98.63
SY_48_kirkas_area1	2.00	0.04	0.10	0.02	0.05	0.02	0.00	0.00	95.99	98.22
SY_48_kirkas_area1	1.89	0.03	0.10	0.00	0.08	0.05	0.00	0.00	95.86	98.01
SY_48_kirkas_area1	2.09	0.04	0.10	0.00	0.08	0.06	0.00	0.00	95.70	98.06
SY_48_kirkas_area1	2.04	0.04	0.10	0.00	0.03	0.03	0.00	0.00	95.66	97.90
SY_48_kirkas_area1	2.00	0.03	0.10	0.03	0.07	0.04	0.00	0.00	95.34	97.61
SY_48_kirkas_area1	2.07	0.04	0.11	0.02	0.07	0.05	0.00	0.00	95.40	97.77
SY_48_kirkas_area1	2.10	0.05	0.10	0.01	0.06	0.03	0.01	0.00	95.29	97.66
SY_48_kirkas_area1	2.13	0.05	0.10	0.00	0.09	0.02	0.00	0.00	94.90	97.30
SY_48_kirkas_area1	2.10	0.04	0.12	0.00	0.07	0.03	0.02	0.01	95.02	97.41
SY_48_kirkas_area2	2.23	0.02	0.01	0.00	0.09	0.03	0.00	0.00	97.79	100.18
SY_48_kirkas_area2	2.26	0.02	0.01	0.00	0.06	0.05	0.00	0.00	97.83	100.23
SY_48_kirkas_area2	2.31	0.01	0.04	0.01	0.08	0.02	0.02	0.00	97.25	99.74
SY_48_kirkas_area2	2.33	0.03	0.05	0.00	0.09	0.05	0.00	0.00	97.24	99.78
SY_48_kirkas_area2	2.21	0.02	0.05	0.01	0.08	0.02	0.00	0.00	97.11	99.48

SY_48_kirkas_area2	2.04	0.04	0.05	0.00	0.06	0.03	0.01	0.00	96.99	99.22
SY_48_kirkas_area2	2.45	0.03	0.05	0.00	0.08	0.01	0.00	0.00	96.86	99.48
SY_48_kirkas_area2	2.25	0.02	0.05	0.00	0.07	0.03	0.00	0.00	96.59	99.01
SY_48_kirkas_area2	2.40	0.04	0.06	0.02	0.08	0.05	0.02	0.00	96.43	99.09
SY_48_kirkas_area2	2.18	0.04	0.06	0.00	0.07	0.03	0.00	0.00	96.41	98.80
SY_48_kirkas_area2	2.18	0.03	0.07	0.00	0.05	0.02	0.00	0.00	96.21	98.57
SY_49_kirkas_area1	5.94	0.11	0.00	0.00	0.06	0.05	0.00	0.00	92.98	99.15
SY_49_kirkas_area1	5.88	0.16	0.01	0.01	0.06	0.05	0.00	0.00	93.50	99.67
SY_49_kirkas_area1	5.85	0.25	0.00	0.01	0.05	0.02	0.00	0.00	93.73	99.91
SY_49_kirkas_area1	5.68	0.40	0.00	0.00	0.06	0.03	0.00	0.00	93.35	99.52
SY_49_kirkas_area1	5.70	0.48	0.00	0.01	0.07	0.05	0.00	0.00	93.12	99.44
SY_49_kirkas_area1	5.55	0.67	0.00	0.00	0.03	0.03	0.00	0.01	92.75	99.04
SY_49_kirkas_area1	5.40	0.74	0.00	0.00	0.08	0.02	0.00	0.00	92.62	98.86
SY_49_kirkas_area1	5.32	0.87	0.00	0.02	0.03	0.01	0.00	0.00	92.59	98.85
SY_49_kirkas_area1	5.48	0.88	0.01	0.00	0.08	0.03	0.00	0.00	92.42	98.92
SY_49_kirkas_area1	5.46	1.02	0.00	0.01	0.05	0.02	0.00	0.00	92.28	98.85
SY_49_kirkas_area1	5.71	0.98	0.01	0.01	0.03	0.02	0.01	0.00	92.36	99.13
SY_49_kirkas_area1	5.62	1.17	0.00	0.00	0.06	0.03	0.00	0.00	91.95	98.82
SY_49_kirkas_area1	5.46	1.18	0.01	0.00	0.06	0.03	0.00	0.00	91.81	98.55
SY_49_kirkas_area1	5.32	1.36	0.00	0.00	0.06	0.04	0.00	0.00	91.52	98.30
Sy33_kirkas_alue1	1.58	0.08	0.01	0.01	0.03	0.04	0.00	0.00	97.28	99.02
Sy33_kirkas_alue1	1.67	0.09	0.00	0.01	0.04	0.03	0.00	0.00	96.91	98.75
Sy33_kirkas_alue1	1.72	0.08	0.01	0.03	0.03	0.05	0.00	0.00	97.15	99.06
Sy33_kirkas_alue1	1.93	0.09	0.00	0.02	0.06	0.06	0.01	0.00	97.12	99.29
Sy33_kirkas_alue1	1.66	0.07	0.01	0.01	0.04	0.04	0.00	0.00	97.23	99.07
Sy33_kirkas_alue1	1.53	0.09	0.01	0.00	0.06	0.00	0.00	0.00	97.33	99.03
Sy33_kirkas_alue1	1.65	0.07	0.00	0.00	0.04	0.03	0.00	0.00	97.10	98.90
Sy33_kirkas_alue1	1.60	0.10	0.02	0.00	0.03	0.06	0.00	0.00	97.43	99.24
Sy33_kirkas_alue2	2.71	0.39	0.05	0.02	0.06	0.01	0.01	0.00	96.54	99.77
Sy33_kirkas_alue2	2.66	0.38	0.04	0.03	0.08	0.03	0.00	0.00	96.67	99.88
Sy33_kirkas_alue2	2.62	0.38	0.06	0.01	0.06	0.00	0.00	0.00	96.70	99.84
Sy33_kirkas_alue2	2.89	0.40	0.04	0.00	0.09	0.07	0.00	0.00	96.30	99.79
Sy33_kirkas_alue2	2.67	0.39	0.03	0.03	0.05	0.02	0.00	0.00	96.54	99.73
Sy33_kirkas_alue2	2.74	0.38	0.04	0.01	0.10	0.00	0.04	0.00	96.22	99.53
Sy33_kirkas_alue2	2.75	0.39	0.05	0.01	0.06	0.03	0.00	0.00	96.41	99.70
Sy33_kirkas_alue2	2.86	0.41	0.06	0.02	0.08	0.04	0.01	0.00	95.93	99.41
SY34_kirkas_alue1	3.23	0.22	0.09	0.00	0.05	0.05	0.00	0.00	96.74	100.38
SY34_kirkas_alue1	3.22	0.39	0.37	0.02	0.11	0.04	0.00	0.02	96.66	100.83
SY34_kirkas_alue1	2.69	0.19	0.02	0.00	0.07	0.04	0.00	0.00	96.61	99.62
SY34_kirkas_alue1	3.06	0.30	0.16	0.01	0.04	0.03	0.00	0.00	96.97	100.57
SY34_kirkas_alue1	3.41	0.25	0.12	0.00	0.09	0.05	0.00	0.00	96.85	100.79
SY34_kirkas_alue1	2.53	0.19	0.06	0.01	0.09	0.02	0.01	0.00	96.22	99.11
SY34_kirkas_alue1	2.88	0.21	0.04	0.01	0.04	0.07	0.00	0.00	96.72	99.96

SY34_kirkas_alue1	2.93	0.20	0.03	0.00	0.11	0.02	0.00	0.00	96.55	99.85
SY34_kirkas_alue1	3.11	0.19	0.04	0.01	0.06	0.05	0.01	0.00	96.81	100.29
SY34_kirkas_alue1	2.61	0.21	0.02	0.02	0.09	0.00	0.00	0.00	96.71	99.67
SY34_kirkas_alue1	2.81	0.16	0.04	0.01	0.08	0.02	0.00	0.00	96.28	99.41
SY34_kirkas_alue1	2.33	0.14	0.03	0.00	0.04	0.02	0.00	0.00	95.95	98.52
SY34_kirkas_alue1	2.57	0.18	0.04	0.02	0.09	0.00	0.02	0.00	96.24	99.16
SY34_kirkas_alue1	2.96	0.17	0.03	0.01	0.06	0.00	0.01	0.00	96.38	99.62
SY34_kirkas_alue1	3.03	0.20	0.01	0.02	0.08	0.05	0.00	0.00	96.26	99.64
SY34_kirkas_alue1	3.32	0.21	0.02	0.01	0.05	0.02	0.00	0.01	96.40	100.04
SY47_kirkas_alue1	3.81	0.36	0.00	0.00	0.02	0.03	0.01	0.09	96.05	100.37
SY47_kirkas_alue1	4.08	0.32	0.02	0.04	0.07	0.06	0.02	0.05	95.97	100.64
SY47_kirkas_alue1	3.62	0.35	0.01	0.00	0.02	0.04	0.02	0.07	95.93	100.06
SY47_kirkas_alue1	3.84	0.35	0.00	0.02	0.08	0.04	0.04	0.04	96.05	100.46
SY47_kirkas_alue1	3.95	0.37	0.00	0.00	0.06	0.01	0.01	0.06	95.50	99.97
SY47_kirkas_alue1	3.64	0.34	0.00	0.00	0.05	0.02	0.03	0.05	95.63	99.76
SY47_kirkas_alue1	3.73	0.35	0.00	0.00	0.07	0.03	0.04	0.08	94.96	99.25
SY47_kirkas_alue1	3.83	0.37	0.01	0.01	0.09	0.00	0.02	0.05	95.68	100.07
SY47_kirkas_alue1	4.09	0.36	0.00	0.00	0.03	0.01	0.02	0.06	95.03	99.61
SY47_kirkas_alue1	3.84	0.36	0.01	0.00	0.06	0.01	0.02	0.05	95.00	99.36
SY47_kirkas_alue1	3.90	0.35	0.01	0.00	0.03	0.01	0.00	0.03	94.82	99.15
SY47_kirkas_alue1	3.97	0.35	0.00	0.00	0.08	0.02	0.01	0.05	94.33	98.82
SY25_kirkas area1	1.56	0.05	0.01	0.02	0.06	0.02	0.00	0.06	97.74	99.52
SY25_kirkas area1	1.34	0.07	0.02	0.00	0.06	0.01	0.00	0.06	97.58	99.14
SY25_kirkas area1	1.66	0.06	0.03	0.01	0.07	0.03	0.00	0.06	97.48	99.39
SY25_kirkas area1	1.15	0.04	0.02	0.02	0.04	0.03	0.01	0.05	97.37	98.72
SY25_kirkas area1	1.53	0.05	0.02	0.00	0.06	0.05	0.00	0.04	97.41	99.17
SY25_kirkas area1	1.40	0.06	0.02	0.02	0.05	0.03	0.00	0.06	97.36	99.01
SY25_kirkas area1	1.66	0.08	0.01	0.00	0.03	0.01	0.01	0.05	97.25	99.09
SY25_kirkas area1	1.75	0.08	0.01	0.02	0.08	0.04	0.00	0.06	97.24	99.28
SY25_kirkas area1	1.59	0.07	0.01	0.00	0.08	0.01	0.01	0.04	97.31	99.13
SY25_kirkas area1	1.51	0.06	0.01	0.02	0.07	0.01	0.00	0.05	97.18	98.92
SY25_kirkas area1	1.79	0.05	0.01	0.00	0.07	0.02	0.01	0.06	97.24	99.24
SY25_kirkas area1	1.54	0.06	0.01	0.03	0.07	0.01	0.01	0.05	96.99	98.78
SY29_kirkas_alue1	3.73	0.14	0.00	0.03	0.07	0.03	0.30	0.26	94.55	99.12
SY29_kirkas_alue1	3.54	0.14	0.02	0.00	0.04	0.05	0.30	0.28	95.01	99.39
SY29_kirkas_alue1	3.93	0.15	0.00	0.03	0.07	0.05	0.29	0.29	94.74	99.55
SY29_kirkas_alue1	3.55	0.13	0.02	0.01	0.06	0.02	0.28	0.27	94.84	99.18
SY29_kirkas_alue1	3.38	0.17	0.01	0.00	0.06	0.02	0.27	0.26	95.17	99.34
SY29_kirkas_alue1	3.99	0.15	0.01	0.00	0.07	0.03	0.25	0.29	94.98	99.78
SY29_kirkas_alue1	3.83	0.15	0.01	0.01	0.05	0.01	0.30	0.25	95.08	99.70
SY29_kirkas_alue1	3.75	0.14	0.03	0.01	0.01	0.05	0.27	0.28	95.28	99.81
SY29_kirkas_alue1	3.58	0.17	0.02	0.00	0.04	0.00	0.29	0.27	94.96	99.33
SY29_kirkas_alue1	3.56	0.16	0.03	0.00	0.09	0.00	0.28	0.27	95.39	99.79

SY29_kirkas_alue1	3.46	0.15	0.00	0.00	0.04	0.02	0.25	0.25	95.03	99.20
SY29_kirkas_alue1	3.51	0.17	0.01	0.01	0.06	0.04	0.26	0.25	95.31	99.61
SY29_kirkas_alue1	3.41	0.17	0.01	0.01	0.08	0.05	0.24	0.24	95.26	99.47
SY30_kirkas_alue1	5.51	0.13	0.02	0.00	0.09	0.00	0.23	0.23	93.70	99.90
SY30_kirkas_alue1	5.48	0.17	0.01	0.00	0.10	0.03	0.22	0.25	93.29	99.54
SY30_kirkas_alue1	5.39	0.14	0.02	0.00	0.05	0.04	0.25	0.26	93.02	99.16
SY30_kirkas_alue1	5.49	0.14	0.03	0.02	0.00	0.04	0.20	0.24	93.22	99.39
SY30_kirkas_alue1	5.07	0.14	0.01	0.00	0.08	0.02	0.26	0.23	93.03	98.86
SY30_kirkas_alue1	5.70	0.17	0.03	0.00	0.06	0.03	0.24	0.22	93.16	99.61
SY30_kirkas_alue1	5.47	0.16	0.02	0.00	0.05	0.08	0.23	0.24	92.85	99.10
SY30_kirkas_alue1	5.63	0.15	0.04	0.02	0.05	0.03	0.23	0.24	92.86	99.24
SY30_kirkas_alue1	5.46	0.15	0.03	0.00	0.04	0.00	0.24	0.25	93.60	99.78
SY30_kirkas_alue1	5.32	0.17	0.00	0.03	0.07	0.00	0.22	0.26	94.11	100.18
SY30_kirkas_alue1	5.60	0.16	0.02	0.02	0.07	0.03	0.24	0.23	93.23	99.60
SY30_kirkas_alue1	5.35	0.17	0.02	0.01	0.05	0.00	0.22	0.24	93.62	99.67
SY41_kirkas_alue1	6.17	0.35	0.36	0.06	0.11	0.14	0.27	0.35	91.06	98.88
SY41_kirkas_alue1	5.95	0.36	0.37	0.08	0.11	0.11	0.26	0.32	90.84	98.38
SY41_kirkas_alue1	6.31	0.35	0.36	0.03	0.07	0.12	0.27	0.35	90.74	98.62
SY41_kirkas_alue1	6.16	0.34	0.36	0.05	0.09	0.10	0.24	0.32	90.41	98.08
SY41_kirkas_alue1	6.41	0.35	0.35	0.06	0.11	0.10	0.21	0.32	90.54	98.44
SY41_kirkas_alue1	6.27	0.35	0.35	0.02	0.09	0.13	0.22	0.33	90.22	97.98
SY41_kirkas_alue1	5.92	0.34	0.35	0.05	0.08	0.12	0.23	0.35	89.94	97.38
SY41_kirkas_alue2	7.84	0.28	0.03	0.02	0.07	0.04	0.13	0.14	91.49	100.04
SY41_kirkas_alue2	8.17	0.28	0.04	0.02	0.07	0.04	0.12	0.17	91.25	100.16
SY41_kirkas_alue2	7.92	0.29	0.04	0.01	0.07	0.02	0.12	0.18	91.18	99.83
SY41_kirkas_alue2	7.60	0.27	0.03	0.02	0.08	0.02	0.16	0.19	91.12	99.49
SY41_kirkas_alue2	7.77	0.27	0.04	0.03	0.08	0.08	0.17	0.16	90.97	99.59
SY41_kirkas_alue2	7.74	0.26	0.02	0.00	0.03	0.01	0.14	0.23	91.49	99.92
SY41_kirkas_alue2	8.31	0.25	0.04	0.02	0.05	0.02	0.14	0.21	91.33	100.37
SY42_kirkas_alue1	4.68	0.16	0.02	0.05	0.09	0.06	0.46	0.29	93.93	99.75
SY42_kirkas_alue1	4.98	0.12	0.02	0.04	0.10	0.01	0.49	0.28	94.03	100.07
SY42_kirkas_alue1	4.21	0.14	0.02	0.05	0.07	0.04	0.48	0.32	93.70	99.05
SY42_kirkas_alue1	4.60	0.15	0.00	0.04	0.10	0.04	0.48	0.30	93.84	99.54
SY42_kirkas_alue1	4.25	0.14	0.02	0.05	0.09	0.00	0.47	0.29	94.63	99.94
SY42_kirkas_alue1	4.45	0.15	0.00	0.06	0.07	0.04	0.52	0.30	94.17	99.75
SY42_kirkas_alue1	4.38	0.15	0.01	0.03	0.10	0.04	0.49	0.35	94.30	99.86
SY42_kirkas_alue1	5.14	0.15	0.03	0.05	0.08	0.01	0.47	0.35	93.96	100.23
SY42_kirkas_alue1	5.15	0.13	0.02	0.01	0.08	0.04	0.49	0.29	93.75	99.97
SY42_kirkas_alue2	5.08	0.12	0.02	0.04	0.05	0.01	0.62	0.45	93.08	99.47
SY42_kirkas_alue2	5.18	0.14	0.02	0.01	0.09	0.04	0.63	0.42	93.05	99.57
SY42_kirkas_alue2	5.33	0.13	0.02	0.02	0.04	0.05	0.66	0.41	93.08	99.74
SY42_kirkas_alue2	5.25	0.13	0.02	0.00	0.10	0.07	0.63	0.41	93.17	99.80
SY42_kirkas_alue2	4.77	0.11	0.02	0.02	0.05	0.04	0.69	0.40	93.43	99.52

SY42_kirkas_alue2	5.39	0.12	0.01	0.03	0.09	0.04	0.60	0.38	93.61	100.28
SY42_kirkas_alue2	5.45	0.15	0.03	0.02	0.10	0.02	0.62	0.38	93.40	100.18
SY42_kirkas_alue2	5.00	0.14	0.02	0.03	0.09	0.06	0.62	0.36	93.35	99.66
SY42_kirkas_alue2	5.19	0.12	0.02	0.00	0.05	0.04	0.62	0.40	93.32	99.76
SY42_kirkas_alue2	4.66	0.14	0.02	0.06	0.09	0.00	0.64	0.36	93.20	99.16
SY42_kirkas_alue2	5.38	0.15	0.03	0.00	0.07	0.03	0.66	0.37	93.44	100.13
SY45_kirkas-alue1	4.55	0.10	0.09	0.17	0.09	0.09	2.23	1.28	89.79	98.39
SY45_kirkas-alue1	4.69	0.10	0.10	0.16	0.08	0.04	2.05	1.21	89.99	98.42
SY45_kirkas-alue1	4.67	0.09	0.08	0.17	0.12	0.03	1.99	1.13	89.19	97.46
SY45_kirkas-alue1	4.60	0.11	0.09	0.15	0.05	0.05	1.78	1.05	89.31	97.17
SY45_kirkas-alue1	4.59	0.10	0.07	0.17	0.12	0.05	1.76	1.03	89.66	97.55
SY45_kirkas-alue1	6.08	0.10	0.09	0.18	0.10	0.09	1.63	0.95	89.90	99.12
SY45_kirkas-alue1	7.81	0.08	0.08	0.15	0.11	0.09	1.65	0.94	88.49	99.40
SY45_kirkas-alue1	9.72	0.09	0.09	0.16	0.09	0.06	1.54	0.95	87.87	100.59
SY45_kirkas-alue1	9.83	0.10	0.08	0.19	0.08	0.08	1.62	0.94	86.88	99.78
SY45_kirkas-alue1	9.37	0.11	0.08	0.15	0.07	0.05	1.62	0.90	86.63	98.98
SY45_kirkas-alue1	7.70	0.12	0.10	0.17	0.09	0.09	1.62	0.96	86.79	97.63
SY45_kirkas-alue1	6.56	0.11	0.09	0.20	0.10	0.07	1.60	0.88	87.68	97.29

Lead phase normalised wt-%

	Norm Weight%								
Sample	Si	Ca	Fe	Ga	Ge	In	Sn	Pb	Total
SY_50_kirkas_area1	0.49	0.32	0.00	0.06	0.02	0.01	0.00	99.09	100.00
SY_50_kirkas_area1	0.44	0.20	0.00	0.06	0.03	0.00	0.00	99.27	100.00
SY_50_kirkas_area1	0.38	0.18	0.01	0.08	0.02	0.00	0.00	99.33	100.00
SY_50_kirkas_area1	0.35	0.15	0.01	0.08	0.02	0.00	0.00	99.40	100.00
SY_50_kirkas_area1	0.33	0.15	0.01	0.07	0.05	0.01	0.00	99.39	100.00
SY_50_kirkas_area1	0.33	0.11	0.00	0.08	0.05	0.01	0.00	99.43	100.00
SY_50_kirkas_area1	0.30	0.12	0.00	0.07	0.03	0.00	0.00	99.48	100.00
SY_50_kirkas_area1	0.31	0.10	0.01	0.06	0.03	0.00	0.00	99.49	100.00
SY_50_kirkas_area1	0.32	0.10	0.00	0.06	0.04	0.00	0.01	99.48	100.00
SY_50_kirkas_area1	0.28	0.10	0.01	0.06	0.01	0.00	0.00	99.54	100.00
SY_50_kirkas_area1	0.30	0.10	0.00	0.07	0.03	0.00	0.00	99.49	100.00
SY_50_kirkas_area1	0.30	0.09	0.00	0.05	0.01	0.00	0.00	99.55	100.00
SY_50_kirkas_area1	0.29	0.09	0.00	0.05	0.03	0.00	0.00	99.55	100.00
SY_51_kirkas_area1	2.32	0.10	0.00	0.06	0.06	0.00	0.01	97.44	100.00
SY_51_kirkas_area1	6.00	0.10	0.01	0.11	0.02	0.00	0.00	93.77	100.00
SY_51_kirkas_area1	7.37	0.12	0.01	0.08	0.05	0.00	0.00	92.38	100.00
SY_51_kirkas_area1	7.52	0.11	0.00	0.09	0.03	0.00	0.00	92.25	100.00
SY_51_kirkas_area1	7.53	0.12	0.01	0.06	0.03	0.00	0.02	92.23	100.00
SY_51_kirkas_area1	7.07	0.12	0.02	0.08	0.02	0.00	0.00	92.70	100.00
SY_51_kirkas_area1	6.81	0.11	0.01	0.07	0.06	0.00	0.00	92.94	100.00

SY_51_kirkas_area1	6.68	0.11	0.00	0.08	0.04	0.00	0.00	93.09	100.00
SY_51_kirkas_area1	5.82	0.11	0.02	0.07	0.04	0.00	0.00	93.94	100.00
SY_51_kirkas_area1	5.20	0.09	0.02	0.09	0.02	0.00	0.00	94.58	100.00
SY_51_kirkas_area1	5.01	0.11	0.02	0.07	0.01	0.00	0.00	94.78	100.00
SY_51_kirkas_area1	4.62	0.10	0.03	0.07	0.01	0.00	0.00	95.17	100.00
SY_51_kirkas_area1	4.39	0.10	0.00	0.05	0.04	0.00	0.00	95.43	100.00
SY31_kirkas_alue1	0.00	0.03	0.00	0.05	0.06	0.00	0.00	99.85	100.00
SY31_kirkas_alue1	0.01	0.03	0.00	0.07	0.05	0.00	0.02	99.82	100.00
SY31_kirkas_alue1	0.00	0.03	0.00	0.05	0.05	0.00	0.00	99.87	100.00
SY31_kirkas_alue1	0.00	0.03	0.00	0.05	0.00	0.01	0.00	99.90	100.00
SY31_kirkas_alue1	0.00	0.04	0.00	0.06	0.03	0.00	0.03	99.84	100.00
SY31_kirkas_alue1	0.00	0.03	0.00	0.10	0.00	0.00	0.00	99.86	100.00
SY31_kirkas_alue1	0.03	0.03	0.01	0.04	0.00	0.00	0.00	99.90	100.00
SY31_kirkas_alue1	0.00	0.03	0.00	0.07	0.05	0.00	0.00	99.85	100.00
SY31_kirkas_alue1	0.02	0.02	0.01	0.09	0.01	0.00	0.00	99.84	100.00
SY31_kirkas_alue1	0.02	0.03	0.03	0.06	0.02	0.00	0.01	99.84	100.00
SY31_kirkas_alue1	0.02	0.02	0.00	0.08	0.04	0.00	0.00	99.85	100.00
SY31_kirkas_alue1	0.01	0.03	0.01	0.10	0.00	0.00	0.01	99.84	100.00
SY31_kirkas_alue1	0.02	0.03	0.01	0.02	0.01	0.00	0.00	99.91	100.00
SY31_kirkas_alue1	0.00	0.02	0.00	0.03	0.02	0.01	0.00	99.92	100.00
SY31_kirkas_alue1	0.03	0.02	0.04	0.08	0.01	0.00	0.00	99.83	100.00
SY37_kirkas_alue1	0.62	0.00	0.01	0.09	0.03	0.00	0.02	99.23	100.00
SY37_kirkas_alue1	0.62	0.01	0.03	0.07	0.02	0.00	0.00	99.25	100.00
SY37_kirkas_alue1	0.56	0.01	0.00	0.09	0.00	0.00	0.01	99.33	100.00
SY37_kirkas_alue1	0.77	0.01	0.00	0.10	0.00	0.00	0.00	99.10	100.00
SY37_kirkas_alue1	0.79	0.01	0.00	0.07	0.03	0.00	0.02	99.08	100.00
SY37_kirkas_alue1	0.75	0.00	0.00	0.07	0.03	0.00	0.01	99.13	100.00
SY37_kirkas_alue2	0.20	0.00	0.00	0.06	0.02	0.00	0.00	99.72	100.00
SY37_kirkas_alue2	0.13	0.01	0.00	0.03	0.00	0.00	0.00	99.84	100.00
SY37_kirkas_alue2	0.07	0.02	0.01	0.08	0.01	0.00	0.03	99.79	100.00
SY37_kirkas_alue2	0.15	0.03	0.00	0.06	0.05	0.00	0.00	99.71	100.00
SY37_kirkas_alue2	0.24	0.01	0.00	0.09	0.00	0.00	0.00	99.66	100.00
SY37_kirkas_alue2	0.26	0.00	0.01	0.08	0.02	0.00	0.00	99.63	100.00
SY37_kirkas_alue2	0.15	0.01	0.00	0.06	0.02	0.01	0.02	99.73	100.00
SY23_kirkas_alue1	0.27	0.00	0.02	0.07	0.01	0.08	0.14	99.41	100.00
SY23_kirkas_alue1	0.27	0.02	0.00	0.06	0.00	0.06	0.14	99.44	100.00
SY23_kirkas_alue1	0.28	0.02	0.00	0.07	0.04	0.06	0.16	99.38	100.00
SY23_kirkas_alue1	0.27	0.00	0.00	0.06	0.05	0.09	0.15	99.38	100.00
SY23_kirkas_alue1	0.24	0.01	0.00	0.08	0.03	0.07	0.15	99.42	100.00
SY23_kirkas_alue1	0.25	0.01	0.00	0.05	0.00	0.08	0.13	99.50	100.00
SY23_kirkas_alue1	0.25	0.01	0.00	0.05	0.05	0.10	0.11	99.43	100.00
SY23_kirkas_alue1	0.23	0.01	0.00	0.08	0.06	0.07	0.15	99.40	100.00
SY23_kirkas_alue1	0.23	0.00	0.01	0.08	0.03	0.09	0.16	99.41	100.00

SY23_kirkas_alue1	0.25	0.02	0.02	0.06	0.04	0.09	0.12	99.40	100.00
SY23_kirkas_alue1	0.25	0.01	0.03	0.08	0.05	0.08	0.09	99.42	100.00
SY23_kirkas_alue1	0.24	0.02	0.01	0.05	0.02	0.10	0.10	99.45	100.00
SY11_kirkas_alue1	0.02	0.00	0.04	0.08	0.01	0.11	0.11	99.64	100.00
SY11_kirkas_alue1	0.03	0.00	0.00	0.04	0.03	0.04	0.04	99.83	100.00
SY11_kirkas_alue1	0.02	0.00	0.02	0.07	0.05	0.05	0.04	99.75	100.00
SY11_kirkas_alue1	0.00	0.01	0.00	0.08	0.01	0.12	0.10	99.68	100.00
SY11_kirkas_alue1	0.02	0.00	0.01	0.08	0.06	0.05	0.05	99.72	100.00
SY11_kirkas_alue1	0.01	0.00	0.03	0.08	0.03	0.05	0.09	99.70	100.00
SY11_kirkas_alue1	0.04	0.00	0.02	0.09	0.04	0.06	0.02	99.73	100.00
SY11_kirkas_alue1	0.03	0.00	0.05	0.09	0.03	0.05	0.05	99.70	100.00
SY11_kirkas_alue2	0.05	0.00	0.03	0.07	0.07	0.05	0.08	99.65	100.00
SY11_kirkas_alue2	0.05	0.00	0.01	0.06	0.00	0.08	0.09	99.70	100.00
SY11_kirkas_alue2	0.03	0.01	0.01	0.10	0.02	0.06	0.07	99.71	100.00
SY27_kirkas_alue1	0.11	0.00	0.00	0.07	0.03	2.67	2.50	94.62	100.00
SY27_kirkas_alue1	0.10	0.02	0.00	0.08	0.02	2.69	2.37	94.73	100.00
SY27_kirkas_alue1	0.11	0.01	0.02	0.05	0.04	2.79	2.50	94.48	100.00
SY27_kirkas_alue1	0.08	0.03	0.00	0.07	0.01	2.75	2.41	94.65	100.00
SY27_kirkas_alue1	0.08	0.01	0.00	0.05	0.08	2.80	2.51	94.47	100.00
SY27_kirkas_alue1	0.12	0.02	0.00	0.06	0.02	2.80	2.41	94.56	100.00
SY27_kirkas_alue1	0.09	0.01	0.00	0.06	0.03	2.83	2.45	94.52	100.00
SY27_kirkas_alue2	0.15	0.03	0.01	0.12	0.01	2.92	2.57	94.18	100.00
SY27_kirkas_alue2	0.12	0.04	0.01	0.04	0.03	2.95	2.65	94.15	100.00
SY27_kirkas_alue2	0.13	0.06	0.01	0.09	0.03	2.94	2.57	94.17	100.00
SY27_kirkas_alue2	0.15	0.03	0.02	0.07	0.04	3.03	2.70	93.97	100.00
SY27_kirkas_alue2	0.11	0.02	0.02	0.08	0.03	3.00	2.66	94.08	100.00
SY27_kirkas_alue2	0.15	0.03	0.00	0.11	0.05	3.00	2.73	93.93	100.00
SY13_kirkas_alue1	0.26	0.02	0.01	0.08	0.04	0.80	0.53	98.27	100.00
SY13_kirkas_alue1	0.27	0.03	0.00	0.05	0.00	0.80	0.54	98.31	100.00
SY13_kirkas_alue1	0.26	0.03	0.03	0.07	0.02	0.77	0.56	98.27	100.00
SY13_kirkas_alue1	0.26	0.01	0.01	0.06	0.02	0.77	0.57	98.30	100.00
SY13_kirkas_alue1	0.27	0.02	0.00	0.08	0.05	0.77	0.53	98.28	100.00
SY13_kirkas_alue1	0.26	0.02	0.02	0.09	0.02	0.83	0.56	98.22	100.00
SY13_kirkas_alue1	0.27	0.03	0.03	0.06	0.00	0.80	0.55	98.25	100.00
SY13_kirkas_alue1	0.19	0.03	0.02	0.08	0.02	0.86	0.61	98.18	100.00
SY13_kirkas_alue1	0.18	0.03	0.00	0.10	0.03	0.86	0.59	98.22	100.00
SY13_kirkas_alue1	0.18	0.02	0.02	0.06	0.02	0.85	0.60	98.25	100.00
SY13_kirkas_alue1	0.19	0.02	0.03	0.07	0.00	0.86	0.60	98.23	100.00
SY13_kirkas_alue1	0.18	0.03	0.01	0.08	0.05	0.88	0.60	98.19	100.00
SY13_kirkas_alue1	0.19	0.02	0.02	0.08	0.05	0.86	0.57	98.21	100.00
SY13_kirkas_alue1	0.19	0.03	0.02	0.09	0.00	0.90	0.60	98.17	100.00
SY14_kirkas_alue1	0.56	0.71	1.12	0.43	0.07	1.04	0.67	95.39	100.00
SY14_kirkas_alue1	0.58	0.72	1.07	0.43	0.05	1.06	0.65	95.43	100.00

SY14_kirkas_alue1	0.59	0.72	1.10	0.46	0.10	1.07	0.62	95.33	100.00
SY14_kirkas_alue1	0.56	0.73	1.10	0.44	0.07	1.06	0.63	95.41	100.00
SY14_kirkas_alue1	0.57	0.71	1.11	0.42	0.10	1.00	0.63	95.47	100.00
SY14_kirkas_alue1	0.57	0.75	1.17	0.41	0.10	1.05	0.64	95.31	100.00
SY14_kirkas_alue1	0.58	0.71	1.13	0.43	0.04	1.03	0.65	95.44	100.00
SY14_kirkas_alue1	0.56	0.73	1.07	0.45	0.07	1.05	0.63	95.44	100.00
SY14_kirkas_alue1	0.59	0.74	1.10	0.49	0.09	1.05	0.61	95.33	100.00
SY14_kirkas_alue1	0.58	0.74	1.17	0.40	0.10	1.04	0.64	95.33	100.00
SY14_kirkas_alue1	0.61	0.72	1.11	0.46	0.07	1.06	0.62	95.35	100.00
SY14_kirkas_alue1	0.57	0.74	1.14	0.42	0.04	1.03	0.63	95.42	100.00
SY15_kirkas_area1	0.37	0.65	1.30	0.19	0.10	2.17	1.86	93.36	100.00
SY15_kirkas_area1	0.44	0.79	1.31	0.21	0.15	2.21	2.17	92.72	100.00
SY15_kirkas_area1	0.58	0.87	1.38	0.22	0.10	2.21	2.16	92.47	100.00
SY15_kirkas_area1	0.68	0.98	1.41	0.18	0.11	2.33	2.33	91.99	100.00
SY15_kirkas_area1	0.78	1.07	1.58	0.24	0.12	2.30	2.31	91.61	100.00
SY15_kirkas_area1	1.07	1.42	1.76	0.25	0.11	2.40	2.45	90.54	100.00
SY15_kirkas_area1	1.22	1.54	1.82	0.24	0.10	2.46	2.44	90.18	100.00
SY15_kirkas_area1	1.38	1.77	1.90	0.24	0.05	2.39	2.49	89.78	100.00
SY15_kirkas_area1	1.53	1.92	2.10	0.29	0.08	2.36	2.39	89.34	100.00
SY15_kirkas_area1	1.66	1.98	2.16	0.25	0.08	2.38	2.33	89.16	100.00
SY15_kirkas_area1	1.70	2.13	2.24	0.27	0.14	2.39	2.28	88.84	100.00
SY15_kirkas_area1	1.75	2.22	2.16	0.24	0.07	2.35	2.28	88.92	100.00
SY15_kirkas_area1	2.03	2.50	2.45	0.31	0.08	2.37	2.37	87.89	100.00
SY16_kirkas_area1	0.27	0.39	0.73	0.44	0.06	1.60	0.93	95.58	100.00
SY16_kirkas_area1	0.27	0.39	0.71	0.41	0.06	1.63	0.91	95.62	100.00
SY16_kirkas_area1	0.26	0.44	0.74	0.42	0.05	1.62	0.88	95.59	100.00
SY16_kirkas_area1	0.29	0.41	0.76	0.43	0.06	1.59	0.89	95.57	100.00
SY16_kirkas_area1	0.28	0.47	0.76	0.42	0.05	1.72	0.92	95.37	100.00
SY16_kirkas_area1	0.30	0.43	0.80	0.43	0.07	1.65	0.90	95.41	100.00
SY16_kirkas_area1	0.29	0.44	0.83	0.42	0.09	1.68	0.93	95.32	100.00
SY16_kirkas_area1	0.28	0.44	0.79	0.43	0.06	1.71	0.92	95.37	100.00
SY16_kirkas_area1	0.30	0.47	0.77	0.42	0.09	1.75	0.95	95.26	100.00
SY16_kirkas_area1	0.32	0.46	0.80	0.43	0.10	1.69	0.95	95.26	100.00
SY16_kirkas_area1	0.31	0.46	0.81	0.44	0.06	1.72	0.95	95.24	100.00
SY16_kirkas_area1	0.30	0.46	0.76	0.44	0.07	1.72	0.95	95.30	100.00
SY16_kirkas_area1	0.32	0.47	0.77	0.44	0.07	1.74	0.95	95.23	100.00
SY46_kirkas_area1	1.34	2.43	1.60	0.31	0.04	0.00	0.00	94.28	100.00
SY46_kirkas_area1	1.31	2.18	1.57	0.33	0.02	0.00	0.00	94.58	100.00
SY46_kirkas_area1	1.16	2.29	1.55	0.34	0.06	0.02	0.00	94.58	100.00
SY46_kirkas_area1	1.12	2.10	1.55	0.31	0.04	0.00	0.00	94.88	100.00
SY46_kirkas_area1	1.06	2.12	1.49	0.33	0.08	0.00	0.00	94.92	100.00
SY46_kirkas_area1	1.08	2.17	1.54	0.32	0.05	0.01	0.00	94.83	100.00
SY46_kirkas_area1	1.06	2.15	1.56	0.34	0.03	0.01	0.00	94.84	100.00

SY_48_kirkas_area1	0.04	0.10	0.02	0.09	0.01	0.01	0.00	99.73	100.00
SY_48_kirkas_area1	0.02	0.10	0.00	0.05	0.06	0.00	0.00	99.78	100.00
SY_48_kirkas_area1	0.04	0.11	0.02	0.05	0.04	0.00	0.00	99.75	100.00
SY_48_kirkas_area1	0.04	0.10	0.02	0.06	0.03	0.00	0.00	99.76	100.00
SY_48_kirkas_area1	0.03	0.10	0.00	0.09	0.05	0.00	0.00	99.73	100.00
SY_48_kirkas_area1	0.04	0.10	0.00	0.08	0.06	0.00	0.00	99.72	100.00
SY_48_kirkas_area1	0.04	0.10	0.00	0.03	0.03	0.00	0.00	99.79	100.00
SY_48_kirkas_area1	0.03	0.11	0.03	0.07	0.04	0.00	0.00	99.71	100.00
SY_48_kirkas_area1	0.04	0.11	0.02	0.07	0.06	0.00	0.00	99.69	100.00
SY_48_kirkas_area1	0.06	0.11	0.01	0.07	0.04	0.01	0.00	99.72	100.00
SY_48_kirkas_area1	0.05	0.11	0.00	0.10	0.02	0.00	0.00	99.71	100.00
SY_48_kirkas_area1	0.05	0.12	0.00	0.07	0.03	0.02	0.01	99.69	100.00
SY_48_kirkas_area2	0.02	0.01	0.00	0.10	0.03	0.00	0.00	99.85	100.00
SY_48_kirkas_area2	0.02	0.01	0.00	0.06	0.05	0.00	0.00	99.85	100.00
SY_48_kirkas_area2	0.01	0.04	0.01	0.08	0.03	0.02	0.00	99.81	100.00
SY_48_kirkas_area2	0.03	0.05	0.00	0.10	0.05	0.00	0.00	99.78	100.00
SY_48_kirkas_area2	0.02	0.05	0.01	0.08	0.02	0.00	0.00	99.83	100.00
SY_48_kirkas_area2	0.04	0.05	0.00	0.06	0.03	0.01	0.00	99.80	100.00
SY_48_kirkas_area2	0.03	0.06	0.00	0.09	0.01	0.00	0.00	99.82	100.00
SY_48_kirkas_area2	0.02	0.05	0.00	0.07	0.03	0.00	0.00	99.82	100.00
SY_48_kirkas_area2	0.04	0.06	0.02	0.08	0.05	0.02	0.00	99.73	100.00
SY_48_kirkas_area2	0.04	0.06	0.00	0.08	0.04	0.00	0.00	99.79	100.00
SY_48_kirkas_area2	0.03	0.07	0.00	0.05	0.02	0.00	0.00	99.82	100.00
SY_49_kirkas_area1	0.12	0.00	0.00	0.07	0.05	0.00	0.00	99.76	100.00
SY_49_kirkas_area1	0.18	0.01	0.01	0.07	0.05	0.00	0.00	99.69	100.00
SY_49_kirkas_area1	0.27	0.00	0.01	0.06	0.02	0.00	0.00	99.65	100.00
SY_49_kirkas_area1	0.42	0.00	0.00	0.06	0.03	0.00	0.00	99.49	100.00
SY_49_kirkas_area1	0.52	0.00	0.01	0.08	0.05	0.00	0.01	99.35	100.00
SY_49_kirkas_area1	0.71	0.00	0.00	0.03	0.03	0.00	0.01	99.21	100.00
SY_49_kirkas_area1	0.80	0.00	0.00	0.08	0.02	0.00	0.00	99.10	100.00
SY_49_kirkas_area1	0.93	0.00	0.02	0.04	0.01	0.00	0.00	99.00	100.00
SY_49_kirkas_area1	0.95	0.01	0.00	0.09	0.04	0.00	0.00	98.92	100.00
SY_49_kirkas_area1	1.10	0.00	0.01	0.06	0.03	0.00	0.00	98.81	100.00
SY_49_kirkas_area1	1.05	0.01	0.01	0.03	0.02	0.01	0.00	98.86	100.00
SY_49_kirkas_area1	1.25	0.00	0.00	0.06	0.03	0.00	0.00	98.65	100.00
SY_49_kirkas_area1	1.26	0.01	0.00	0.07	0.03	0.00	0.00	98.63	100.00
SY_49_kirkas_area1	1.46	0.00	0.00	0.06	0.04	0.00	0.00	98.43	100.00
Sy33_kirkas_alue1	0.08	0.01	0.01	0.03	0.04	0.00	0.00	99.83	100.00
Sy33_kirkas_alue1	0.09	0.00	0.01	0.04	0.03	0.00	0.00	99.82	100.00
Sy33_kirkas_alue1	0.08	0.01	0.03	0.03	0.05	0.00	0.00	99.80	100.00
Sy33_kirkas_alue1	0.09	0.00	0.02	0.06	0.07	0.01	0.00	99.75	100.00
Sy33_kirkas_alue1	0.08	0.01	0.01	0.04	0.04	0.00	0.00	99.82	100.00
Sy33_kirkas_alue1	0.09	0.01	0.00	0.06	0.00	0.00	0.00	99.83	100.00

Sy33_kirkas_alue1	0.07	0.00	0.00	0.05	0.03	0.00	0.00	99.85	100.00
Sy33_kirkas_alue1	0.10	0.02	0.00	0.03	0.06	0.00	0.00	99.79	100.00
Sy33_kirkas_alue2	0.40	0.05	0.02	0.06	0.01	0.01	0.00	99.45	100.00
Sy33_kirkas_alue2	0.39	0.04	0.03	0.08	0.03	0.00	0.00	99.43	100.00
Sy33_kirkas_alue2	0.39	0.06	0.02	0.07	0.00	0.00	0.00	99.46	100.00
Sy33_kirkas_alue2	0.41	0.04	0.00	0.09	0.07	0.00	0.00	99.38	100.00
Sy33_kirkas_alue2	0.40	0.03	0.03	0.06	0.02	0.00	0.00	99.46	100.00
Sy33_kirkas_alue2	0.39	0.04	0.01	0.10	0.00	0.04	0.00	99.41	100.00
Sy33_kirkas_alue2	0.41	0.05	0.01	0.06	0.03	0.00	0.00	99.44	100.00
Sy33_kirkas_alue2	0.43	0.06	0.02	0.08	0.04	0.01	0.00	99.36	100.00
SY34_kirkas_alue1	0.22	0.09	0.00	0.06	0.05	0.00	0.00	99.58	100.00
SY34_kirkas_alue1	0.40	0.38	0.02	0.11	0.04	0.00	0.03	99.03	100.00
SY34_kirkas_alue1	0.20	0.02	0.00	0.07	0.05	0.00	0.00	99.67	100.00
SY34_kirkas_alue1	0.31	0.17	0.01	0.04	0.03	0.00	0.00	99.45	100.00
SY34_kirkas_alue1	0.25	0.13	0.00	0.09	0.05	0.00	0.00	99.47	100.00
SY34_kirkas_alue1	0.19	0.06	0.01	0.09	0.02	0.01	0.00	99.63	100.00
SY34_kirkas_alue1	0.21	0.04	0.01	0.04	0.07	0.00	0.00	99.62	100.00
SY34_kirkas_alue1	0.20	0.03	0.00	0.11	0.02	0.00	0.00	99.62	100.00
SY34_kirkas_alue1	0.20	0.04	0.01	0.06	0.05	0.01	0.00	99.62	100.00
SY34_kirkas_alue1	0.22	0.02	0.02	0.09	0.00	0.00	0.00	99.64	100.00
SY34_kirkas_alue1	0.17	0.04	0.01	0.08	0.02	0.00	0.00	99.67	100.00
SY34_kirkas_alue1	0.15	0.03	0.00	0.05	0.02	0.00	0.00	99.75	100.00
SY34_kirkas_alue1	0.19	0.04	0.02	0.09	0.00	0.02	0.00	99.64	100.00
SY34_kirkas_alue1	0.17	0.03	0.01	0.06	0.00	0.01	0.00	99.71	100.00
SY34_kirkas_alue1	0.21	0.01	0.02	0.08	0.05	0.00	0.00	99.64	100.00
SY34_kirkas_alue1	0.22	0.02	0.01	0.05	0.02	0.00	0.01	99.68	100.00
SY47_kirkas_alue1	0.37	0.00	0.00	0.02	0.03	0.01	0.09	99.47	100.00
SY47_kirkas_alue1	0.33	0.02	0.05	0.07	0.06	0.02	0.05	99.39	100.00
SY47_kirkas_alue1	0.36	0.01	0.00	0.02	0.04	0.02	0.07	99.47	100.00
SY47_kirkas_alue1	0.36	0.00	0.02	0.09	0.04	0.05	0.04	99.40	100.00
SY47_kirkas_alue1	0.39	0.00	0.00	0.07	0.01	0.01	0.06	99.47	100.00
SY47_kirkas_alue1	0.36	0.00	0.00	0.06	0.02	0.03	0.05	99.48	100.00
SY47_kirkas_alue1	0.36	0.00	0.00	0.07	0.03	0.04	0.08	99.41	100.00
SY47_kirkas_alue1	0.39	0.01	0.01	0.10	0.00	0.02	0.05	99.42	100.00
SY47_kirkas_alue1	0.37	0.00	0.00	0.03	0.01	0.02	0.06	99.49	100.00
SY47_kirkas_alue1	0.37	0.01	0.00	0.07	0.01	0.02	0.05	99.46	100.00
SY47_kirkas_alue1	0.36	0.01	0.00	0.03	0.01	0.00	0.03	99.56	100.00
SY47_kirkas_alue1	0.37	0.00	0.00	0.09	0.03	0.01	0.05	99.45	100.00
SY25_kirkas area1	0.05	0.01	0.02	0.06	0.02	0.00	0.06	99.78	100.00
SY25_kirkas area1	0.07	0.02	0.00	0.06	0.01	0.00	0.06	99.77	100.00
SY25_kirkas area1	0.06	0.03	0.01	0.07	0.03	0.00	0.06	99.74	100.00
SY25_kirkas area1	0.04	0.02	0.02	0.04	0.03	0.01	0.05	99.79	100.00
SY25_kirkas area1	0.06	0.02	0.00	0.06	0.05	0.00	0.04	99.77	100.00

SY25_kirkas area1	0.07	0.02	0.02	0.05	0.03	0.00	0.06	99.75	100.00
SY25_kirkas area1	0.08	0.01	0.00	0.03	0.01	0.01	0.05	99.82	100.00
SY25_kirkas area1	0.08	0.01	0.02	0.08	0.04	0.00	0.06	99.71	100.00
SY25_kirkas area1	0.07	0.01	0.00	0.08	0.01	0.01	0.04	99.77	100.00
SY25_kirkas area1	0.06	0.01	0.02	0.08	0.02	0.00	0.05	99.76	100.00
SY25_kirkas area1	0.05	0.01	0.00	0.07	0.02	0.01	0.06	99.78	100.00
SY25_kirkas area1	0.06	0.01	0.03	0.07	0.01	0.01	0.05	99.75	100.00
SY29_kirkas_alue1	0.15	0.00	0.03	0.07	0.04	0.31	0.27	99.13	100.00
SY29_kirkas_alue1	0.14	0.03	0.01	0.05	0.05	0.31	0.30	99.12	100.00
SY29_kirkas_alue1	0.15	0.00	0.03	0.08	0.05	0.30	0.31	99.08	100.00
SY29_kirkas_alue1	0.14	0.02	0.01	0.06	0.02	0.29	0.29	99.16	100.00
SY29_kirkas_alue1	0.18	0.01	0.00	0.07	0.02	0.28	0.27	99.17	100.00
SY29_kirkas_alue1	0.16	0.01	0.00	0.07	0.03	0.26	0.31	99.15	100.00
SY29_kirkas_alue1	0.16	0.01	0.01	0.05	0.01	0.31	0.26	99.18	100.00
SY29_kirkas_alue1	0.14	0.03	0.01	0.01	0.05	0.28	0.29	99.18	100.00
SY29_kirkas_alue1	0.18	0.02	0.00	0.05	0.00	0.30	0.28	99.18	100.00
SY29_kirkas_alue1	0.17	0.03	0.00	0.09	0.00	0.29	0.28	99.13	100.00
SY29_kirkas_alue1	0.15	0.00	0.00	0.05	0.02	0.26	0.26	99.26	100.00
SY29_kirkas_alue1	0.18	0.01	0.01	0.07	0.04	0.27	0.26	99.17	100.00
SY29_kirkas_alue1	0.17	0.01	0.01	0.08	0.05	0.25	0.24	99.17	100.00
SY30_kirkas_alue1	0.13	0.02	0.00	0.09	0.01	0.24	0.25	99.26	100.00
SY30_kirkas_alue1	0.18	0.01	0.00	0.11	0.03	0.23	0.26	99.18	100.00
SY30_kirkas_alue1	0.15	0.02	0.00	0.06	0.04	0.26	0.28	99.20	100.00
SY30_kirkas_alue1	0.15	0.03	0.02	0.00	0.04	0.22	0.26	99.28	100.00
SY30_kirkas_alue1	0.15	0.02	0.00	0.09	0.02	0.27	0.25	99.20	100.00
SY30_kirkas_alue1	0.18	0.03	0.00	0.06	0.03	0.25	0.24	99.20	100.00
SY30_kirkas_alue1	0.17	0.02	0.00	0.06	0.09	0.25	0.26	99.17	100.00
SY30_kirkas_alue1	0.16	0.04	0.02	0.05	0.03	0.24	0.25	99.21	100.00
SY30_kirkas_alue1	0.16	0.03	0.00	0.04	0.00	0.25	0.26	99.25	100.00
SY30_kirkas_alue1	0.17	0.00	0.03	0.07	0.00	0.23	0.27	99.21	100.00
SY30_kirkas_alue1	0.17	0.02	0.02	0.07	0.03	0.26	0.25	99.18	100.00
SY30_kirkas_alue1	0.18	0.02	0.01	0.05	0.00	0.23	0.25	99.26	100.00
SY41_kirkas_alue1	0.38	0.39	0.07	0.12	0.15	0.29	0.38	98.22	100.00
SY41_kirkas_alue1	0.39	0.40	0.08	0.11	0.11	0.28	0.35	98.28	100.00
SY41_kirkas_alue1	0.38	0.40	0.03	0.08	0.13	0.29	0.38	98.30	100.00
SY41_kirkas_alue1	0.37	0.40	0.05	0.10	0.11	0.26	0.35	98.36	100.00
SY41_kirkas_alue1	0.39	0.38	0.06	0.12	0.11	0.23	0.34	98.37	100.00
SY41_kirkas_alue1	0.38	0.38	0.03	0.10	0.14	0.24	0.36	98.38	100.00
SY41_kirkas_alue1	0.37	0.38	0.06	0.09	0.13	0.25	0.39	98.34	100.00
SY41_kirkas_alue2	0.30	0.03	0.02	0.08	0.04	0.14	0.15	99.23	100.00
SY41_kirkas_alue2	0.31	0.04	0.02	0.07	0.05	0.13	0.18	99.20	100.00
SY41_kirkas_alue2	0.32	0.04	0.01	0.08	0.02	0.13	0.20	99.21	100.00
SY41_kirkas_alue2	0.29	0.04	0.02	0.09	0.02	0.17	0.21	99.16	100.00

SY41_kirkas_alue2	0.30	0.04	0.04	0.09	0.09	0.19	0.18	99.08	100.00
SY41_kirkas_alue2	0.28	0.02	0.00	0.04	0.01	0.16	0.25	99.25	100.00
SY41_kirkas_alue2	0.27	0.04	0.02	0.06	0.02	0.15	0.23	99.21	100.00
SY42_kirkas_alue1	0.17	0.02	0.06	0.10	0.07	0.49	0.30	98.80	100.00
SY42_kirkas_alue1	0.13	0.02	0.04	0.11	0.01	0.52	0.30	98.88	100.00
SY42_kirkas_alue1	0.15	0.02	0.06	0.08	0.04	0.50	0.34	98.81	100.00
SY42_kirkas_alue1	0.15	0.00	0.04	0.11	0.04	0.50	0.31	98.84	100.00
SY42_kirkas_alue1	0.15	0.02	0.05	0.09	0.00	0.49	0.31	98.90	100.00
SY42_kirkas_alue1	0.15	0.00	0.06	0.07	0.04	0.54	0.31	98.82	100.00
SY42_kirkas_alue1	0.15	0.01	0.03	0.11	0.05	0.51	0.36	98.77	100.00
SY42_kirkas_alue1	0.16	0.03	0.05	0.08	0.01	0.50	0.36	98.81	100.00
SY42_kirkas_alue1	0.14	0.02	0.02	0.09	0.05	0.52	0.30	98.87	100.00
SY42_kirkas_alue2	0.12	0.02	0.05	0.05	0.01	0.66	0.48	98.61	100.00
SY42_kirkas_alue2	0.15	0.02	0.01	0.09	0.04	0.67	0.44	98.58	100.00
SY42_kirkas_alue2	0.13	0.02	0.02	0.04	0.05	0.70	0.44	98.59	100.00
SY42_kirkas_alue2	0.14	0.02	0.00	0.11	0.08	0.67	0.44	98.54	100.00
SY42_kirkas_alue2	0.12	0.02	0.02	0.05	0.04	0.73	0.42	98.60	100.00
SY42_kirkas_alue2	0.13	0.01	0.03	0.10	0.04	0.64	0.40	98.65	100.00
SY42_kirkas_alue2	0.16	0.03	0.02	0.11	0.02	0.65	0.40	98.60	100.00
SY42_kirkas_alue2	0.15	0.02	0.03	0.09	0.06	0.65	0.38	98.62	100.00
SY42_kirkas_alue2	0.13	0.02	0.00	0.05	0.05	0.66	0.43	98.67	100.00
SY42_kirkas_alue2	0.15	0.02	0.06	0.09	0.00	0.68	0.38	98.62	100.00
SY42_kirkas_alue2	0.16	0.03	0.00	0.07	0.03	0.70	0.39	98.62	100.00
SY45_kirkas-alue1	0.11	0.09	0.18	0.10	0.10	2.37	1.36	95.68	100.00
SY45_kirkas-alue1	0.10	0.11	0.17	0.09	0.05	2.19	1.29	96.01	100.00
SY45_kirkas-alue1	0.09	0.09	0.18	0.13	0.03	2.15	1.22	96.11	100.00
SY45_kirkas-alue1	0.12	0.09	0.16	0.05	0.05	1.92	1.13	96.47	100.00
SY45_kirkas-alue1	0.11	0.07	0.18	0.13	0.05	1.89	1.11	96.45	100.00
SY45_kirkas-alue1	0.10	0.10	0.20	0.11	0.09	1.75	1.02	96.63	100.00
SY45_kirkas-alue1	0.09	0.08	0.16	0.12	0.10	1.80	1.03	96.62	100.00
SY45_kirkas-alue1	0.10	0.10	0.18	0.10	0.06	1.70	1.04	96.71	100.00
SY45_kirkas-alue1	0.11	0.09	0.21	0.09	0.09	1.80	1.05	96.58	100.00
SY45_kirkas-alue1	0.13	0.09	0.16	0.08	0.06	1.81	1.00	96.67	100.00
SY45_kirkas-alue1	0.14	0.11	0.19	0.10	0.10	1.80	1.06	96.50	100.00
SY45_kirkas-alue1	0.12	0.10	0.22	0.11	0.07	1.76	0.97	96.64	100.00

Slag phase wt-%

Weight%										
Sample	O	Si	Ca	Fe	Ga	Ge	In	Sn	Pb	Total
SY_50_kuona_area1	20.53	10.13	6.16	5.68	0.73	0.22	0.59	0.20	54.77	99.01
SY_50_kuona_area1	20.45	10.17	6.14	5.69	0.76	0.20	0.58	0.19	54.85	99.04

SY_50_kuona_area1	20.44	10.13	6.14	5.73	0.75	0.19	0.59	0.20	54.77	98.94
SY_50_kuona_area1	20.56	10.13	6.13	5.64	0.73	0.22	0.56	0.17	54.78	98.94
SY_50_kuona_area1	20.50	10.19	6.11	5.68	0.74	0.22	0.60	0.17	54.52	98.73
SY_50_kuona_area1	20.53	10.13	6.16	5.66	0.75	0.21	0.60	0.19	54.77	99.00
SY_50_kuona_area1	20.35	10.15	6.16	5.71	0.73	0.21	0.60	0.19	54.60	98.71
SY_50_kuona_area1	20.05	10.23	6.18	5.67	0.75	0.20	0.58	0.18	54.67	98.51
SY_50_kuona_area2	19.87	10.52	5.55	6.10	0.82	0.20	0.65	0.20	54.16	98.05
SY_50_kuona_area2	19.72	10.49	5.58	5.97	0.80	0.19	0.65	0.19	53.75	97.35
SY_50_kuona_area2	19.79	10.54	5.65	6.12	0.79	0.21	0.68	0.21	53.65	97.63
SY_50_kuona_area2	19.60	10.45	5.41	6.10	0.82	0.20	0.64	0.21	54.54	97.98
SY_50_kuona_area2	19.37	10.59	5.58	6.06	0.81	0.23	0.68	0.19	54.08	97.60
SY_50_kuona_area2	20.34	10.66	5.73	6.06	0.80	0.17	0.66	0.20	53.42	98.03
SY_50_kuona_area2	20.32	10.58	5.75	6.11	0.82	0.21	0.66	0.20	53.44	98.09
SY_50_kuona_area2	20.05	10.66	5.59	6.07	0.80	0.19	0.66	0.18	53.68	97.88
SY_51_kuona_area1	19.41	10.21	6.30	5.83	0.49	0.25	0.63	0.22	54.58	97.93
SY_51_kuona_area1	19.62	10.20	6.33	5.87	0.49	0.24	0.66	0.23	54.97	98.62
SY_51_kuona_area1	19.72	10.20	6.29	5.85	0.48	0.26	0.66	0.21	54.94	98.61
SY_51_kuona_area1	21.06	10.21	6.31	5.91	0.49	0.26	0.68	0.21	54.97	100.11
SY_51_kuona_area1	20.12	10.31	6.27	5.87	0.49	0.23	0.63	0.21	54.50	98.63
SY_51_kuona_area1	19.84	10.22	6.31	5.90	0.51	0.24	0.68	0.23	54.85	98.76
SY_51_kuona_area1	19.80	10.26	6.28	5.86	0.49	0.26	0.65	0.21	54.43	98.23
SY_51_kuona_area2	20.80	10.16	6.30	5.91	0.45	0.26	0.65	0.22	55.28	100.03
SY_51_kuona_area2	20.27	10.10	6.28	5.85	0.46	0.25	0.63	0.21	55.02	99.06
SY_51_kuona_area2	20.67	10.01	6.30	5.92	0.43	0.24	0.65	0.20	55.74	100.16
SY_51_kuona_area2	20.29	10.14	6.28	5.87	0.45	0.26	0.62	0.18	55.03	99.13
SY_51_kuona_area2	19.86	10.10	6.31	5.90	0.46	0.26	0.67	0.22	55.12	98.88
SY_51_kuona_area2	20.18	10.05	6.26	5.89	0.45	0.26	0.67	0.22	55.66	99.64
SY_51_kuona_area2	19.73	10.21	6.25	5.89	0.43	0.25	0.66	0.22	55.28	98.93
SY_51_kuona_area2	20.42	10.15	6.27	5.86	0.46	0.23	0.62	0.20	55.03	99.23
SY_51_kuona_area2	19.77	10.09	6.26	5.80	0.46	0.24	0.64	0.23	55.31	98.80
SY31_kuona_alue1	27.84	16.13	8.20	9.42	0.12	0.12	0.37	0.14	37.40	99.73
SY31_kuona_alue1	28.37	16.08	8.09	9.32	0.12	0.06	0.34	0.15	37.43	99.95
SY31_kuona_alue1	27.65	16.20	8.04	9.34	0.13	0.11	0.35	0.15	37.27	99.25
SY31_kuona_alue1	27.98	16.05	8.08	9.31	0.12	0.10	0.32	0.17	37.17	99.31
SY31_kuona_alue1	27.74	16.18	8.13	9.37	0.13	0.11	0.31	0.13	36.94	99.03
SY31_kuona_alue1	28.18	16.21	7.98	9.38	0.12	0.11	0.30	0.14	37.12	99.54
SY31_kuona_alue1	27.28	16.09	8.09	9.36	0.10	0.10	0.33	0.13	37.42	98.92
SY31_kuona_alue1	27.05	16.13	8.02	9.35	0.13	0.06	0.34	0.13	37.13	98.34
SY31_kuona_alue1	28.21	16.19	8.01	9.44	0.15	0.08	0.34	0.15	37.36	99.93
SY31_kuona_alue1	28.32	16.13	8.02	9.36	0.15	0.10	0.32	0.16	37.48	100.04
SY31_kuona_alue1	27.61	16.06	8.06	9.28	0.16	0.08	0.31	0.15	37.02	98.72
SY31_kuona_alue1	27.05	16.08	7.95	9.16	0.12	0.09	0.34	0.13	37.37	98.30
SY31_kuona_alue1	26.92	16.14	8.05	9.27	0.13	0.11	0.34	0.16	37.04	98.17

SY31_kuona_alue1	27.50	16.14	8.09	9.28	0.16	0.09	0.32	0.14	37.11	98.83
SY31_kuona_alue1	26.96	16.15	7.97	9.31	0.16	0.08	0.34	0.14	36.93	98.04
SY31_kuona_alue1	26.52	16.10	8.01	9.22	0.12	0.06	0.33	0.15	36.87	97.39
SY37_kuona_alue1 (20 µm from the edge of Pb)	25.14	13.88	7.74	7.01	2.13	0.22	1.61	0.66	40.00	98.38
SY37_kuona_alue1 (20 µm from the edge of Pb)	24.54	13.94	7.73	7.05	2.17	0.21	1.62	0.64	40.27	98.16
SY37_kuona_alue1 (20 µm from the edge of Pb)	24.24	13.89	7.79	7.08	2.16	0.21	1.64	0.67	39.78	97.44
SY37_kuona_alue1 (20 µm from the edge of Pb)	25.11	13.96	7.73	7.02	2.19	0.15	1.60	0.66	40.39	98.81
SY37_kuona_alue1 (20 µm from the edge of Pb)	24.37	13.96	7.83	7.04	2.17	0.24	1.62	0.62	39.61	97.47
SY37_kuona_alue1 (20 µm from the edge of Pb)	25.41	13.89	7.42	6.96	2.19	0.20	1.67	0.64	40.84	99.21
SY37_kuona_alue1 (20 µm from the edge of Pb)	24.44	13.96	7.73	7.01	2.21	0.19	1.65	0.65	40.13	97.98
SY37_kuona_alue2 (20 µm from the edge of Pb)	25.16	13.69	7.54	6.92	2.08	0.19	1.60	0.63	40.71	98.52
SY37_kuona_alue2 (20 µm from the edge of Pb)	24.62	13.66	7.55	7.00	2.06	0.19	1.69	0.66	40.91	98.33
SY37_kuona_alue2 (20 µm from the edge of Pb)	24.72	13.59	7.45	6.87	2.07	0.17	1.66	0.64	40.57	97.74
SY37_kuona_alue2 (20 µm from the edge of Pb)	25.15	13.81	7.44	7.04	2.08	0.19	1.72	0.68	40.70	98.81
SY37_kuona_alue2 (20 µm from the edge of Pb)	24.99	13.69	7.52	6.94	2.08	0.17	1.64	0.61	40.42	98.08
SY37_kuona_alue2 (20 µm from the edge of Pb)	23.83	13.65	7.53	6.98	2.07	0.18	1.66	0.65	40.91	97.46
SY37_kuona_alue2 (20 µm from the edge of Pb)	23.84	13.70	7.57	6.93	2.08	0.18	1.64	0.63	40.73	97.31

Sy23_kuona_alue1	31.37	19.31	8.59	9.13	0.09	0.03	0.65	0.47	28.44	98.07
Sy23_kuona_alue1	30.88	19.40	8.61	9.16	0.08	0.00	0.67	0.45	28.32	97.58
Sy23_kuona_alue1	30.89	19.34	8.58	9.28	0.10	0.04	0.65	0.46	28.58	97.93
Sy23_kuona_alue1	31.01	19.46	8.62	9.13	0.07	0.01	0.66	0.48	28.49	97.94
Sy23_kuona_alue1	30.11	19.28	8.58	9.20	0.10	0.04	0.66	0.46	28.40	96.83
Sy23_kuona_alue1	30.27	19.50	8.63	8.97	0.07	0.05	0.64	0.47	28.78	97.39
Sy23_kuona_alue1	30.60	19.47	8.63	9.10	0.09	0.03	0.65	0.43	28.48	97.49
Sy23_kuona_alue1	30.86	19.46	8.65	8.99	0.09	0.06	0.67	0.49	28.43	97.71
Sy23_kuona_alue1	31.22	19.45	8.55	9.07	0.08	0.07	0.64	0.45	28.24	97.78
Sy23_kuona_alue2	29.48	17.14	8.73	5.54	3.70	0.89	2.33	0.91	29.12	97.85
Sy23_kuona_alue2	28.93	17.30	8.75	5.65	3.72	0.93	2.27	0.87	28.91	97.34
Sy23_kuona_alue2	30.11	17.15	8.73	5.63	3.70	0.90	2.33	0.88	29.33	98.77
Sy23_kuona_alue2	29.62	17.25	8.71	5.59	3.71	0.90	2.33	0.86	28.93	97.89
Sy23_kuona_alue2	29.02	17.07	8.74	5.57	3.71	0.90	2.37	0.89	29.19	97.48
Sy23_kuona_alue2	29.01	17.04	8.73	5.71	3.65	0.93	2.28	0.86	29.13	97.34
Sy23_kuona_alue2	29.63	17.12	8.80	5.52	3.68	0.89	2.32	0.91	29.33	98.20
Sy23_kuona_alue2	28.80	17.01	8.77	5.58	3.64	0.87	2.26	0.85	29.19	96.97
Sy23_kuona_alue2	29.47	17.16	8.75	5.58	3.66	0.89	2.32	0.91	29.79	98.53
Sy23_kuona_alue2	29.55	17.19	8.71	5.63	3.67	0.92	2.28	0.87	29.28	98.10
Sy23_kuona_alue2	28.62	17.22	8.68	5.56	3.70	0.86	2.34	0.90	29.41	97.29
SY11_kuona_alue1	29.71	16.10	10.26	15.01	0.85	0.02	1.77	0.70	25.11	99.53
SY11_kuona_alue1	29.62	16.11	10.28	15.11	0.82	0.01	1.73	0.65	25.06	99.39
SY11_kuona_alue1	29.41	16.05	10.24	15.09	0.82	0.06	1.72	0.67	25.21	99.27
SY11_kuona_alue1	29.33	16.14	10.32	14.99	0.82	0.04	1.72	0.64	24.99	99.00
SY11_kuona_alue1	28.74	16.17	10.29	14.94	0.85	0.01	1.75	0.67	24.98	98.40
SY11_kuona_alue2	33.01	18.86	12.36	19.06	1.13	0.13	1.66	0.56	10.80	97.57
SY11_kuona_alue2	33.20	18.87	12.30	19.35	1.15	0.11	1.72	0.58	11.00	98.28
SY11_kuona_alue2	33.82	18.70	12.38	19.15	1.12	0.09	1.67	0.55	11.06	98.55
SY11_kuona_alue2	33.49	18.77	12.40	19.17	1.14	0.12	1.74	0.57	11.04	98.43
SY11_kuona_alue2	33.55	18.74	12.34	19.16	1.15	0.10	1.68	0.58	10.97	98.27
SY11_kuona_alue2	33.36	18.94	12.35	19.22	1.16	0.11	1.71	0.56	10.88	98.29
SY11_kuona_alue2	33.24	18.94	12.43	19.25	1.14	0.06	1.74	0.54	10.91	98.26
SY11_kuona_alue3	33.29	19.53	12.35	20.65	0.66	0.06	1.29	0.48	9.60	97.90
SY11_kuona_alue3	33.09	19.47	12.38	20.60	0.66	0.07	1.25	0.46	9.50	97.47
SY11_kuona_alue3	33.04	19.47	12.38	20.53	0.64	0.03	1.28	0.47	9.55	97.39
SY11_kuona_alue3	32.81	19.61	12.28	20.81	0.62	0.08	1.26	0.45	9.57	97.50
SY11_kuona_alue3	33.55	19.61	12.28	20.91	0.60	0.08	1.25	0.48	9.74	98.51
SY11_kuona_alue3	33.71	19.59	12.33	20.97	0.61	0.07	1.24	0.45	9.81	98.77
SY27_kuona_alue1	38.35	21.25	12.27	12.66	3.10	0.07	3.27	2.38	6.56	99.91
SY27_kuona_alue1	38.00	21.41	12.33	12.40	3.10	0.07	3.26	2.41	6.58	99.57
SY27_kuona_alue1	38.83	21.26	12.30	12.53	3.08	0.05	3.26	2.34	6.68	100.33
SY27_kuona_alue1	38.45	21.25	12.28	12.48	3.09	0.05	3.25	2.36	6.72	99.93
SY27_kuona_alue1	38.27	21.20	12.38	12.47	3.12	0.04	3.30	2.43	6.66	99.86

SY27_kuona_alue1	38.09	21.15	12.28	12.38	3.11	0.07	3.21	2.31	6.55	99.15
SY27_kuona_alue2	37.08	21.08	11.95	11.35	3.61	0.08	3.58	1.91	8.77	99.42
SY27_kuona_alue2	37.70	20.93	12.01	11.27	3.63	0.06	3.57	1.89	8.68	99.74
SY27_kuona_alue2	37.31	21.05	12.07	11.30	3.57	0.08	3.61	1.94	8.71	99.62
SY27_kuona_alue2	37.31	21.02	11.99	11.07	3.55	0.09	3.61	1.88	8.90	99.41
SY27_kuona_alue2	37.45	21.01	12.05	11.23	3.60	0.07	3.64	1.94	8.88	99.87
SY27_kuona_alue2	37.53	21.01	12.02	11.13	3.61	0.05	3.61	1.89	8.90	99.75
SY13_kuona_alue1	35.65	20.37	11.63	14.78	0.80	0.09	3.24	2.13	10.49	99.19
SY13_kuona_alue1	35.21	20.33	11.68	14.75	0.77	0.08	3.15	2.05	10.41	98.44
SY13_kuona_alue1	35.23	20.20	11.67	14.70	0.80	0.07	3.18	2.10	10.23	98.18
SY13_kuona_alue1	35.10	20.27	11.71	14.87	0.77	0.11	3.06	2.06	10.58	98.53
SY13_kuona_alue1	35.67	20.15	11.64	14.80	0.79	0.10	3.05	2.03	10.62	98.87
SY13_kuona_alue1	35.26	20.09	11.70	14.97	0.78	0.10	2.92	1.94	10.69	98.45
SY13_kuona_alue2	33.75	16.47	14.07	15.02	10.74	0.23	0.66	0.35	6.80	98.09
SY13_kuona_alue2	34.24	16.59	14.13	14.66	10.84	0.22	0.60	0.32	6.78	98.38
SY13_kuona_alue2	34.90	16.79	14.20	14.21	10.84	0.24	0.63	0.32	6.69	98.82
SY13_kuona_alue2	34.46	16.92	14.22	14.15	10.78	0.19	0.60	0.33	6.86	98.52
SY13_kuona_alue2	34.77	16.43	14.39	14.75	10.69	0.25	0.66	0.36	6.83	99.12
SY13_kuona_alue2	34.66	16.36	14.37	15.29	10.69	0.27	0.65	0.31	6.73	99.33
SY13_kuona_alue2	33.60	16.31	14.18	15.58	10.66	0.30	0.68	0.34	6.34	97.99
SY14_kuona_alue1	36.34	19.26	14.29	18.76	7.59	0.07	0.75	0.59	0.51	98.16
SY14_kuona_alue1	36.56	19.19	14.30	18.88	7.55	0.10	0.79	0.60	0.52	98.49
SY14_kuona_alue1	36.10	19.21	14.26	18.82	7.60	0.09	0.74	0.58	0.64	98.03
SY14_kuona_alue1	36.15	19.28	14.29	18.66	7.63	0.05	0.76	0.62	0.52	97.96
SY14_kuona_alue1	36.51	19.25	14.38	18.64	7.59	0.06	0.75	0.57	0.61	98.35
SY14_kuona_alue1	36.35	19.15	14.38	18.64	7.65	0.06	0.77	0.59	0.61	98.20
SY14_kuona_alue2	36.65	18.98	14.24	17.03	8.79	0.14	0.77	0.60	1.93	99.13
SY14_kuona_alue2	37.47	18.92	14.28	16.97	8.64	0.11	0.76	0.64	1.94	99.74
SY14_kuona_alue2	36.48	19.04	14.20	16.97	8.67	0.11	0.75	0.61	1.99	98.84
SY14_kuona_alue2	36.91	18.86	14.27	17.03	8.61	0.13	0.78	0.66	2.14	99.38
SY14_kuona_alue2	36.40	18.84	14.32	17.25	8.66	0.10	0.73	0.62	2.06	98.98
SY14_kuona_alue2	37.39	18.96	14.32	17.83	7.86	0.12	0.81	0.64	2.19	100.13
SY14_kuona_alue2	36.90	18.88	14.26	17.29	8.61	0.10	0.78	0.62	2.13	99.55
SY14_kuona_alue2	37.02	18.95	14.34	17.06	8.52	0.12	0.77	0.64	1.97	99.39
SY14_kuona_alue2	36.49	19.00	14.28	17.35	8.51	0.13	0.77	0.60	1.99	99.12
SY15_kuona_area1	36.36	17.30	15.04	27.77	1.76	0.00	0.49	0.57	0.00	99.29
SY15_kuona_area1	36.57	17.29	15.17	27.65	1.78	0.01	0.47	0.55	0.00	99.50
SY15_kuona_area1	35.43	17.36	15.05	27.75	1.79	0.01	0.48	0.55	0.02	98.44
SY15_kuona_area1	35.88	17.34	14.98	27.83	1.79	0.02	0.48	0.53	0.00	98.85
SY15_kuona_area1	36.35	17.23	15.09	27.80	1.74	0.02	0.43	0.52	0.00	99.17
SY15_kuona_area1	35.94	17.20	15.15	28.10	1.82	0.00	0.40	0.48	0.00	99.10
SY15_kuona_area2	35.78	17.35	14.67	26.81	1.91	0.06	0.77	0.82	0.09	98.25
SY15_kuona_area2	35.34	17.52	14.65	27.16	1.86	0.02	0.76	0.81	0.00	98.12

SY15_kuona_area2	36.03	17.65	14.64	26.93	1.91	0.04	0.77	0.83	0.06	98.85
SY15_kuona_area2	35.11	17.42	14.67	27.06	1.85	0.00	0.74	0.82	0.10	97.79
SY15_kuona_area2	35.88	17.43	14.77	26.94	1.87	0.03	0.76	0.85	0.11	98.64
SY15_kuona_area2	36.25	17.53	14.76	26.92	1.88	0.04	0.77	0.80	0.09	99.05
SY15_kuona_area2	35.05	17.49	14.73	26.93	1.88	0.05	0.79	0.81	0.07	97.82
SY15_kuona_area2	35.70	17.46	14.64	26.78	1.94	0.04	0.77	0.78	0.03	98.16
SY16_kuona_area1	38.24	20.87	14.37	16.86	7.46	0.02	0.33	0.32	0.44	98.90
SY16_kuona_area1	37.81	20.75	14.47	17.05	7.57	0.01	0.33	0.32	0.46	98.77
SY16_kuona_area1	37.93	20.82	14.31	16.84	7.51	0.02	0.35	0.34	0.49	98.61
SY16_kuona_area1	38.58	20.83	14.39	17.09	7.55	0.01	0.32	0.32	0.46	99.53
SY16_kuona_area1	37.86	20.79	14.30	16.79	7.57	0.02	0.33	0.36	0.47	98.49
SY16_kuona_area1	38.39	20.73	14.29	16.97	7.52	0.01	0.31	0.34	0.39	98.94
SY16_kuona_area1	37.40	20.95	14.43	16.86	7.55	0.01	0.33	0.33	0.55	98.42
SY16_kuona_area1	38.12	20.94	14.30	16.77	7.55	0.00	0.33	0.34	0.49	98.85
SY16_kuona_area1	38.31	20.87	14.39	16.90	7.53	0.03	0.32	0.32	0.51	99.18
SY16_kuona_area1	37.62	21.00	14.33	16.91	7.55	0.01	0.30	0.30	0.62	98.65
SY16_kuona_area1	37.00	20.75	14.27	16.83	7.53	0.02	0.33	0.34	0.44	97.52
SY16_kuona_area1	37.66	20.90	14.28	16.84	7.55	0.02	0.32	0.32	0.47	98.35
SY16_kuona_area1	37.03	20.86	14.37	16.85	7.55	0.01	0.33	0.33	0.38	97.72
SY16_kuona_area1	37.62	20.95	14.21	17.01	7.51	0.00	0.32	0.32	0.53	98.47
SY16_kuona_area1	37.39	20.90	14.45	16.80	7.43	0.02	0.33	0.32	0.63	98.27
SY16_kuona_area1	37.82	21.05	14.52	16.74	7.35	0.00	0.33	0.32	0.43	98.57
SY46_kuona_alue1	33.95	17.81	16.02	28.12	2.21	0.00	0.00	0.16	0.01	98.26
SY46_kuona_alue1	33.45	17.82	16.03	27.97	2.23	0.00	0.00	0.16	0.00	97.65
SY46_kuona_alue1	34.08	17.86	16.00	28.21	2.21	0.01	0.00	0.16	0.02	98.55
SY46_kuona_alue1	35.05	17.87	16.14	28.02	2.23	0.00	0.01	0.16	0.00	99.48
SY46_kuona_alue1	34.84	17.86	16.15	28.32	2.27	0.00	0.00	0.17	0.00	99.61
SY46_kuona_alue1	34.32	17.87	16.12	28.00	2.25	0.01	0.00	0.15	0.09	98.80
SY46_kuona_alue2	34.19	18.07	16.21	28.62	2.26	0.00	0.01	0.16	0.04	99.55
SY46_kuona_alue2	34.30	18.10	16.21	28.44	2.28	0.03	0.00	0.14	0.00	99.51
SY46_kuona_alue2	34.00	18.01	16.18	28.44	2.27	0.01	0.01	0.16	0.00	99.07
SY46_kuona_alue2	33.48	18.06	16.20	28.30	2.28	0.00	0.00	0.14	0.10	98.55
SY46_kuona_alue2	32.96	18.09	16.18	28.67	2.24	0.00	0.00	0.17	0.00	98.32
SY46_kuona_alue2	32.86	18.05	16.21	28.16	2.25	0.00	0.00	0.14	0.00	97.68
SY_48_kuona_area1	15.98	7.00	2.82	5.58	0.10	0.19	0.17	0.06	67.01	98.93
SY_48_kuona_area1	15.84	6.87	2.68	5.52	0.11	0.22	0.17	0.06	66.41	97.89
SY_48_kuona_area1	17.42	6.89	2.76	5.55	0.10	0.21	0.17	0.05	66.23	99.38
SY_48_kuona_area1	17.61	7.20	3.11	5.34	0.10	0.16	0.15	0.08	65.93	99.68
SY_48_kuona_area1	16.70	7.41	3.41	5.32	0.13	0.19	0.17	0.05	64.56	97.94
SY_48_kuona_area1	16.40	7.82	4.05	5.12	0.10	0.16	0.16	0.07	63.73	97.60
SY_48_kuona_area2	19.73	8.85	5.83	5.04	0.12	0.21	0.16	0.06	60.14	100.13
SY_48_kuona_area2	18.76	8.69	5.72	4.96	0.11	0.18	0.17	0.06	60.15	98.80
SY_48_kuona_area2	18.04	8.52	5.46	5.15	0.09	0.21	0.16	0.05	60.65	98.34

SY_48_kuona_area2	18.12	8.52	5.55	5.02	0.10	0.23	0.18	0.05	60.65	98.42
SY_48_kuona_area2	17.71	8.31	5.20	5.09	0.10	0.22	0.19	0.07	61.35	98.23
SY_48_kuona_area2	16.93	8.09	4.97	5.14	0.11	0.19	0.19	0.05	62.27	97.95
SY_48_kuona_area2	17.52	8.23	5.23	5.11	0.06	0.20	0.16	0.05	61.76	98.31
SY_49_kuona area1	22.56	11.40	6.18	6.92	0.10	0.29	0.64	0.18	50.20	98.46
SY_49_kuona area1	22.42	11.68	6.42	7.16	0.09	0.29	0.67	0.21	50.67	99.61
SY_49_kuona area1	21.79	11.60	6.42	7.08	0.07	0.31	0.63	0.19	50.63	98.73
SY_49_kuona area1	21.74	11.62	6.41	7.07	0.07	0.31	0.67	0.19	50.27	98.35
SY_49_kuona area1	21.72	11.59	6.42	7.00	0.09	0.33	0.65	0.20	50.36	98.36
SY_49_kuona area1	21.63	11.63	6.43	7.12	0.06	0.32	0.67	0.20	50.51	98.57
SY_49_kuona area1	21.74	11.62	6.46	7.08	0.05	0.34	0.64	0.21	50.21	98.34
SY_49_kuona area1	21.28	11.63	6.44	7.05	0.07	0.32	0.66	0.20	50.24	97.90
SY_49_kuona area1	21.82	11.63	6.40	7.02	0.06	0.31	0.66	0.18	50.12	98.20
SY_49_kuona area1	21.14	11.48	6.41	7.04	0.11	0.35	0.67	0.20	50.11	97.50
Sy33_kuona_alue1	24.73	14.17	6.89	5.40	1.32	0.21	0.79	0.55	44.34	98.41
Sy33_kuona_alue1	24.39	14.19	6.96	5.40	1.32	0.19	0.79	0.54	44.58	98.35
Sy33_kuona_alue1	24.54	14.20	6.93	5.34	1.36	0.19	0.81	0.55	44.78	98.69
Sy33_kuona_alue1	24.29	14.13	6.90	5.38	1.34	0.19	0.76	0.56	44.60	98.15
Sy33_kuona_alue1	24.72	14.11	6.92	5.39	1.34	0.15	0.78	0.55	44.77	98.74
Sy33_kuona_alue1	24.62	14.14	6.88	5.41	1.34	0.12	0.77	0.55	44.88	98.70
Sy33_kuona_alue2	25.54	14.71	7.39	4.69	2.60	0.42	1.49	0.75	40.52	98.12
Sy33_kuona_alue2	25.21	14.83	7.37	4.68	2.60	0.45	1.48	0.72	41.06	98.39
Sy33_kuona_alue2	25.54	14.64	7.35	4.70	2.59	0.49	1.45	0.73	40.95	98.43
Sy33_kuona_alue2	25.55	14.69	7.32	4.69	2.61	0.47	1.45	0.70	40.98	98.46
Sy33_kuona_alue2	25.83	14.65	7.39	4.69	2.58	0.44	1.45	0.71	40.97	98.72
Sy33_kuona_alue2	25.59	14.78	7.29	4.74	2.58	0.45	1.46	0.73	40.80	98.42
SY34_kuona_alue1	33.29	20.23	10.13	7.44	2.53	0.71	2.53	1.15	21.42	99.44
SY34_kuona_alue1	32.53	20.23	10.07	7.47	2.50	0.72	2.58	1.17	21.63	98.90
SY34_kuona_alue1	33.43	20.30	10.16	7.35	2.47	0.70	2.52	1.14	21.42	99.48
SY34_kuona_alue1	34.00	20.35	10.13	7.56	2.49	0.72	2.55	1.16	21.52	100.49
SY34_kuona_alue1	33.38	20.40	10.16	7.45	2.49	0.68	2.51	1.14	21.59	99.79
SY34_kuona_alue1	32.76	20.33	10.10	7.47	2.47	0.73	2.55	1.16	21.52	99.09
SY34_kuona_alue1	33.61	20.38	10.12	7.42	2.50	0.73	2.52	1.15	21.59	100.02
SY34_kuona_alue1	32.42	20.52	10.11	7.49	2.44	0.73	2.54	1.17	21.68	99.09
SY34_kuona_alue1	33.44	20.44	10.10	7.41	2.46	0.70	2.51	1.15	21.75	99.95
SY34_kuona_alue2	32.72	19.59	9.53	5.80	3.72	1.10	2.36	1.87	24.02	100.71
SY34_kuona_alue2	32.46	19.56	9.47	5.69	3.70	1.14	2.31	1.76	23.61	99.70
SY34_kuona_alue2	32.49	19.64	9.44	5.74	3.73	1.06	2.33	1.82	23.90	100.15
SY34_kuona_alue2	32.11	19.62	9.53	5.59	3.68	1.10	2.29	1.80	23.64	99.36
SY34_kuona_alue2	31.66	19.56	9.53	5.80	3.73	1.08	2.35	1.82	23.66	99.19
SY34_kuona_alue2	32.37	19.61	9.50	5.66	3.76	1.09	2.29	1.77	23.86	99.91
SY34_kuona_alue2	31.47	19.54	9.45	5.72	3.75	1.09	2.35	1.83	23.86	99.07
SY34_kuona_alue2	31.15	19.63	9.48	5.67	3.74	1.09	2.33	1.76	23.54	98.40

SY34_kuona_alue3 (500 µm from the edge of Pb)	28.25	18.43	8.34	5.34	1.63	0.89	2.18	1.33	31.63	98.01
SY34_kuona_alue3 (500 µm from the edge of Pb)	29.91	18.30	8.36	5.32	1.60	0.85	2.17	1.26	31.99	99.76
SY34_kuona_alue3 (500 µm from the edge of Pb)	29.77	18.20	8.32	5.37	1.61	0.89	2.21	1.32	32.15	99.83
SY34_kuona_alue3 (500 µm from the edge of Pb)	29.34	18.31	8.32	5.37	1.62	0.86	2.19	1.28	32.40	99.69
SY34_kuona_alue3 (500 µm from the edge of Pb)	28.78	18.30	8.37	5.36	1.59	0.87	2.19	1.32	31.93	98.70
SY34_kuona_alue3 (500 µm from the edge of Pb)	29.01	18.23	8.34	5.33	1.63	0.89	2.18	1.26	32.01	98.88
SY47_kuona_alue1	30.37	17.88	9.04	7.75	2.84	0.37	1.70	0.67	27.98	98.60
SY47_kuona_alue1	30.85	18.01	9.01	7.68	2.82	0.31	1.62	0.66	28.10	99.05
SY47_kuona_alue1	30.76	17.95	8.99	7.77	2.73	0.30	1.59	0.67	28.32	99.07
SY47_kuona_alue1	30.66	17.96	8.99	7.74	2.76	0.32	1.61	0.65	28.29	98.98
SY47_kuona_alue1	30.32	18.00	8.93	7.66	2.76	0.33	1.64	0.66	28.04	98.34
SY47_kuona_alue1	30.60	17.98	8.95	7.79	2.78	0.33	1.59	0.65	28.08	98.75
SY47_kuona_alue1	30.56	18.04	8.88	7.83	2.69	0.25	1.55	0.66	28.16	98.63
SY47_kuona_alue2	30.23	18.29	8.73	7.52	2.33	0.17	1.21	0.59	28.82	97.89
SY47_kuona_alue2	30.07	18.33	8.69	7.63	2.39	0.19	1.27	0.62	28.68	97.88
SY47_kuona_alue2	31.23	17.92	8.88	7.66	2.73	0.31	1.57	0.65	28.11	99.05
SY47_kuona_alue2	29.58	18.23	8.74	7.59	2.44	0.18	1.34	0.63	28.62	97.36
SY47_kuona_alue2	30.23	17.91	8.92	7.69	2.67	0.26	1.54	0.65	28.10	97.98
SY47_kuona_alue2	30.52	17.83	8.98	7.81	2.78	0.31	1.63	0.67	28.17	98.70
SY47_kuona_alue2	30.54	18.05	8.83	7.61	2.57	0.22	1.44	0.63	28.34	98.22
SY47_kuona_alue2	30.09	17.84	8.92	7.76	2.73	0.34	1.66	0.68	28.02	98.04
SY47_kuona_alue2	30.00	17.70	8.95	7.77	2.86	0.41	1.75	0.65	27.75	97.83
SY25_kuona_area1	32.99	20.38	9.76	9.31	1.46	0.87	2.16	1.50	20.36	98.78
SY25_kuona_area1	32.80	20.57	9.99	9.63	1.49	0.93	2.18	1.50	20.67	99.77
SY25_kuona_area1	33.12	20.73	9.90	9.51	1.46	0.87	2.19	1.56	20.70	100.04
SY25_kuona_area1	32.87	20.64	9.95	9.57	1.45	0.91	2.18	1.51	20.86	99.94
SY25_kuona_area1	33.03	20.52	9.94	9.51	1.45	0.91	2.21	1.56	20.75	99.88
SY25_kuona_area1	31.69	20.61	9.91	9.57	1.45	0.92	2.15	1.50	20.73	98.53
SY25_kuona_area1	32.05	20.52	9.92	9.62	1.45	0.90	2.23	1.57	20.98	99.24
SY25_kuona_area1	32.50	20.52	9.92	9.50	1.47	0.91	2.14	1.50	20.62	99.08
SY25_kuona_area1	33.05	20.71	9.98	9.51	1.41	0.91	2.24	1.51	20.88	100.20
SY25_kuona_area2	31.44	20.83	9.52	10.16	0.87	0.51	1.23	1.07	22.96	98.59

SY25_kuona_area2	31.07	20.73	9.60	9.95	0.88	0.51	1.25	1.10	23.11	98.20
SY25_kuona_area2	31.35	20.75	9.58	10.00	0.89	0.47	1.25	1.04	23.04	98.38
SY25_kuona_area2	31.09	20.81	9.53	9.98	0.90	0.50	1.25	1.07	23.20	98.32
SY25_kuona_area2	30.91	20.62	9.51	10.02	0.89	0.54	1.25	1.06	22.98	97.77
SY25_kuona_area2	30.79	20.74	9.54	10.00	0.90	0.51	1.23	1.10	22.89	97.71
SY25_kuona_area2	31.36	20.70	9.61	9.96	0.89	0.50	1.24	1.02	23.16	98.43
SY25_kuona_area2	30.74	20.82	9.56	10.04	0.89	0.48	1.25	1.07	23.16	98.03
SY25_kuona_area2	30.69	20.84	9.47	10.00	0.88	0.50	1.24	1.06	22.78	97.45
SY29_kuona_alue1	36.09	21.14	10.67	13.86	0.22	0.05	0.32	0.38	17.28	100.02
SY29_kuona_alue1	35.45	21.09	10.62	14.13	0.22	0.06	0.33	0.35	17.23	99.48
SY29_kuona_alue1	34.86	21.14	10.64	13.88	0.19	0.09	0.29	0.36	17.06	98.51
SY29_kuona_alue1	34.81	21.10	10.60	13.90	0.21	0.07	0.30	0.35	16.95	98.31
SY29_kuona_alue1	34.81	21.13	10.63	13.81	0.23	0.04	0.31	0.39	16.91	98.26
SY29_kuona_alue1	34.57	21.08	10.62	14.07	0.23	0.08	0.32	0.34	16.89	98.21
SY29_kuona_alue2	34.80	20.81	11.04	15.01	0.07	0.12	0.19	0.20	16.59	98.82
SY29_kuona_alue2	34.35	20.88	10.95	14.93	0.07	0.09	0.17	0.19	16.47	98.11
SY29_kuona_alue2	34.79	20.82	10.92	14.91	0.07	0.09	0.18	0.19	16.23	98.20
SY29_kuona_alue2	34.32	20.75	10.96	15.00	0.07	0.10	0.21	0.22	16.32	97.94
SY29_kuona_alue2	34.30	20.79	10.97	14.82	0.06	0.09	0.18	0.19	16.43	97.83
SY29_kuona_alue2	34.36	20.80	10.93	14.93	0.07	0.13	0.22	0.21	16.21	97.85
SY29_kuona_alue2	33.88	20.82	11.04	14.98	0.09	0.10	0.16	0.20	16.35	97.61
SY30_kuona_alue1	34.95	21.29	11.16	15.43	0.07	0.06	0.20	0.22	15.73	99.10
SY30_kuona_alue1	34.75	21.07	11.20	15.65	0.08	0.06	0.19	0.20	16.10	99.30
SY30_kuona_alue1	34.53	21.03	11.23	15.41	0.08	0.06	0.20	0.20	15.97	98.70
SY30_kuona_alue1	33.53	21.13	11.21	15.58	0.07	0.05	0.21	0.20	15.96	97.96
SY30_kuona_alue1	34.64	21.07	11.19	15.46	0.08	0.06	0.21	0.20	16.01	98.92
SY30_kuona_alue1	34.27	21.14	11.16	15.78	0.07	0.04	0.21	0.21	15.96	98.85
SY30_kuona_alue1	33.87	21.07	11.25	15.45	0.06	0.06	0.20	0.22	15.77	97.93
SY30_kuona_alue2	34.95	21.48	11.29	15.66	0.08	0.05	0.15	0.18	15.10	98.93
SY30_kuona_alue2	35.11	21.46	11.35	15.64	0.08	0.04	0.15	0.19	15.27	99.29
SY30_kuona_alue2	34.99	21.57	11.29	15.61	0.08	0.04	0.13	0.18	15.34	99.22
SY30_kuona_alue2	35.33	21.44	11.26	15.61	0.05	0.04	0.14	0.18	15.26	99.32
SY30_kuona_alue2	34.50	21.46	11.26	15.66	0.07	0.07	0.13	0.16	15.30	98.61
SY41_kuona_alue1 (20 µm from the edge of Pb)	29.74	18.16	8.43	6.11	2.09	0.83	2.23	1.66	29.52	98.76
SY41_kuona_alue1 (20 µm from the edge of Pb)	29.56	18.06	8.36	6.05	2.12	0.86	2.18	1.61	29.39	98.19
SY41_kuona_alue1 (20 µm from the edge of Pb)	29.50	17.96	8.32	6.04	2.10	0.83	2.22	1.67	29.35	98.00

SY41_kuona_alue1 (20 µm from the edge of Pb)	29.80	18.07	8.31	6.09	2.12	0.87	2.19	1.64	29.52	98.61
SY41_kuona_alue1 (20 µm from the edge of Pb)	29.43	18.12	8.39	6.18	2.13	0.90	2.21	1.67	29.63	98.66
SY41_kuona_alue1 (20 µm from the edge of Pb)	29.55	18.10	8.39	6.06	2.12	0.85	2.20	1.60	29.38	98.26
SY41_kuona_alue2 (35 µm from the edge of Pb)	29.57	17.82	8.44	6.42	2.09	1.03	2.22	1.70	29.53	98.82
SY41_kuona_alue2 (35 µm from the edge of Pb)	30.08	17.78	8.41	6.42	2.10	0.99	2.17	1.59	29.56	99.10
SY41_kuona_alue2 (35 µm from the edge of Pb)	29.37	17.70	8.42	6.43	2.08	1.03	2.19	1.66	29.72	98.60
SY41_kuona_alue2 (35 µm from the edge of Pb)	29.41	17.96	8.37	6.37	1.89	0.97	1.97	1.60	29.78	98.32
SY41_kuona_alue2 (35 µm from the edge of Pb)	29.12	17.80	8.35	6.39	1.97	0.96	2.12	1.68	30.05	98.44
SY41_kuona_alue2 (35 µm from the edge of Pb)	29.07	17.96	8.36	6.33	1.99	0.96	2.10	1.59	29.10	97.46
SY41_kuona_alue2 (35 µm from the edge of Pb)	29.40	17.92	8.38	6.49	1.95	0.91	2.07	1.61	29.77	98.50
SY42_kuona_alue1	35.72	21.62	11.74	14.14	2.38	1.38	1.09	0.82	10.28	99.17
SY42_kuona_alue1	35.15	21.65	11.82	14.26	2.37	1.37	1.15	0.86	10.27	98.90
SY42_kuona_alue1	35.29	21.64	11.75	14.03	2.39	1.31	1.10	0.81	10.02	98.34
SY42_kuona_alue1	35.21	21.51	11.73	14.22	2.40	1.31	1.17	0.82	10.23	98.61
SY42_kuona_alue1	34.63	21.76	11.82	14.00	2.44	1.36	1.10	0.78	10.18	98.07
SY42_kuona_alue1	34.78	21.65	11.76	14.14	2.41	1.39	1.13	0.85	10.19	98.29
SY42_kuona_alue1	35.69	21.64	11.78	14.01	2.39	1.35	1.16	0.80	10.18	99.00
SY42_kuona_alue1	34.87	21.56	11.71	14.11	2.40	1.33	1.13	0.82	10.26	98.18
SY42_kuona_alue1	35.34	21.65	11.75	13.92	2.43	1.34	1.07	0.80	10.23	98.53
SY42_kuona_alue2	34.46	21.76	11.87	13.46	2.88	1.19	1.40	0.95	9.73	97.70
SY42_kuona_alue2	35.32	21.61	11.90	13.38	2.90	1.20	1.31	0.90	10.03	98.55
SY42_kuona_alue2	35.47	21.73	11.82	13.55	2.90	1.19	1.41	0.95	9.99	99.01
SY42_kuona_alue2	35.82	21.55	11.83	13.29	2.94	1.24	1.35	0.95	9.85	98.82
SY42_kuona_alue2	35.11	21.72	11.83	13.29	2.92	1.21	1.44	0.98	9.74	98.24

SY42_kuona_alue2	35.31	21.83	11.88	13.21	2.97	1.23	1.35	0.94	9.73	98.43
SY42_kuona_alue2	34.69	21.88	11.78	13.40	2.99	1.21	1.40	0.93	9.85	98.12
SY42_kuona_alue2	35.82	21.67	11.81	13.23	2.98	1.26	1.34	0.94	9.64	98.68
SY45_kuona_alue1	37.94	23.77	13.87	15.43	6.13	0.01	0.09	0.92	0.00	98.16
SY45_kuona_alue1	37.79	24.16	13.92	15.54	6.12	0.00	0.09	0.89	0.04	98.53
SY45_kuona_alue1	37.63	24.08	14.02	15.78	6.15	0.00	0.08	0.96	0.01	98.72
SY45_kuona_alue1	37.44	24.39	14.15	15.67	6.15	0.00	0.09	0.89	0.00	98.78
SY45_kuona_alue1	37.03	24.38	14.15	15.64	6.08	0.00	0.09	0.94	0.03	98.35
SY45_kuona_alue1	37.15	24.39	14.10	15.50	6.20	0.00	0.07	0.97	0.07	98.45
SY45_kuona_alue1	38.23	24.64	14.16	16.05	6.17	0.03	0.09	0.96	0.00	100.33
SY45_kuona_alue1	38.70	24.62	14.25	15.63	6.20	0.00	0.07	0.89	0.02	100.39
SY45_kuona_alue1	35.96	24.36	14.00	15.61	6.06	0.00	0.09	0.93	0.00	97.01
SY45_kuona_alue1	36.82	24.27	14.03	15.57	6.06	0.01	0.09	0.89	0.06	97.79
SY45_kuona_alue1	37.08	24.53	14.11	16.02	6.18	0.00	0.07	0.96	0.00	98.96
SY45_kuona_alue1	36.98	24.44	14.07	15.67	6.20	0.00	0.08	0.91	0.00	98.35

Slag phase normalised wt-%

	Norm Weight%									
Sample	O	Si	Ca	Fe	Ga	Ge	In	Sn	Pb	Total
SY_50_kuona_area1	20.73	10.23	6.22	5.74	0.74	0.22	0.60	0.21	55.31	100.00
SY_50_kuona_area1	20.65	10.27	6.20	5.75	0.76	0.20	0.59	0.19	55.39	100.00
SY_50_kuona_area1	20.66	10.24	6.20	5.79	0.76	0.19	0.59	0.20	55.36	100.00
SY_50_kuona_area1	20.78	10.24	6.20	5.70	0.74	0.23	0.57	0.17	55.37	100.00
SY_50_kuona_area1	20.76	10.32	6.19	5.75	0.75	0.22	0.61	0.17	55.23	100.00
SY_50_kuona_area1	20.74	10.23	6.22	5.72	0.76	0.21	0.61	0.19	55.32	100.00
SY_50_kuona_area1	20.61	10.29	6.24	5.79	0.74	0.22	0.61	0.19	55.32	100.00
SY_50_kuona_area1	20.36	10.38	6.27	5.76	0.76	0.20	0.59	0.18	55.50	100.00
SY_50_kuona_area2	20.26	10.73	5.66	6.22	0.84	0.21	0.66	0.20	55.23	100.00
SY_50_kuona_area2	20.26	10.78	5.73	6.14	0.83	0.20	0.67	0.20	55.21	100.00
SY_50_kuona_area2	20.27	10.80	5.78	6.27	0.81	0.21	0.70	0.21	54.95	100.00
SY_50_kuona_area2	20.01	10.66	5.53	6.23	0.84	0.21	0.65	0.21	55.66	100.00
SY_50_kuona_area2	19.84	10.85	5.72	6.21	0.83	0.24	0.70	0.20	55.42	100.00
SY_50_kuona_area2	20.75	10.87	5.84	6.18	0.82	0.17	0.68	0.21	54.49	100.00
SY_50_kuona_area2	20.72	10.79	5.86	6.23	0.83	0.21	0.68	0.20	54.48	100.00
SY_50_kuona_area2	20.48	10.89	5.71	6.20	0.82	0.20	0.67	0.18	54.84	100.00
SY_51_kuona_area1	19.82	10.43	6.43	5.96	0.51	0.26	0.64	0.23	55.73	100.00
SY_51_kuona_area1	19.89	10.35	6.42	5.95	0.50	0.24	0.67	0.23	55.74	100.00
SY_51_kuona_area1	20.00	10.34	6.38	5.93	0.49	0.27	0.67	0.21	55.71	100.00
SY_51_kuona_area1	21.04	10.20	6.30	5.90	0.49	0.26	0.68	0.21	54.91	100.00
SY_51_kuona_area1	20.40	10.45	6.36	5.95	0.50	0.23	0.63	0.21	55.26	100.00
SY_51_kuona_area1	20.09	10.34	6.39	5.97	0.51	0.25	0.69	0.23	55.54	100.00
SY_51_kuona_area1	20.15	10.44	6.39	5.96	0.50	0.26	0.66	0.21	55.41	100.00

SY_51_kuona_area2	20.80	10.16	6.29	5.91	0.45	0.26	0.65	0.22	55.26	100.00
SY_51_kuona_area2	20.46	10.19	6.34	5.90	0.46	0.25	0.63	0.21	55.54	100.00
SY_51_kuona_area2	20.64	10.00	6.29	5.91	0.43	0.24	0.64	0.20	55.65	100.00
SY_51_kuona_area2	20.47	10.23	6.34	5.92	0.46	0.26	0.62	0.18	55.51	100.00
SY_51_kuona_area2	20.09	10.21	6.38	5.96	0.46	0.26	0.67	0.22	55.75	100.00
SY_51_kuona_area2	20.25	10.09	6.28	5.91	0.45	0.26	0.67	0.23	55.86	100.00
SY_51_kuona_area2	19.94	10.32	6.32	5.95	0.44	0.26	0.67	0.23	55.88	100.00
SY_51_kuona_area2	20.58	10.23	6.31	5.90	0.47	0.23	0.62	0.20	55.45	100.00
SY_51_kuona_area2	20.01	10.21	6.34	5.87	0.46	0.24	0.65	0.24	55.98	100.00
SY31_kuona_alue1	27.91	16.17	8.22	9.45	0.12	0.12	0.37	0.14	37.50	100.00
SY31_kuona_alue1	28.39	16.09	8.09	9.32	0.12	0.06	0.34	0.15	37.45	100.00
SY31_kuona_alue1	27.86	16.32	8.10	9.41	0.13	0.11	0.35	0.16	37.55	100.00
SY31_kuona_alue1	28.18	16.16	8.14	9.38	0.12	0.10	0.33	0.17	37.43	100.00
SY31_kuona_alue1	28.01	16.34	8.21	9.46	0.13	0.11	0.31	0.13	37.30	100.00
SY31_kuona_alue1	28.31	16.28	8.02	9.43	0.12	0.11	0.30	0.14	37.29	100.00
SY31_kuona_alue1	27.58	16.27	8.18	9.47	0.10	0.10	0.34	0.13	37.83	100.00
SY31_kuona_alue1	27.51	16.40	8.15	9.51	0.13	0.06	0.35	0.13	37.76	100.00
SY31_kuona_alue1	28.23	16.20	8.01	9.45	0.15	0.08	0.34	0.15	37.39	100.00
SY31_kuona_alue1	28.31	16.12	8.02	9.36	0.15	0.10	0.32	0.16	37.47	100.00
SY31_kuona_alue1	27.96	16.26	8.17	9.40	0.16	0.08	0.31	0.15	37.50	100.00
SY31_kuona_alue1	27.52	16.35	8.09	9.32	0.13	0.09	0.35	0.14	38.02	100.00
SY31_kuona_alue1	27.42	16.44	8.20	9.45	0.14	0.11	0.35	0.16	37.73	100.00
SY31_kuona_alue1	27.83	16.33	8.19	9.39	0.16	0.09	0.32	0.14	37.55	100.00
SY31_kuona_alue1	27.50	16.47	8.13	9.49	0.16	0.09	0.35	0.14	37.67	100.00
SY31_kuona_alue1	27.23	16.53	8.23	9.47	0.12	0.06	0.34	0.16	37.86	100.00
SY37_kuona_alue1 (20 µm from the edge of Pb)	25.55	14.11	7.86	7.13	2.17	0.22	1.64	0.67	40.65	100.00
SY37_kuona_alue1 (20 µm from the edge of Pb)	25.00	14.20	7.87	7.19	2.21	0.22	1.65	0.65	41.02	100.00
SY37_kuona_alue1 (20 µm from the edge of Pb)	24.87	14.26	7.99	7.27	2.21	0.21	1.68	0.69	40.82	100.00
SY37_kuona_alue1 (20 µm from the edge of Pb)	25.41	14.13	7.82	7.11	2.21	0.15	1.62	0.66	40.88	100.00
SY37_kuona_alue1 (20 µm from the edge of Pb)	25.00	14.33	8.04	7.22	2.22	0.25	1.66	0.64	40.64	100.00
SY37_kuona_alue1 (20 µm from the edge of Pb)	25.61	14.00	7.48	7.01	2.20	0.21	1.68	0.64	41.16	100.00
SY37_kuona_alue1 (20 µm from the edge of Pb)	24.94	14.25	7.89	7.16	2.25	0.20	1.69	0.66	40.96	100.00
SY37_kuona_alue2 (20 µm from the edge of Pb)	25.53	13.89	7.66	7.03	2.11	0.19	1.63	0.64	41.32	100.00
SY37_kuona_alue2 (20 µm from the edge of Pb)	25.04	13.89	7.67	7.12	2.09	0.19	1.72	0.67	41.60	100.00

SY37_kuona_alue2 (20 µm from the edge of Pb)	25.29	13.90	7.62	7.03	2.12	0.18	1.70	0.66	41.50	100.00
SY37_kuona_alue2 (20 µm from the edge of Pb)	25.45	13.97	7.53	7.13	2.11	0.19	1.74	0.69	41.19	100.00
SY37_kuona_alue2 (20 µm from the edge of Pb)	25.48	13.96	7.67	7.08	2.13	0.17	1.67	0.63	41.22	100.00
SY37_kuona_alue2 (20 µm from the edge of Pb)	24.45	14.01	7.73	7.16	2.13	0.18	1.71	0.67	41.97	100.00
SY37_kuona_alue2 (20 µm from the edge of Pb)	24.50	14.08	7.78	7.12	2.14	0.18	1.69	0.65	41.86	100.00
Sy23_kuona_alue1	31.99	19.69	8.75	9.31	0.09	0.03	0.67	0.48	29.00	100.00
Sy23_kuona_alue1	31.65	19.88	8.82	9.39	0.08	0.00	0.69	0.47	29.02	100.00
Sy23_kuona_alue1	31.54	19.75	8.77	9.47	0.10	0.04	0.67	0.47	29.19	100.00
Sy23_kuona_alue1	31.66	19.87	8.80	9.33	0.07	0.01	0.67	0.49	29.09	100.00
Sy23_kuona_alue1	31.10	19.91	8.87	9.50	0.10	0.04	0.68	0.48	29.33	100.00
Sy23_kuona_alue1	31.08	20.03	8.87	9.21	0.08	0.05	0.66	0.48	29.55	100.00
Sy23_kuona_alue1	31.39	19.97	8.86	9.33	0.10	0.03	0.66	0.44	29.22	100.00
Sy23_kuona_alue1	31.59	19.91	8.86	9.20	0.10	0.06	0.69	0.50	29.09	100.00
Sy23_kuona_alue1	31.93	19.89	8.75	9.28	0.08	0.07	0.65	0.46	28.88	100.00
Sy23_kuona_alue2	30.13	17.52	8.92	5.66	3.78	0.91	2.38	0.93	29.76	100.00
Sy23_kuona_alue2	29.72	17.77	8.99	5.80	3.83	0.95	2.34	0.90	29.70	100.00
Sy23_kuona_alue2	30.49	17.37	8.84	5.70	3.75	0.91	2.36	0.89	29.70	100.00
Sy23_kuona_alue2	30.26	17.62	8.89	5.71	3.79	0.92	2.38	0.88	29.55	100.00
Sy23_kuona_alue2	29.77	17.51	8.97	5.72	3.81	0.93	2.43	0.91	29.95	100.00
Sy23_kuona_alue2	29.80	17.51	8.97	5.87	3.75	0.96	2.34	0.88	29.93	100.00
Sy23_kuona_alue2	30.17	17.43	8.96	5.63	3.75	0.91	2.37	0.92	29.86	100.00
Sy23_kuona_alue2	29.70	17.54	9.04	5.76	3.75	0.90	2.33	0.88	30.11	100.00
Sy23_kuona_alue2	29.91	17.41	8.88	5.66	3.72	0.91	2.35	0.92	30.24	100.00
Sy23_kuona_alue2	30.12	17.52	8.88	5.74	3.74	0.94	2.32	0.89	29.85	100.00
Sy23_kuona_alue2	29.42	17.70	8.93	5.71	3.81	0.88	2.40	0.93	30.23	100.00
SY11_kuona_alue1	29.85	16.18	10.31	15.09	0.85	0.02	1.78	0.70	25.23	100.00
SY11_kuona_alue1	29.81	16.21	10.34	15.20	0.82	0.01	1.74	0.65	25.21	100.00
SY11_kuona_alue1	29.63	16.16	10.31	15.20	0.83	0.06	1.73	0.68	25.39	100.00
SY11_kuona_alue1	29.63	16.30	10.42	15.14	0.83	0.04	1.74	0.65	25.25	100.00
SY11_kuona_alue1	29.21	16.44	10.46	15.18	0.86	0.01	1.78	0.68	25.39	100.00
SY11_kuona_alue2	33.83	19.33	12.66	19.54	1.16	0.13	1.70	0.58	11.07	100.00
SY11_kuona_alue2	33.78	19.20	12.52	19.69	1.17	0.11	1.75	0.59	11.19	100.00
SY11_kuona_alue2	34.32	18.98	12.56	19.43	1.13	0.09	1.70	0.56	11.22	100.00
SY11_kuona_alue2	34.02	19.07	12.59	19.47	1.16	0.13	1.76	0.58	11.21	100.00
SY11_kuona_alue2	34.14	19.07	12.56	19.50	1.17	0.10	1.71	0.59	11.16	100.00
SY11_kuona_alue2	33.95	19.27	12.57	19.55	1.18	0.11	1.74	0.57	11.07	100.00
SY11_kuona_alue2	33.83	19.28	12.65	19.59	1.16	0.07	1.77	0.55	11.10	100.00
SY11_kuona_alue3	34.00	19.95	12.61	21.09	0.68	0.06	1.32	0.49	9.80	100.00

SY11_kuona_alue3	33.95	19.98	12.70	21.13	0.68	0.08	1.28	0.47	9.75	100.00
SY11_kuona_alue3	33.93	19.99	12.71	21.08	0.66	0.04	1.31	0.48	9.81	100.00
SY11_kuona_alue3	33.65	20.12	12.60	21.34	0.63	0.09	1.29	0.47	9.82	100.00
SY11_kuona_alue3	34.06	19.90	12.47	21.23	0.61	0.08	1.27	0.48	9.89	100.00
SY11_kuona_alue3	34.13	19.83	12.48	21.23	0.61	0.07	1.25	0.46	9.93	100.00
SY27_kuona_alue1	38.38	21.27	12.28	12.67	3.11	0.07	3.27	2.38	6.57	100.00
SY27_kuona_alue1	38.16	21.51	12.39	12.46	3.11	0.07	3.27	2.42	6.61	100.00
SY27_kuona_alue1	38.70	21.19	12.26	12.49	3.07	0.05	3.25	2.33	6.66	100.00
SY27_kuona_alue1	38.48	21.26	12.28	12.49	3.09	0.05	3.25	2.36	6.72	100.00
SY27_kuona_alue1	38.32	21.23	12.39	12.48	3.13	0.04	3.30	2.43	6.67	100.00
SY27_kuona_alue1	38.42	21.33	12.39	12.49	3.14	0.07	3.24	2.33	6.60	100.00
SY27_kuona_alue2	37.30	21.20	12.02	11.42	3.63	0.08	3.60	1.92	8.83	100.00
SY27_kuona_alue2	37.80	20.98	12.04	11.30	3.64	0.06	3.58	1.89	8.70	100.00
SY27_kuona_alue2	37.45	21.13	12.11	11.34	3.58	0.08	3.62	1.94	8.74	100.00
SY27_kuona_alue2	37.53	21.14	12.06	11.14	3.57	0.09	3.63	1.90	8.95	100.00
SY27_kuona_alue2	37.50	21.03	12.07	11.24	3.60	0.07	3.65	1.94	8.90	100.00
SY27_kuona_alue2	37.62	21.07	12.05	11.16	3.62	0.05	3.62	1.89	8.92	100.00
SY13_kuona_alue1	35.94	20.54	11.73	14.90	0.81	0.09	3.27	2.15	10.57	100.00
SY13_kuona_alue1	35.77	20.66	11.87	14.98	0.79	0.08	3.20	2.08	10.58	100.00
SY13_kuona_alue1	35.88	20.57	11.89	14.98	0.81	0.07	3.24	2.14	10.42	100.00
SY13_kuona_alue1	35.62	20.58	11.88	15.09	0.79	0.11	3.11	2.09	10.73	100.00
SY13_kuona_alue1	36.08	20.38	11.77	14.97	0.80	0.10	3.09	2.06	10.74	100.00
SY13_kuona_alue1	35.82	20.40	11.88	15.21	0.79	0.10	2.96	1.97	10.86	100.00
SY13_kuona_alue2	34.40	16.79	14.34	15.32	10.95	0.23	0.67	0.35	6.94	100.00
SY13_kuona_alue2	34.80	16.86	14.36	14.91	11.02	0.22	0.61	0.33	6.89	100.00
SY13_kuona_alue2	35.32	16.99	14.37	14.38	10.96	0.24	0.64	0.33	6.77	100.00
SY13_kuona_alue2	34.98	17.17	14.44	14.36	10.94	0.19	0.61	0.34	6.97	100.00
SY13_kuona_alue2	35.08	16.58	14.51	14.88	10.78	0.25	0.66	0.37	6.89	100.00
SY13_kuona_alue2	34.89	16.47	14.47	15.39	10.76	0.27	0.66	0.31	6.78	100.00
SY13_kuona_alue2	34.29	16.65	14.47	15.90	10.88	0.31	0.70	0.34	6.47	100.00
SY14_kuona_alue1	37.02	19.62	14.56	19.11	7.73	0.08	0.77	0.60	0.52	100.00
SY14_kuona_alue1	37.12	19.48	14.52	19.17	7.67	0.10	0.80	0.61	0.53	100.00
SY14_kuona_alue1	36.83	19.60	14.55	19.20	7.75	0.09	0.76	0.59	0.65	100.00
SY14_kuona_alue1	36.90	19.69	14.59	19.05	7.79	0.05	0.78	0.63	0.53	100.00
SY14_kuona_alue1	37.12	19.57	14.62	18.95	7.72	0.06	0.76	0.58	0.62	100.00
SY14_kuona_alue1	37.02	19.50	14.64	18.98	7.79	0.06	0.78	0.60	0.63	100.00
SY14_kuona_alue2	36.97	19.15	14.36	17.18	8.87	0.14	0.78	0.61	1.95	100.00
SY14_kuona_alue2	37.57	18.97	14.32	17.01	8.67	0.11	0.76	0.65	1.95	100.00
SY14_kuona_alue2	36.91	19.26	14.37	17.17	8.77	0.12	0.76	0.62	2.01	100.00
SY14_kuona_alue2	37.14	18.98	14.35	17.13	8.67	0.13	0.79	0.66	2.15	100.00
SY14_kuona_alue2	36.77	19.04	14.47	17.43	8.75	0.10	0.74	0.62	2.08	100.00
SY14_kuona_alue2	37.34	18.94	14.30	17.81	7.85	0.12	0.81	0.64	2.19	100.00
SY14_kuona_alue2	37.06	18.96	14.32	17.37	8.65	0.10	0.78	0.62	2.14	100.00

SY14_kuona_alue2	37.25	19.06	14.43	17.16	8.57	0.12	0.78	0.65	1.98	100.00
SY14_kuona_alue2	36.81	19.17	14.40	17.50	8.59	0.13	0.77	0.61	2.01	100.00
SY15_kuona_area1	36.62	17.42	15.14	27.97	1.77	0.00	0.49	0.57	0.00	100.00
SY15_kuona_area1	36.76	17.38	15.25	27.79	1.79	0.01	0.47	0.55	0.00	100.00
SY15_kuona_area1	36.00	17.63	15.29	28.19	1.82	0.01	0.48	0.56	0.02	100.00
SY15_kuona_area1	36.30	17.54	15.16	28.16	1.81	0.02	0.48	0.54	0.00	100.00
SY15_kuona_area1	36.66	17.37	15.22	28.03	1.75	0.02	0.43	0.53	0.00	100.00
SY15_kuona_area1	36.27	17.36	15.29	28.36	1.83	0.00	0.41	0.49	0.00	100.00
SY15_kuona_area2	36.42	17.66	14.93	27.29	1.94	0.06	0.78	0.83	0.09	100.00
SY15_kuona_area2	36.02	17.86	14.93	27.67	1.90	0.02	0.77	0.83	0.00	100.00
SY15_kuona_area2	36.45	17.85	14.81	27.24	1.93	0.05	0.78	0.84	0.07	100.00
SY15_kuona_area2	35.90	17.81	15.01	27.68	1.89	0.00	0.76	0.84	0.11	100.00
SY15_kuona_area2	36.38	17.67	14.97	27.32	1.90	0.03	0.77	0.86	0.11	100.00
SY15_kuona_area2	36.60	17.70	14.91	27.18	1.90	0.04	0.77	0.80	0.09	100.00
SY15_kuona_area2	35.84	17.88	15.06	27.53	1.92	0.05	0.81	0.83	0.07	100.00
SY15_kuona_area2	36.37	17.79	14.92	27.29	1.98	0.04	0.79	0.79	0.03	100.00
SY16_kuona_area1	38.66	21.11	14.53	17.04	7.55	0.02	0.33	0.32	0.45	100.00
SY16_kuona_area1	38.28	21.01	14.65	17.26	7.66	0.01	0.34	0.33	0.47	100.00
SY16_kuona_area1	38.46	21.11	14.51	17.08	7.61	0.02	0.36	0.34	0.49	100.00
SY16_kuona_area1	38.76	20.93	14.46	17.17	7.58	0.01	0.32	0.32	0.47	100.00
SY16_kuona_area1	38.44	21.11	14.52	17.05	7.69	0.02	0.34	0.36	0.48	100.00
SY16_kuona_area1	38.80	20.95	14.45	17.16	7.60	0.01	0.32	0.34	0.39	100.00
SY16_kuona_area1	38.00	21.29	14.67	17.13	7.67	0.01	0.34	0.33	0.56	100.00
SY16_kuona_area1	38.57	21.18	14.47	16.97	7.64	0.00	0.34	0.34	0.49	100.00
SY16_kuona_area1	38.62	21.04	14.51	17.04	7.60	0.03	0.32	0.32	0.52	100.00
SY16_kuona_area1	38.14	21.28	14.52	17.14	7.65	0.01	0.30	0.31	0.63	100.00
SY16_kuona_area1	37.94	21.28	14.64	17.26	7.72	0.02	0.34	0.35	0.45	100.00
SY16_kuona_area1	38.29	21.25	14.52	17.12	7.68	0.02	0.33	0.33	0.48	100.00
SY16_kuona_area1	37.90	21.34	14.70	17.24	7.73	0.01	0.34	0.34	0.39	100.00
SY16_kuona_area1	38.20	21.27	14.43	17.28	7.63	0.00	0.33	0.33	0.54	100.00
SY16_kuona_area1	38.05	21.27	14.70	17.10	7.56	0.02	0.33	0.33	0.64	100.00
SY16_kuona_area1	38.37	21.35	14.74	16.98	7.46	0.00	0.33	0.33	0.43	100.00
SY46_kuona_alue1	34.55	18.12	16.30	28.62	2.25	0.00	0.00	0.16	0.01	100.00
SY46_kuona_alue1	34.26	18.25	16.42	28.64	2.28	0.00	0.00	0.16	0.00	100.00
SY46_kuona_alue1	34.59	18.12	16.24	28.63	2.24	0.01	0.00	0.16	0.02	100.00
SY46_kuona_alue1	35.23	17.97	16.23	28.17	2.24	0.00	0.01	0.16	0.00	100.00
SY46_kuona_alue1	34.97	17.93	16.22	28.43	2.28	0.00	0.00	0.17	0.00	100.00
SY46_kuona_alue1	34.74	18.08	16.31	28.34	2.28	0.01	0.00	0.15	0.09	100.00
SY46_kuona_alue2	34.34	18.16	16.28	28.75	2.27	0.00	0.01	0.16	0.04	100.00
SY46_kuona_alue2	34.47	18.19	16.29	28.58	2.29	0.03	0.00	0.14	0.00	100.00
SY46_kuona_alue2	34.32	18.18	16.33	28.71	2.29	0.01	0.01	0.16	0.00	100.00
SY46_kuona_alue2	33.97	18.32	16.44	28.72	2.31	0.00	0.00	0.14	0.10	100.00
SY46_kuona_alue2	33.53	18.40	16.46	29.16	2.28	0.00	0.00	0.17	0.00	100.00

SY46_kuona_alue2	33.64	18.48	16.59	28.83	2.30	0.00	0.00	0.15	0.00	100.00
SY_48_kuona_area1	16.15	7.08	2.85	5.65	0.10	0.19	0.18	0.07	67.74	100.00
SY_48_kuona_area1	16.18	7.02	2.74	5.64	0.12	0.22	0.18	0.06	67.84	100.00
SY_48_kuona_area1	17.53	6.93	2.78	5.58	0.10	0.21	0.18	0.05	66.64	100.00
SY_48_kuona_area1	17.67	7.22	3.12	5.35	0.10	0.17	0.15	0.08	66.14	100.00
SY_48_kuona_area1	17.06	7.57	3.48	5.43	0.13	0.19	0.17	0.05	65.92	100.00
SY_48_kuona_area1	16.80	8.01	4.15	5.25	0.10	0.16	0.16	0.07	65.29	100.00
SY_48_kuona_area2	19.70	8.84	5.82	5.03	0.12	0.21	0.16	0.06	60.06	100.00
SY_48_kuona_area2	18.99	8.80	5.79	5.02	0.11	0.19	0.17	0.06	60.88	100.00
SY_48_kuona_area2	18.34	8.67	5.55	5.24	0.09	0.22	0.17	0.05	61.67	100.00
SY_48_kuona_area2	18.41	8.66	5.64	5.10	0.10	0.23	0.18	0.05	61.63	100.00
SY_48_kuona_area2	18.03	8.46	5.29	5.18	0.10	0.23	0.19	0.07	62.46	100.00
SY_48_kuona_area2	17.29	8.26	5.08	5.24	0.11	0.20	0.19	0.05	63.58	100.00
SY_48_kuona_area2	17.82	8.37	5.32	5.20	0.06	0.20	0.16	0.05	62.82	100.00
SY_49_kuona area1	22.91	11.58	6.27	7.03	0.10	0.30	0.65	0.18	50.98	100.00
SY_49_kuona area1	22.51	11.73	6.44	7.19	0.09	0.29	0.68	0.21	50.87	100.00
SY_49_kuona area1	22.07	11.75	6.50	7.17	0.07	0.32	0.64	0.20	51.28	100.00
SY_49_kuona area1	22.10	11.82	6.52	7.19	0.07	0.32	0.68	0.19	51.11	100.00
SY_49_kuona area1	22.08	11.78	6.53	7.12	0.09	0.33	0.66	0.21	51.20	100.00
SY_49_kuona area1	21.95	11.80	6.52	7.23	0.07	0.32	0.68	0.20	51.24	100.00
SY_49_kuona area1	22.11	11.81	6.57	7.20	0.05	0.35	0.65	0.21	51.05	100.00
SY_49_kuona area1	21.74	11.88	6.58	7.21	0.08	0.32	0.67	0.20	51.32	100.00
SY_49_kuona area1	22.22	11.84	6.52	7.15	0.06	0.32	0.68	0.18	51.04	100.00
SY_49_kuona area1	21.68	11.78	6.57	7.22	0.11	0.36	0.69	0.20	51.40	100.00
Sy33_kuona_alue1	25.13	14.39	7.00	5.49	1.34	0.22	0.81	0.56	45.06	100.00
Sy33_kuona_alue1	24.80	14.43	7.07	5.49	1.35	0.19	0.80	0.55	45.32	100.00
Sy33_kuona_alue1	24.86	14.39	7.02	5.41	1.38	0.19	0.82	0.56	45.37	100.00
Sy33_kuona_alue1	24.75	14.40	7.03	5.48	1.37	0.19	0.78	0.57	45.44	100.00
Sy33_kuona_alue1	25.04	14.29	7.01	5.46	1.36	0.16	0.79	0.56	45.34	100.00
Sy33_kuona_alue1	24.94	14.33	6.97	5.48	1.36	0.12	0.78	0.55	45.47	100.00
Sy33_kuona_alue2	26.03	15.00	7.53	4.78	2.65	0.43	1.52	0.76	41.30	100.00
Sy33_kuona_alue2	25.62	15.07	7.49	4.76	2.64	0.46	1.50	0.74	41.73	100.00
Sy33_kuona_alue2	25.94	14.87	7.47	4.77	2.63	0.50	1.47	0.74	41.60	100.00
Sy33_kuona_alue2	25.94	14.92	7.44	4.76	2.65	0.48	1.48	0.71	41.62	100.00
Sy33_kuona_alue2	26.17	14.84	7.48	4.75	2.62	0.45	1.47	0.72	41.50	100.00
Sy33_kuona_alue2	26.00	15.01	7.41	4.82	2.63	0.46	1.48	0.74	41.46	100.00
SY34_kuona_alue1	33.48	20.35	10.19	7.48	2.55	0.71	2.54	1.16	21.55	100.00
SY34_kuona_alue1	32.89	20.46	10.19	7.55	2.52	0.73	2.61	1.19	21.87	100.00
SY34_kuona_alue1	33.61	20.41	10.21	7.39	2.48	0.70	2.53	1.14	21.53	100.00
SY34_kuona_alue1	33.83	20.25	10.08	7.53	2.48	0.72	2.54	1.15	21.42	100.00
SY34_kuona_alue1	33.45	20.44	10.18	7.47	2.49	0.68	2.52	1.14	21.63	100.00
SY34_kuona_alue1	33.06	20.52	10.19	7.54	2.49	0.74	2.58	1.17	21.72	100.00
SY34_kuona_alue1	33.60	20.38	10.12	7.42	2.50	0.73	2.52	1.15	21.58	100.00

SY34_kuona_alue1	32.72	20.71	10.20	7.56	2.46	0.74	2.56	1.18	21.88	100.00
SY34_kuona_alue1	33.45	20.45	10.10	7.42	2.46	0.70	2.51	1.15	21.76	100.00
SY34_kuona_alue2	32.49	19.46	9.47	5.76	3.70	1.09	2.34	1.85	23.85	100.00
SY34_kuona_alue2	32.55	19.62	9.50	5.71	3.71	1.14	2.32	1.77	23.69	100.00
SY34_kuona_alue2	32.44	19.61	9.42	5.73	3.72	1.06	2.33	1.82	23.86	100.00
SY34_kuona_alue2	32.32	19.74	9.60	5.62	3.70	1.10	2.31	1.81	23.80	100.00
SY34_kuona_alue2	31.92	19.72	9.60	5.84	3.77	1.09	2.37	1.83	23.85	100.00
SY34_kuona_alue2	32.40	19.63	9.51	5.67	3.77	1.09	2.29	1.77	23.88	100.00
SY34_kuona_alue2	31.77	19.73	9.54	5.78	3.79	1.10	2.37	1.85	24.08	100.00
SY34_kuona_alue2	31.66	19.95	9.64	5.76	3.80	1.11	2.37	1.79	23.93	100.00
SY34_kuona_alue3 (500 µm from the edge of Pb)	28.83	18.80	8.51	5.44	1.67	0.91	2.22	1.36	32.27	100.00
SY34_kuona_alue3 (500 µm from the edge of Pb)	29.98	18.34	8.38	5.33	1.60	0.86	2.17	1.27	32.07	100.00
SY34_kuona_alue3 (500 µm from the edge of Pb)	29.82	18.23	8.34	5.37	1.61	0.89	2.21	1.32	32.20	100.00
SY34_kuona_alue3 (500 µm from the edge of Pb)	29.43	18.37	8.35	5.39	1.62	0.86	2.20	1.28	32.50	100.00
SY34_kuona_alue3 (500 µm from the edge of Pb)	29.16	18.54	8.48	5.43	1.61	0.88	2.22	1.33	32.35	100.00
SY34_kuona_alue3 (500 µm from the edge of Pb)	29.34	18.44	8.44	5.39	1.64	0.90	2.20	1.28	32.37	100.00
SY47_kuona_alue1	30.80	18.13	9.17	7.86	2.88	0.38	1.72	0.68	28.38	100.00
SY47_kuona_alue1	31.14	18.18	9.10	7.75	2.85	0.31	1.63	0.67	28.37	100.00
SY47_kuona_alue1	31.04	18.12	9.07	7.84	2.75	0.30	1.61	0.68	28.58	100.00
SY47_kuona_alue1	30.97	18.15	9.09	7.82	2.78	0.32	1.63	0.66	28.58	100.00
SY47_kuona_alue1	30.83	18.30	9.08	7.79	2.81	0.33	1.67	0.67	28.51	100.00
SY47_kuona_alue1	30.99	18.20	9.07	7.89	2.82	0.33	1.61	0.66	28.43	100.00
SY47_kuona_alue1	30.99	18.29	9.01	7.94	2.73	0.26	1.57	0.67	28.55	100.00
SY47_kuona_alue2	30.88	18.69	8.92	7.69	2.38	0.17	1.24	0.60	29.44	100.00
SY47_kuona_alue2	30.72	18.73	8.88	7.80	2.45	0.19	1.30	0.64	29.30	100.00
SY47_kuona_alue2	31.53	18.09	8.97	7.73	2.76	0.31	1.59	0.65	28.37	100.00
SY47_kuona_alue2	30.39	18.73	8.98	7.80	2.50	0.18	1.38	0.64	29.40	100.00
SY47_kuona_alue2	30.85	18.28	9.11	7.84	2.73	0.27	1.57	0.67	28.68	100.00
SY47_kuona_alue2	30.93	18.06	9.10	7.91	2.82	0.32	1.65	0.68	28.54	100.00
SY47_kuona_alue2	31.10	18.38	8.99	7.74	2.62	0.22	1.46	0.64	28.85	100.00
SY47_kuona_alue2	30.69	18.20	9.10	7.91	2.78	0.34	1.69	0.69	28.59	100.00
SY47_kuona_alue2	30.66	18.10	9.14	7.94	2.92	0.42	1.79	0.66	28.36	100.00
SY25_kuona_area1	33.40	20.63	9.88	9.43	1.48	0.88	2.18	1.52	20.61	100.00
SY25_kuona_area1	32.88	20.61	10.02	9.65	1.49	0.94	2.18	1.51	20.72	100.00
SY25_kuona_area1	33.11	20.72	9.90	9.51	1.46	0.87	2.19	1.56	20.69	100.00
SY25_kuona_area1	32.89	20.65	9.96	9.57	1.45	0.91	2.18	1.51	20.88	100.00
SY25_kuona_area1	33.07	20.55	9.95	9.52	1.46	0.91	2.21	1.56	20.77	100.00

SY25_kuona_area1	32.16	20.91	10.06	9.71	1.47	0.93	2.19	1.52	21.04	100.00
SY25_kuona_area1	32.29	20.67	10.00	9.70	1.47	0.91	2.25	1.58	21.14	100.00
SY25_kuona_area1	32.80	20.71	10.01	9.58	1.48	0.92	2.16	1.51	20.82	100.00
SY25_kuona_area1	32.98	20.67	9.96	9.49	1.41	0.91	2.23	1.51	20.84	100.00
SY25_kuona_area2	31.89	21.13	9.66	10.31	0.88	0.51	1.25	1.08	23.29	100.00
SY25_kuona_area2	31.64	21.11	9.78	10.13	0.90	0.52	1.27	1.12	23.53	100.00
SY25_kuona_area2	31.87	21.09	9.74	10.17	0.90	0.48	1.27	1.06	23.42	100.00
SY25_kuona_area2	31.62	21.16	9.69	10.15	0.91	0.51	1.27	1.09	23.60	100.00
SY25_kuona_area2	31.62	21.09	9.72	10.25	0.91	0.55	1.28	1.08	23.50	100.00
SY25_kuona_area2	31.52	21.22	9.76	10.24	0.92	0.53	1.26	1.13	23.43	100.00
SY25_kuona_area2	31.86	21.03	9.76	10.12	0.90	0.51	1.26	1.03	23.53	100.00
SY25_kuona_area2	31.36	21.24	9.76	10.24	0.91	0.49	1.28	1.10	23.63	100.00
SY25_kuona_area2	31.49	21.39	9.72	10.26	0.91	0.51	1.27	1.09	23.37	100.00
SY29_kuona_alue1	36.08	21.14	10.66	13.86	0.22	0.05	0.32	0.38	17.28	100.00
SY29_kuona_alue1	35.63	21.20	10.68	14.21	0.22	0.06	0.33	0.35	17.32	100.00
SY29_kuona_alue1	35.39	21.46	10.80	14.09	0.20	0.09	0.29	0.36	17.32	100.00
SY29_kuona_alue1	35.41	21.47	10.78	14.14	0.21	0.08	0.31	0.36	17.24	100.00
SY29_kuona_alue1	35.43	21.50	10.82	14.06	0.23	0.04	0.32	0.39	17.21	100.00
SY29_kuona_alue1	35.20	21.47	10.82	14.33	0.23	0.08	0.33	0.35	17.20	100.00
SY29_kuona_alue2	35.22	21.06	11.17	15.18	0.07	0.12	0.20	0.20	16.78	100.00
SY29_kuona_alue2	35.01	21.29	11.16	15.22	0.07	0.09	0.18	0.19	16.79	100.00
SY29_kuona_alue2	35.42	21.20	11.13	15.19	0.07	0.09	0.19	0.19	16.53	100.00
SY29_kuona_alue2	35.04	21.19	11.19	15.31	0.07	0.10	0.21	0.22	16.66	100.00
SY29_kuona_alue2	35.06	21.25	11.22	15.15	0.06	0.09	0.18	0.20	16.79	100.00
SY29_kuona_alue2	35.12	21.25	11.17	15.26	0.07	0.13	0.22	0.22	16.57	100.00
SY29_kuona_alue2	34.71	21.33	11.31	15.34	0.09	0.10	0.17	0.20	16.75	100.00
SY30_kuona_alue1	35.27	21.48	11.26	15.57	0.07	0.06	0.21	0.22	15.87	100.00
SY30_kuona_alue1	35.00	21.21	11.28	15.76	0.08	0.06	0.19	0.20	16.22	100.00
SY30_kuona_alue1	34.98	21.31	11.38	15.61	0.08	0.06	0.21	0.20	16.18	100.00
SY30_kuona_alue1	34.23	21.57	11.45	15.91	0.07	0.05	0.22	0.21	16.29	100.00
SY30_kuona_alue1	35.01	21.30	11.31	15.63	0.08	0.06	0.22	0.20	16.19	100.00
SY30_kuona_alue1	34.67	21.38	11.29	15.97	0.07	0.04	0.22	0.21	16.15	100.00
SY30_kuona_alue1	34.58	21.51	11.49	15.77	0.06	0.06	0.20	0.23	16.10	100.00
SY30_kuona_alue2	35.33	21.71	11.41	15.83	0.08	0.05	0.15	0.19	15.26	100.00
SY30_kuona_alue2	35.36	21.62	11.43	15.75	0.09	0.04	0.15	0.19	15.38	100.00
SY30_kuona_alue2	35.27	21.73	11.38	15.73	0.08	0.04	0.13	0.18	15.46	100.00
SY30_kuona_alue2	35.58	21.59	11.34	15.72	0.05	0.04	0.14	0.18	15.36	100.00
SY30_kuona_alue2	34.99	21.77	11.42	15.88	0.07	0.07	0.13	0.16	15.52	100.00
SY41_kuona_alue1 (20 µm from the edge of Pb)	30.12	18.38	8.54	6.19	2.11	0.84	2.25	1.68	29.89	100.00
SY41_kuona_alue1 (20 µm from the edge of Pb)	30.10	18.40	8.52	6.16	2.16	0.87	2.22	1.64	29.93	100.00

SY41_kuona_alue1 (20 µm from the edge of Pb)	30.10	18.33	8.49	6.17	2.14	0.85	2.27	1.71	29.95	100.00
SY41_kuona_alue1 (20 µm from the edge of Pb)	30.22	18.33	8.42	6.17	2.15	0.88	2.22	1.66	29.94	100.00
SY41_kuona_alue1 (20 µm from the edge of Pb)	29.84	18.37	8.51	6.26	2.16	0.91	2.24	1.69	30.04	100.00
SY41_kuona_alue1 (20 µm from the edge of Pb)	30.08	18.42	8.54	6.16	2.16	0.86	2.24	1.63	29.90	100.00
SY41_kuona_alue2 (35 µm from the edge of Pb)	29.92	18.04	8.54	6.49	2.11	1.04	2.25	1.72	29.88	100.00
SY41_kuona_alue2 (35 µm from the edge of Pb)	30.35	17.94	8.49	6.48	2.12	0.99	2.18	1.61	29.83	100.00
SY41_kuona_alue2 (35 µm from the edge of Pb)	29.78	17.95	8.54	6.52	2.11	1.04	2.22	1.69	30.14	100.00
SY41_kuona_alue2 (35 µm from the edge of Pb)	29.92	18.26	8.52	6.48	1.92	0.98	2.01	1.63	30.29	100.00
SY41_kuona_alue2 (35 µm from the edge of Pb)	29.58	18.08	8.48	6.49	2.00	0.97	2.16	1.70	30.53	100.00
SY41_kuona_alue2 (35 µm from the edge of Pb)	29.83	18.43	8.58	6.49	2.04	0.99	2.15	1.63	29.86	100.00
SY41_kuona_alue2 (35 µm from the edge of Pb)	29.84	18.19	8.51	6.59	1.98	0.93	2.10	1.63	30.23	100.00
SY42_kuona_alue1	36.02	21.80	11.84	14.26	2.40	1.39	1.10	0.83	10.37	100.00
SY42_kuona_alue1	35.54	21.89	11.95	14.42	2.40	1.38	1.16	0.87	10.38	100.00
SY42_kuona_alue1	35.89	22.01	11.95	14.27	2.43	1.33	1.12	0.82	10.19	100.00
SY42_kuona_alue1	35.71	21.81	11.90	14.42	2.43	1.33	1.19	0.83	10.38	100.00
SY42_kuona_alue1	35.31	22.19	12.06	14.27	2.49	1.38	1.13	0.79	10.38	100.00
SY42_kuona_alue1	35.38	22.02	11.97	14.38	2.45	1.41	1.15	0.87	10.36	100.00
SY42_kuona_alue1	36.05	21.86	11.90	14.15	2.42	1.36	1.17	0.81	10.28	100.00
SY42_kuona_alue1	35.51	21.96	11.92	14.37	2.44	1.35	1.15	0.83	10.45	100.00
SY42_kuona_alue1	35.86	21.98	11.92	14.13	2.46	1.36	1.09	0.81	10.38	100.00
SY42_kuona_alue2	35.27	22.27	12.15	13.77	2.95	1.22	1.43	0.98	9.96	100.00
SY42_kuona_alue2	35.84	21.93	12.08	13.57	2.94	1.22	1.33	0.91	10.18	100.00
SY42_kuona_alue2	35.82	21.95	11.94	13.68	2.93	1.20	1.43	0.96	10.09	100.00
SY42_kuona_alue2	36.25	21.81	11.97	13.45	2.98	1.25	1.37	0.96	9.96	100.00
SY42_kuona_alue2	35.74	22.11	12.04	13.53	2.98	1.23	1.46	0.99	9.91	100.00
SY42_kuona_alue2	35.87	22.17	12.07	13.42	3.02	1.24	1.37	0.95	9.88	100.00
SY42_kuona_alue2	35.35	22.29	12.01	13.65	3.05	1.23	1.43	0.95	10.04	100.00
SY42_kuona_alue2	36.30	21.96	11.97	13.41	3.02	1.28	1.36	0.95	9.76	100.00
SY45_kuona_alue1	38.65	24.21	14.13	15.72	6.25	0.01	0.09	0.94	0.00	100.00
SY45_kuona_alue1	38.35	24.52	14.13	15.77	6.21	0.00	0.09	0.90	0.04	100.00
SY45_kuona_alue1	38.12	24.40	14.20	15.99	6.23	0.00	0.08	0.97	0.01	100.00
SY45_kuona_alue1	37.91	24.70	14.32	15.86	6.22	0.00	0.09	0.90	0.00	100.00
SY45_kuona_alue1	37.65	24.79	14.39	15.90	6.18	0.00	0.09	0.96	0.03	100.00

SY45_kuona_alue1	37.73	24.77	14.32	15.75	6.30	0.00	0.07	0.99	0.07	100.00
SY45_kuona_alue1	38.11	24.56	14.12	16.00	6.15	0.03	0.09	0.96	0.00	100.00
SY45_kuona_alue1	38.55	24.53	14.19	15.57	6.17	0.00	0.07	0.89	0.02	100.00
SY45_kuona_alue1	37.07	25.11	14.43	16.09	6.24	0.00	0.09	0.96	0.00	100.00
SY45_kuona_alue1	37.65	24.82	14.35	15.92	6.19	0.01	0.09	0.91	0.06	100.00
SY45_kuona_alue1	37.47	24.79	14.26	16.19	6.25	0.00	0.07	0.97	0.00	100.00
SY45_kuona_alue1	37.60	24.85	14.31	15.93	6.30	0.00	0.09	0.93	0.00	100.00

Appendix 3 Average, Standard deviation and their ratio of elements in lead phase

Calculated from normalised data

Series 1

Average										
Sample	log pO2	log pO2	Si	Ca	Fe	Ga	Ge	In	Sn	Pb
SY50	-7	-6.27	0.34	0.14	0.01	0.06	0.03	0.01	0.00	99.42
SY51	-7	-6.41	5.87	0.11	0.01	0.07	0.03	0.00	0.02	93.90
SY31	-8	-7.82	0.01	0.03	0.02	0.06	0.03	0.01	0.01	99.86
SY37	-8	-7.76	0.41	0.01	0.01	0.07	0.02	0.01	0.02	99.48
SY23	-9	-8.84	0.25	0.01	0.02	0.07	0.03	0.08	0.13	99.42
SY11	-9	-8.96	0.03	0.00	0.02	0.08	0.03	0.07	0.07	99.71
SY27	-10	-9.95	0.12	0.02	0.01	0.07	0.03	2.86	2.54	94.35
SY13	-10	-9.96	0.22	0.02	0.02	0.07	0.03	0.83	0.57	98.24
SY14	-11	-10.95	0.58	0.73	1.12	0.44	0.08	1.04	0.64	95.39
SY15	-11	-10.99	1.17	1.53	1.81	0.24	0.10	2.33	2.30	90.52
SY16	-12	-11.20	0.29	0.44	0.77	0.43	0.07	1.68	0.93	95.39
SY46	-12	-11.99	1.16	2.21	1.55	0.33	0.05	0.01	0.00	94.70
Standard deviation										
Sample	log pO2	log pO2	Si	Ca	Fe	Ga	Ge	In	Sn	Pb
SY50	-7	-6.27	0.06	0.07	0.00	0.01	0.01	0.00	0.01	0.13
SY51	-7	-6.41	1.53	0.01	0.01	0.01	0.02	0.00	0.01	1.54
SY31	-8	-7.82	0.01	0.01	0.01	0.02	0.02	0.01	0.01	0.03
SY37	-8	-7.76	0.28	0.01	0.01	0.02	0.01	0.00	0.01	0.29
SY23	-9	-8.84	0.02	0.01	0.01	0.01	0.02	0.01	0.02	0.03
SY11	-9	-8.96	0.02	0.00	0.01	0.02	0.02	0.03	0.03	0.05
SY27	-10	-9.95	0.02	0.01	0.01	0.02	0.02	0.12	0.12	0.28
SY13	-10	-9.96	0.04	0.01	0.01	0.01	0.01	0.04	0.03	0.04
SY14	-11	-10.95	0.02	0.01	0.03	0.02	0.02	0.02	0.02	0.06
SY15	-11	-10.99	0.56	0.61	0.39	0.04	0.03	0.09	0.16	1.74
SY16	-12	-11.20	0.02	0.03	0.03	0.01	0.02	0.05	0.02	0.15
SY46	-12	-11.99	0.12	0.11	0.03	0.01	0.02	0.01	0.00	0.23
Standard deviation/Average										
Sample	log pO2	log pO2	Si	Ca	Fe	Ga	Ge	In	Sn	Pb
SY50	-7	-6.27	0.19	0.48	0.62	0.17	0.42	0.51	1.48	0.00
SY51	-7	-6.41	0.26	0.08	0.77	0.19	0.52	0.00	0.62	0.02
SY31	-8	-7.82	0.71	0.23	0.80	0.39	0.65	0.93	0.99	0.00
SY37	-8	-7.76	0.68	0.68	1.31	0.26	0.68	0.42	0.45	0.00
SY23	-9	-8.84	0.07	0.68	0.54	0.20	0.60	0.18	0.18	0.00
SY11	-9	-8.96	0.56	0.75	0.56	0.21	0.56	0.40	0.40	0.00

SY27	-10	-9.95	0.22	0.63	0.65	0.31	0.58	0.04	0.05	0.00
SY13	-10	-9.96	0.19	0.26	0.56	0.19	0.43	0.05	0.05	0.00
SY14	-11	-10.95	0.03	0.02	0.03	0.06	0.29	0.02	0.03	0.00
SY15	-11	-10.99	0.48	0.40	0.22	0.15	0.27	0.04	0.07	0.02
SY16	-12	-11.20	0.07	0.06	0.05	0.03	0.22	0.03	0.03	0.00
SY46	-12	-11.99	0.10	0.05	0.02	0.04	0.45	0.80	0.00	0.00

Series 2

Average										
Sample	log pO2	log pO2	Si	Ca	Fe	Ga	Ge	In	Sn	Pb
SY48	-7	-6.46	0.03	0.08	0.01	0.07	0.04	0.01	0.01	99.77
SY49	-7	-6.52	0.79	0.01	0.01	0.06	0.03	0.00	0.00	99.11
SY33	-8	-7.83	0.24	0.03	0.02	0.06	0.04	0.01	0.00	99.62
SY34	-8	-7.83	0.22	0.07	0.01	0.07	0.03	0.01	0.02	99.59
SY47	-9	-8.92	0.37	0.01	0.02	0.06	0.03	0.02	0.06	99.46
SY25	-9	-8.85	0.06	0.02	0.02	0.06	0.02	0.01	0.05	99.77
SY29	-10	-9.95	0.16	0.02	0.01	0.06	0.03	0.29	0.28	99.16
SY30	-10	-9.94	0.16	0.02	0.02	0.07	0.03	0.25	0.26	99.22
SY41	-11	-10.94	0.34	0.21	0.04	0.09	0.08	0.21	0.28	98.76
SY42	-11	-10.95	0.14	0.02	0.04	0.08	0.04	0.60	0.37	98.71
SY45	-12	-11.96	0.11	0.09	0.18	0.10	0.07	1.91	1.11	96.42
Standard deviation										
Sample	log pO2	log pO2	Si	Ca	Fe	Ga	Ge	In	Sn	Pb
SY48	-7	-6.46	0.01	0.03	0.01	0.02	0.02	0.01	0.01	0.05
SY49	-7	-6.52	0.43	0.00	0.01	0.02	0.01	0.00	0.00	0.43
SY33	-8	-7.83	0.16	0.02	0.01	0.02	0.02	0.01	0.00	0.20
SY34	-8	-7.83	0.06	0.09	0.01	0.02	0.02	0.01	0.01	0.17
SY47	-9	-8.92	0.02	0.01	0.02	0.03	0.02	0.01	0.02	0.05
SY25	-9	-8.85	0.01	0.01	0.01	0.02	0.01	0.01	0.01	0.03
SY29	-10	-9.95	0.02	0.01	0.01	0.02	0.02	0.02	0.02	0.04
SY30	-10	-9.94	0.01	0.01	0.01	0.02	0.02	0.02	0.01	0.04
SY41	-11	-10.94	0.05	0.18	0.02	0.02	0.05	0.06	0.09	0.45
SY42	-11	-10.95	0.01	0.01	0.02	0.02	0.02	0.09	0.06	0.12
SY45	-12	-11.96	0.01	0.01	0.02	0.02	0.02	0.21	0.12	0.32
Standard deviation/Average										
Sample	log pO2	log pO2	Si	Ca	Fe	Ga	Ge	In	Sn	Pb
SY48	-7	-6.46	0.39	0.43	0.74	0.23	0.44	0.48	1.17	0.00
SY49	-7	-6.52	0.55	0.58	0.54	0.28	0.37	1.14	1.11	0.00
SY33	-8	-7.83	0.67	0.69	0.53	0.40	0.58	1.08	0.77	0.00

SY34	-8	-7.83	0.27	1.27	0.37	0.32	0.59	0.69	0.37	0.00
SY47	-9	-8.92	0.04	0.82	0.83	0.44	0.61	0.59	0.29	0.00
SY25	-9	-8.85	0.20	0.41	0.50	0.25	0.62	0.50	0.17	0.00
SY29	-10	-9.95	0.09	0.55	0.88	0.35	0.53	0.07	0.07	0.00
SY30	-10	-9.94	0.09	0.45	0.43	0.30	0.72	0.07	0.04	0.00
SY41	-11	-10.94	0.14	0.86	0.65	0.27	0.63	0.30	0.32	0.00
SY42	-11	-10.95	0.09	0.31	0.45	0.26	0.50	0.15	0.15	0.00
SY45	-12	-11.96	0.12	0.11	0.09	0.22	0.33	0.11	0.11	0.00

Appendix 4 Average, Standard deviation and their ratio of elements in slag phase

Calculated from normalised data

Series 1

Average											
Sample	log pO2	log pO2	O	Si	Ca	Fe	Ga	Ge	In	Sn	Pb
SY50	-7	-6.27	20.49	10.54	5.97	5.98	0.79	0.21	0.64	0.20	55.19
SY51	-7	-6.41	20.29	10.26	6.35	5.93	0.47	0.25	0.66	0.22	55.57
SY31	-8	-7.82	27.86	16.30	8.13	9.42	0.13	0.09	0.33	0.15	37.58
SY37	-8	-7.76	25.15	14.07	7.76	7.12	2.16	0.20	1.68	0.66	41.20
SY23	-9	-8.84	30.67	18.59	8.88	7.35	2.11	0.52	1.60	0.71	29.56
SY11	-9	-8.96	29.62	16.26	10.37	15.16	0.84	0.03	1.75	0.67	25.29
SY27	-10	-9.95	37.97	21.20	12.20	11.89	3.36	0.06	3.44	2.15	7.74
SY13	-10	-9.96	35.30	18.51	13.23	15.02	6.24	0.17	1.80	1.14	8.59
SY14	-11	-10.95	37.06	19.27	14.45	18.02	8.26	0.10	0.77	0.62	1.46
SY15	-11	-10.99	36.33	17.64	15.06	27.69	1.87	0.03	0.64	0.70	0.07
SY16	-12	-11.20	38.34	21.17	14.56	17.13	7.63	0.01	0.33	0.33	0.49
SY46	-12	-11.99	34.38	18.18	16.34	28.63	2.28	0.00	0.00	0.16	0.04
Standard deviation											
Sample	log pO2	log pO2	O	Si	Ca	Fe	Ga	Ge	In	Sn	Pb
SY50	-7	-6.27	0.29	0.28	0.26	0.24	0.04	0.02	0.04	0.01	0.34
SY51	-7	-6.41	0.35	0.13	0.04	0.03	0.03	0.01	0.02	0.01	0.27
SY31	-8	-7.82	0.36	0.12	0.07	0.06	0.02	0.02	0.02	0.01	0.20
SY37	-8	-7.76	0.38	0.15	0.16	0.07	0.05	0.02	0.03	0.02	0.42
SY23	-9	-8.84	0.87	1.20	0.08	1.85	1.88	0.45	0.87	0.22	0.43
SY11	-9	-8.96	0.25	0.11	0.07	0.05	0.02	0.02	0.02	0.02	0.09
SY27	-10	-9.95	0.49	0.14	0.15	0.66	0.26	0.01	0.19	0.24	1.15
SY13	-10	-9.96	0.60	1.95	1.34	0.40	5.24	0.08	1.30	0.90	2.00
SY14	-11	-10.95	0.21	0.28	0.12	0.92	0.49	0.03	0.02	0.02	0.75
SY15	-11	-10.99	0.29	0.19	0.16	0.40	0.07	0.02	0.17	0.15	0.03
SY16	-12	-11.20	0.29	0.14	0.10	0.10	0.07	0.01	0.01	0.01	0.07
SY46	-12	-11.99	0.50	0.16	0.11	0.25	0.02	0.01	0.00	0.01	0.04
Standard deviation/Average											
Sample	log pO2	log pO2	O	Si	Ca	Fe	Ga	Ge	In	Sn	Pb
SY50	-7	-6.27	0.01	0.03	0.04	0.04	0.05	0.07	0.07	0.06	0.01
SY51	-7	-6.41	0.02	0.01	0.01	0.00	0.05	0.05	0.03	0.06	0.00
SY31	-8	-7.82	0.01	0.01	0.01	0.01	0.14	0.20	0.05	0.07	0.01
SY37	-8	-7.76	0.02	0.01	0.02	0.01	0.02	0.12	0.02	0.03	0.01
SY23	-9	-8.84	0.03	0.06	0.01	0.25	0.89	0.86	0.54	0.31	0.01
SY11	-9	-8.96	0.01	0.01	0.01	0.00	0.02	0.86	0.01	0.03	0.00

SY27	-10	-9.95	0.01	0.01	0.01	0.06	0.08	0.22	0.05	0.11	0.15
SY13	-10	-9.96	0.02	0.11	0.10	0.03	0.84	0.48	0.72	0.79	0.23
SY14	-11	-10.95	0.01	0.01	0.01	0.05	0.06	0.29	0.02	0.04	0.51
SY15	-11	-10.99	0.01	0.01	0.01	0.01	0.04	0.82	0.26	0.21	0.45
SY16	-12	-11.20	0.01	0.01	0.01	0.01	0.01	0.68	0.04	0.04	0.15
SY46	-12	-11.99	0.01	0.01	0.01	0.01	0.01	2.10	0.95	0.06	1.00

Series 2

Average											
Sample	log pO2	log pO2	O	Si	Ca	Fe	Ga	Ge	In	Sn	Pb
SY48	-7	-6.46	17.69	7.99	4.43	5.30	0.10	0.20	0.17	0.06	64.05
SY49	-7	-6.52	22.14	11.78	6.50	7.17	0.08	0.32	0.67	0.20	51.15
SY33	-8	-7.83	25.43	14.66	7.24	5.12	2.00	0.32	1.14	0.65	43.43
SY34	-8	-7.83	31.92	19.66	9.49	6.33	2.70	0.89	2.38	1.42	25.20
SY47	-9	-8.92	30.91	18.29	9.05	7.83	2.72	0.29	1.57	0.66	28.68
SY25	-9	-8.85	32.25	20.92	9.85	9.89	1.18	0.71	1.73	1.31	22.16
SY29	-10	-9.95	35.29	21.29	10.99	14.72	0.14	0.09	0.25	0.28	16.96
SY30	-10	-9.94	35.02	21.52	11.37	15.76	0.07	0.05	0.18	0.20	15.83
SY41	-11	-10.94	29.98	18.24	8.51	6.36	2.09	0.94	2.19	1.66	30.03
SY42	-11	-10.95	35.75	22.00	11.98	13.95	2.69	1.30	1.26	0.89	10.17
SY45	-12	-11.96	37.91	24.67	14.26	15.89	6.22	0.01	0.08	0.94	0.04
Standard deviation											
Sample	log pO2	log pO2	O	Si	Ca	Fe	Ga	Ge	In	Sn	Pb
SY48	-7	-6.46	1.03	0.73	1.27	0.22	0.02	0.02	0.01	0.01	2.68
SY49	-7	-6.52	0.36	0.08	0.09	0.06	0.02	0.02	0.02	0.01	0.17
SY33	-8	-7.83	0.56	0.31	0.24	0.36	0.67	0.15	0.36	0.09	1.99
SY34	-8	-7.83	1.64	0.82	0.71	0.96	0.85	0.17	0.14	0.30	4.42
SY47	-9	-8.92	0.25	0.23	0.08	0.08	0.16	0.07	0.15	0.02	0.37
SY25	-9	-8.85	0.68	0.27	0.13	0.34	0.29	0.20	0.48	0.23	1.37
SY29	-10	-9.95	0.34	0.14	0.23	0.59	0.08	0.03	0.07	0.09	0.31
SY30	-10	-9.94	0.38	0.18	0.07	0.12	0.01	0.01	0.04	0.02	0.40
SY41	-11	-10.94	0.21	0.18	0.04	0.17	0.08	0.07	0.07	0.04	0.21
SY42	-11	-10.95	0.32	0.16	0.08	0.40	0.28	0.07	0.14	0.07	0.22
SY45	-12	-11.96	0.47	0.24	0.11	0.17	0.05	0.01	0.01	0.03	0.02
Standard deviation/Average											
Sample	log pO2	log pO2	O	Si	Ca	Fe	Ga	Ge	In	Sn	Pb
SY48	-7	-6.46	0.06	0.09	0.29	0.04	0.16	0.11	0.07	0.18	0.04
SY49	-7	-6.52	0.02	0.01	0.01	0.01	0.24	0.06	0.02	0.06	0.00
SY33	-8	-7.83	0.02	0.02	0.03	0.07	0.33	0.47	0.32	0.14	0.05
SY34	-8	-7.83	0.05	0.04	0.07	0.15	0.32	0.19	0.06	0.21	0.18
SY47	-9	-8.92	0.01	0.01	0.01	0.01	0.06	0.24	0.10	0.03	0.01
SY25	-9	-8.85	0.02	0.01	0.01	0.03	0.24	0.29	0.28	0.18	0.06

SY29	-10	-9.95	0.01	0.01	0.02	0.04	0.55	0.29	0.27	0.31	0.02
SY30	-10	-9.94	0.01	0.01	0.01	0.01	0.14	0.17	0.20	0.09	0.03
SY41	-11	-10.94	0.01	0.01	0.00	0.03	0.04	0.08	0.03	0.02	0.01
SY42	-11	-10.95	0.01	0.01	0.01	0.03	0.11	0.06	0.11	0.08	0.02
SY45	-12	-11.96	0.01	0.01	0.01	0.01	0.01	0.97	0.10	0.03	0.58

Appendix 5 Trace elements distribution coefficients with errors

Series 1

Sample	log pO2	L Ga	Δ L Ga	L Ge	Δ L Ge	L In	Δ L In	L Sn	Δ L Sn
SY50	-6.27	8.18E-02	1.77E-02	1.32E-01	6.56E-02	9.52E-03	5.49E-03	1.76E-02	2.71E-02
SY51	-6.41	1.57E-01	3.85E-02	1.26E-01	7.09E-02	0.00E+00	0.00E+00	7.31E-02	3.11E-02
SY31	-7.82	4.75E-01	2.48E-01	3.17E-01	2.71E-01	1.77E-02	1.74E-02	5.99E-02	6.35E-02
SY37	-7.76	3.40E-02	9.57E-03	1.10E-01	8.75E-02	3.83E-03	1.69E-03	2.68E-02	1.28E-02
SY23	-8.84	3.15E-02	3.43E-02	6.67E-02	9.43E-02	4.94E-02	3.57E-02	1.86E-01	9.18E-02
SY11	-8.96	9.06E-02	2.11E-02	1.31E+00	1.86E+00	3.78E-02	1.57E-02	1.19E-01	4.31E-02
SY27	-9.95	2.18E-02	8.39E-03	5.18E-01	4.13E-01	8.31E-01	7.99E-02	1.18E+00	1.90E-01
SY13	-9.96	1.18E-02	1.21E-02	1.79E-01	1.64E-01	4.60E-01	3.56E-01	5.00E-01	4.20E-01
SY14	-10.95	5.29E-02	6.05E-03	7.71E-01	4.48E-01	1.35E+00	5.75E-02	1.03E+00	6.52E-02
SY15	-10.99	1.28E-01	2.38E-02	3.39E+00	3.31E+00	3.63E+00	1.07E+00	3.26E+00	9.32E-01
SY16	-11.20	5.62E-02	2.03E-03	4.37E+00	2.79E+00	5.07E+00	3.59E-01	2.78E+00	1.85E-01
SY46	-11.99	1.44E-01	7.22E-03	4.37E+00	5.80E+00	2.03E+00	2.43E+00	2.82E-02	1.71E-03

Series 2

Sample	log pO2	L Ga	Δ L Ga	L Ge	Δ L Ge	L In	Δ L In	L Sn	Δ L Sn
SY48	-6.46	7.05E-01	2.75E-01	1.85E-01	9.60E-02	8.41E-02	4.60E-02	1.24E-01	1.66E-01
SY49	-6.52	7.88E-01	4.10E-01	1.00E-01	4.39E-02	5.05E-03	5.85E-03	2.14E-02	2.49E-02
SY33	-7.83	2.95E-02	2.15E-02	1.12E-01	1.17E-01	1.12E-02	1.56E-02	3.58E-03	3.28E-03
SY34	-7.83	2.71E-02	1.74E-02	3.82E-02	2.97E-02	3.37E-03	2.54E-03	1.42E-02	8.27E-03
SY47	-8.92	2.19E-02	1.09E-02	9.09E-02	7.73E-02	1.39E-02	9.54E-03	8.77E-02	2.86E-02
SY25	-8.85	5.30E-02	2.62E-02	3.30E-02	2.98E-02	6.05E-03	4.71E-03	4.19E-02	1.45E-02
SY29	-9.95	4.28E-01	3.84E-01	3.70E-01	3.03E-01	1.15E+00	3.96E-01	1.00E+00	3.77E-01
SY30	-9.94	9.33E-01	4.12E-01	6.16E-01	5.45E-01	1.36E+00	3.60E-01	1.30E+00	1.74E-01
SY41	-10.94	4.15E-02	1.28E-02	8.63E-02	6.15E-02	9.50E-02	3.16E-02	1.69E-01	5.76E-02
SY42	-10.95	3.14E-02	1.14E-02	3.05E-02	1.69E-02	4.75E-01	1.21E-01	4.21E-01	9.58E-02
SY45	-11.96	1.62E-02	3.65E-03	6.64E+00	8.66E+00	2.26E+01	4.76E+00	1.18E+00	1.71E-01

Appendix 6 Oxygen mole-% calculated in HSC

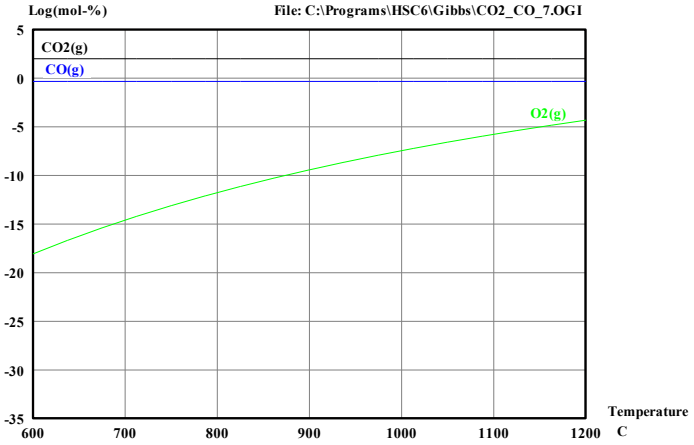

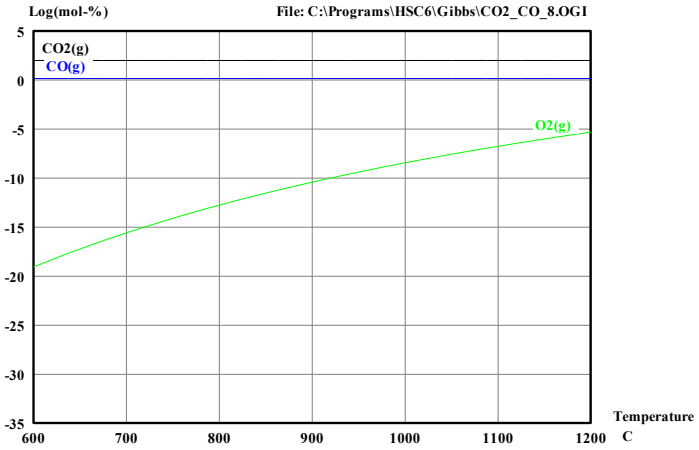

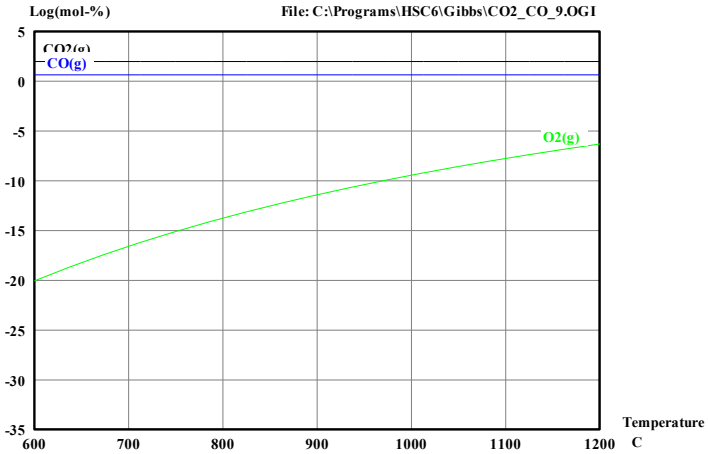

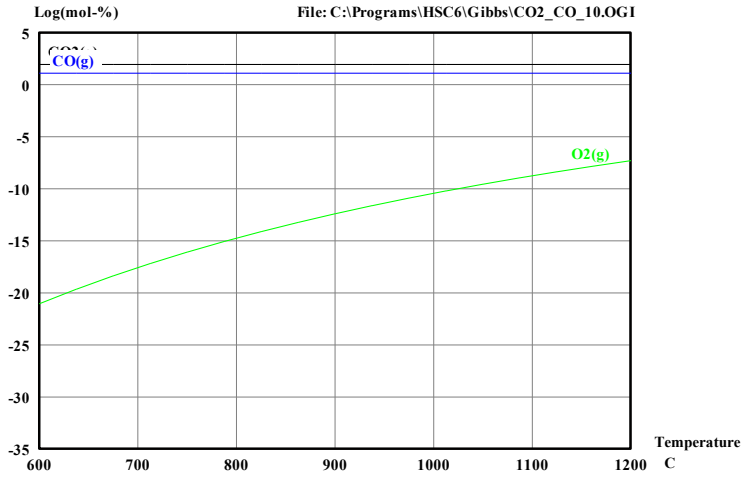
Log(mol-%)
File: C:\Programs\HSC6\Gibbs\CO2_CO_10.OGI
CO(g)
O2(g)
5
0
-5
-10
-15
-20
-25
-30
-35
600
700
800
900
1000
1100
1200
Temperature
C

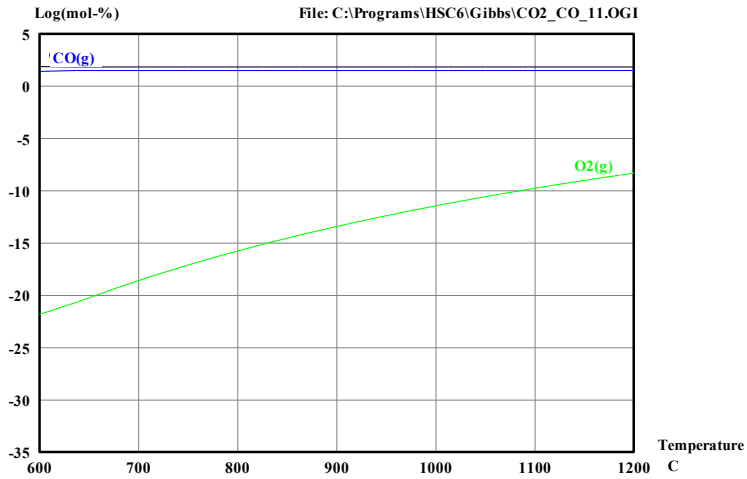
Log(mol-%)
File: C:\Programs\HSC6\Gibbs\CO2_CO_11.OGI
CO(g)
O2(g)
5
0
-5
-10
-15
-20
-25
-30
-35
600
700
800
900
1000
1100
1200
Temperature
C

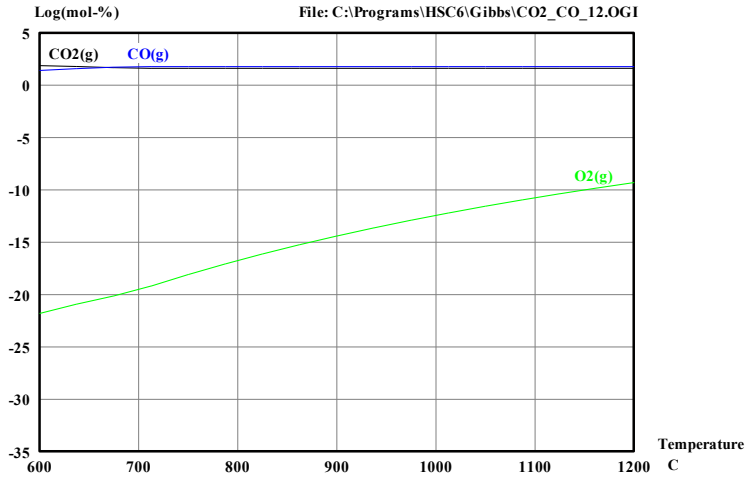
Log(mol-%)
File: C:\Programs\HSC6\Gibbs\CO2_CO_12.OGI
CO2(g)
CO(g)
O2(g)
5
0
-5
-10
-15
-20
-25
-30
-35
600
700
800
900
1000
1100
1200
Temperature
C